GL-TR-89-0179

Analysis of Significant Weather on Meso-Alpha
Scales Using Conventional and Remotely Sensed
Data - Exploratory Studies

Gregory S. Forbes   Paul J. Neiman
Dennis W. Thomson   Scott R. Williams
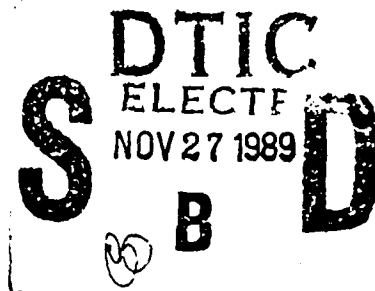John J. Cahir   Arthur A. Person
Catherine A. Carlson

Pennsylvania State University
Department of Meteorology
University Park, PA 16802

July 1989

Final Report
October 1984-September 1985

DTIC
ELECTF
NOV 27 1989
S   B   D

AD-A214 563
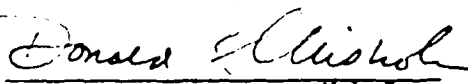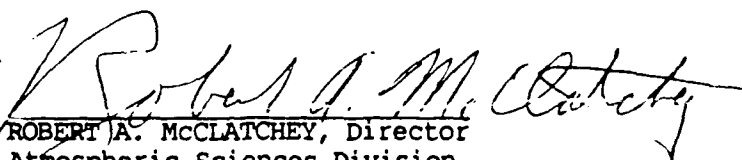
89 11 21 135

"This technical report has been reviewed and is approved for publication"

ARTHUR JACKSON
Contract Manager

DONALD A. CHISHOLM, Chief
Atmospheric Prediction Branch

/ROBERT A. McCLATCHEY, Director
Atmospheric Sciences Division

This document has been reviewed by the ESD Public Affairs Office (PA) and is releasable to the National Technical Information Service (NTIS).

Qualified requestors may obtain additional copies from the Defense Technical Information Center. All others should apply to the National Technical Information Service.

If your address has changed, or if you wish to be removed from the mailing list, or if the addressee is no longer employed by your organization, please notify AFGL/DAA, Hanscom AFB MA 01731-5000. This will assist us in maintaining a current mailing list.

Do not return copies of this report unless contractual obligations or notices on a specific document requires that it be returned.

REPORT DOCUMENTATION PAGE

1a REPORT SECURITY CLASSIFICATION Unclassified		1b RESTRICTIVE MARKINGS		
2a SECURITY CLASSIFICATION AUTHORITY		3 DISTRIBUTION/AVAILABILITY OF REPORT **Approved for public release; Distribution unlimited.**		
2b DECLASSIFICATION/DOWNGRADING SCHEDULE				
4 PERFORMING ORGANIZATION REPORT NUMBER(S)		5 MONITORING ORGANIZATION REPORT NUMBER(S) GL-TR-89-0179		
6a NAME OF PERFORMING ORGANIZATION Pennsylvania State University	6b OFFICE SYMBOL (If applicable)	7a NAME OF MONITORING ORGANIZATION Geophysics Laboratory		
6c ADDRESS (City, State, and ZIP Code) Department of Meteorology University Park, PA 16802		7b ADDRESS (City, State, and ZIP Code) Hanscom AFB Massachusetts 01731-5000		
8a NAME OF FUNDING/SPONSORING ORGANIZATION	8b OFFICE SYMBOL (If applicable)	9 PROCUREMENT INSTRUMENT IDENTIFICATION NUMBER F19628-85-K-0011		
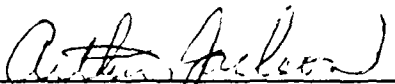
8c ADDRESS (City, State, and ZIP Code)	10 SOURCE OF FUNDING NUMBERS			
	PROGRAM ELEMENT NO	PROJECT NO	TASK NO	WORK UNIT ACCESSION NO
	61101F	ILIR	5J	AA

11 TITLE (Include Security Classification)

Analysis of Significant Weather on Meso-Alpha Scales Using Conventional and Remotely Sensed Data - Exploratory Studies

12 PERSONAL AUTHOR(S) Gregory S. Forbes, Dennis W. Thomson, John J. Cahir, Catherine A. Carlson, Paul J. Neiman, Scott R. Williams, Arthur A. Person

13a TYPE OF REPORT FINAL REPORT	13b TIME COVERED FROM Oct 1984 TO Sep 1985	14 DATE OF REPORT (Year, Month, Day) 1989 July	15 PAGE COUNT 228

16 SUPPLEMENTARY NOTATION

17	COSATI CODES		18 SUBJECT TERMS (Continue on reverse if necessary and identify by block number)
FIELD	GROUP	SUB-GROUP	Wind profiler Winds Jet streams
			Weather forecasting Fronts weather Systems
			VHF Dopper radar wind profiler

19 ABSTRACT (Continue on reverse if necessary and identify by block number)

Studies have been made regarding the use of Doppler wind profiler data in weather analysis and forecasting. Wind profiler from the Fleming, CO and McAlevy's Fort,PA sites were used to examine a number of cases of subtle weather situations. Use of the wind profiler data, together with conventional National Weather Service rawinsonde data proved quite helpful in understanding the cause of subtle weather systems seen in either satellite imagery or in the profiler wind variations. In addition to examining the profiler winds, studies were made of the utility of profiler-derived temperature gradients, temperature advections, and lapse rate gradient information. These quantities were derived from the observed vertical wind shears, assuming that the thermal wind relationship was reasonably valid. The framework is set forth for future studies involving profiler networks.

20 DISTRIBUTION/AVAILABILITY OF ABSTRACT ☐ UNCLASSIFIED/UNLIMITED ☐ SAME AS RPT ☐ DTIC USERS	21 ABSTRACT SECURITY CLASSIFICATION Unclassified	
22a NAME OF RESPONSIBLE INDIVIDUAL Arthur Jackson	22b TELEPHONE (Include Area Code)	22c OFFICE SYMBOL GL/LYP

DD FORM 1473, 84 MAR   83 APR edition may be used until exhausted   SECURITY CLASSIFICATION OF THIS PAGE

All other editions are obsolete

TABLE OF CONTENTS

TABLE OF CONTENTS, Continued

PREFACE

Between 1985 and 1989, two Air Force Geophysics Laboratory Contracts with the lead author have supported research on the use of wind profiler data for meteorological analysis and forecasting. This manuscript is a delayed publication of the final report on the first contract, F19628-85-K-0011. It is intended to provide the framework upon which the reader can more readily and thoroughly comprehend the studies reported in the publications resulting from the second contract, F19628-86-C-0092. Indeed, the research summarized in this Final Report set the framework upon which the research of the second contract was based. Stated in another way, this Final Report introduces a set of research topics which have been pursued in greater detail during the subsequent contract period.

The delay in the publication of this final report on the first contract allows this Preface to contain information concerning "subsequent" reports, which have been written not to be sequential works, but rather to be more like individual volumes of a pre-planned set. This Preface, then, shall serve as a guide to the set of publications during the 4-year project. The reader desiring to comprehensively examine the results of the project should acquire (in addition to this report, obviously) the M.S. Thesis of Cathy Carlson (published as AFGL-TR-87-0265), the M.S. Theses of Paul Neiman and Larry Knowlton (available from Penn State Department of Meteorology), and the Final Report of Contract F19628-86-C-0092 (available from AFGL). The latter report does contain a brief summary of the research reported in the

above Theses, but deals more thoroughly with the research of the lead author and by graduate students Tim Dye and Ming-Tzer Lee, partially supported by AFGL (and whose M.S. Theses will be available from Penn State).

The topics treated by the other reports can be capsulized as follows:

Carlson Thesis: Calculations using a triangle of wind profilers

Neiman Thesis: Thermodynamic information estimated from single-station profiler winds

Knowlton Thesis: Frontal zone structure and circulations

Dye Thesis: Mesoscale precipitation bands

Lee Thesis: Time-Space-Conversion analysis of profiler and rawinsonde data

1. INTRODUCTION

This report documents research performed during the first year of operation of a VHF Doppler wind profiler in Pennsylvania, and studies using Colorado profiler-triangle data in preparation for profiler triangle deployment in Pennsylvania. Inasmuch as the field of profiler technology is in a rapidly growing stage, many of the topics discussed herein are still being actively researched. Similarly, with less than a year to collect and analyze data, meteorological studies completed during the first year necessarily involved primarily case studies. Examples of this type are presented in chapters 4 and 5, as illustrations of some of the ways in which wind profiler data can be used in weather analysis and forecasting. More systematic studies of series of cases and their composited data have been pursued during subsequent years, and results are presented in subsequent reports. Refer to the Preface for an "outline" of the topics of these studies, and to Appendix 2 for a list of publications emanating from this first-year research.

1.1 Meteorological Applications of Profiler Technology

Essentially continuous measurements of many atmospheric parameters required for a variety of operational purposes are now possible as a consequence of the use of new and highly reliable remote sensing techniques and relatively inexpensive, yet powerful, computers. For continuous wind measurements, VHF and UHF Doppler wind profilers are ready for operational deployment.

The VHF Doppler wind profilers are pulsed clear-air Doppler radars that operate at about 50 MHz frequency and are capable of measuring the three-dimensional wind field essentially continuously (i.e., at intervals as short as about 2 minutes). An obvious first impact of the deployment of wind profilers is the ability to detect small-scale meteorolgical features and intrastation variations presently transparent to the synoptic-scale rawinsonde network.

Figure 1.1.1 is a time-height diagram illustrating how much meteorological detail can be missed by operational 12-hourly rawinsonde launches. Hourly wind profiler data enabled the mapping of the analyzed wind speeds as a function of height and time, including the brief maximum between about 1900 and 2200 UTC on 19 January 1987. Heavy lines with arrows and balloon symbols on the diagram indicate the approximate sampling that would have been obtained had conventional rawinsondes been launched at the site as a poor substitute for the wind profiler. It should be pointed out that the slope of the rawinsonde ascent on the diagram has been deliberately exaggerated, and the ascent appears to take longr than in reality, in order to allow for the eastward movement of the weather system and qualitatively portray the portions of the wind field sampled by the ascending (and mainly northward-moving) rawinsonde. This case is examined in detail by Forbes and Bankert (1987) and in the Final Report of the subsequent contract (Forbes et. al. 1989b).

Carlson and Sundararaman (1982) compiled a useful summary of the potential value of the Doppler wind profilers to the aviation
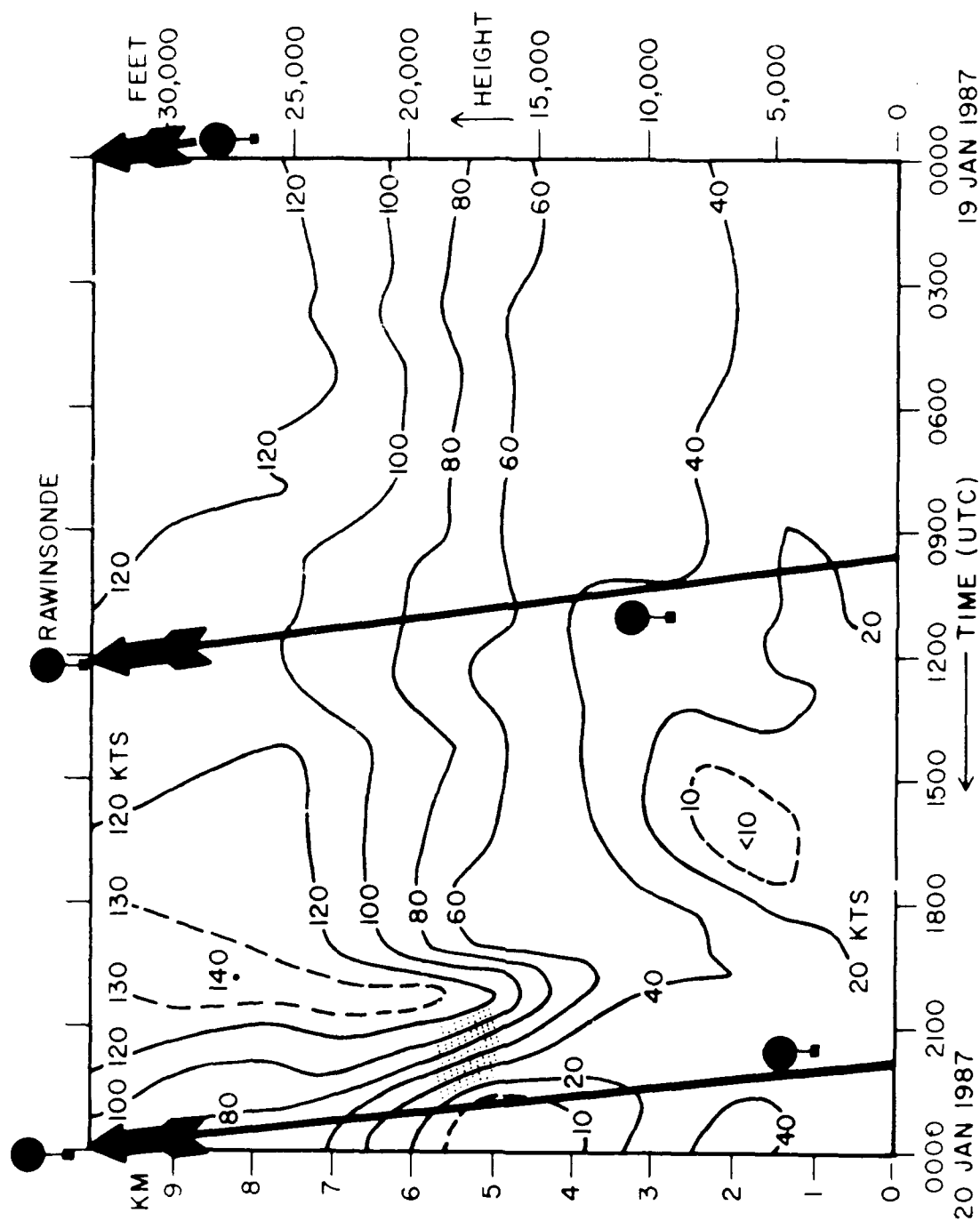
Figure 1.1.1. Time-height section of wind speeds on 19-20 January 1987, with hypothetical rawinsonde ascents superimposed, illustrating how much meteorological detail can be missed by operational 12-hourly rawinsonde launches.

community. According to their estimates, the improved knowledge of winds provided by a dense National network of profilers could result in the savings of 1 to 3% in annual aviation fuel costs, or a savings of 100 to 300 million dollars. There are countless other potential gains for public and private weather forecasts to be had because of improved weather analyses and forecasts which can result from the use of the high-temporal-resolution profiler data, both interactively by weather forecasters and by the inser-tion of the data into numerical weather prediction models.

While a National network is not yet a reality, the interest in profilers among the meteorological community is skyrocketing, and at least parts of what may grow into a national network should become a reality in the very near future. At present, the Wave Propagation Laboratory (WPL) of the National Oceanic and Atmospheric Administration (NOAA) is operating a network in eastern Colorado. A second network is being installed in west-ern and central Pennsylvania by the Pennsylvania State Univer-sity. NOAA has issued a contract for 30 UHF (about 405 MHz) Doppler wind profilers to be built and installed between rawin-sonde sites throughout approximately the central third of the United States. A number of other systems are in operation or are being prepared for operation at sites scattered throughout the world.

1.2 Overview of Profiler Hardware and Software Operation

Figure 1.2.1 shows the 1985 layout plan of the Pennsylvania State University three-wind-profiler network (Forbes et. al,
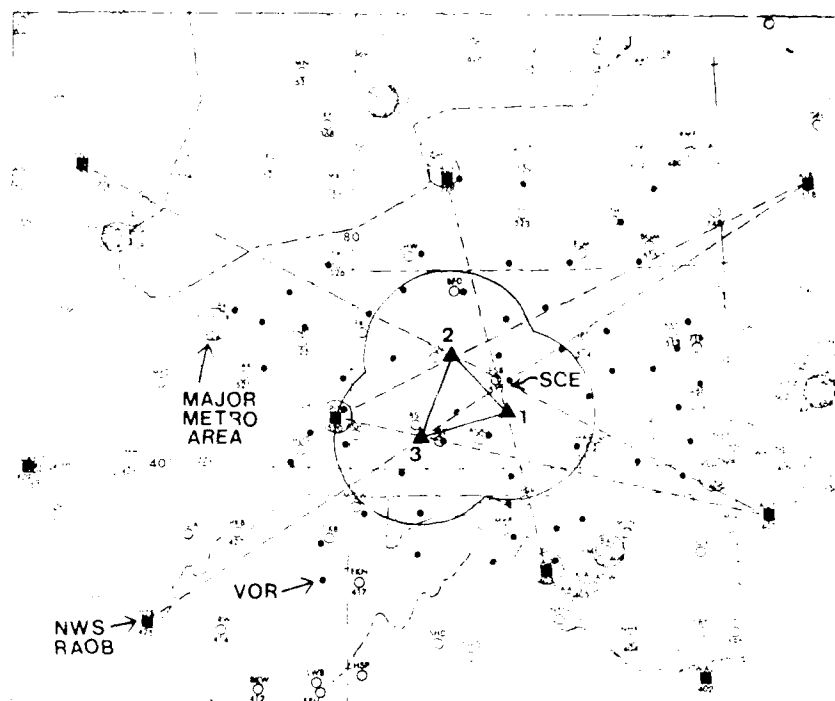
Figure 1.2.1. The Penn State profiler network (triangles), as planned in
1985, in relation to National Weather Service rawinsonde sites (squares),
operational surface weather reporting sites (small open circles), VORTAC
locations (dots), and major metropolitan areas (large open circles). Site 1
is at McAlevy's Fort, or "Shantytown". Site 2 was actually moved to Crown,
PA, about 40 km northwest of DUJ. Site 3 is expected to begin operation in
1989 about 15 km N of BSI.

1985; Williams and Peters, 1986), in relation to National Weather Service rawinsonde sites, surface observing sites, and major metropolitan areas. Circles of 100 km radius have been drawn around the profilers to suggest a reasonable influence radius for the real-time wind data. Dots on Fig. 1.2.1 indicate the locations of VORTACs (which are used for aeronautical navigational purposes) in the vicinity of the profiler network.

Site 1 of Fig. 1.2.1 is the McAlevy's Fort, PA site (sometimes nicknamed "Shantytown" after the various outbuildings along the roads through this part of rural Appalachia), and was operated throughout the period of this research. Site 2 was actually chosen at Crown, PA, about 40 km northwest of DUJ (Dubois), and began operating during the late spring of 1986. The third profiler of Fig. 1.2.1 has not yet been deployed at the time of this writing, but is expected to begin operation before the end of 1989. Its location has recently been chosen to be somewhat different from that shown, and will be in less hilly terrain near Indiana, PA, about 15 km north of BSI (Blairsville).

Some additional profiling instruments not shown on Fig. 1.2.1 either have been obtained or are planned. A fourth Doppler wind profiler, this one of the UHF type, has been acquired as a "mobile" research instrument that will participate in field experiments. It began operation in Alabama during the summer of 1986 as part of the Cooperative Huntsville Meteorological Experiment, COHMEX, (Dodge et. al, 1986) and has been to field experiment sites on San Nicholas Island, CA, in Arizona, and at Otis Air Force Base, MA in the interim. Between field experiments,

the UHF Doppler wind profiler is sited slightly south of State College, PA (SCE) on Penn State land about 15 km north of the McAlevy's Fort site. Temperature and humidity-sensing profilers are being constructed for deployment at the UHF site, and a RASS (radar-acoustic sounding system) has been obtained for use with the UHF Doppler wind profiler. Additional details of the chronology of the profiler system deployment are given in Section 2.

The principles of operation of the VHF and UHF Doppler radar wind profilers are given by Gage and Balsley (1978), Balsley (1981), Balsley and Gage (1982), Lassen and Rottger (1982), Hogg et. al (1983), and Thomson (1988), among others. Only a brief review is given here, dealing primarily with the methodology of the software for obtaining individual wind samples and hourly "averages" from series of individual samples.

Figure 1.2.2 is a photograph of the McAlevy's Fort wind profiler antenna. The upper mesh of cables is used to transmit VHF radio-wave energy, at about 50 MHz frequency. By varying the phasing over the array, the antenna controller enables the sequential simulation of three beams: one vertical beam and two "horizontal" beams at angles about 15 degrees from zenith. The lower mesh (almost at the ground level and not easily visible in the photograph) establishes a uniform plane of reference.

By measuring the phase shift of the returned signal, the radial velocity is computed according to

$$V_R = - \frac{\Delta f \, \lambda}{2} ,$$ (1.1)

where Δf is the frequency shift and λ is the wavelength. Positive frequency shifts occur when air approaches the antenna.

Figure 1.2.2. The mesh of cables which comprise the McAlevy's Fort VHF wind profiler, being inspected by H. Stuart Muench (left) and Artie Jackson (center) of AFGL. Scott Williams (right) leads the tour.

Air vertical velocity, with sign positive when motion is upward, has sign opposite to, and magnitude equal to, the radial velocity of the vertical beam.

As shown schematically in Figure 1.2.3, the off-zenith beams are at a large angle ($75-76^o$) to the horizontal air flow, such that the radial velocity measured is only about 24% (= $\cos 76^o$) of the horizontal velocity component along the beam azimuth. The measured radial velocity is used to deduce the component of horizontal velocity along each beam azimuth; obtained, therefore, by multiplying the radial velocity (i.e., the right side of (1.1)) by $(\cos 76^o)-1 = 4.1336$. Further, if the wind direction is along an azimuth different from that of the off-zenith beam, then the horizontal velocity component along the individual beam azimuth is Vh $\cos \theta$, which is less than the total horizontal speed, Vh. The total horizontal wind can be obtained by vector addition of the two horizontal velocity components retrieved from the orthogonal off-zenith beams.

It is clear from Fig. 1.2.3, and should be pointed out at this juncture, that the presence of non-zero air vertical velocity would "contaminate" the radial velocities measured in the off-zenith beams. This, in turn, would "contaminate" the horizontal velocity retrieved from the radial velocities. Hence, it is necessary to "correct" the retrieved horizontal velocities by eliminating the effects of the vertical velocity (measured by the vertical beam). This is discussed in greater detail in a subsequent paragraph.

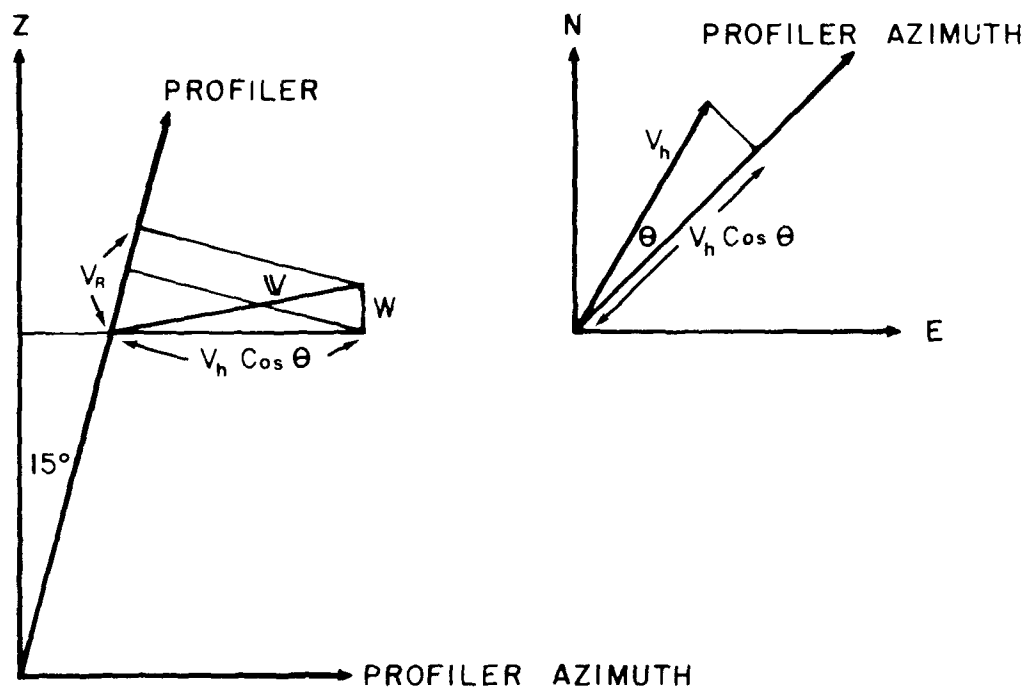Pulses of signal of duration T (3.67 or 9.67 microseconds),

Figure 1.2.3. Geometry of one of the profiler off-zenith beams with respect to the wind.

are transmitted at interval T (239 or 672 microseconds, for high-resolution and low-resolution data, respectively). The intervening period is used to measure the power and frequency of the returned signal. The time of arrival is related to the range of the target, according to the two-way path at the speed of electromagnetic propagation, 3×10^{8} ms^{-1}. After allowing for a brief period of time for the profiler electronics to switch from transmitter to receiver mode, the remainder of the inter-pulse interval is broken into 24 periods which correspond to 24 finite-volume range bins or "gates". A mean velocity and amplitude (power returned) is measured for each gate, and referenced to the center range.

In the presence of turbulence or other velocity inhomogeneities within the beam, the frequency may vary appreciably from one pulse to the next. In order to measure the prevailing flow velocity (by averaging out the microscale fluctuations), many samples (about 1500) are composited over a period of integration (i.e., sample period). Even if there were no velocity variations within the beam, the returned signal would be at an assortment of frequencies, since the transmitted signal is not of uniform frequency. In addition to the 50 MHz frequency, the transmitter also leaks low-intensity "tails" at slightly higher and lower frequencies.

The period of integration is 90 seconds in high-resolution (290 m gate spacing), near-range mode and about 3.5 minutes in low-resolution (870 m gate spacing), far-range mode. The McAlevy's Fort profiler measures winds at altitudes of about 1.3

- 7.4 km MSL (1.1 - 7.2 km AGL) in near-range (high-resolution) mode and about 1.3 - 16.1 km MSL (1.1 - 15.9 km AGL) in far-range (low resolution) mode. The ranges sampled by the Crown profiler are about 1.6 - 7.7 km MSL (1.1 - 7.2 km AGL) and 1.6-16.4 km MSL (1.1 - 15.9 km AGL) in the near- and far-range modes, respective- ly. In order to sample the entire troposphere and lower stratos- phere, near and far mode profiles are measured sequentially, re- quiring a total of 5 minutes. Thus, 12 sets of tropospheric winds can be obtained per hour.

The result at the end of the period of integration is the most fundamental profiler quantity, a vertical profile of spec- tra. An example is shown in Figure 1.2.4.   The display contains one spectrum from each of the range gates--highest one at the top of the diagram--with frequency shift (velocity) along the abscis- sa and the vertical extent of the spectrum presentation propor- tional to power returned at that frequency.

The spectra profile is one of three output data sets pre- sently generated by the profiler software. One spectra profile is generated for each beam. The other two types of output data are Moments Tables and Winds Tables, as shown in Figures 1.2.5 and 1.2.6. These are derived from the spectra profiles.

The Moments Table data are powers and weighted-mean veloci- ties that are computed from the spectra profiles through use of a "simple" algorithm developed at NOAA Wave Propagation Lab that (1) finds the primary peak (frequency of peak power) of the spec- trum, (2) searches left and right (toward lower and higher fre- quencies) to determine the frequencies at which the noise-level

FREQUENCY SHIFT →

HEIGHT →
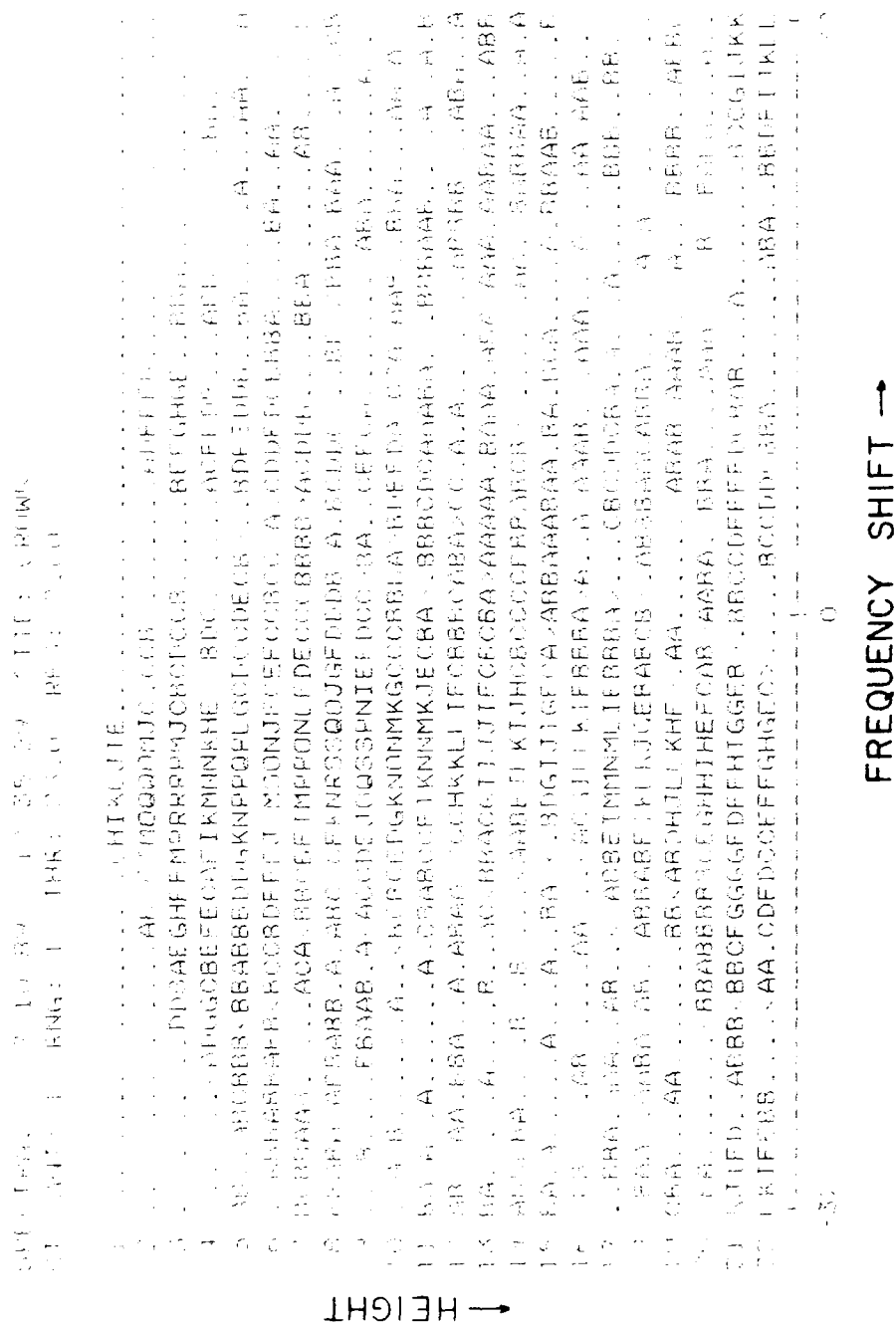
Figure 1.2.4a. Sample of raw output of wind profiler spectra.
Successive letters represent increments of 2db of returned power.

T I M E   2 2 0 7 3 0

HEIGHT →

FREQUENCY SHIFT →

←— RADIAL VELOCITY

− 0 +

POWER
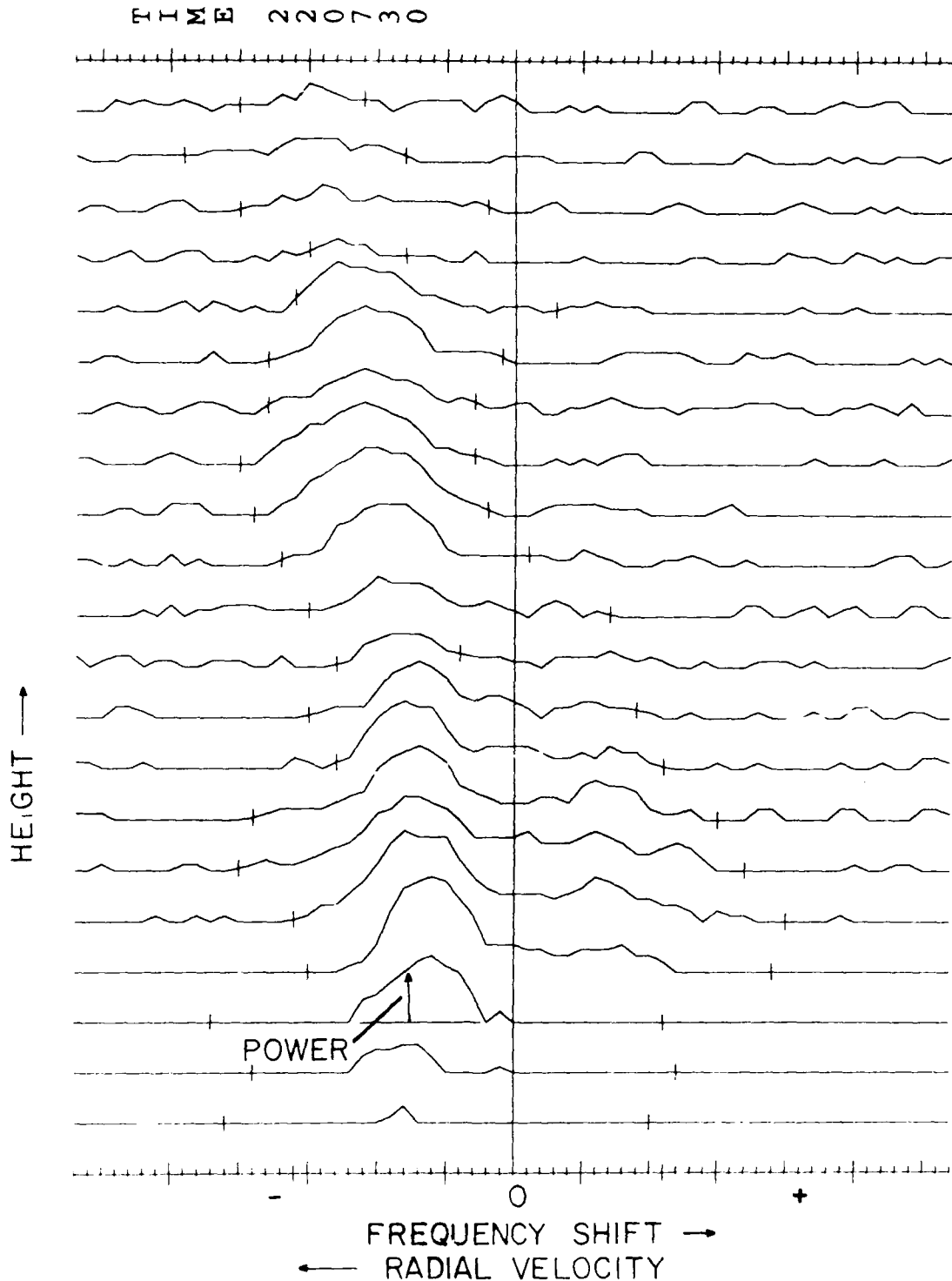
Figure 1.2.4b Sample profile of wind profiler spectra data. The x-axis represents frequency shift, scaled such that 32 and -32 represent the unambiguous (maximum) freqency shift. The y-axis represents height, and each trace represents a separate altitude ("gate"). The altitude is determined in the tails of the trace, where power diminished to the noise level. Near the center of the trace, where there is meteorological (or occasionally some other type of) return, the trace is displaced away from the reference level by an amount proportional to the log of the power of the returned signal.

```
MOMENTS:     7 10 89    12 35 36   SITE: CROWN
ANT: 1   RNG: 1
```

GATE	HOR VEL M/S	POWER DB	NOISE DB	SNR DB	WIDTH M/S
1	20.93	49.11	1.61	29.44	1.56
2	-21.43	59.86	8.08	35.71	2.28
3	-22.32	63.46	12.76	32.64	2.73
4	-21.39	55.99	21.26	14.66	3.02
5	-19.84	59.98	23.47	18.44	1.69
6	-19.64	57.03	23.83	15.14	1.84
7	-18.16	58.16	23.03	17.06	1.68
8	-17.02	64.68	23.75	22.87	1.34
9	-17.40	63.93	22.34	23.03	1.31
10	-17.48	56.49	23.16	15.26	1.59
11	-16.01	54.04	23.31	12.67	1.65
12	-16.22	50.99	23.48	9.45	1.68
13	-15.87	47.86	23.28	6.52	1.90
14	-15.40	49.49	23.17	3.26	2.23
15	-15.72	45.62	22.81	4.74	1.47
16	-16.20	50.11	23.07	8.98	1.42
17	-18.37	54.08	22.73	13.24	1.73
18	-20.21	49.82	23.09	8.67	1.73
19	-19.05	50.23	23.26	8.90	1.48
20	-19.89	44.67	23.19	3.42	2.45
21	-23.20	45.79	23.62	4.11	4.55
22	-20.26	43.32	22.58	2.68	3.49

Figure 1.2.5. Sample of a Moments Table. See text for explanation.

```
SITE:  SHANTY TOWN
DATE:   6 28 85
TIME:   7  0  0
NPRO:   12  NTDA:   419  NOSP:    9  PULW:  3.67  PRPR:  2050.07
MAX HOR VEL:      58.15
FIRST HT (AGL):    1.69
NUMBER OF HEIGHTS:   24
DELTA HEIGHT (FM):  .29
POWER ANTENNA:       EW
```

GATE	SPEED	DIRECT	HEIGHT	#E	#N	POWER
1	5.98	21.1	1.94	12	12	34.9
2	4.21	26.2	2.23	12	12	43.9
3	4.06	24.5	2.52	12	12	55.2
4	3.61	12.7	2.81	12	12	63.2
5	4.14	.7	3.10	12	12	65.5
6	5.46	352.6	3.39	12	12	63.2
7	8.29	350.7	3.68	12	12	63.1
8	9.69	350.2	3.97	12	12	63.2
9	10.57	346.9	4.26	12	12	62.8
10	12.36	343.2	4.55	12	12	60.0
11	13.71	343.1	4.84	12	12	58.7
12	14.22	340.5	5.12	12	12	56.0
13	14.87	338.4	5.41	12	12	52.5
14	15.70	337.0	5.70	12	12	50.8
15	16.11	337.3	5.99	12	12	49.2
16	16.12	340.2	6.28	12	12	48.9
17	16.43	341.3	6.57	12	12	49.7
18	17.17	342.2	6.86	12	12	48.6
19	16.41	344.2	7.15	12	12	47.4
20	14.78	347.8	7.44	12	12	45.0
21	13.28	351.1	7.73	12	12	43.8
22	13.46	350.5	8.02	11	10	43.0
23	12.63	251.6	8.31	12	10	43.2
24	12.99	349.1	8.60	12	10	40.0

Figure 1.2.6a. Sample of a Winds Table, high resolution portion.
See text for explanation.

SITE: SHANTY TOWN
DATE:
TIME:
DESC: NDOA: 124   NUSP: 22   PULW: 9.67   PRF: 672.00
MAX HOR VEL: 69.78
FIRST HT (ANG): 2.61
NUMBER OF HEIGHTS: 18
DELTA HEIGHT (KM):   .87
POWER ANTENNA: EW

GATE	SPEED	DIRECT	HEIGHT	#E	#N	POWER
1		5.5	2.85	12	12	57.6
2		353.6	3.72	12	12	65.6
3		346.1	4.59	11	12	65.4
4		341.1	5.46	11	11	59.8
5		341.6	6.33	12	12	54.7
6		344.5	7.20	12	12	52.1
7		348.5	8.07	11	10	48.6
8		349.9	8.94	11	11	42.7
9		340.0	9.81	9	10	35.6
10		337.8	10.68	12	10	38.9
11		331.4	11.55	12	11	41.9
12		337.5	12.42	12	12	38.0
13		341.2	13.29	9	12	34.2
14		8.9	14.16	8	12	32.7
15			15.03	7	10	999.0
16		331.1	15.89	5	7	32.0
17		349.3	16.76	4	7	32.1
18		349.0	17.63	2	5	999.0

Figure 1.2.6b. Sample of a Winds Table, low resolution portion. See text for explanation.

power returns are reached, and (3) computes the power weighted mean frequency shift between the noise-level frequency limits. This mean frequency shift corresponds to a measured radial velocity (see Eq. 1.1), which is displayed in the Moments Table as the radial velocity in the case of the vertical beam. As described in the discussion of Fig. 1.2.3, the radial velocities from the two off zenith beams are used to compute the mean horizontal velocity components. The Moments Table velocities retain the sign of the frequency shift (positive when flow is toward the antenna).

The Winds Table is a modification of the Moments Table, with velocities displayed in a more conventional meteorological format. The vertical velocity is displayed by magnitude and indicated as upward or downward. The horizontal velocity is presented as the speed and direction from which the wind is blowing.

Hourly "averages" are obtained by finding the mean value of up to 12 individual sets of Moments Table values available during an hour. Before the mean velocity is computed, a consensus process is imposed. The end product is a set of $\leq$ 12 spectra means which fall within ± 1.5 m/s of a mean value. The number of "concurring" spectra is termed the "consensus number", and is output to the Winds Table along with the raw mean velocity.

Data from the Winds Table is used as input by a number of meteorological-quantity derivation computation schemes and graphical display programs developed in the course of the period of funded research (discussed further beginning in section 2). As a mild quality check, winds accompanied by consensus numbers

than 4 are rejected as questionable in all calculation and display programs, unless the consensus number is specified higher the researcher.

The consensus method is far from a perfect noise suppression quality checking technique. When only a small number of spectra are required to agree, noise can enter the meteorological lations and displays. When a large number of spectra are required to agree, most of the noise is eliminated along with apparently valid data. In the latter case, the intra-hour passage of meso-gamma-scale wave phenomena (causing large changes velocity) may be the culprit.

Figure 1.2.7 illustrates the impact of varying the consensus number on a case that happens to be noisier than typical, especially below 7 km. Whereas increasing the consensus number from 4 to 7, and from 7 to 10 (out of 12) progressively removed more of the noise, increasing amounts of apparently good data were also eliminated. In this case, it was necessary to increase the consensus number to 12 before all of the noise was eliminated. In the process, however, as much as 55% of the good data was also eliminated, unfortunately. Obviously, more sophisticated noise removal schemes will ultimately need to be developed. This task will be undertaken in the future. In the interim, a choice of consensus number of about 7 is used. Use of that number appears to remove the most bad data without eliminating much good data.

There are many potential sources of noise in the radial velocities. One is electromagnetic noise present within the
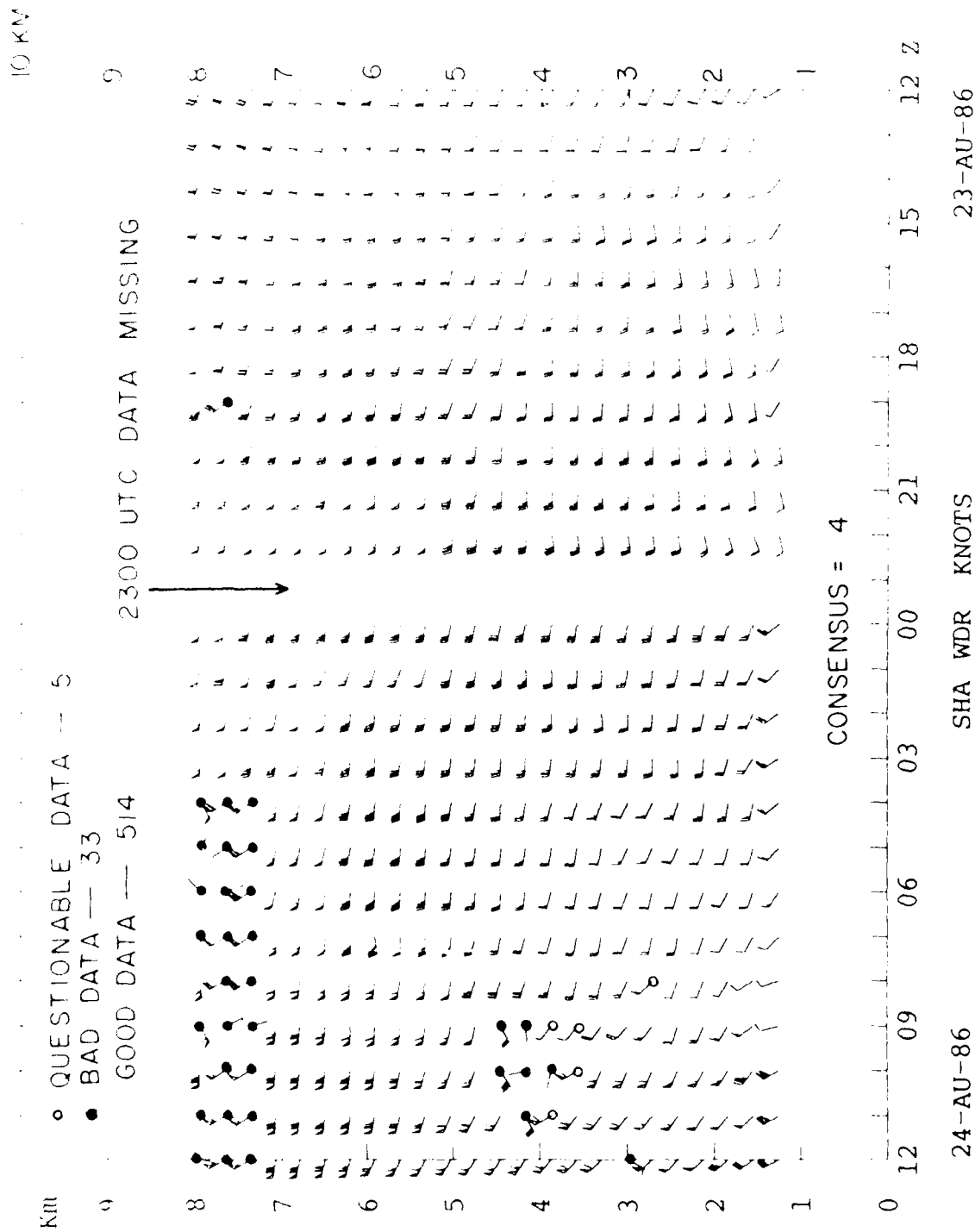
Figure 1.2.7. The impact of varying the consensus number on a case that is noisier than typical.
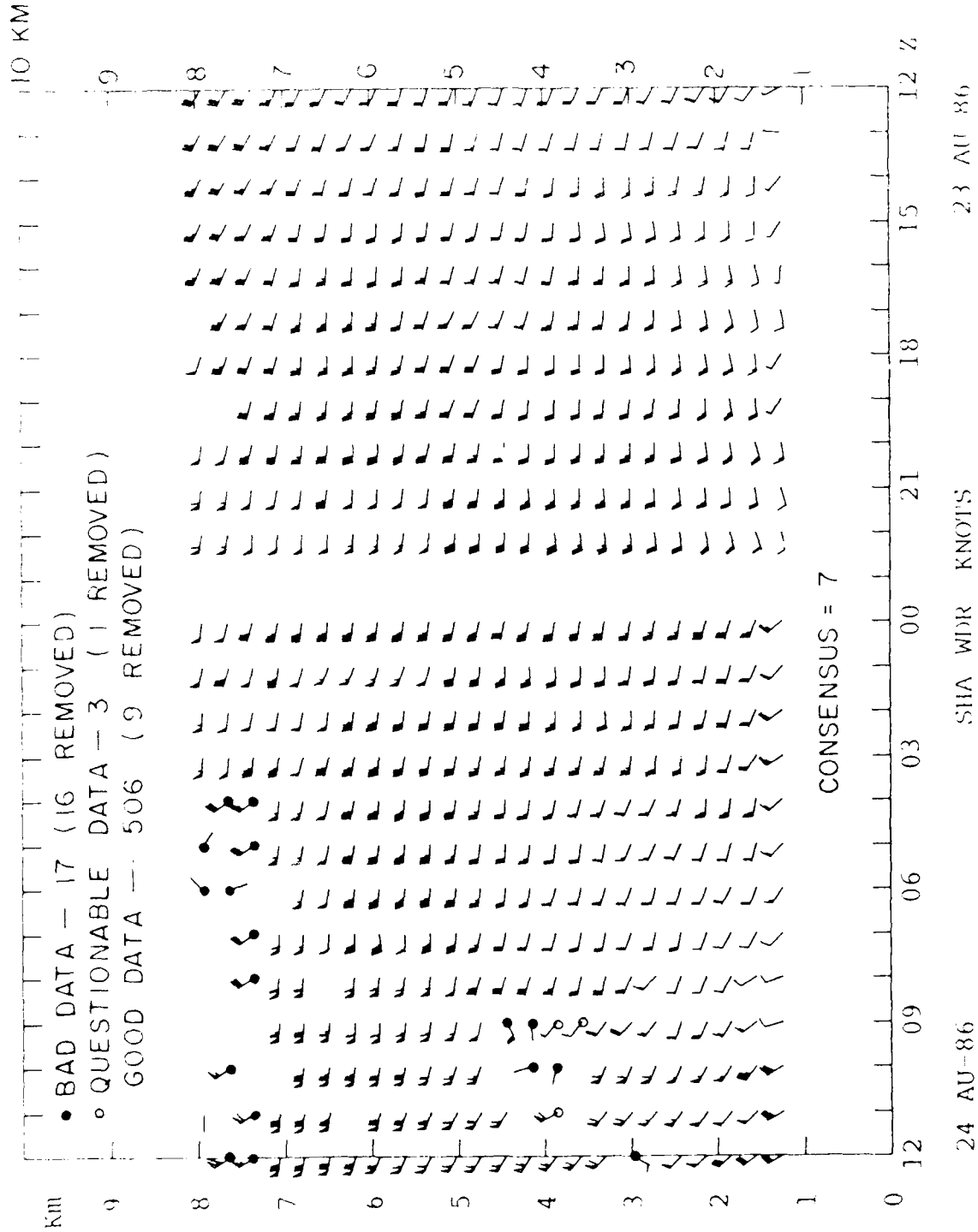
a. Consensus number 4

Fig. 1.2.7, cont'd. The impact of varying the consensus number.
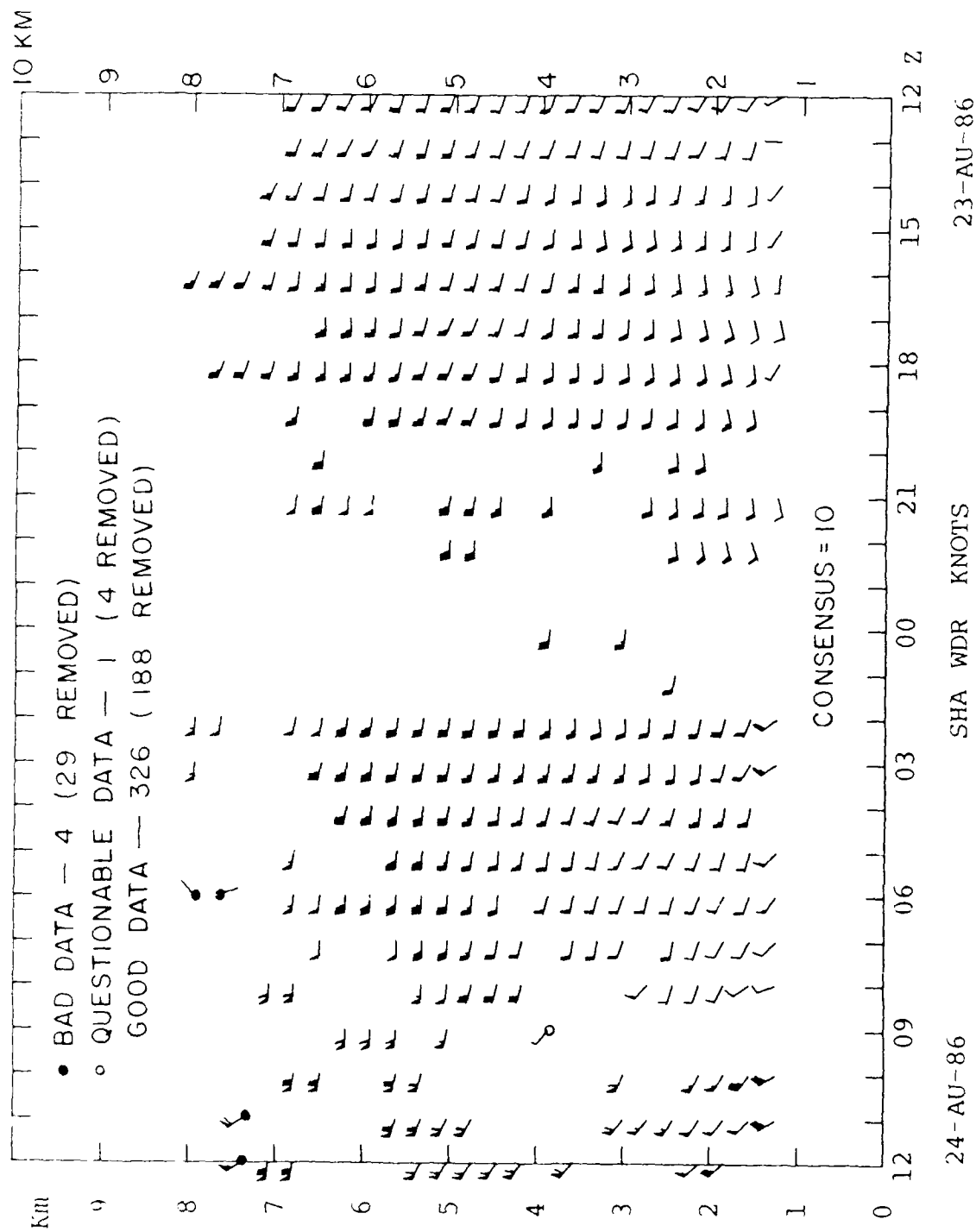
b. Consensus number 7

Fig. 1.2.7, cont'd. The impact of varying the consensus number.
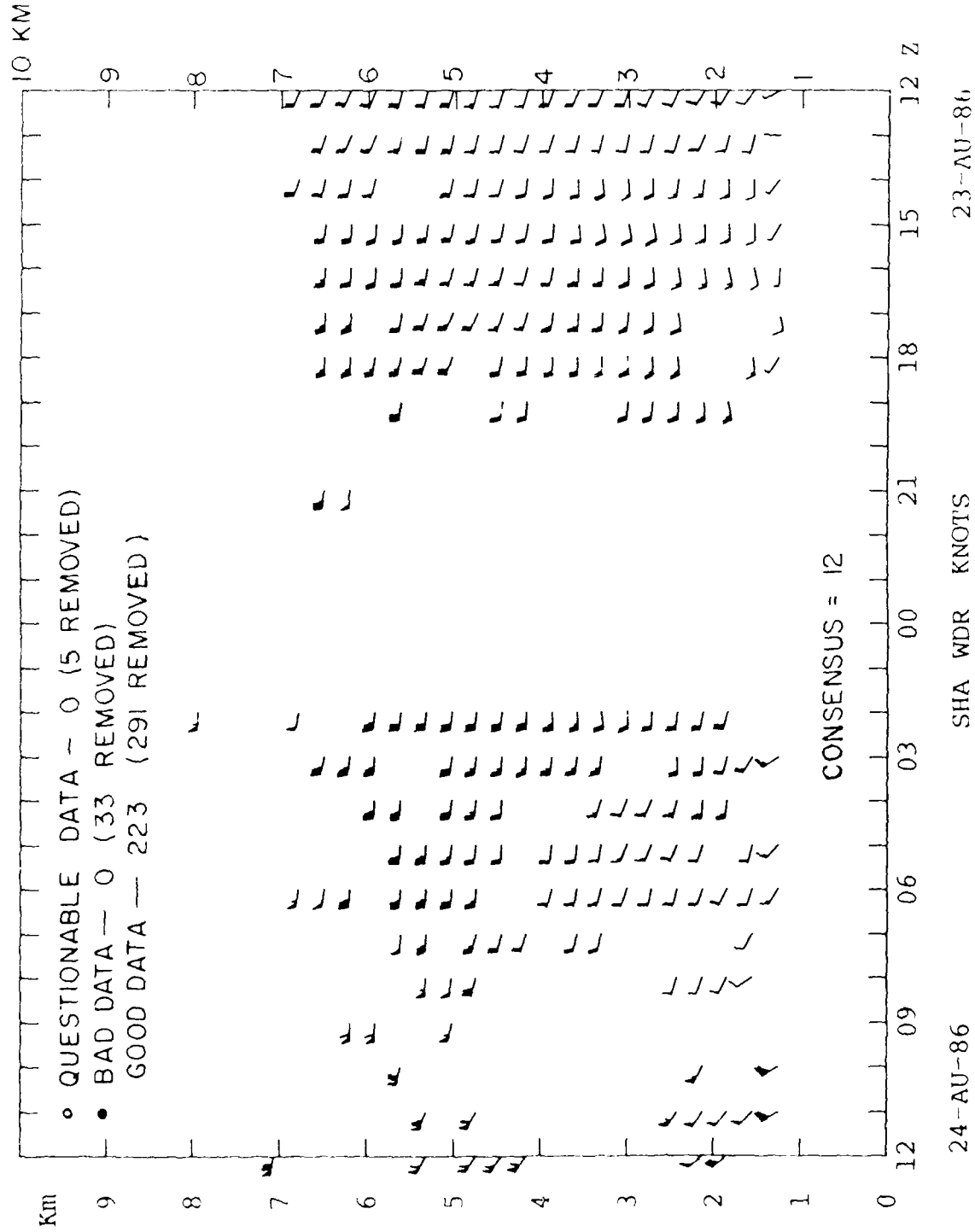
c. Consensus number 10

Fig. 1.2.7, cont'd. The impact of varying the consensus number.

d. Consensus number 12

pulse volume as a result of nearby power lines or machinery. Another is contamination of data through contributions from side lobes (power "leaking" from the antenna at angles other than the desired angle).

Noisy wind vectors can result from an imbalance of the sensitivities of the individual beams, since one beam may detect the weak atmospheric signal and the other may intermittently lock in on background noise or atmospheric signal. In the event that the atmosphere is quite dry and the associated profiler backscatter weak while there is a fairly strong persistent background frequency present, the insensitive beam may "lock in on" the background frequency. The result is a high consensus number but an unrealistic wind.

Contributions from persistent vertical velocity, such as in the vicinity of sloping terrain, may cause appreciable contamination of the "horizontal" velocity measured by the off-zenith beams, especially when the horizontal wind speed is low. Since the "horizontal" beams are only $14-15^{o}$ from zenith, 97% of the vertical velocity is sensed as off-zenith radial velocity. The horizontal velocity required to produce that radial component is 4.01 w (ratio of $\cos 14^{o}$ and $\cos 76^{o}$). Synoptic-scale vertical velocities ($\sim$ 5 cm/s) clearly do not pose a problem, but smaller-scale systems which may contain vertical velocities as great as several meters per second are clearly a potential source of horizontal beam contamination.

The WPL software contains provisions for systematically removing the effect of measured vertical velocity from the "hori-

zontal" velocity measured by the off-zenith beams. This step has not been used in this research, since the vertical beam was not yet installed in the McAlevy's Fort profiler during the first year of operation.

It must also be recognized that the vertical beam and the two off-zenith beams do not sample the same volume of air, in either space or time. This is especially troublesome in the presence of mesoscale weather systems which have both large vertical velocities and large horizontal and vertical variations. As a result, it may not be possible to unambiguously retrieve the horizontal velocity in the presence of strong vertical velocities in the vicinity of the profiler.

If more than one spectral peak of vertical velocity exists, the horizontal velocity spectra might also have multiple peaks, to the extent that the spectral processing algorithm fails to yield a meaningful velocity. Again, this type of problem could occur when vigorous mesoscale systems are present.

Similarly, when precipitation is present in the profiler beam—in the case of the UHF radar—the spectra may contain multiple peaks or at least a broadened spectrum. That is, the air velocity and velocities of precipitation particles of one or more sizes may be detected within the beam simultaneously. The simple scheme described above for obtaining the mean velocity from the spectral data tends to average over all of the individual peaks and obtain a weighted value not representative of any one of contributors. It will be necessary to develop and deploy algorithms not presently in our arsenal in order to decompose such

complex spectra into a finite number of contributing spectra.

Inspection of returned powers over wide ranges of meteoro-logical conditions reveals that humidity plays a crucial role in the process of wind profiling with VHF and UHF Doppler radar. Drying aloft can easily be recognized in the form of powers that approach the noise level. Days with deep cloud layers in middle and upper troposphere are associated with above-average powers and consistently high consensus numbers. Future research will attempt to determine if humidity can be accurately estimated quantitatively by this means.

The enhanced probability of bad winds under conditions of low power (dry atmosphere) and background noise at preferred frequencies suggests that a hybrid technique is merited which uses consensus numbers when powers are high and some other means when powers are low. This remains a topic for future research.

During the early months of operations of the McAlevy's Fort profiler, weather systems accompanied by thunderstorms caused data losses either because the Department computer system lost power or because power went out at the profiler site. A backup power supply and an automatic re-start program was soon added to the profiler system to minimize such future losses. When repeated power disruptions occur, however, many spectra may be lost and the consensus numbers of the hourly winds are reduced. When the Deparment computer "crashes" near the time scheduled for it to interrogate of the profiler for the data from the past hour, the hourly data may be lost unless an operator is present to restart the collection of that hour's data. A Department computer crash

is the likely reason for the missing hour of data in Fig. 1.2.7.

2. STATUS OF PROFILER NETWORK HARDWARE AND SOFTWARE DEVELOPMENT

The layout of the Pennsylvania State University profiler network, Fig. 1.2.1, has already been examined in Chapter 1. Three of the wind profilers operate at about 50 MHz (VHF): at site 1 -- near McAlevys Fort, PA, about 20 km south of State College (SCE on Fig. 1.2.1 denotes the town; note that the airport call letters are UNV) and at site 2 -- near Crown, northwest of Dubois (DUJ). The third wind profiler will be sited near Indiana, PA. A 405 MHz (UHF) wind profiler has been acquired and will split time between Penn State's Rock Springs experimental site (about 10 km southwest of State College) and various off-site measurement programs.

The wind profilers are located in the western portion of a region presently devoid of routine upper-air soundings. Twice-daily soundings are launched at National Weather Service (NWS) sites, the nearest of which are shown by boxes in Fig. 1.2.1. Rawinsonde facilities are available at the University, but are used only when research support is available for special projects. Remote sensing temperature and moisture profilers to complement the wind profiler network are now under construction.

The wind profiler sites were selected so that the new wind (and other derived parameter) data would fit into cross-sections between the rawinsonde sites at Pittsburgh, PA (PIT, 72520); Atlantic City, NJ (ACY, 72407); Buffalo,NY (BUF, 72528); Albany, NY (ALB, 72518); Washington, DC (IAD, 72403); and Flint, MI (FNT, 72637). These cross-section orientations are shown as dashed lines on Fig. 1.2.1.

Table 2.1 gives a chronology of the development of the Penn State profiler network in terms of the most significant hardware acquisitions.

Before the first Penn State wind profiler began operation, much effort was put into the development of analysis and display schemes. These were first tested on data obtained on tape from the Fleming, CO wind profiler of the Wave Propagation Laboratory. Some of these techniques are illustrated with Penn State data in the sections that follow. Among the schemes developed are:

- Power spectra displays
- Tabulations of wind components, returned power, consensus statistics
- Displays of u and v component vertical profiles
- Time-height section displays of u, v, velocity vectors, wind speed, wind direction, returned power
- Time series displays of u, v, wind speed, wind direction at a selected level
- Tabulations of vertical wind shear and layer-mean component normal to the shear vector
- Tabulations and profile displays of temperature gradient, temperature advection, lapse rate gradient, and lapse rate advection
- Hodograph displays

The software listed in Table 2.2 has been developed for computing and displaying profiler winds and derived quantities. The meteorological and mathematical bases for these parameters are presented in Chapter 3.

The wind profilers have been designed to provide data essentially automatically from each site. The wind profiler data are pre-processed by Eclipse minicomputers at each site, and fed via telephone line to the Digital Equipment Corporation VAX Cluster computer system at the Department of Meteorology. There the data can be displayed in various formats, such as time-height sections

and hodographs. The data can also be meshed with other meteoro-logical data such as surface data, upper-air data, and National Meteorological Center (NMC) forecast data in various displays, such as cross-sections, constant-pressure analyses, and isentropic analyses.

As will be discussed in chapter 3, there are additional quantities that can be computed and displayed from single and multiple-profiler measurements. Software to compute and display most of these has been developed.

TABLE 2.1

CHRONOLOGY OF MAJOR HARDWARE ACQUISITIONS
IN THE PENN STATE PROFILER NETWORK

Hardware Acquisition/Event	Date
Work Begins at Penn State	Oct 1982
Antennae Acquired for McAlevy's Fort VHF	July 1984
Transmitter and Receiver Borrowed for McAlevy's Fort	Sept 1984
Test Data Collection with Borrowed Equipment	Sept 1984
Return of Borrowed Equipment	Nov 1984
Acquisition of Penn State Transmitter and Receiver	June 1985
McAlevy's Fort VHF begins test operation	June 1985
McAlevy's Fort VHF begins routine operation	1 July 1985
Backup power supply installed at McAlevy's Fort	4 Oct 1985
Acquisition of antenna for Crown VHF site	July 1984
Acquisition of transmitter/receiver of Crown site	Apr 1986
Crown site begins test data collection	Apr 1986
Crown site begins routine operation	28 May 1986
Acquisition of UHF antenna	Apr 1986
Acquisition of UHF transmitter/receiver	Apr 1986
Installation of UHF profiler at Rock Springs site	Apr 1986
UHF profiler begins testing operations	Apr 1986
UHF profiler moves to Athens Alabama	10 June 1986
Data collection in MIST/SPACE/COHMEX begins	26 June 1986

TABLE 2.2

SOFTWARE FOR COMPUTING AND DISPLAYING PROFILER WINDS

AND DERIVED QUANTITIES

Software	Functions
LASTHOUR	Generates table of data for last hour's "real-time" data
LASTDAY	Generates time-height section of wind vectors, direction isopleths for last day (25 hourly observations); generates data needed for isopleth displays of wind speed, wind direction, consensus numbers, power in time-height sections in high-resolution (low range) mode with "real-time" data
MAKE3D	Transforms any x-y grid of values of a field into a 3-dimensional display of the function value transformed to location along the z axis
XY	Interactively generates vertical profiles of the u and v wind components at individual times; hodograph for individual time; time-height sections of of wind vectors; time series of u or v at selected height levels for data in "real-time" format; options regarding smoothing, resolution
DELTEMP	Calculates single-station vertical profiles of horizontal temperature gradient, lapse rate gradient, temperature advection, lapse rate advection; generates data files that can be used to plot time-height sections of these quantities; generates table of values for selected levels for data in "real-time" format
STATRITE	Generates temporal-mean profiles of u, v, single-station horizontal temperature gradient, temperature advection; calculates standard deviation (temporal) profiles and displays these as error bounds on profiles of mean values for data in "real-time" format
TSECTRITE	generates time series of temperature gradient, temperature and lapse rate advection for selected levels
PROSEC	Generates data for time-height sections of wind vectors, speed, and direction for raw, temporal mean, and perturbation winds for data in "real-time" format
WINDDATA	generates wind shear vector and component normal to the shear vector for data in CO format
NETWORK	generates data for time-height sections and time series at selected levels of divergence and vorticity; time-height sections of vector velocity, wind speed and direction and perturbation wind for profiler triangles with CO data format

3.   KINEMATIC, DYNAMIC, AND THERMODYNAMIC BASES FOR SINGLE AND
MULTIPLE PROFILER COMPUTATIONS OF METEOROLOGICAL PARAMETERS

3.1   Single Station Time Series; Time-Height Sections; Pattern
Recognition

Meteorologists are used to looking at "synoptic" (i.e., si-

multaneous) maps and cross-sections. Because the most comprehen-

sive way of looking at single wind profiler data is in a time-

height section, some familiarization with the appearance of com-

mon meteorological phenomena in this mode of presentation may be

necessary.

Since most weather systems travel across the countryside

with some component of movement from the west, time-height sec-

tions can be made to resemble west-east cross sections by revers-

ing the normal time axis, such that time increases to the left.

In this manner of display, the leading portions of a weather

system (i.e., those observed first) are displayed on the left

side of the time-height section, and the rear portions (observed

later) are displayed on the left side of the time-height section.

Figures shown in this manuscript follow this convention, and usu-

ally encompass a period of 24 hours.

Temporal changes of the wind, of course, can arise due to

local processes that do not move. However, the temporal changes

due to the movement of large-scale and mesoscale weather systems

can readily be identified in profiler time-height sections.   This

section reviews the temporal evolution of winds within large-

scale cyclones and anticyclones, and frontal zones.   These fea-

tures are assumed to be measured at altitudes above the friction

layer, such that winds are nearly in gradient balance.

The temporal changes that occur during the passage of cyclones and anticyclones are different in various sections of these systems. In particular, winds back (turn counterclockwise as time progresses) when a cyclone center is passing to the left (as the observer faces toward the approaching cyclone) of the observation point. Winds veer (turn clockwise as time progresses) when a cyclone center is passing to the right (facing toward the approaching cyclone) of the observation point. Figure 3.1.1 illustrates this concept for cyclones moving from the N, S, E, and W. It should be noted that a cyclone passing directly overhead may be associated with a rather abrupt change of wind direction, rather than a prolonged period of veering or backing.

Fig. 3.1.1 also illustrates the evolution of winds during the passage of an anticyclone. Like the cyclone, winds back when the anticyclone center is passing south of the observation point, and veer when the anticyclone center is passing north of the observation point.

Table 3.1 summarizes the changes of wind direction that might be seen in watching the wind evolution at a particular level on a profiler time-height section. It can be seen that there is some ambiguity in the cause of the changes (i.e., whether due to a cyclone or anticyclone), if only the winds at that level as input to the decision. For example, a wind veering through a southerly direction could arise either at a location west of an anticyclone moving toward the south or at a location east of a cyclone moving toward the north. This ambiguity can normally be resolved by looking at the direction of the mid-
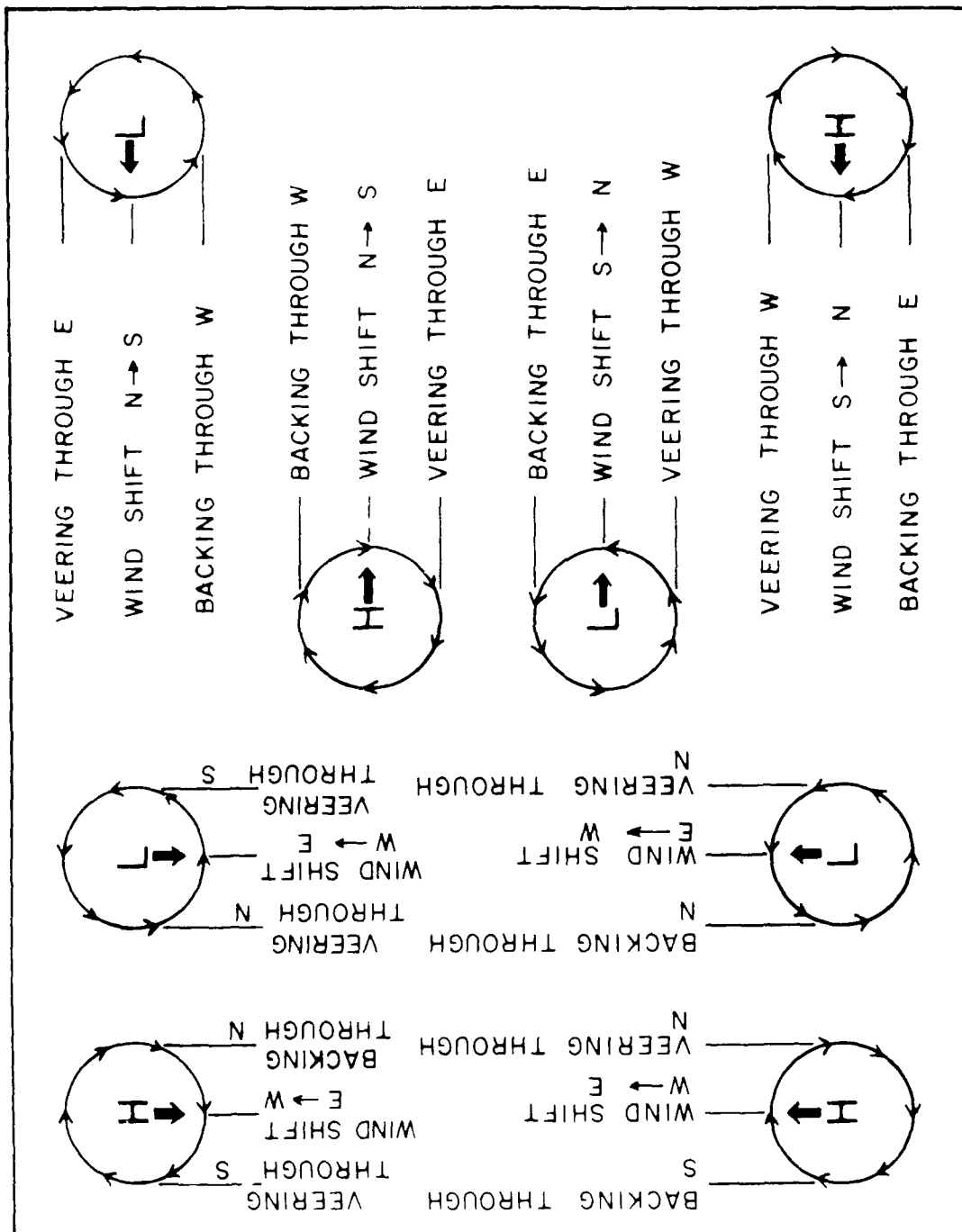
Figure 3.1.1. Schematic diagram of the evolution of the winds during passage of cyclones and anticyclones from different directions of movement.

	through N	through S	through E	through W
veering	west of L moving S — (east of H moving N)	west of H moving S — east of L moving N	north of H moving E — (north of L moving W)	south of L moving E — (north of H moving W)
backing	east of H moving S — west of L moving N	east of L moving S — (west of H moving N)	north of L moving E — (south of H moving W)	north of H moving E — (south of L moving W)
	ending N	ending S	ending E	ending W
~ 180 degree windshift	L moving E — (H moving W)	H moving E — (L moving W)	L moving S — (H moving N)	H moving S — L moving N

Table 3.1.   Temporal changes of wind at a level above the friction layer due to the passage of a low pressure or high pressure system.   Backing signifies a counterclockwise shift of direction; veering signifies, a clockwise shift.

tropospheric winds (or at the mean mid-tropospheric winds), and recognizing that large-scale weather systems tend to be steered with the mid-tropospheric or mean-tropospheric winds. If the mean mid-tropospheric winds were determined to be from the south, then in the example above the observed wind direction changes would have been due to a northward-moving cyclone passing west of the observation site. Other additional clues can include the veering or backing of winds with height, which give a measure of the sign of the temperature advection.

Figure 3.1.2 illustrates a typical large-scale weather situation involving the retreat of an anticyclone, and the approach and passage of a front and cyclone. It can be seen that the frontal zone, associated with a pressure trough, is characterized by a cycloneic wind shift. Subtle anticyclonic ridging in some areas on the periphery of the cyclone can cause temporal wind shifts characteristic of an anticyclone retreating or advancing. This more complicated situation, typical of the real environment, suggests that a coherent picture of the large-scale weather situation can only be obtained after carefully examining several contiguous levels of a profiler time-height section, and considering the secondary clues mentioned in the preceding paragraph.

3.2 Single-Station Calculations

A single VHF or UHF Doppler wind profiler measures:

$$u \; , \; \frac{\partial u}{\partial z} \; , \; \frac{\partial u}{\partial t} \qquad ;$$

$$v \; , \; \frac{\partial v}{\partial z} \; , \; \frac{\partial v}{\partial t} \qquad ;$$
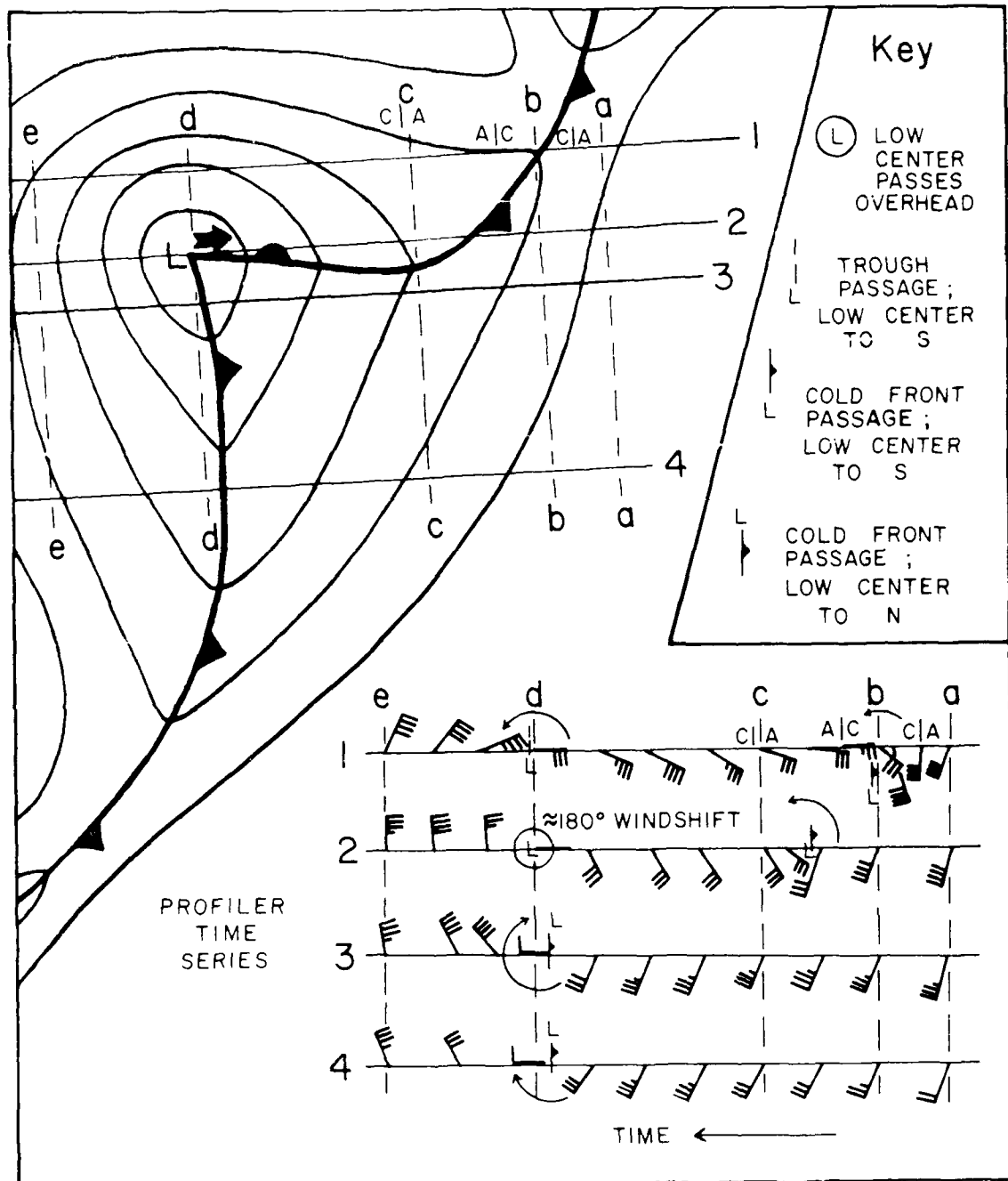
Figure 3.1.2. Schematic diagram of the evolution of winds at several locations within a travelling weather system. The letter "L" signifies the cyclone center. The broad arrow near the cyclone indicates the direction of its movement. The symbol C/A indicates a point (time) of transition from anticyclonic to cyclonic isobar curvature along transect 1.

$$w \ , \ \frac{\partial w}{\partial z} \ , \ \frac{\partial w}{\partial t}$$

If w can be measured with sufficient accuracy, then it may be possible to get a meaningful value for $\frac{\partial w}{\partial z}$ which, when used in combination with the equation of continuity for an incompressible fluid gives the horizontal divergence,

$$\frac{\partial u}{\partial x} + \frac{\partial v}{\partial y} = - \frac{\partial w}{\partial z} \qquad . \qquad (3.1)$$

The vertical wind shear vectors are composed of geostrophic and ageostrophic components. Wheareas the observed winds at an individual level possess considerable ageostrophic components, the vertical shear of the wind does not typically depart as significantly from the geostrophic shear. This is due in part to the fact that there is a fair amount of "coupling" between levels, especially where the lapse rates are conditionally unstable, and mixing is taking place. In addition, many of the processes that induce ageostrophic wind components (such as jet streaks) affect an appreciable portion of the troposphere; hence adjacent profiler wind levels tend to have rather similar ageostrophic velocities.

Subject to the validity of the assumption that the measured vertical wind shear vector is a good approximation to the vertical shear of the geostrophic velocity, then it is possible to estimate several thermodynamic parameters from single-station measurements of vertical wind shear. The thermal wind relationship is

$$\frac{\partial \bar{T}}{\partial y} = - \frac{f \bar{T}}{g} \frac{\partial u_g}{\partial z} - \frac{\gamma f}{g} \bar{u}_g \qquad ,$$

$$\frac{\partial \bar{T}}{\partial x} = - \frac{f \bar{T}}{g} \frac{\partial v_g}{\partial z} + \frac{\gamma f}{g} \bar{v}_g \qquad . \qquad (3.2)$$

The second terms on the right-hand side of (3.2) are typically rather small; when neglected, equations (3.2) become the thermal wind equations. In (3.2), all temperatures are virtual temperatures in degrees Kelvin, and γ is the lapse rate of virtual temperature,

$$\gamma = -\frac{\partial \overline{T}}{\partial z} \qquad (3.3)$$

When (3.2) is differentiated in the vertical, profiler winds can be used to estimate horizontal gradients of virtual temperature lapse rate. The two components are

$$\frac{\partial \gamma}{\partial x} = -\frac{\partial}{\partial z}\left(\frac{\partial \overline{T}}{\partial x}\right) \quad ; \quad \frac{\partial \gamma}{\partial y} = -\frac{\partial}{\partial z}\left(\frac{\partial \overline{T}}{\partial y}\right) \qquad (3.4)$$

When the horizontal temperature gradient derived from the vertical wind shear in a layer is used in conjunction with the mean winds in that layer, then the average horizontal temperature advection for the layer can be computed as

$$\text{Adv} \ (T) = -\overline{V}\cdot\nabla T = -u\frac{\partial T}{\partial x} - v\frac{\partial T}{\partial y} \qquad (3.5)$$

Figure 3.2.1 illustrates graphically the mathematical concept of using profiler winds at two levels to estimate horizontal temperature advection in a layer.

When the profiler-derived lapse rate gradient is utilized with the mean wind through the two adjacent layers used to calculate the lapse rate gradient, then the lapse rate advection by the mean wind is

$$\text{Adv} \ (\gamma) = -\overline{V}\cdot\nabla\gamma = -u\frac{\partial \gamma}{\partial x} - v\frac{\partial \gamma}{\partial y} \qquad (3.6)$$
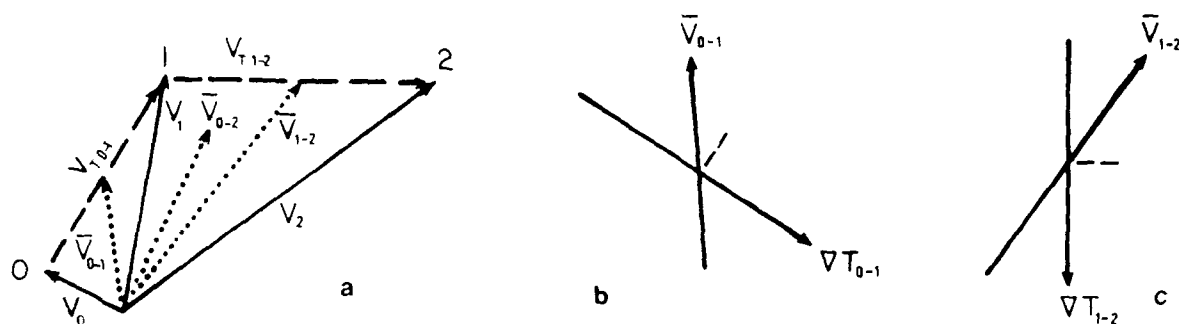
Figure 3.2.1. Derivation of temperature gradient and temperature advection from measurements of near-geostrophic winds at three levels: 0 (lowest), 1, and 2 (highest).

    a. Hodograph, showing wind vectors at the three levels (solid), shear vectors (or, thermal wind vectors) between levels (dashed), and the mean wind vectors in the layers 0-1, 1-2, and 0-2 (dotted).

    b. Determination of the temperature advection in layer 0-1.

    c. Determination of the temperature advection in layer 1-2.
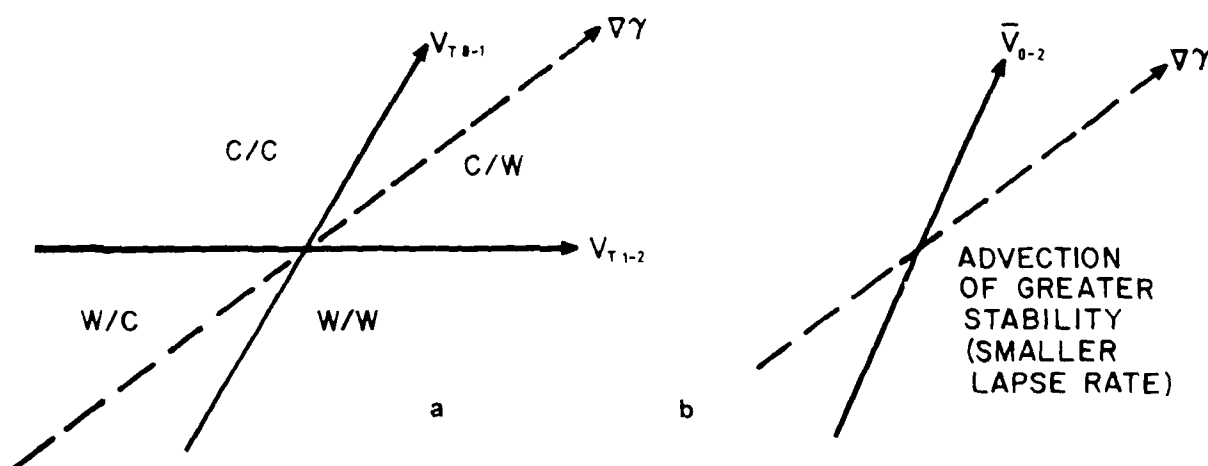
Figure 3.2.2. Derivation of lapse rate gradient and lapse rate advection from measurements of near-geostrophic shear vectors in the two layers of Figure 3.2.1.

    a. Determination of the lapse rate gradient from the thermal winds in two layers. The two intersecting thermal winds generate 4 quadrants, with respect to the point of intersection. In this case, the quadrant north and east of the intersection has colder air in layer 1-2 and warmer air in layer 0-1 than at the intersection and, therefore, has largest lapse rates. The lapse rate gradient is dashed.

    b. Determination of lapse rate advection from the lapse rate gradient and the mean wind in layer 0-2.

Figure 3.2.2 illustrates graphically the concept of computing advection of lapse rate from profiler winds measured at three levels.

The quantitative accuracy of the single-profiler-derived estimates of the horizontal gradients of temperature and lapse rate and advections of temperature and lapse rate are, clearly, only as good as the assumption that the measured vertical wind shear is equal to the vertical shear of the geostrophic wind. Qualitatively, however, the computed values of these thermodynamic quantities—and especially their patterns on time sections —appear to have diagnostic and prognostic value. Examples of time sections of these parameters will be shown in Chapter 5. A more thorough quantitative examination of these parameters is being completed as part of the M.S. Thesis of Paul Neiman (1987).

The existence of horizontal temperature gradients and horizontal lapse rate gradients does not necessarily imply that temperature and lapse rate will change at the profiler site. Horizontal advections can be offset by vertical advections and adiabatic cooling and either offset or augmented by diabatic processes. However, the isotherm and lapse rate patterns tend to move from one region to another in a state of fairly slow evolution, accompanying the propagation of an atmospheric wave or mesoscale weather system. That is,

$$\frac{\partial T}{\partial t} = -C_x \frac{\partial T}{\partial x} - C_y \frac{\partial T}{\partial y} \qquad , \qquad (3.7)$$

where C_x and C_y are the components of the velocity of movement in the x and y directions, respectively.

The velocity of movement of these systems can probably be

estimated best using radar or satellite imagery. In the absence
of this indepedent type of data, it would be desirable to be able
to use profiler-derived winds to estimate the velocity of move-
ment of the weather systems and their associated temperature pat-
terns and weather. The velocity of movement of the phenomena can
be quite different from the wind velocity at any particular lev-
el. The systems, however, tend to move more nearly with the mean
velocity obtained by averaging vertically through the depth of
the weather system. The mean wind tends to give a reasonable
estimate of the direction of movement of the system and an upper
bound or overestimate of the speed of the weather system, which
moves slower than the mean wind (more so as the scale of the
system increases). Thus, a vertically averaged wind may serve to
give a reasonable estimate of the velocity of movement needed in
(3.7). Frontal systems tend to move more with the component of
the wind normal to the temperature gradient in the boundary lay-
er. Thus, the front-normal winds in the lowest few gates may be
used as a first approximation to the velocity of the baroclinic
zone.

In a related matter, the winds observed by the wind profiler
are the result of the combined effects of local (stationary, ter-
rain-related) influences plus travelling disturbances of differ-
ent scales. The smaller systems tend to move as if they were
"steered" by the winds of the larger-scale system. Such winds
can be obtained by averaging not only in the vertical but also
over time.

Furthermore, the presence of a stationary velocity pattern

combined with a slowly-varying velocity pattern of large scale, tends to mask the presence of the superimposed mesoscale velocity perturbations. In order to better reveal these meteorologically significant winds, it is useful to subtract from the individual winds at a particular level the temporally averaged winds at the level. That is,

$$V' = V - \hat{V} \quad , \tag{3.8}$$

where V' is the perturbation velocity and $\hat{V}$ is the temporally averaged velocity at the same level. Examples of the utility of the perturbation field are given in Chapter 4.

3.3 Multi-Profiler Kinematic Quantities

If winds are measured by three profilers sited in a triangular arrangement, then the kinematic quantities of network-mean wind, horizontal divergence, vertical vorticity, stretching deformation, and shearing devormation can be computed. Unless additional wind data are available which suggest that variations of the winds within the triangle are non-linear, then winds at any point within the triangle can be estimated through linear interpolation between the profiler-measured winds at the three sites.

Referring to Figure 3.3.1, the wind at the centroid point 0 (x_0, y_0) can be deduced from the winds at the profiler sites: point 1 (x_1, y_1), point 2 (x_2, y_2), and point 3 (x_3, y_3). The centroid value can be determined by first deducing the coordinates of points a,b,c:

a: $([x_2 + x_3]/2, [y_2 + y_3]/2)$

b: $([x_1 + x_3]/2, [y_1 + y_3]/2)$
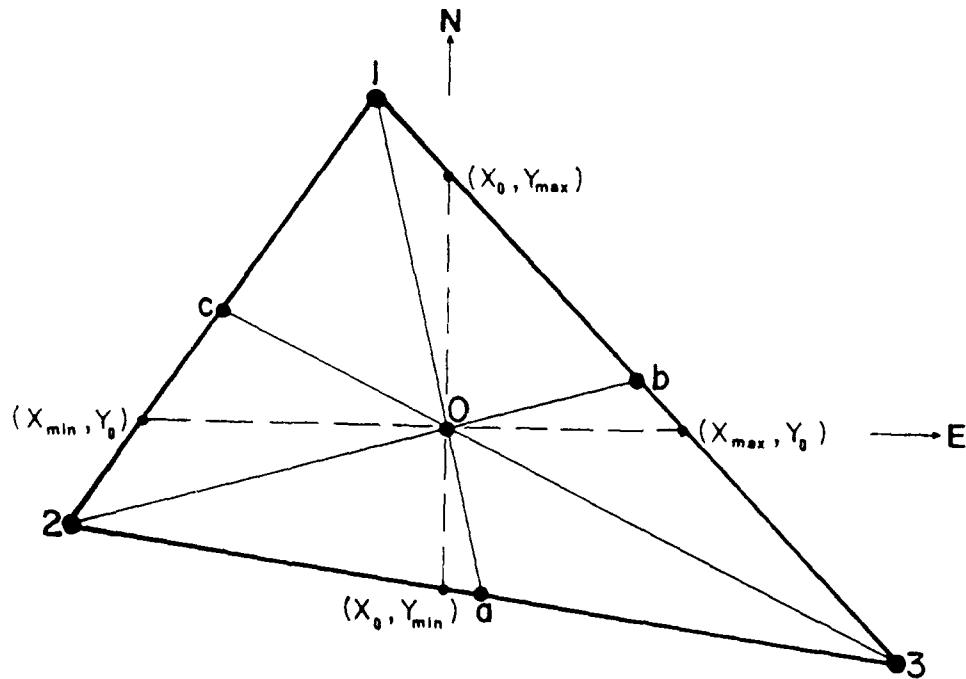
Figure 3.3.1. Schematic diagram labelling the three wind profiler locations (subscripts 1, 2, and 3), the location of the centroid of the triangle (subscript 0), points a-c needed in determining the centroid location, and points used in computing kinematic quantities (subscripts min and max).

$$c: \quad ([x_1 + x_2]/2, \ [y_1 + y_2]/2).$$

Using the generic equation for a line through point 0,

$$y - y_0 = m(x - x_0),$$ (3.9)

where m is the slope of the line. The two unknowns, coordinates x_0 and y_0, can be determined by solving a set of two equations of the form of (3.9), such as the lines connecting point 0 to points 2 and 3. In this case (3.9) takes the forms

$$y_2 - y_0 = ([y_b - y_2]/[x_b - x_2])(x_2 - x_0) \text{ for line 2-0}$$

$$y_3 - y_0 = ([y_c - y_3]/[x_c - x_3])(x_3 - x_0) \text{ for line 3-0,}$$ (3.10)

which can be solved to isolate x_0 and then used to yield y_0.

Once x_0 and y_0 are computed, then the distances to points 1, 2, and 3 can be computed and used to compute weighting factors w_1, w_2, and w_3:

$$r_{1-0} = ([x_1 - x_0]^2 + [y_1 - y_0]^2)^{1/2},$$

$$r_{2-0} = ([x_2 - x_0]^2 + [y_2 - y_0]^2)^{1/2},$$

$$r_{3-0} = ([x_3 - x_0]^2 + [y_3 - y_0]^2)^{1/2},$$ (3.11)

and $\quad w_1 = 1/r_{1-0}, \quad w_2 = 1/r_{2-0}, \quad w_3 = 1/r_{3-0}.$ (3.12)

The velocity components at the centroid, then, are

$$U_0 = (w_1 U_1 + w_2 U_2 + w_3 U_3)/(w_1 + w_2 + w_3)$$

$$V_0 = (w_1 V_1 + w_2 V_2 + w_3 V_3)/(w1 + w2 + w3).$$ (3.13)

The kinematic quantities of divergence, vorticity and deformation are dependent upon the horizontal derivatives of the wind components. In order to compute the gradients it is necessary to compute the coordinates of points along the periphery of the triangle (x_{min}, y_0), (x_{max}, y_0), (x_0, y_{min}), and (x_0, y_{max}).

This is done by solving equations of the form (referring to Fig. 3.3.1)

$$y_{max} = ([y_1 - y_2]/[x_1 - x_2])(x_0 - x_2) + y_2 ,$$

$$y_{min} = ([y_3 - y_2]/[x_3 - x_2])(x_0 - x_2) + y_2 ,$$

$$x_{max} = ([x_3 - x_1]/[y_3 - y_1])(y_0 - y_1) + x_1 ,$$

$$x_{min} = ([x_1 - x_2]/[y_1 - y_2])(x_0 - x_2) + x_2 . \tag{3.14}$$

Thereafter, the gradient values can be computed using weighted mean values in a manner similar to that for computing the mean value at the centroid (3.13), except that velocity components at the four points (x_{max}, y_0), (x_{min}, y_0), (x_0, y_{max}), (x_0, y_{min}) are desired.

Horizontal divergence: $\dfrac{\partial u}{\partial x} + \dfrac{\partial v}{\partial y}$

Vertical vorticity: $\zeta \approx \dfrac{\partial v}{\partial x} - \dfrac{\partial u}{\partial y}$

Stretching deformation: $\dfrac{\partial u}{\partial x} - \dfrac{\partial v}{\partial y}$

Shearing deformation: $\dfrac{\partial v}{\partial x} + \dfrac{\partial u}{\partial y}$ (15)

Mathematically, there are alternative techniques for computing divergence and vorticity. Using Stokes' theorem, the vorticity is the line integral of the tangential wind component divided by the area of the triangle:

$$\zeta = \int \frac{\vec{V} \cdot d\vec{l}}{A} = \frac{\sum^i \vec{V_i} \cos\theta_i \, l_i}{A} \tag{16}$$

where A is the area of the profiler triangle, $d\vec{l}$ is a unit vector along one of the sides of the triangle in a counter clockwise orientation, the subscript i indicates one of three sides, $\vec{V}$ is the vector velocity, l is the length of a side of

the triangle, θ is the angle between the wind and the side of the triangle, and $\bar{V}_i$ is the mean wind speed along the side of the triangle.

By Gauss' theorem, the horizontal divergence is the line integral of the normal wind component divided by the area of the triangle:

$$\text{Div} = \int \frac{\vec{V} \cdot \vec{n} \, dl}{A} = \frac{\overset{i}{\sum} V_i \cos\phi_i l_i}{A} \qquad , \qquad (3.17)$$

where $\vec{n}$ is a unit vector directed outward away from the centroid of the triangle, ϕ_i is the angle between the wind along the side and the unit vector, and the other symbols are as defined above.

If the atmosphere is assumed to be incompressible, then it is possible to use the three horizontal velocities, and in particular the calculated divergence, to deduce the triangle-mean vertical velocity. This makes use of the equation of continuity,

$$-\frac{\partial w}{\partial z} = \frac{\partial u}{\partial x} + \frac{\partial v}{\partial y} \qquad (3.18)$$

and yields
$$w(z) = -\int \text{Div}(z) \, dz + W(z_0) \quad . \qquad (3.19)$$

The boundary value $W(z0)$ is normally set equal to zero unless there is a horizontal wind blowing over sloping terrain, in which case
$$W(z_0) = \bar{V} \cdot \nabla h \quad , \qquad (3.20)$$
where ∇h is the horizontal gradient of the terrain elevation.

3.4 Profiler Dynamic Quantities

If friction and turbulence are neglected, it is possible to use velocities measured at three points of a profiler triangle to compute geostrophic and ageostrophic velocity components, horizontal geopotential gradients, and radius of flow curvature.

With the radius of curvature known, it then becomes possible to also discern whether the flow is ir gradient balance.

The radius of curvature of the flow is a direct byproduct of the vorticity computation. In natural coordinates, the relative vorticity can be written

$$\zeta = \frac{V}{R} + \frac{\partial V}{\partial n} \qquad , \qquad (3.21)$$

where V is the tangential component of the wind, n is directed outward along a radial, and R is the radius of curvature. From the profiler winds,

$$R = \bar{V} \left(\zeta - \frac{\partial V}{\partial n} \right)^{-1} \qquad , \qquad (3.22)$$

where $\bar{V}$ is the mean or centroid value of wind speed measured by the profilers and the positive n direction is directed 90o to the right (clockwise) from the mean direction. This requires a gradient calculation along an orientation somewhat different from the that used for the kinematic quantities in (3.17).

The equations of horizontal momentum, neglecting viscosity, diffusion, and turbulence, are

$$\frac{dv}{dt} = -fu_{ag} \quad ; \quad \frac{du}{dt} = fv_{ag} \qquad , \qquad (3.23)$$

where f is the Coriolis parameter and the subscript ag indicates the ageostrophic wind component. These forms of the momentum equations, in Lagrangian form, can be rewritten in Eulerian coordinates and rearranged to give

$$\bar{u}_{ag} = -f^{-1} \left(\frac{\partial \bar{v}}{\partial t} + \bar{u}\frac{\partial v}{\partial x} + \bar{v}\frac{\partial v}{\partial y} + \bar{w}\frac{\partial \bar{v}}{\partial z} \right)$$

$$\bar{v}_{ag} = f^{-1} \left(\frac{\partial \bar{u}}{\partial t} + \bar{u}\frac{\partial u}{\partial x} + \bar{v}\frac{\partial u}{\partial y} + \bar{w}\frac{\partial \bar{u}}{\partial z} \right)$$

$$(3.24)$$

Thus, a combination of the tendency of the triangle-mean velocity and the instantaneous mean velocity components and their gradients allows for the determination of the ageostrophic velocity. The geostrophic velocity is then deduced from

$$\bar{U}_g = \bar{U} - \bar{U}_{ag} \quad ; \quad \bar{V}_g = \bar{V} - \bar{V}_{ag} \quad . \qquad (3.25)$$

Accordingly, the horizontal gradients of geopotential can be deduced:

$$\frac{\partial h}{\partial x} = \frac{f}{g}\bar{v}_g \quad ; \quad \frac{\partial h}{\partial y} = -\frac{f}{g}\bar{u}_g \qquad . \qquad (3.26)$$

In these equations, h represents the geopotential height of the pressure surface intersecting the centroid at level z.

Studies of the profiler-triangle-derived kinematic and dynamic quantities discussed above have been performed by Cathy Carlson (1987) as part of her M.S. Thesis.

3.5 Multi-Profiler Thermodynamic Quantities

By taking the vertical derivatives of the formula for the geostrophic wind,

$$Ug = -(\rho f)^{-1}\frac{\partial p}{\partial x} \quad ; \quad Vg = (\rho f)^{-1}\frac{\partial p}{\partial y} \quad , \qquad (3.27)$$

it is possible to derive formulae for computing horizontal gradients of virtual temperature based primarily upon profiler wind measurements. These have the form

$$\frac{\partial \bar{T}}{\partial y} = \frac{f\bar{T}}{g}\frac{\partial \bar{u}_g}{\partial z} - \frac{\gamma f}{g}\bar{u}_g$$

$$\frac{\partial \bar{T}}{\partial x} = -\frac{f\bar{T}}{g}\frac{\partial \bar{v}_g}{\partial z} + \frac{\gamma f}{g}\bar{v}_g$$

$$\qquad . \qquad (3.28)$$

The second terms on the right-hand side of (3.28) are typically rather small; when neglected equations (3.28) become the thermal wind equations. In (3.28), all temperatures are virtual temperatures in degrees Kelvin, and γ is the lapse rate of virtual temperature,

$$\gamma = - \frac{\partial \bar{T}}{\partial z} \quad . \tag{3.29}$$

In practice, the values of temperature and lapse rate may not be available with the same temporal frequency as the profiler winds. Since the temperature is in degrees Kelvin, small temperature approximation errors will contribute only on order of 1% error in temperature gradient. Since the second term is negligible, typically only about 1% of the first term, the calculation of horizontal temperature gradient is not very sensitive to the accuracy of the values of T and γ used in the equations. Hence, some approximation of these quantities from large-scale observations and forecasts will suffice.

When (3.28) is differentiated in the vertical, profiler winds can be used to deduce horizontal gradients of virtual temperature lapse rate. That is,

$$\frac{\partial}{\partial x} = - \frac{\partial}{\partial z} \left(\frac{\partial \bar{T}}{\partial x} \right) \quad ; \quad \frac{\partial}{\partial y} = - \frac{\partial}{\partial z} \left(\frac{\partial \bar{T}}{\partial y} \right) \quad . \tag{3.30}$$

These gradients of lapse rate pertain to the center of the vertical layer and to the centroid of the triangle.

3.6 Blending Profiler Data Into the Synoptic-Scale Data Set

Thus far, the thermodynamic parameters derived from the profiler winds have been gradient quantities and advections. If surrounding National Weather Service rawinsonde measurements are available, however, then it is possible to blend in the profiler-derived horizontal temperature gradients with the peripheral temperatures to deduce the temperature at and in the near proximity of the profiler site. The fundamental aspects of a simple blending scheme are presented below.

The blended analysis is subject to two key constraints. The first constraint is that the profiler-derived temperature gradient data are only approximations of the real temperature gradients, since the vertical wind shears may not be fully in thermal wind balance. This suggests that there is no reason to absolutely preserve the magnitudes of the profiler-derived temperature gradients during the blending.

A second constraint is that the profiler data pertain to a limited sampling area, and perhaps a localized weather pattern or mesoscale weather system that cannot be detected with the rawinsonde network. In either event, the true horizontal scales (i.e., the length scales in two orthogonal horizontal dimensions) of the feature being observed cannot necessarily be known from the profiler data alone, even through time-space conversion. This type of weather system, then, is more appropriately studied through single or multiple-profiler data sets, or during special measurement programs when denser meteorological measurements are

available.   The blended   analysis is not of great value in these cases.   The blended analysis is probably of   greatest impact when dealing   with   travelling   sub-synoptic-scale or   meso-alpha-scale disturbances.   The analysis   of features   such as   baroclinic and frontal zones,   jet streams   and streaks,   and short-wave troughs and ridges can be greatly improved through the   blending process, especially if   a modest   amount of   time-space conversion is used with the profiler data.   A more refined position and amplitude of these features   can be   obtained through use of profiler data, as will be illustrated in the examples in Chapters 4 and 5.

The philosophy of   the   blending   scheme   chosen, consistent with   the   two   constraints   above,   is that the blended analysis should strive to improve the analysis of the   location of fronts, and should yield gradient zones with horizontal scale about equal to the distance between the profiler   and the   nearest rawinsonde site.

At   this   juncture,   the   blending scheme has not been fully implemented as   a numerical,   objective procedure.   Instead, the

meteorologist   uses   profiler-derived temperature gradient infor-mation, together with grid-point temperature values from an anal-ysis using   only rawinsonde   data, to determine where to manually enter a "bogus" temperature value and the value to use.   The term "bogus" is used in the same sense as in numerical weather predic-tion, meaning a subjectively introduced value   used to   refine an initial analysis,   based upon   meteorological judgement and prob-ably with   the   aid   of   some   independent   non-conventional data source.

The concepts of the procedure are as follows, and as illustrated in Figure 3.6.1. The profiler temperature gradient data is assumed to pertain to a length scale $d = C T$, where C is the approximate speed of movement of the synoptic-scale weather system, frontal zone, etc., affecting the profiler, as deduced from observed data or from prognoses. T is the averaging period (sampling period) of the profiler data, which is one hour in most cases used in this report. Another scale, D, represents the distance from the profiler observation (which may not be the same as from the profiler site when time-space conversion is being used) to the nearest rawinsonde site. The grid point data are used to interpolate 5 temperatures: one at the profiler location and 4 others at a distance $D + d/2$ from the profiler along the positive and negative x and y (E and N) directions.

Next, the sign and magnitude of the profiler-derived temperature gradient (m_3) is compared to the grid-point-analysis gradients (m_1 and m_2) on either side of the profiler observation point. (Using the convention of Fig. 3.6.1, slope m_1 represents the region west or south of the profiler observation.) If m_3 is closest to m_1, then the "bogus" temperature is inserted at a location a distance d/2 to the north or east of the profiler observation location. The value of the inserted temperature, T', is

$$T' = T_1 + m_1 * D + m_3 * d \quad . \tag{3.30}$$

If m_3 is more comparable to m_2, then the temperature is inserted at a distance d/2 to the south or west of the profiler observation location. The value of the inserted temperature, T',
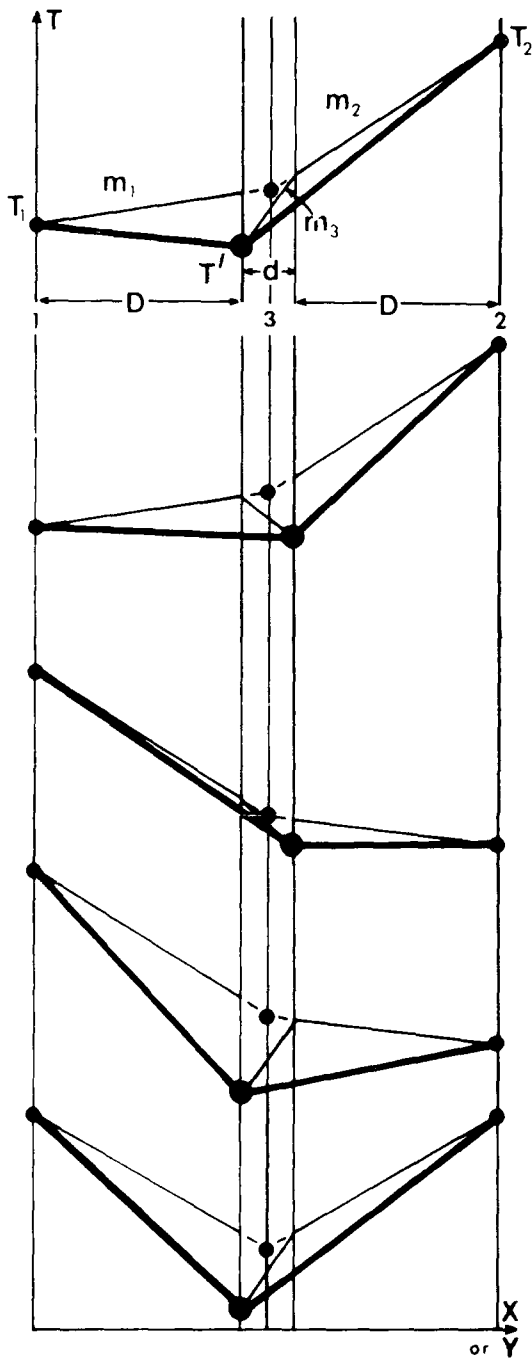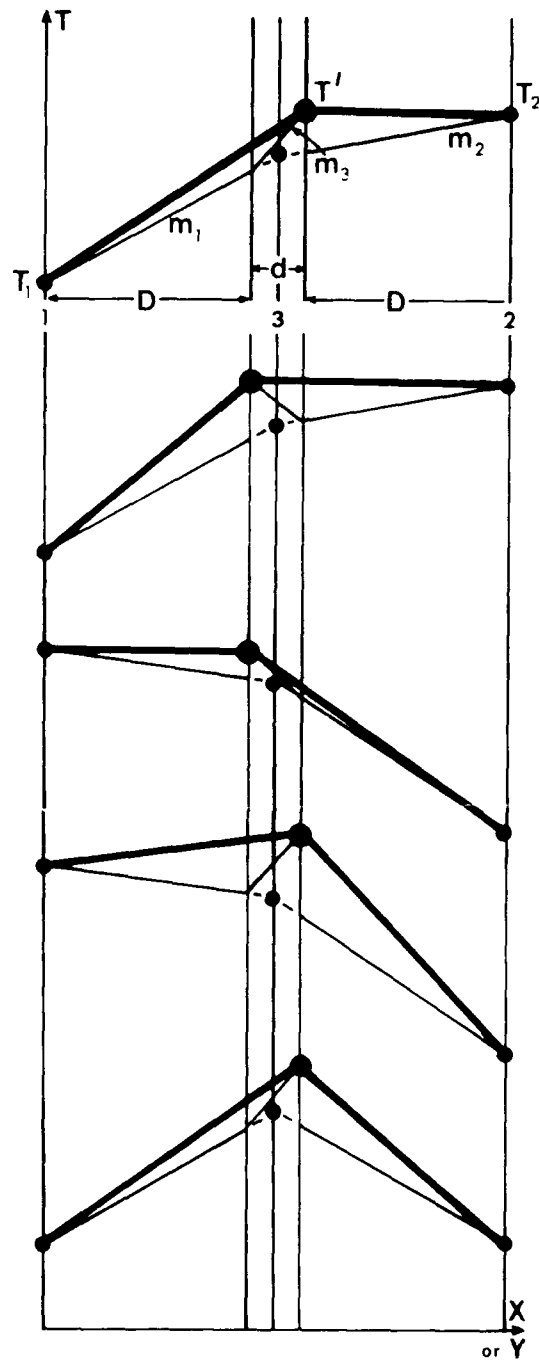
Figure 3.6.1. Schematic diagram of a simple scheme for blending profiler-derived temperature gradient information into synoptic-scale analyses. Y-axis represents temperature and x-axis represents distance east or north. Profiler is at point 3, and has yielded gradient shown by slope m3 on the diagram. The profiler averaging period conforms to a distance d, while the distance to the nearest rawinsonde site is D. Data at points 1 and 2 are obtained from an analysis of the rawinsonde data. The blended analysis is represented by heavy lines, after insertion of temperature data at the point shown by the large dot.

is

$$T' = T_2 - m_2*D - m_3*d \quad . \tag{3.31}$$

As can be seen in Fig. 3.6.1, the resultant blended analysis preserves the integrated temperature difference across the influence distance d, but diffuses the gradient over distances $D + d/2$ or $D - d/2$. However, in each instance it increases the value of the Laplacian of temperature, thereby increasing the sharpness of the baroclinic zone and rendering it more front-like. Except when the synoptic-scale gradient is quite large, the scheme has also preserved the sense of the temperature gradient over the profiler, and merely displaced the maximum or minimum Laplacian to one side or the other.

In the event that m_1 and m_2 are equal (not shown in the Figure); the absolute value of m_3 is greater than m_1, then the temperature is inserted at a distance $d/2$ in a direction toward the warmer temperature side of m_3. If the absolute value of m_3 is less than m_1, then the temperature is inserted at a distance $d/2$ toward the cold temperature side of m_3.

Figure 3.6.1 illustrates the meteorologically most interesting situations, in which the synoptic-scale Laplacian of temperature is either a positive or negative maximum near the profiler observation. When the Laplacian is negative (profiler relatively warm), the profiler is located near the warm side of the frontal zone (which is normally referred to as a front). When the Laplacian is positive (profiler relatively cold), the profiler is located near the cold (rear) side of a distinct frontal zone. In this context, it can be seen that the blending

scheme sharpens the frontal zone and forces it to one side of the profiler or the other, based upon the wind profiler-derived temperature gradient.

Other blending schemes, of course, could be derived. However, further examination of this topic will be postponed, pending field experiments yielding mesoscale data with which the profiler-derived gradients could be assessed.

A real-case test of the blending scheme was performed using wind profiler data from Fleming, Colorado (see Figure 3.6.2), from 0000 UTC 25 November 1984. This case is examined thoroughly in Chapter 5. In this section we shall concentrate merely upon the 500 mb analysis.

Figure 3.6.3 illustrates the objective analysis of rawinsonde data prior to inclusion of profiler-derived temperature information. Figure 3.6.4 shows the analysis after use of the blending scheme described above. It can be seen that the location of the warm tongue has been shifted eastward, and has become slightly warmer. Figure 3.6.5 shows the difference in the analyses resulting from inclusion of profiler-derived temperature gradient information. As expected, most of the change was confined to the immediate vicinity of the bogused temperature location. It will be seen in Section 5.1 that this was a sharp front, so that the refined analysis was an improvement. Additional case studies, however, are needed before the utility of the scheme can be generalized.
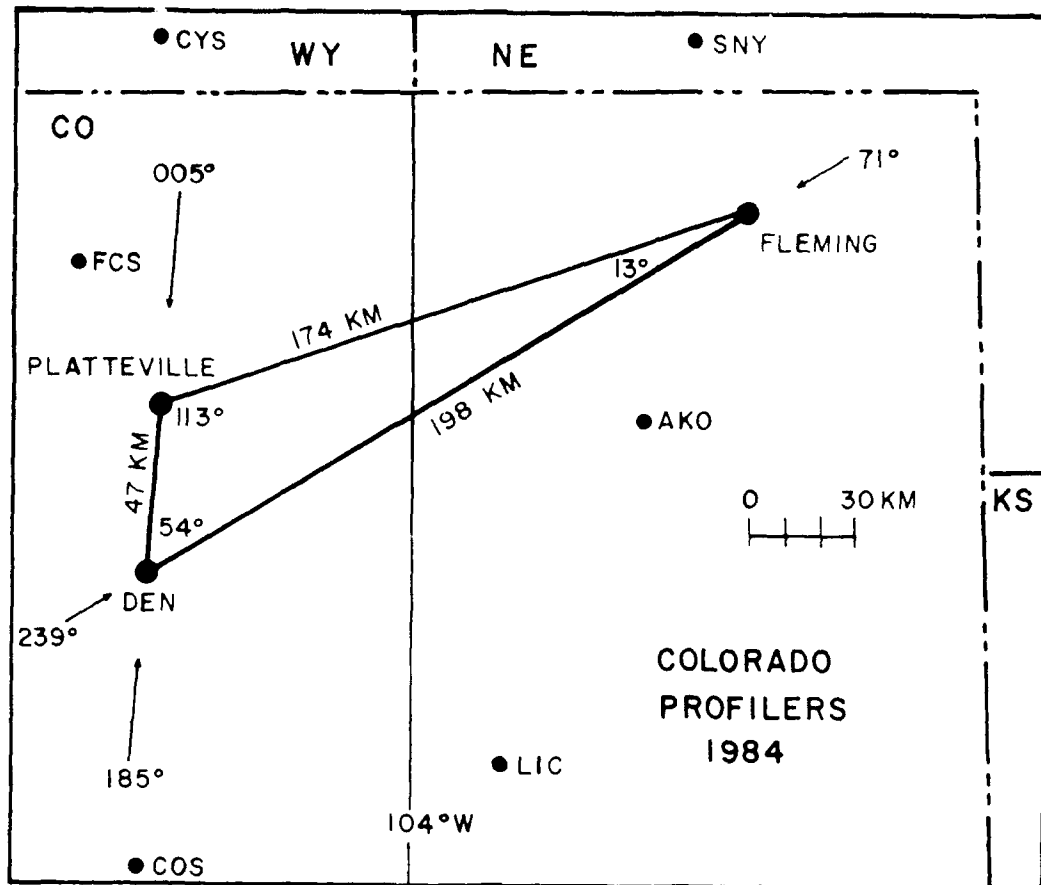
Figure 3.6.2. Configuration of the Colorado profiler triangular network during 1984. Small dots indicate surface observing sites. Data from the Fleming site are used in Chapters 3, 4 and 5.
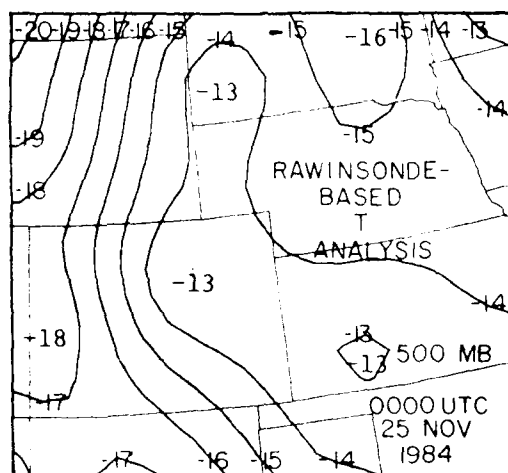
Figure 3.6.3. Rawinsonde-based analysis of 500 mb temperatures (°C) at 0000 UTC on 25 November 1984.
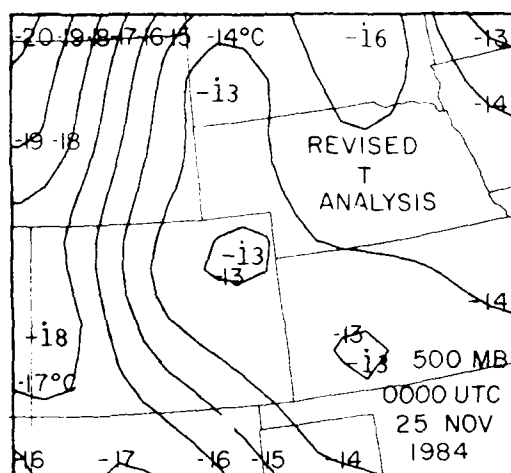
Figure 3.6.4. Revised 500 mb temperature analysis (°C) after blending profiler-derived temperature gradient information with the temperature analysis of Fig. 3.6.3, for 0000 UTC on 25 November 1984.
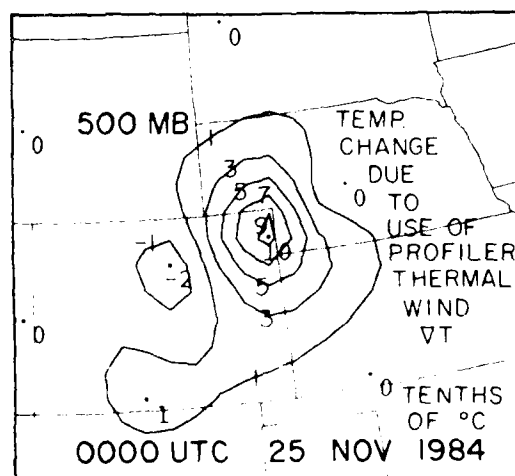
Figure 3.6.5. Change of analyzed 500 mb temperature induced by inclusion of profiler-derived temperature gradient information, for 0000 UTC on 25 November 1984, in tenths of degrees Celsius.

3.7   Accuracy of Profiler Winds

The accuracy of profiler-measured winds has been the subject of a number of past investigations (see Kessler et. al, 1985, for a summary). Vincent (1986) reports that the root-mean-square (rms) error of wind profiler velocities is widely considered to be 3-5 m/s. However, Strauch (1986) indicates that the rms difference between Colorado profiler winds and rawinsondes is about 2-3 m/s. This is in general agreement with values obtained by Lawrence et. al (1986). However, Hoehne (1980) reports that the rms error between two rawinsondes is 3.1 m/s. The rawinsondes, therefore, are thought to contribute errors to the profiler-rawinsonde difference, and the profiler winds themselves are thought to have an rms error of about 1 m/s.

3.7.1   Accuracy Studies

Since previous studies had generally established that profiler winds were accurate, this type of study was not given top priority. Furthermore, such comparisons are difficult to perform in a valid way. While the profiler scans the volume of air drifting across the beam over a certain period of integration, most other means of measuring atmospheric thermodynamic variables --primarily the rawinsonde--sample smaller volumes of air for shorter times as they ascend and drift with the wind. Even if attempts are made to launch a rawinsonde into one or more of the profiler beams, the intersection of the rawinsonde path with the profiler beam is likely to be only a shallow layer. In the

presence of turbulence or other microscale, possibly orographically related, variations in the wind, it is not fair to assign any rawinsonde-profiler differences as errors in profiler winds. Thus, no special wind observations were taken at Penn State during the course of the period of research funded by this contract. However, Williams and Thomson (1986) did identify a potential source of bias in wind speed measurements at low velocities.

Subsequent sections invoke meteorological knowledge of weather systems, inspect analyzed fields where wind profiler data has been blended with rawinsonde data, and examine the temporal and vertical continuity of the profiler-measured winds as alternate ways of assessing the accuracy of profiler winds.

During the subsequent Contract period, Scott Williams and Dennis Thomson performed careful rawinsonde-wind profiler intercomparison studies. These will be reported in the Final Report of that Contract (Forbes et. al, 1989b).

3.7.2 Accuracy of High-Temporal-Resolution Data

No direct method was available to assess the accuracy of the high-time-resolution (1-5 minute) wind profiler data during this Contract period. One indirect method of judging the noise level in profiler winds is to examine sequences of winds measured in quiescent periods, when short-temporal variations should represent noise. This approach has been adopted.

Figures 3.7.1 and 3.7.2 show about one hour of McAlevy's Fort, PA profiler winds collected at 2-minute intervals, begin-

. . .st 0000 UTC on 12 September 1986. There is obvious noise in
. . . pper gates and bad data due to contamination from an air-
. . . . . ar 6 km in the sixth profile. Some eddy-like variations
. . . . seen in the lowest three gates during the early minutes,
. . . . may be due to ground clutter or boundary-layer eddies or
. . . . combination of them. Otherwise, the 2-minute-sampled winds
. . . quite steady.

The high-time-resolution winds of Figs. 3.7.1 and 3.7.2 were
measured during a meteorologically quiescent period, during which
any random noise should have shown up as relatively large varia-
tions with respect to a nearly constant background velocity. That
no significant noise appears at most levels and times suggests
that (1) random fluctuations may not pose a problem for short-
term measurements, and (2) the potential exists for accurate
measurement of short term variations when mesoscale features are
present, when atmospheric signals should be strong.

Research on the accuracy of high-time-resolution wind pro-
filer data, and on the application of high-time-resolution wind
profiler data for nowcasting and very-short-term forecasting,
will continue. A UHF Doppler wind profiler will be deployed in
the MIST/SPACE/COHMEX (Arnold, et. al, 1986) field experiment in
Alabama during the summer of 1986, and high-time-resolution VHF
wind profiler data will be used to examine the structure of Penn-
sylvania rainbands (M.S. Thesis of Tim Dye).
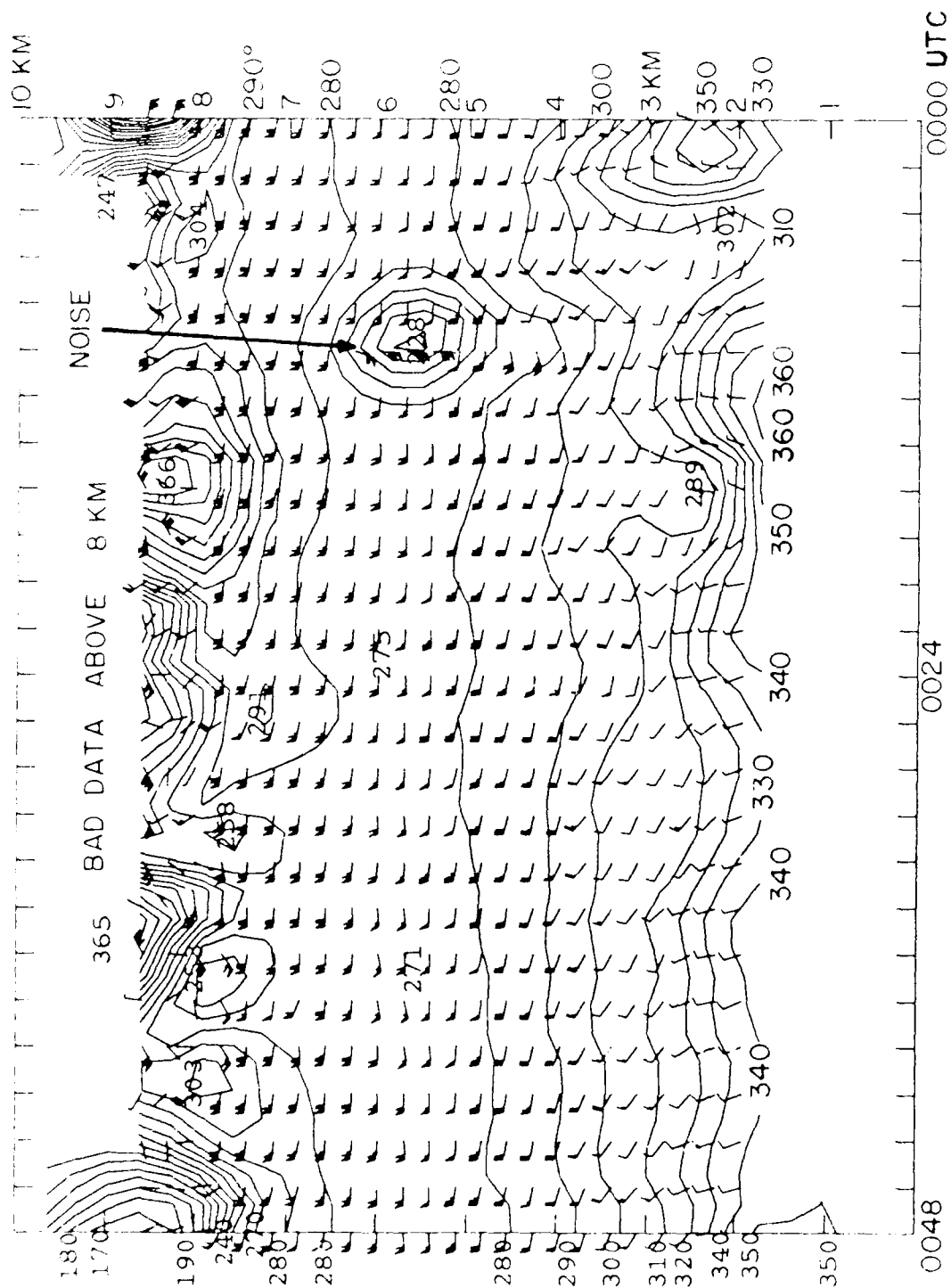
Figure 3.7.1. Time-height section of high-temporal-resolution winds from the McAlevy's Fort, PA wind profiler on 12 September 1986 from 0000 - 0048 UTC. Solid lines are isogons (10-degree azimuth intervals).
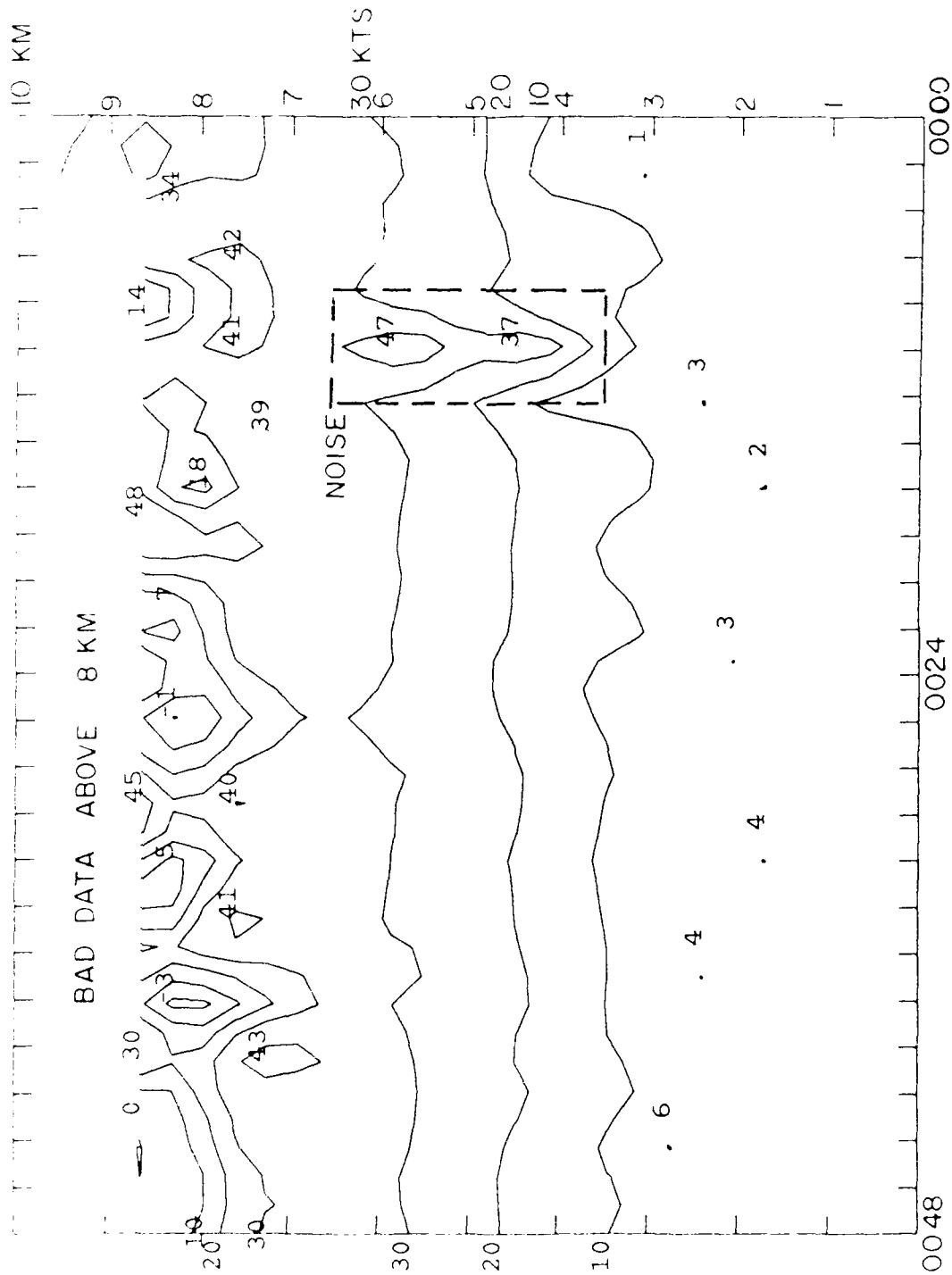
Figure 3.7.2. Time-height section of high-temporal-resolution wind speeds from the McAlevy's Fort, PA wind profiler on 12 September 1986 from 0000 - 0048 UTC (10-knot intervals).

3.7.3 Proximity Rawinsonde Comparisons

Subsequent to the period funded by this research, a local
field program was conducted in the vicinity of the McAlevy's Fort
wind profiler.   Many Loran-tracked rawinsondes were released, and
instrumented   research   aircraft   were   flown.   Results of these
studies will be reported in the Final Report of the subsequent
Contract (Forbes et. al, 1989b).   Some rawinsonde comparisons are
made in the case studies of the following chapters.

3.7.4 Comparison to Interpolated Rawinsonde Data

Although no rawinsondes were released in the vicinity of
the McAlevy's Fort profiler during the period of research funded
by this Contract, comparisons were made upon many occasions be-
tween interpolated NWS rawinsonde winds and those measured by
the McAlevy's Fort profiler.   Most of the time the profiler winds

were quite similar to the interpolated "expected" value and would
blend in rather well to a synoptic-scale analysis. On a fraction
of the occasions, however, the profiler-measured winds were not-
ably "anomalous". In most of these cases, when the weather was
studied carefully for the next 24 hours, evidence for the pro-
filer-detected mesoscale feature was borne out.

3.8 Accuracy of Profiler-Derived Thermodynamic Quantities

In addition to studies which have used profiler "raw" winds,
perturbation winds, and wind shears as diagnostic aids, studies
have also been made regarding the value of analyses of approxi-

mate temperature gradients, lapse rate gradients, temperature advections, and lapse rate advections based upon the thermal wind approximation. Paul Neiman has made this topic the theme of his M.S. Thesis (Neiman, 1987). Accordingly, lengthy discussion of these derived quantities will be deferred to his thesis. In this section only some generalities will be discussed.

While it is a straightforward task to invoke the thermal wind equation (3.2) and infer thermodynamic quantities from profiler-measured wind shears, many practical problems stand in the way of assessing the accuracy of the derived values. Even if one were to use aircraft, it is difficult to measure horizontal gradients of air temperature and lapse rate over length scales comparable to the diameter of the profiler beam. If gradients are measured over larger distances, it becomes necessary to average or filter a time series of profiler winds in order to obtain a comparable sample as inferred from time-space conversion techniques. Questions of steadiness of weather systems and local effects come into play, which damage the credibility of the comparison.

In his M.S. Thesis research, Paul Neiman has compared profiler-derived horizontal temperature gradients and temperature advections to those derived from synoptic-scale NWS rawinsonde-derived analyses interpolated to the profiler sites. Not surprisingly, correlations between the two differently measured sets of values are not large, and had magnitude below 0.3 on average. When "raw" non-filtered profiler data were used, the average (40 cases, 4 levels each) correlation coefficient was 0.20 for tem-

perature gradient and 0.10 for temperature advection. When vertical averaging or modest temporal smoothing was performed on the data the correlation coefficients rose slightly and insignificantly. Correlation coefficients for Fleming, Colorado data were slightly but insignificantly larger. Also not surprisingly, (1) correlation coefficients were larger at 700 and 500 mb (moisture-bearing layers away from the surface) than at 850, 400, and 300 mb; (2) magnitudes of profiler-derived temperature gradients were larger than synoptic-scale-measured gradients by more than a factor of 4—consistent with the profiler detection of mesoscale features; and (3) the effect of vertical and temporal smoothing was to render the profiler-inferred values closer in magnitude to the synoptic-scale values.

In view of these inherent difficulties in directly and quantitatively evaluating the accuracy of the profiler-derived thermodynamic quantities, an alternative approach has been taken, as illustrated in the text to follow. This alternative technique, though somewhat qualitative, takes advantage of the fact that weather systems exhibit a considerable amount of vertical and horizontal (often sloping) continuity which, for certain types of meteorological phenomena, meteorologists understand conceptually. For example, the existence of vertical tilt of fronts and pressure-trough systems has been taught to virtually every meteorology student for decades; the pattern of temperature advection in relation to frontal waves (warm advection in advance and cold advection in the rear) is well known. Thus, in cases

where the meso-alpha-scale (and occasionally meso-beta-scale) surface pressure network shows a series of waves moving along a stationary front near a profiler, for example, an experienced meteorologist knows at least qualitatively what types of changes are taking place aloft. It is this philosophy and synoptic-scale situation that is invoked here in defense of the validity of the "raw" single-profiler-derived temperature gradient and temperature advection calculations.

4.   SINGLE STATION CASE STUDIES: EXAMPLES OF THE USES OF
PROFILER WINDS, WIND SHEARS, AND PERTURBATION WINDS

Many individual cases have been studied in order to deter-
mine in what ways the availability of profiler data might be an
aid to forecasters. This section will try to summarize some of
the findings, and draw illustrations from just a few cases. In
general, these cases are fairly subtle, as it is such circum-
stances where wind profiler data can play the crucial role in
diagnosing and forecasting the situation. The case studies which
follow are extensions of the introductory results presented by
Forbes (1986).

4.1   Perturbation Winds Detect Subtle Features

Section 3.7 briefly discussed the accuracy of profiler
winds. An alternative way to examine the presence or absence of
noise in the data is to examine the perturbation field, i.e., the
vector velocities remaining after a mean value has been removed.
In the research to date, a 24-hour-mean value has been subtract-
ed from each of the hourly values to create the perturbation ve-
locities. A different mean velocity is computed for each range
gate.

The most stringent test of the perturbation field is in a
situation where the raw winds do not exhibit large vertical or
temporal variations despite a moderate or large mean speed. For
example, in Figure 4.1.1, it is difficult at first glance to
detect the variations which are present. Upon very careful in-
spection it can be seen that winds shift from south-southwesterly

to southerly and then back to south-southwesterly. One might be tempted to speculate, however, that most of the variations were noise superimposed upon a uniform velocity.

The perturbation field associated with Fig. 4.1.1 is shown in Figure 4.1.2. From the perturbation velocities it is obvious that the vertical and temporal variations in Fig. 4.1.1 are not noise, but coherent patterns associated with some mesoscale meteorological feature. In this case the feature appeared to be a short-wave trough, and the southerly perturbations resulted in a total wind field that possessed a modest southerly jet. This feature was accompanied by a period of rain, as depicted on the figure.

This case serves well to illustrate the type of situation where the perturbation wind field can be of value to the operational forecaster. When the prevailing flow is weak, even weak mesoscale disturbances can yield directional variations in the total wind field that are readily apparent in the raw winds. In such cases the perturbation field tends to either convey little or is difficult to interpret. On the other hand, when the background flow is strong, equally intense perturbations can be masked, since they only slightly alter the wind directions. Such disturbances can easily be missed by forecasters faced with deadlines and other distractions. Under such circumstances it would be easy to dismiss Fig. 4.1.1 as conveying no message. However, the message conveyed from Fig. 4.1.2 is hard to ignore.

The signature seen in Fig. 4.1.2 on 20 May 1986 is one that has been noticed time and again in association with precipitation
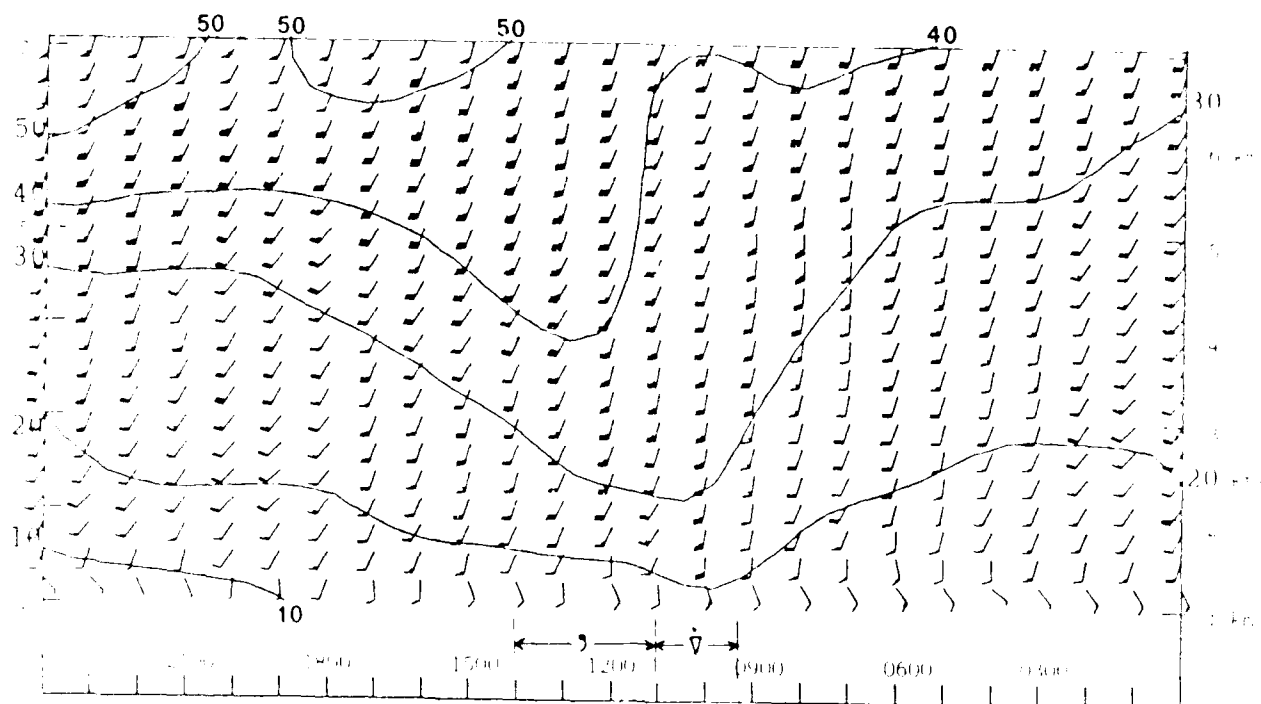
Figure 4.1.1.   Time-height section of McAlevy's Fort, PA,
profiler winds during the passage of a subtle upper-air
disturbance associated with precipitation on 20 May 1986.
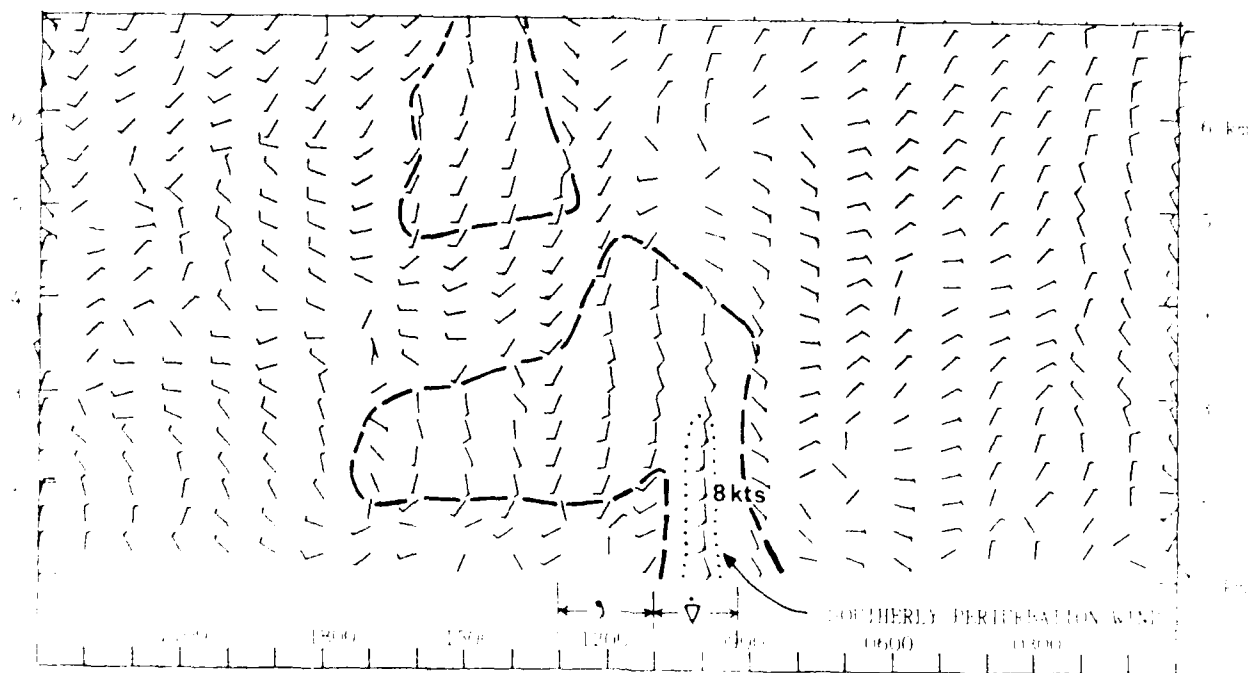
Figure 4.1.2.   Time-height section of perturbation winds,
obtained by subtracting the 24-hour mean winds, level by
level, from the winds of Fig. 4.1.1.   Wind barbs are doubled,
such that a full barb represents 5 kts (2.5 m/s).   Heavy
dashed line delineates perturbation southerlies.

events. A mesoscale "jet" of perturbation southerlies or easter-
lies of about 10 kts (5 m/s) appears in a shallow layer of the
lower troposphere about an hour before precipitation begins, and
the layer bearing these perturbations deepens during the start
and intensification of precipitation. The physical mechanism
relating the mesoscale "jet" to the precipitation event is specu-
lated to be enhanced overrunning in most instances, although en-
hanced convergence may be in effect during others. Spatial cov-
erage of temperature and velocity data have not typically been
adequate to definitively assess either process.

The precipitation event on 20 May 1986 appeared to be from a
pre-cold-frontal rainband. Figure 4.1.3 shows that the surface
cold front was entering Central Pennsylvania at 1200 UTC, but the
heaviest precipitation had already occurred before that time. The
warm front at the surface was in southern New York, clearly north
of the McAlevy's Fort, PA wind profiler site. The pre-frontal
warm sector was almost uniformally warm, both at the surface and
at 850 mb, Figure 4.1.4, so that overrunning was not likely to be
the cause in this case. Indeed, to the extent that the temporal
evolution of the perturbation winds can be interpreted as being
due to a translating spatial pattern, they did show a definite
confluence, which was likely to have been a true convergence if
measurements could have been obtained in two horizontal direc-
tions. Additional studies of precipitation bands are planned for
subsequent years (Tim Dye's M.S. Thesis).
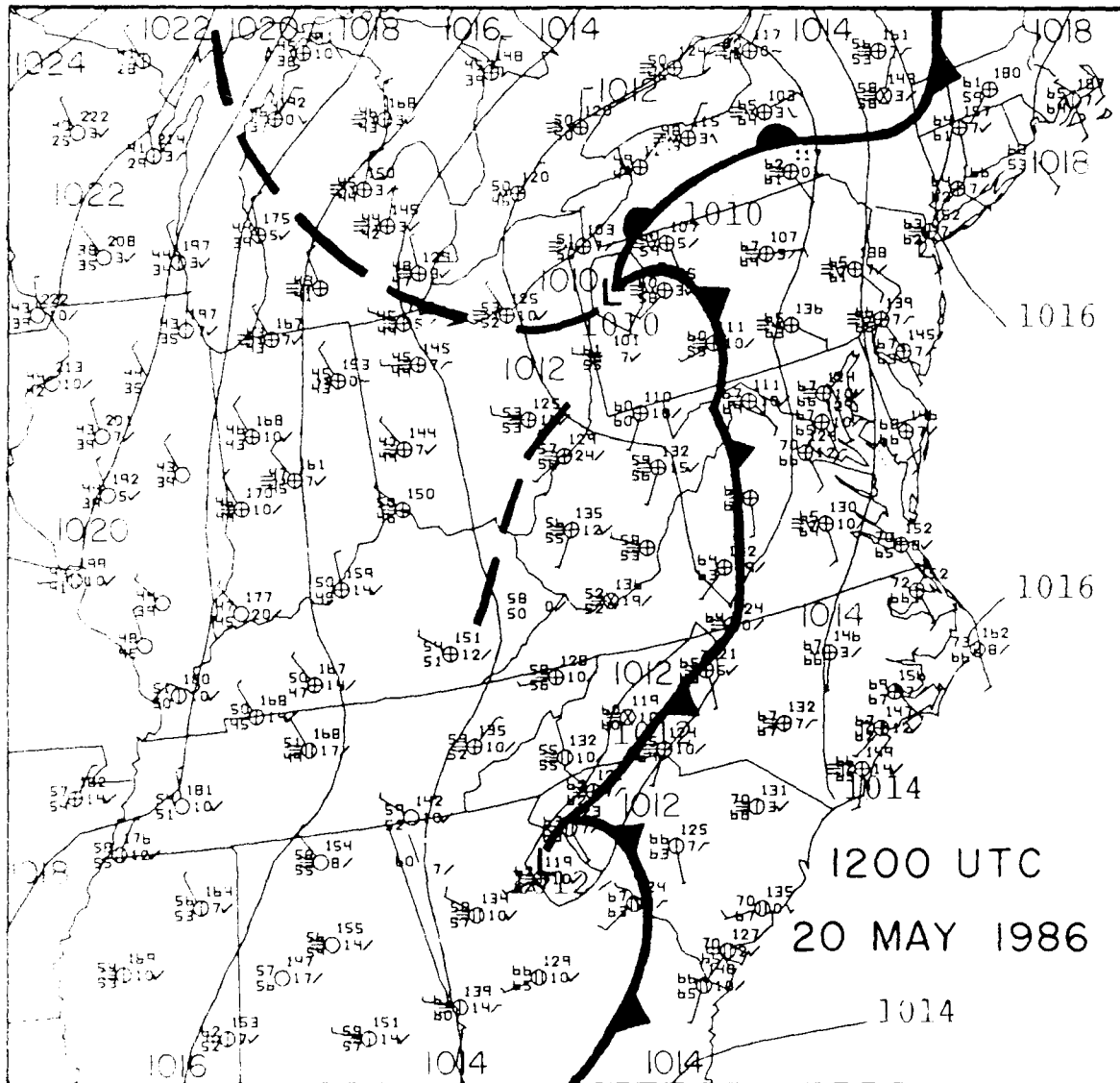
1200 UTC
20 MAY 1986

Surface observations, fronts, wind shift lines, (solid lines, at 2 mb intervals) from 1200 UTC on
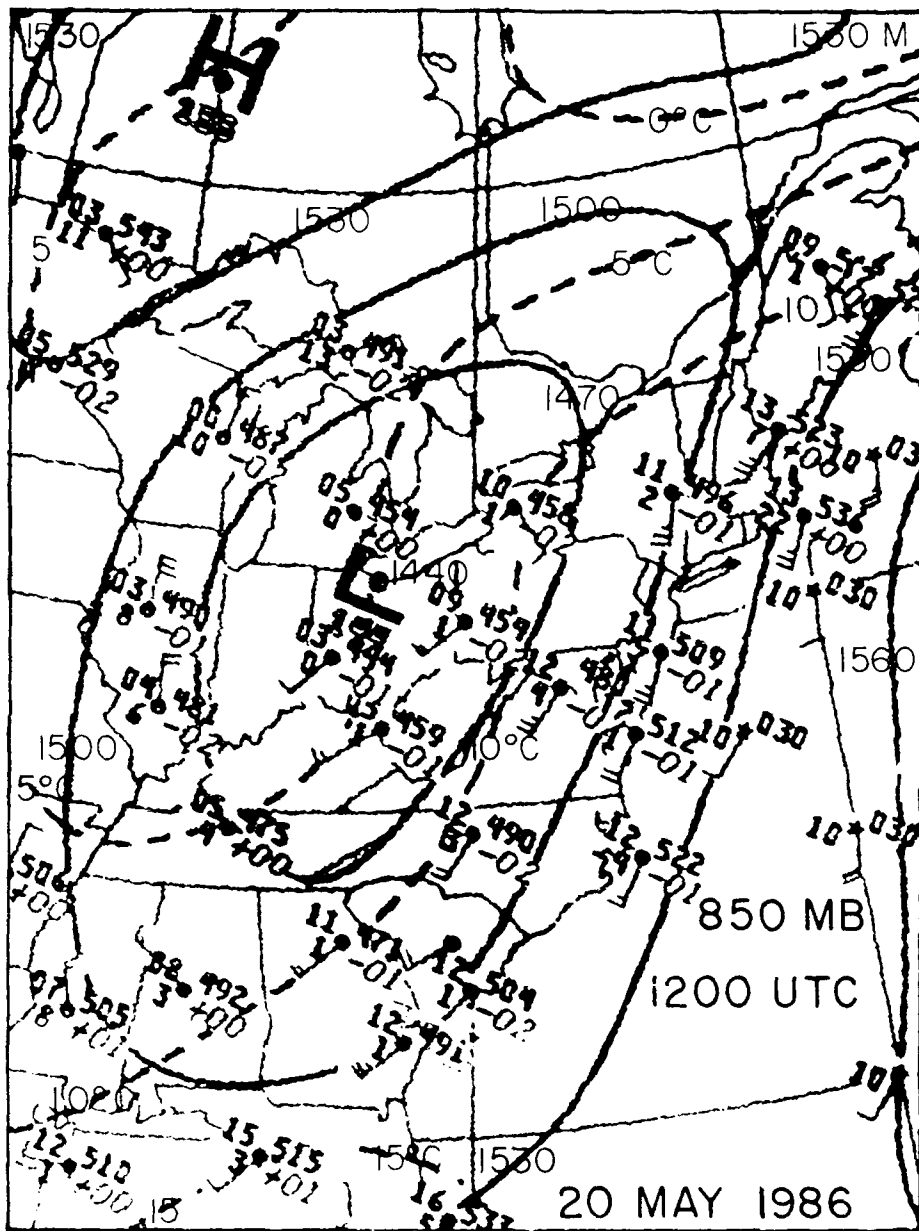
Figure 4.1.4. 850 mb observations, geopotential heights (solid, 30 m intervals) and temperatures (dashed, 5 C intervals) from 1200 UTC on 20 May 1986.

4.2 Detailed Structure of a Lifting-Out, Opening-Up Cutoff Low

The greater temporal resolution of the profiler data over that provided by conventional rawinsondes allows for a much better understanding of the structure of weather systems. This has the potential to allow for detailed mesoscale forecasts, whereas rawinsonde data promotes the issuance of forecasts containing less-abrupt temporal changes. The example case selected is one in which a cutoff low in middle and upper troposphere over southern California was rather abruptly "forced" to move rapidly northeastward under the increasing southwesterly steering flow of a trough approaching from the Pacific. The cutoff subsequently began to "open up", and moved rapidly across the Denver region as a synoptic-scale trough on 16 December 1984. Figure 4.2.1 shows the cloud pattern associated with the cutoff while it was centered over northeastern Arizona on 15 December. The analysis which follows is an extension of that by Forbes et. al (1985).

Figure 4.2.2 illustrates the structure of the trough as it approached Denver, at 300 mb, which was very near the level of the jet stream, based upon rawinsonde data. Though it is apparent from the figure that there are large gradients of wind speed and direction, and despite the rawinsonde sites being adequate to resolve the synoptic-scale wave pattern, the spacing of the rawinsondes was totally inadequate to resolve the true details of the most interesting parts of the trough system from the point of view of a pilot. This can be deduced from inspecting the wind profiler data from the Colorado network.

Figure 4.2.3 shows sets of vertical profiles of the v (N S)

1501 15DE84 38E-2MB 01342 22322 K82
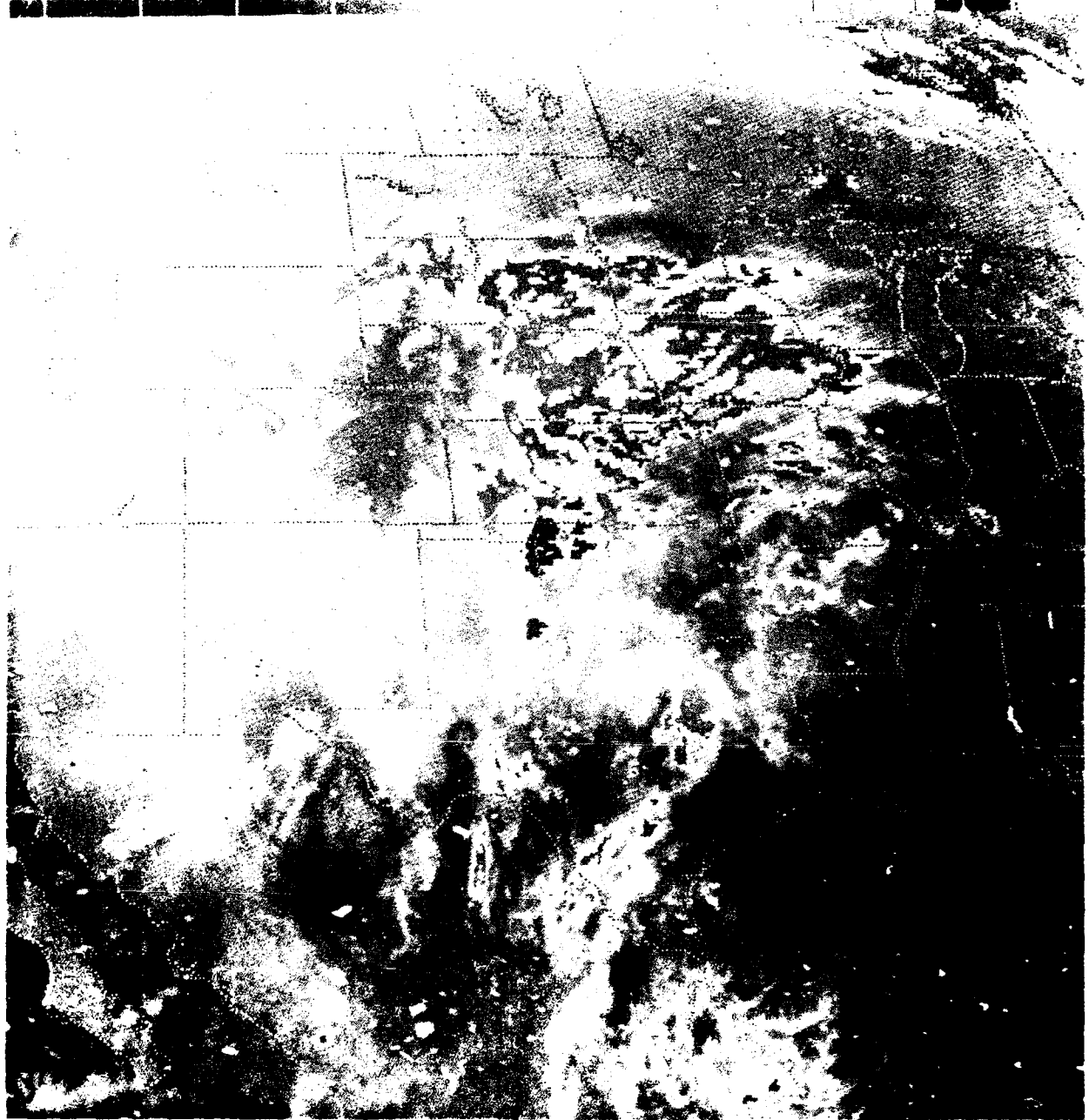
Fig. Enhanced infrared satellite image from 1501 UTC, 15 December
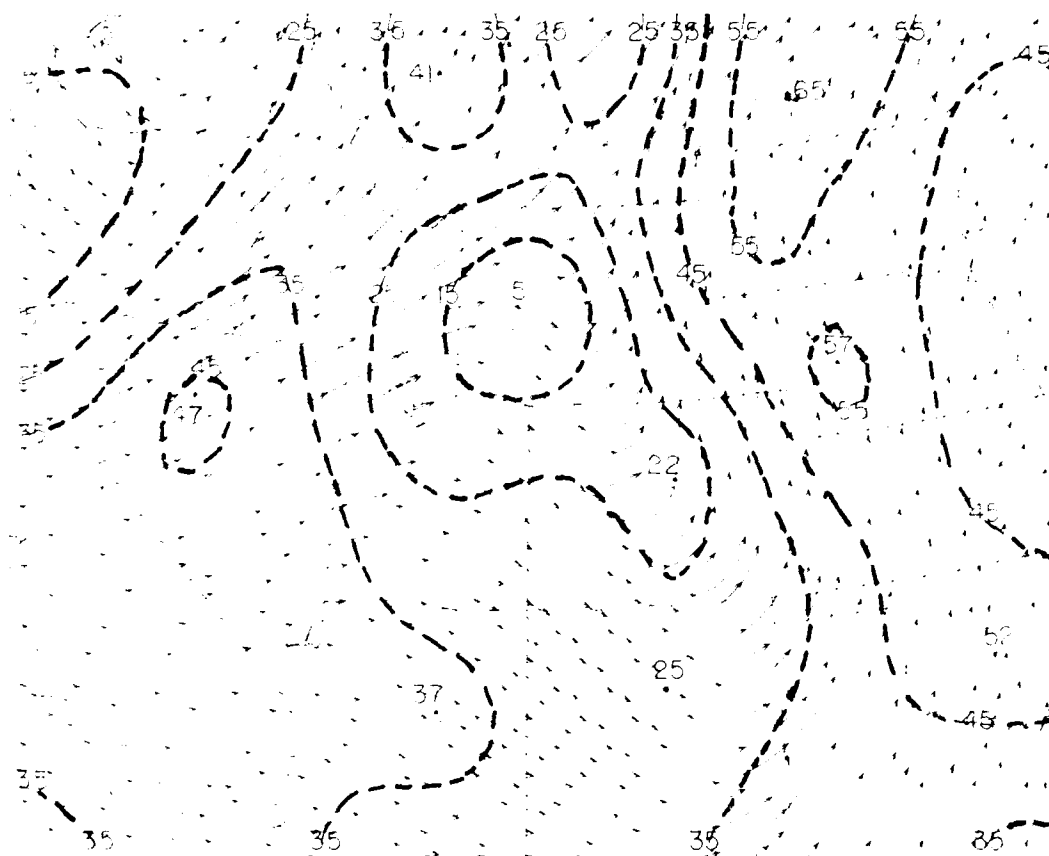
Figure 4.2.2. Streamlines and isotachs (m/s, dashed) of the 300 mb winds at 0000 UTC 16 December 1984, based upon conventional rawinsonde data.

component of the wind at low (a) and high (b) resolutions. It can be seen that during the 6-hour period between 0000 UTC and 0600 UTC on 16 December, while the trough axis approached and passed, the v component changed by up to 66 m/s at levels near the jet stream.

The changes in the u component are shown in Figure 4.2.4. The u (E-W) component also changed considerably, though not as dramatically in this case and, owing to the structure of the wave pattern, not at the same time as the largest changes in v.

As an aside, the rapidity of the changes shown in Fig. 4.2.3 makes it evident that any rawinsonde-wind profiler intercompar- ison studies must be carefully planned in order to ensure nearly identical sample volumes in both space and time. A one-hour mis- match at the 7-8 km levels could have yielded an inconsistency (sometimes erroneously labelled a wind profiler error!) of 10-20 m/s. With this note of caution recognized, it is still possible to see general similarities in an intercomparison between the Fleming profiler winds (Figs. 4.2.3 and 4.2.4) and those from the Denver rawinsonce, Figure 4.2.5. It should be pointed out that the wind at Denver was about 45 m/s in only a very shallow layer, near the 300 mb level, as plotted. Adjacent significant levels in the table to the right of the diagram had winds no larger than 61 kts (about 31 m/s).

Profiler wind observations also have the potential to permit much better resolution of the position and intensity of jet streams and their associated gradients than rawinsondes--provided that temporal changes can be related to horizontal variations
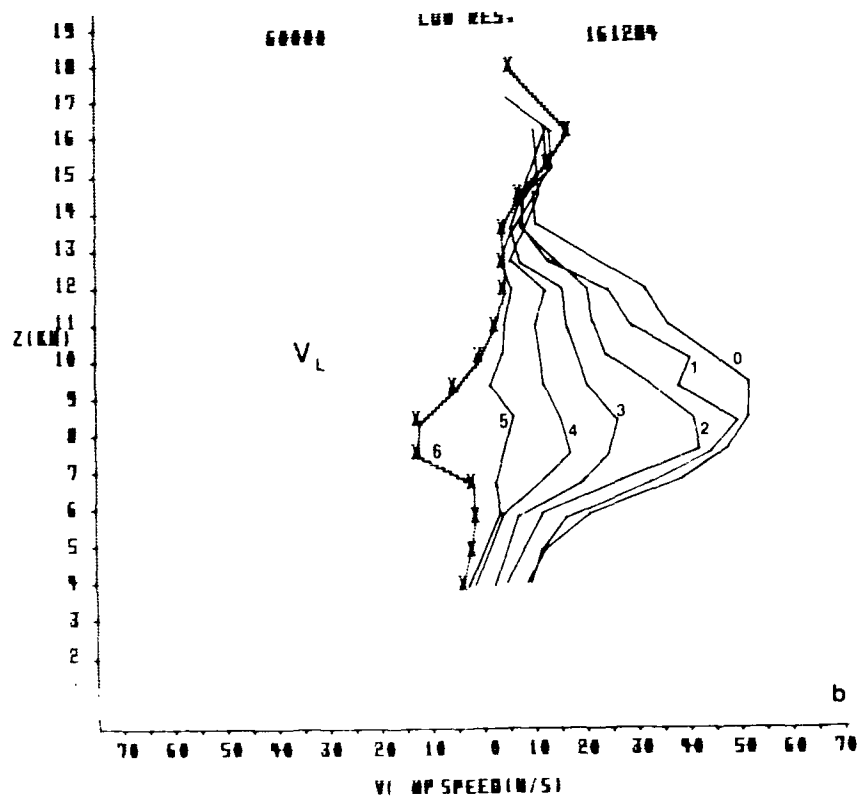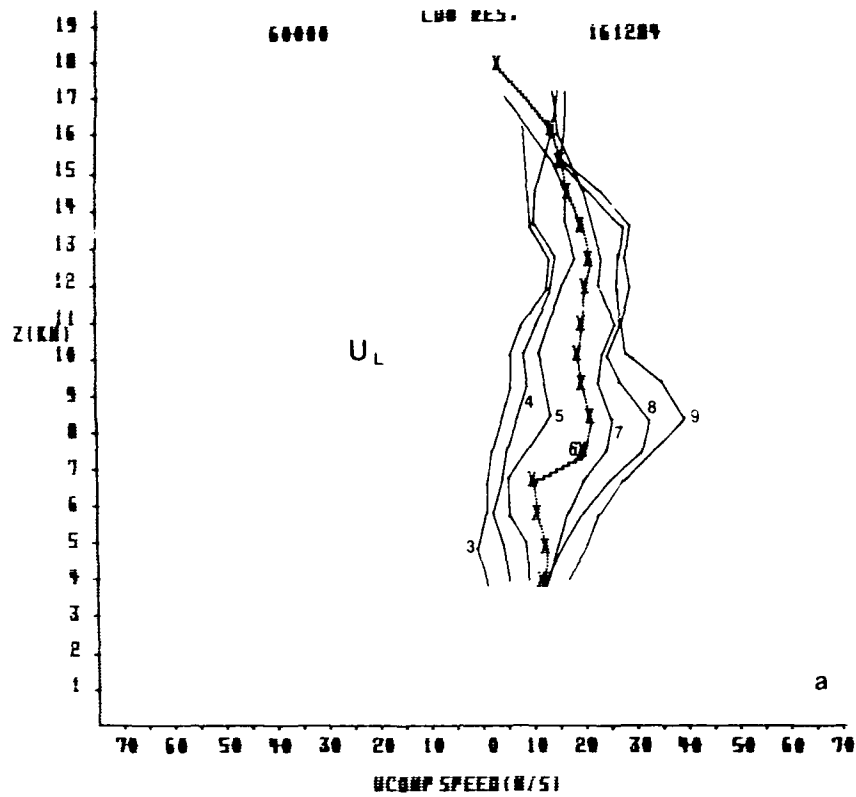
Figure 4.2.3. Vertical profiles of the evolution of the hourly low-resolution average wind components (m/s) at Fleming, CO on 16 December 1984. Numbers beside the profiles indicate the hour in UTC; profiles marked by "x" are from 0600 UTC.

    a. U component; west winds positive

    b. V component; south winds positive
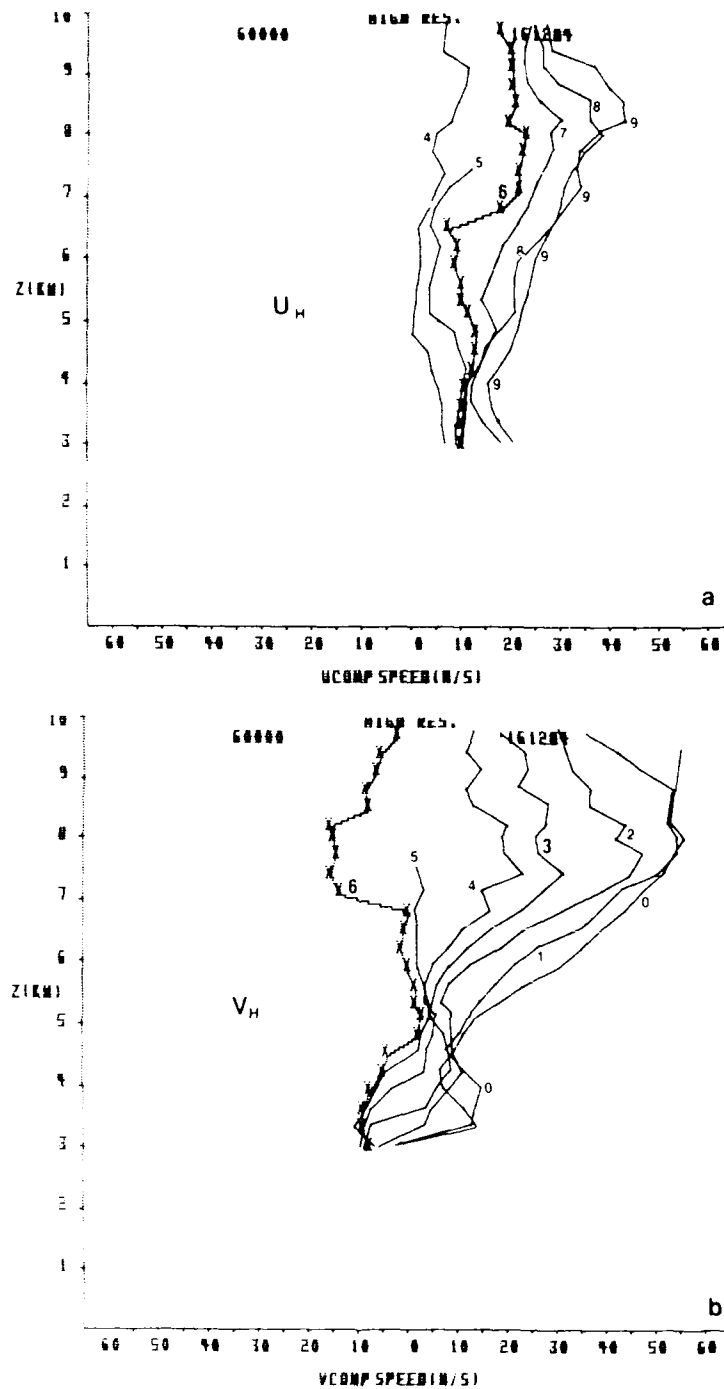
Figure 4.2.4. Vertical profiles of the evolution of the nourly high-resolution average wind components (m/s) at Fleming, CO on 16 December 1984. Numbers beside the profiles indicate the hour in UTC; profiles marked by "x" are from 0600 UTC.

    a. U component; west winds positive
    b. V component; south winds positive

P	T	TD	RH	HT	WS	WD
100	-56			530	25	220
103	-60			500	38	195
158	-48			480	27	195
200	-49			460	42	235
223	-42			430	45	215
321	-40	-52	25	310	43	180
368	-36	-47	30	300	49	180
395	-37	-43	52	250	61	190
455	-28	-39	33	220	64	200
602	-11	-23	35	200	44	210
610	-10	-14	72	190	37	210
700	-2	-8	63	160	22	205
767	-1	-4	79	140	15	200
790	-3	-4	92	120	14	255
796	-5	-6	92	110	17	290
806	-5	-7	85	90	18	310
820	-4	-4	100	80	16	310
				70	16	335
				60	15	350
				00	8	340

STATION: 72469
00Z 16 DE 84
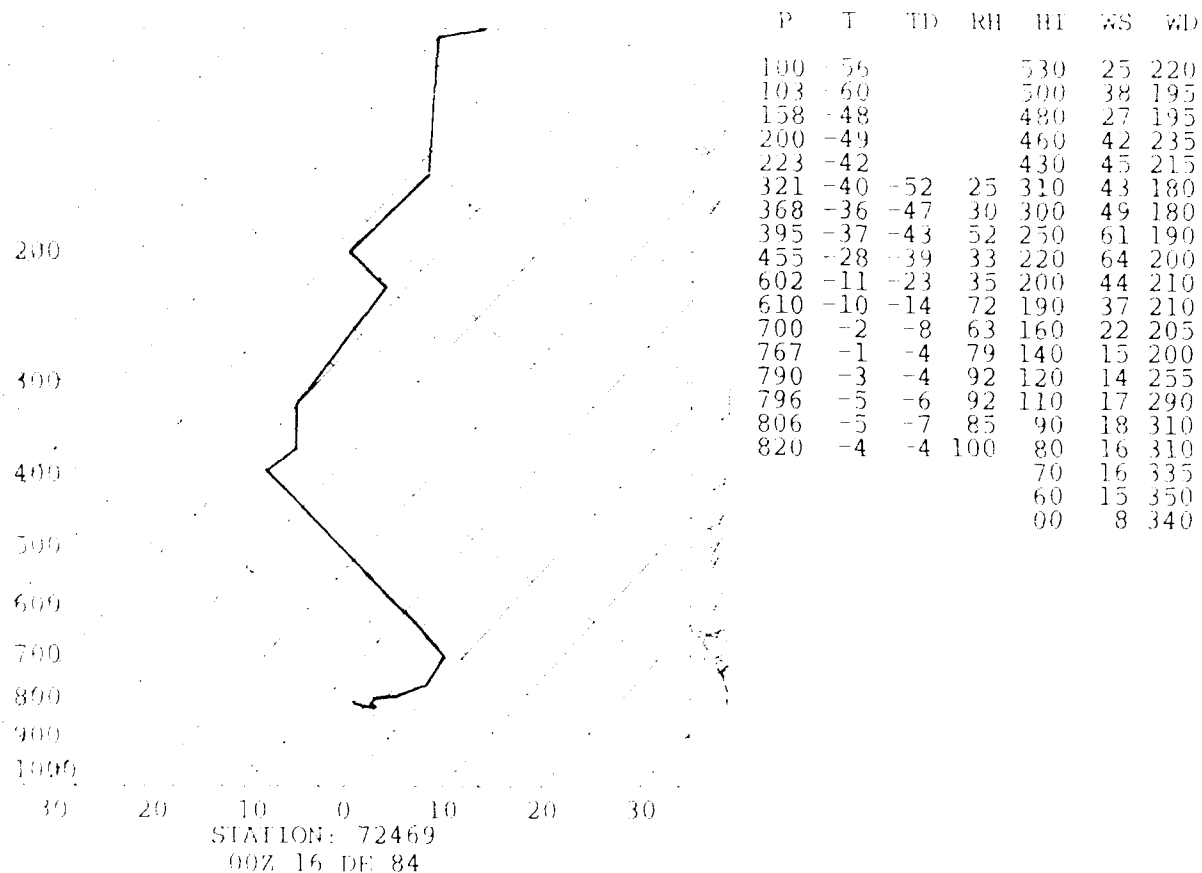
Figure 4.2.5.   Skew-T log P diagram of temperature and humidity from the
Denver, CO rawinsonde of 0000 UTC 16 December 1984.   Conventions:
Heavy line represents dry-bulb air temperature
(^{o}C); thin line represents dew point temperature (^{o}C).   Significant-level
data are tabulated at right: pressure (mb) and corresponding temperature, dew
point, and relative humidity (%); height (hundreds of feet) and
corresponding wind speed (kts) and direction (^{o}); heights do not correspond
to the pressure data.

within a steady-state system translating over the profiler. Figure 4.2.6 shows the temporal variation of the v component of the wind at the 9 km (about 30,000') level, which was generally near the location of the core of the jet stream. It can again be seen that the greatest change occurred in the 6-hour period beginning at 0000 UTC on 16 December, and that changes were considerably more gradual at other times. The southerly and northerly wind maxima were located over Fleming, CO at 15/2000-16/0000 and 16/0600, respectively.

If it is assumed that all of the change of the v component was due to steady-state translation of the wave pattern over the profiler, then measured temporal variations can be used to estimate the horizontal gradient of v. In this case the trough axis was travelling at about 17 m/s, such that in 6 hours the trough axis traveled about 370 km. Thus, the gradient was about 60 ms-1(370 km)-1, or about 0.16 ms-1km-1.

The 370 km distance associated with the above gradient happens to be a typical distance separating radinsonde stations. Thus, only under the most favorable of coincidental circumstances could the entire gradient associated with the rapid change between 0000 and 0600 UTC have been detected by the rawinsonde network. Under more unfavorable (yet typical) circumstances, the gradient would have been underestimated by the rawinsonde network. Under the worst circumstances the wave pattern might have been situated with respect to rawinsondes at the three positions shown by large arrows in Fig. 4.2.6. In this case the gradient inferred from rawinsondes would have appeared to be much weaker
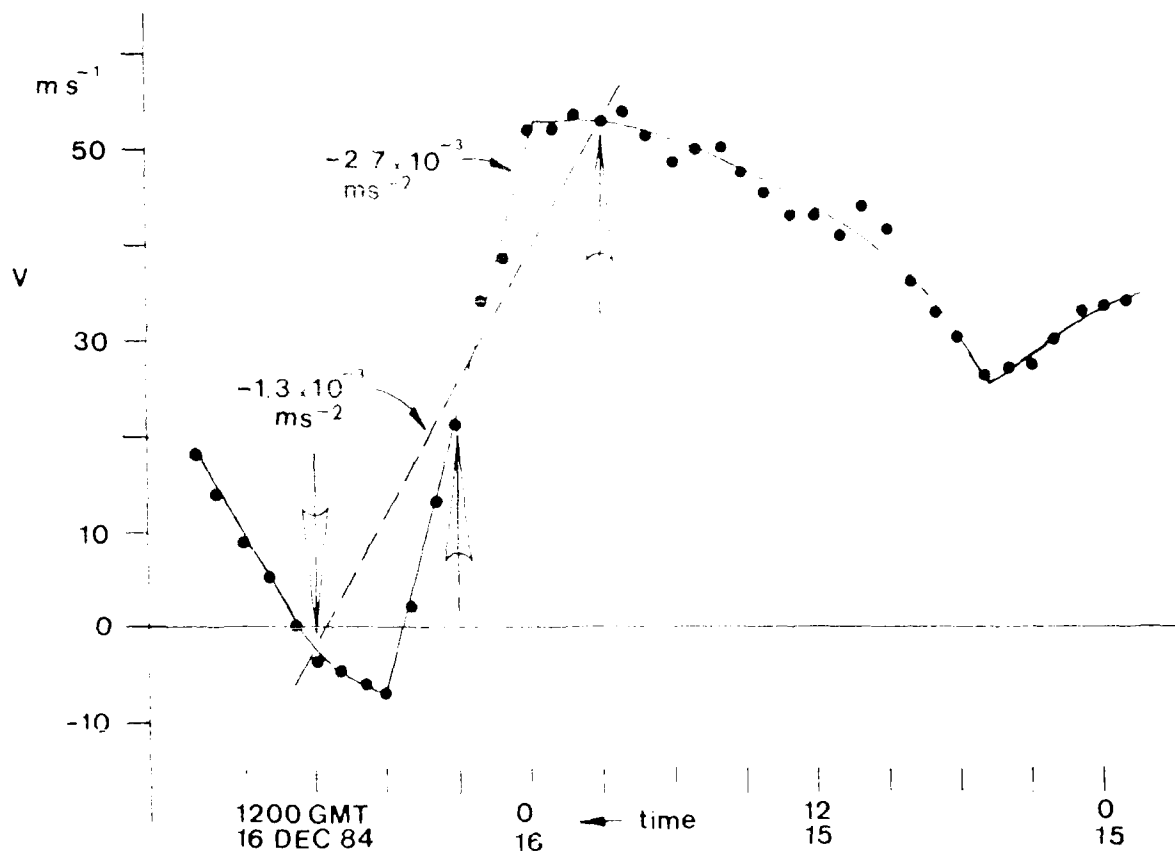
Figure 4.2.6. Time series of the V component of the wind at 9 km MSL at Fleming, CO on 15-16 December 1984 (dots), with a solid line representing a smoothed portrayal of the evolution. The dashed line and arrows represent the approximate profile that would be produced through use of the coarsely spaced, 12-hourly operational rawinsonde data in the region of greatest horizontal variation.

(by a factor of 2) than it actually was. Put another way, an estimate of the rate of change of the v component at some location based upon these ill-placed measurements would have given only about half of the observed rate of change, -1.5 versus -2.7 x $10^{-3} ms^{-2}$.

The linear change of the v-component between 0000 and 0600 UTC on 16 December 1984 shown in Fig. 4.2.6 is not close to the sinusoidal type of variation expected due to the translation of a true wave. Instead, this linear change during the passage of a wind reversal (and trough passage) is suggestive of constant angular velocity. Could it be that the former cutoff low had not fully "opened up" into a wave form, and that there was still a mesoscale cutoff core in constant rotation?

It is recalled that a column of air in "solid-body" rotation possesses a tangential velocity that increases linearly with distance away from the center. In such a case, the relative vorticity is twice the angular velocity, such that if we were to presume this to be the situation on 16 December, and again assumed steady-state translation, the profiler-derived relative vorticity would have been constant over a distance of 370 km (and for 6h during the passage over Fleming), with value $2*(0.16 ms^{-1}km^{-1})$ = 32 x $10^{-5}s^{-1}$. The absolute vorticity would have, therefore, been 41 x $10^{-5}s^{-1}$, which is larger than can ever be seen on a NWS National Meteorological Center (NMC) operational analysis of absolute vorticity!

Figures 4.2.7 and 4.2.8 illustrate the absolute geostrophic and analyzed relative vorticities based upon rawinsonde data at
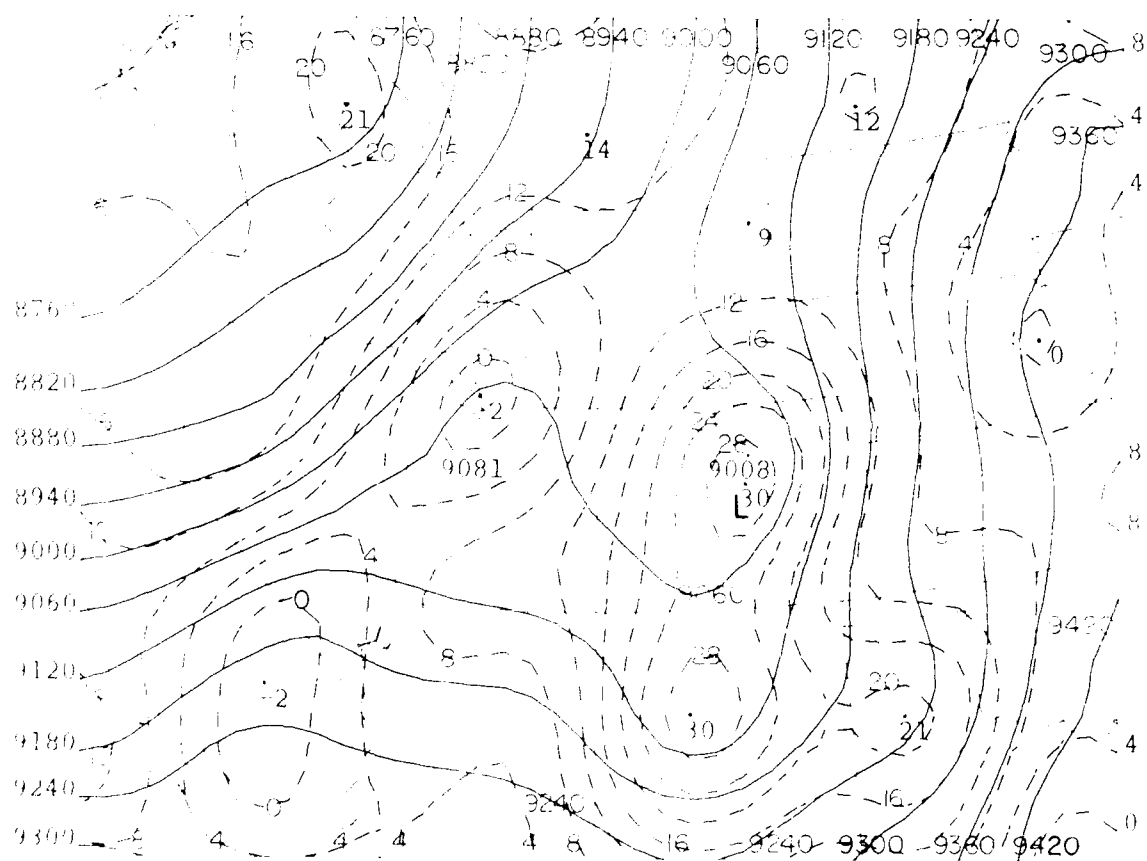
Figure 4.2.7.   Analysis of 300 mb geopotential heights (m, solid) and absolute geostrophic vorticity (units of 10^{-5} s^{-1}, dashed) for 0000 UTC 16 December 1984.
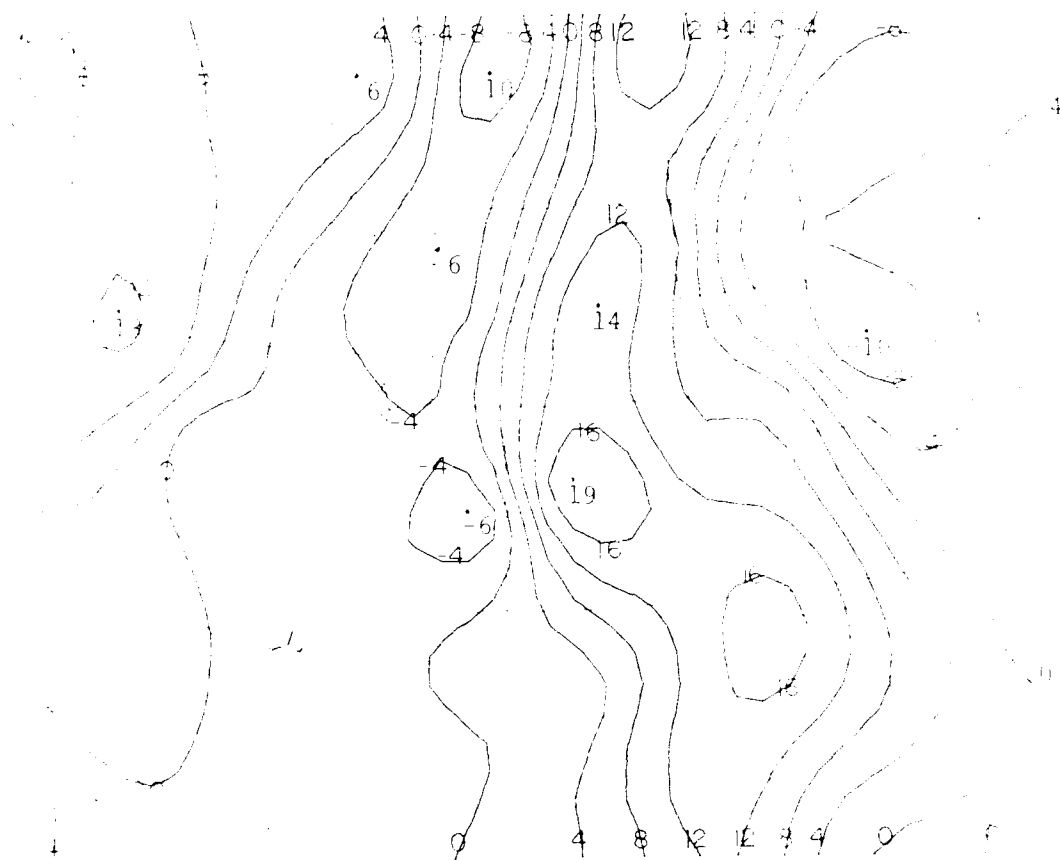
Figure 4.2.8. 300 mb relative vorticity (units of 10^{-5} s^{-1}) corresponding to the winds of Fig. 4.2.15, 0000 UTC 16 December 1984.

mb level.   Maximum values are 30 and 19, respectively.

, this emphasizes the extent to which enhanced meteorolog-

structure can be detected through use of wind profiles.

The notion of solid-body rotation in this case de   as yet

discussion. Based upon the unequal values of the maximum

minimum v component of Fig. 4.2.6 (53 m/s and -7 m/s, respec-

, the vortex could not have been stationary.   (Obviously,

must be true, or else the profiler could not sample cross-

on of the vortex!)   In this case there would have been a

imposed prevailing v-component of 23 m/s from the south,

was almost twice as fast as the v-component speed of trans-

.   This imbalance represents a departure from s   body

rotation of a vortex within a uniform steering flow.   Thus, the

ed v-component changes were not due solely to solid body

tion and translation, but also were due in part to a lateral

of the v component within the steering flow.

The velocity field structure can be further understood by

examining the u-component evolution.   The   u-component did not

undergo sufficient variation to support a 30 m/s tangential

velocity. A tangential velocity of about 20 m/s is about the

largest that can be supported. While the exact 2-dimensional

structure of the flow pattern cannot be fully resolved from

records of a single wind profiler, what appears most likely is

that: (1) there was a core in constant rotation with a radius of

maximum winds of about 185 km, and with maximum tangential veloc-

ity of about 20 m/s; (2) the feature was translating at about 17

m/s northeastward (slightly N of due NE), offsetting a portion of

the "excess" southerlies, and (3) just ahead (north and east) of the core was a south-southwesterly jet stream with about 20 m/s of linear v component shear over 185 km on its cyclonic side that contributed the remainder of the southerlies needed to explain the v-component maximum observed at 0000 UTC. The u-component variations are consistent with this analysis. While the stream-lines of the vector sum of these components take on a trough form, in the relative flow pattern there would remain a closed circulation flanked by a jet stream. The maximum absolute vorticity consistent with this pattern would still be 41 x 10-5s-1, but the isovort pattern would now be somewhat elongated along the jet stream.

Other aspects of the case were interesting, as well. Figure 4.2.9 is a time-height section of the Fleming, CO profiler winds on 15-16 December 1984. Below the 9km level already discussed, sudden variations of wind direction could be seen at all levels, accompanying the passage of the trough axis. Whereas the flow pattern of Fig. 4.2.1 was drawn as wave-like in conjunction with the synoptic-scale data ısity, in time series the disturbance looks much more like a discontinuity. Notice that at all levels there was not a continuous wind shift over a 6-hour period, as was seen in the wind speed. Instead, nearly all of the directional change took place within a period of one hour sometime between 0300 and 0500 UTC on 16 December. Inasmuch as the difference between a headwind, crosswind, and tailwind is of considerable importance to aircraft performance, such profiler data would obviously be of great operational value.
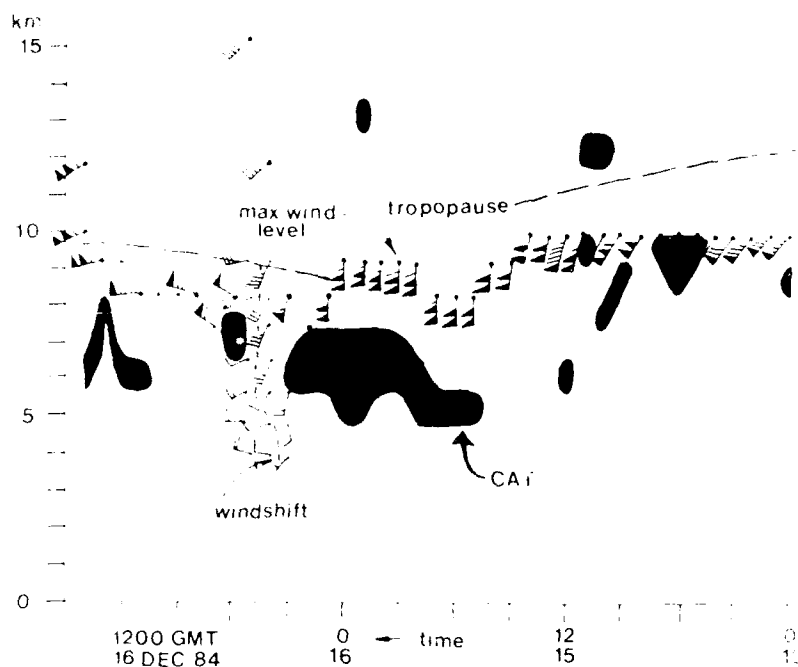
Figure 4.2.9. Selected wind observations from the Fleming, CO wind profiler on 15-16 December 1984. A full barb represents 10 kts (about 5 m... and a pennant represents 50 kts (about 25 m/s). Heavy shading indicates areas likely to have experienced clear-air turbulence (CAT) resulting from vertical wind shear.
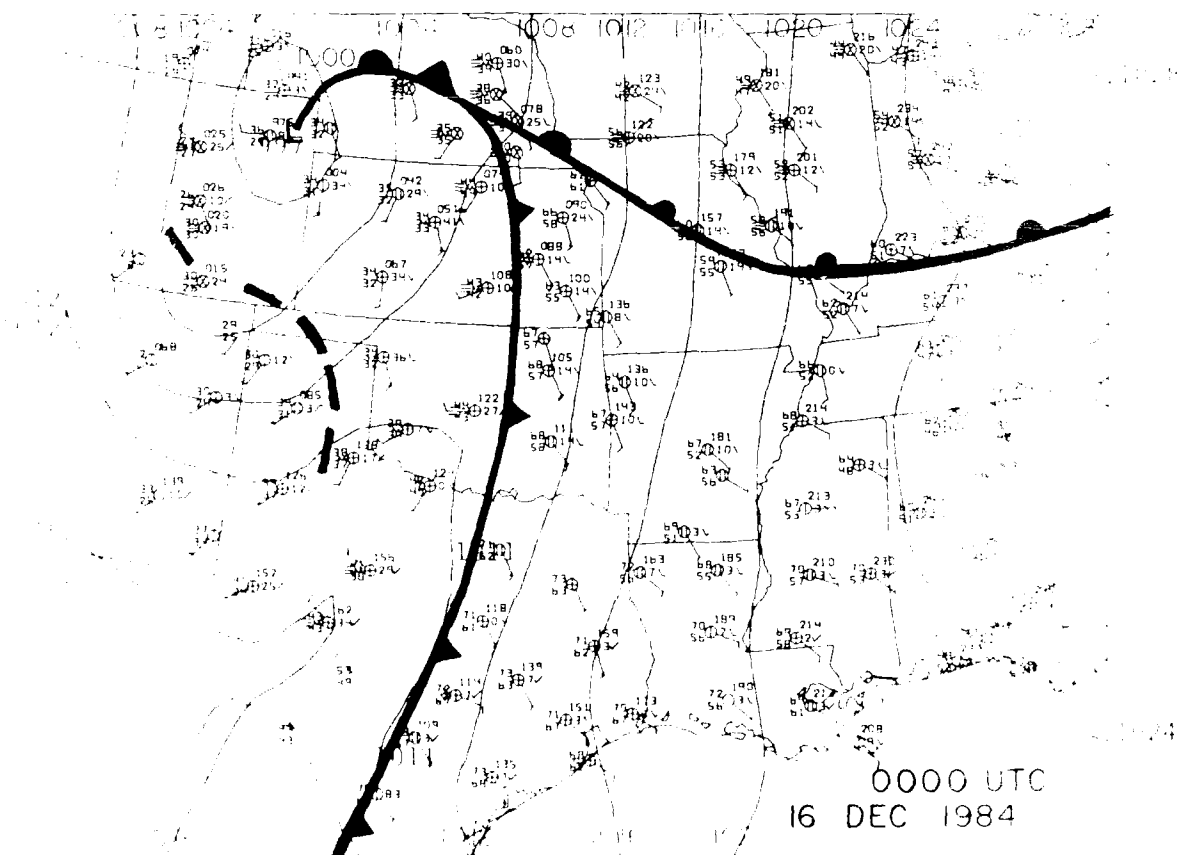
Figure 4.2.10. Surface observations, fronts, and sea-level pressure analysis (4 mb intervals) for 0000 UTC 16 December 1984.

The character of the wind shifts at levels below 9 km can be examined in greater depth. At the surface, Figure 4.2.10, a cold front was located across KS and OK at 0000 UTC on 16 December, tracing back as an occluded front to a surface low pressure center over eastern CO. Figure 4.2.11, a west-east cross-section, does not readily confirm a front at this level because of its revised nature. However, at elevations above about the 850 mb level, a sloping frontal zone can be seen, and appears to cross Denver at about 650 mb. A close inspection of the winds in the Denver sounding, Fig. 4.2.5, bear this out. Above 650 mb winds are from the SSW; between 800 and 650 mb the winds back impressively with height, suggesting cold advection. This suggests strongly that the sudden wind shifts of Fig. 4.2.9 were affiliated with a cold front passage.

There would also appear to be an upper-level front detectable in Fig. 4.2.11, located at about 500 mb over North Platte, NE. This is easily borne out by a 500 mb isotherm analysis, Figure 4.2.12. However, the objective analysis of the 500 mb level data — independent of wind profiler data, detailed sounding examination, and cross-section construction — gives no hint of the lower frontal zone seen in Fig. 4.2.10!

By contrast, the 300 mb isotherm analysis, Figure 4.2.13, does suggest that the wind shift could be accompanied by a front, although the temperature gradient is strong only to the rear (west) of the wind shift. However, intercomparison with Fig. 4.2.10 indicates that this 300 mb front is the upper-level front (i.e., the one over North Platte, NE at 500 mb), and not the low
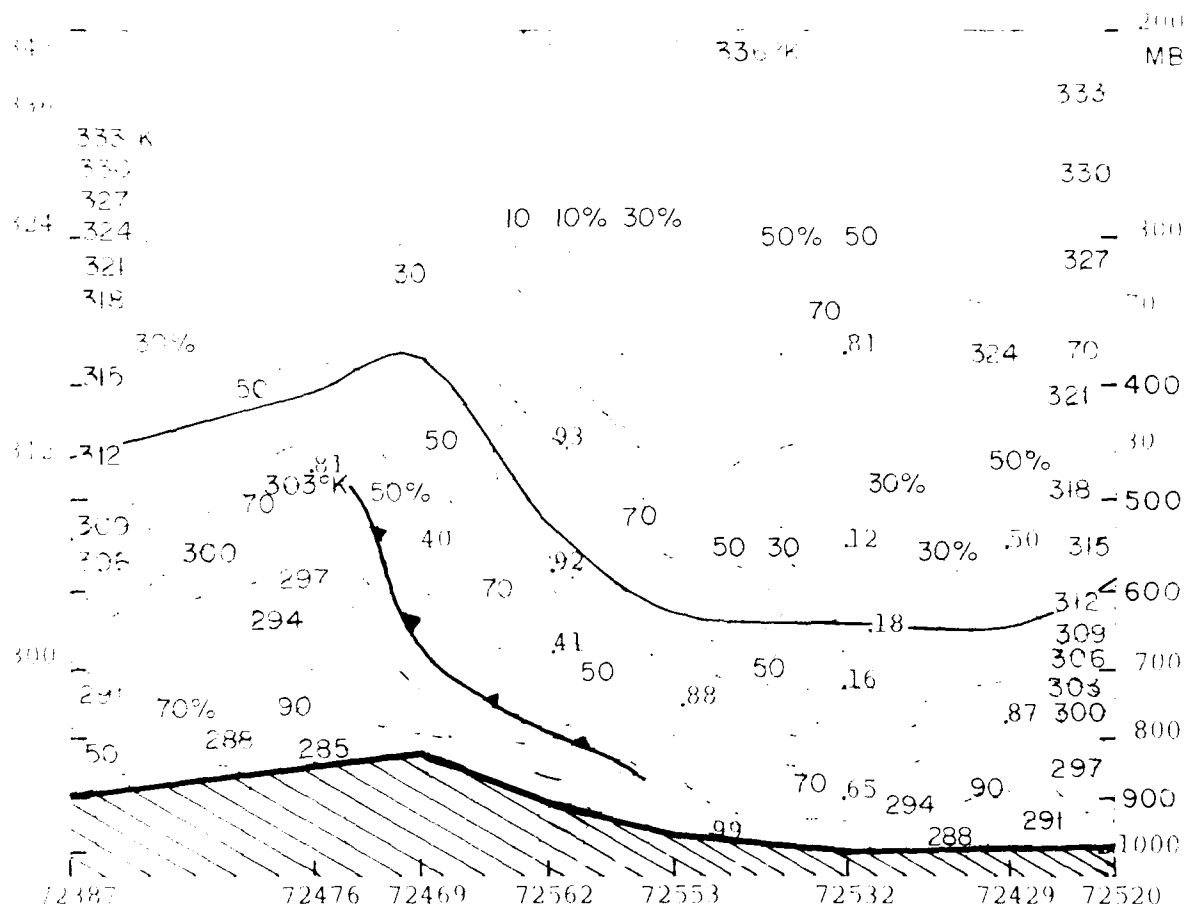
Figure 4.2.11. West-east cross-section of potential temperature (solid, °K) and relative humidity (dashed, %) from 0000 UTC 16 December 1984. Rawinsonde data from 72387, Desert Rock, NV; 72476, Grand Junction, CO; 72469, Denver, CO; 72562, North Platte, NE; 72553, Omaha, NE; 72532, Peoria, IL; 72429, Dayton, OH; 72520, Pittsburgh, PA were used.
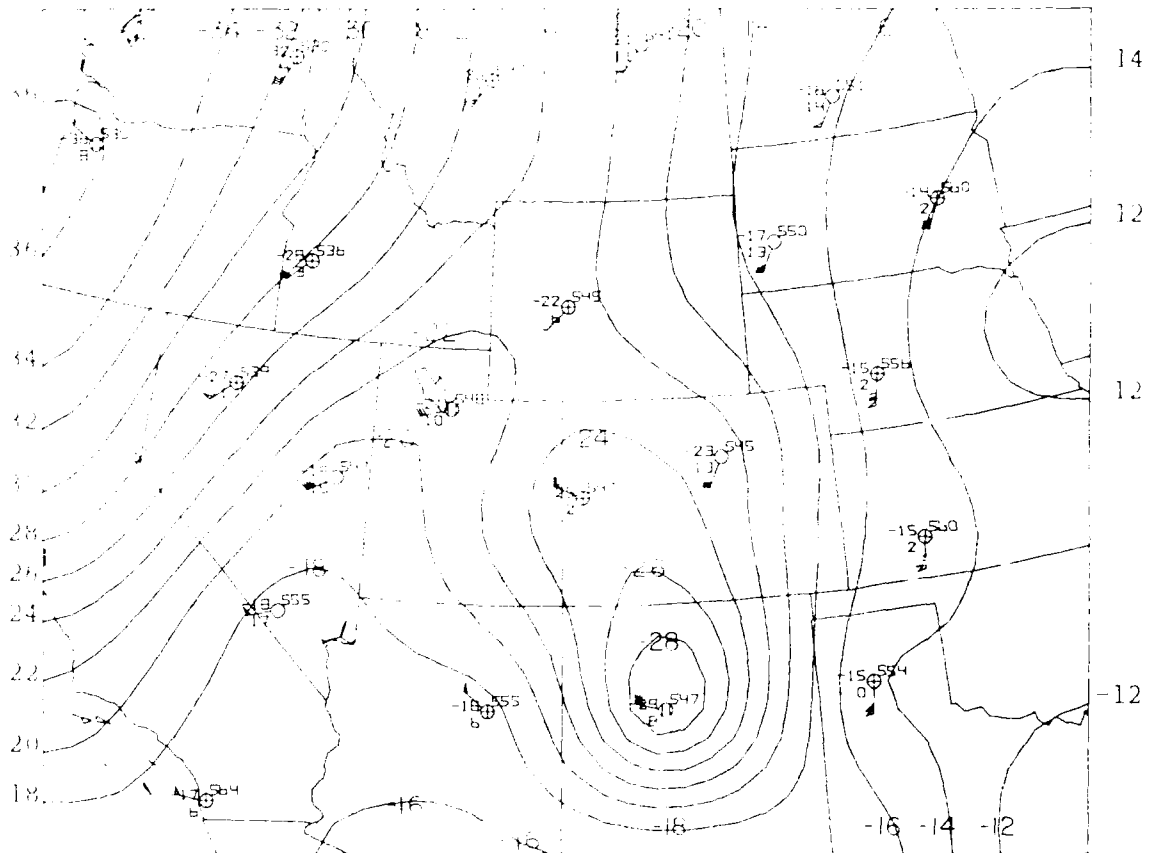
Figure 4.2.12. 500 mb temperatures (^{0}C) at 0000 UTC 16 December 1984.

94
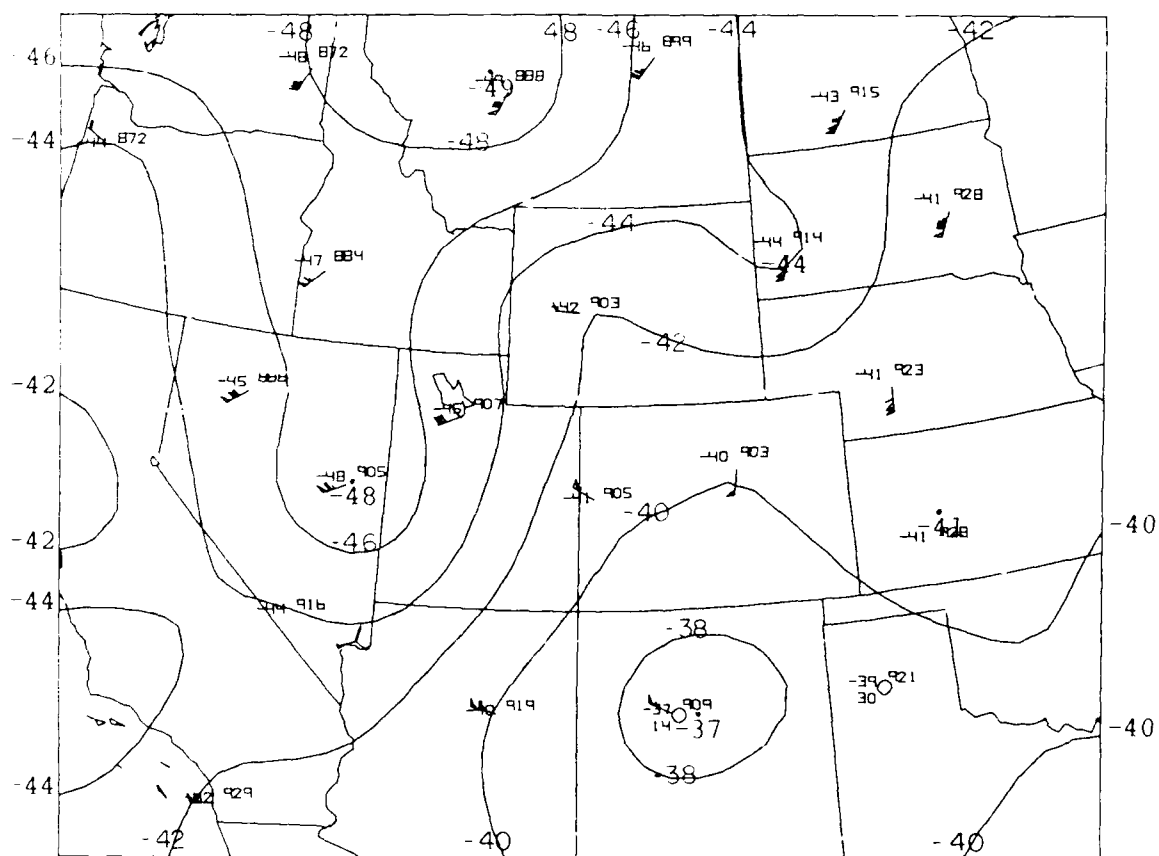
Figure 4.2.13. 300 mb observations and temperature analysis (°C), 0000 UTC 16 December 1984.

er front producing the sudden windshifts in mid-troposphere at Fleming, CO 3-5h later. There is no sign of the latter front at 300 mb.

Finally, the inspection of Figs. 4.2.10 and 4.2.13 suggests that the 300 mb vortex which moved over Fleming, CO, was very near the tropopause. It may have been largely affiliated with a descended statosphere in the region above the subsiding cold dome of the decayed tropospheric cutoff low.

It is rather clear that the availability of the Fleming, CO wind profiler data aided in the after-the-fact interpretation of the weather events of 16 December 1984. There can be little doubt that careful inspection of this type of data in real time would have been helpful to meteorologists preparing forecasts for regions north and east of Colorado on this occasion, and to the users of the forecasts. Knowledge of the exact magnitudes of wind variations of this sort can result in considerable fuel savings while only causing a flight track to be shifted by 100-200 km. Steinberg (1984) has stressed the need for this type of wind information for flight planning. Initialization of meso-scale numerical weather prediction models should also benefit from data of this type.

Another type of information that can be measured or inferred from profiler data is the location of regions of clear air turbu-lence (CAT). The onset of CAT is intimately related to the value of the non-dimensional parameter Ri, the Richardson number:

$$R_i = \frac{g}{\theta} \frac{\partial \theta}{\partial z} \left[\frac{\partial \bar{V}}{\partial z}\right]^{-2} \qquad , \qquad (4.1)$$

where θ is the potential temperature and g is the acceleration due to gravity. Turbulence is favored when Ri is small, owing primarily to strong vertical wind shear. If temperature soundings are available, it is possible to calculate Ri without ambiguity, and values of Ri of about 1 or less when calculated with synoptic-scale data usually are a good measure of a considerable potential for turbulence. If temperature sounding data is not available, it is still possible to estimate CAT regions by virtue of the greater sensitivity of Ri to wind shear than to static stability. For example, a recent, interpolated, forecasted, or even climatological temperature sounding can be used in conjunction with a continually updated wind profile.

Fig. 4.2.9 depicts regions of potential CAT painted black. They were deduced using the Fleming profiler gate-to-gate wind shear data and a climatological temperature profile. Using this approach, a vertical wind shear of about 11 ms^{-1} km^{-1} is indicative of a considerable risk of CAT in the troposphere. A value of about 20 ms^{-1} km^{-1} is indicative of a significant potential for CAT in the stratosphere. These values are slightly higher (i.e., less conservative) than the minimum values often used in the aviation community to signify the onset of turbulence.

4.3. Wind Field Structure in the Tail of a Comma Cloud

The extreme southern end of the tail of a comma cloud pattern passed over the McAlevy's Fort profiler at about 1000 UTC on 19 August 1985. The comma cloud can be seen over eastern Pennsylvania a few hours later in Figure 4.3.1.

Figure 4.3.1. Visible satellite image from 1731 UTC 19 August 1985.

Although the feature was rather distinct in satellite im-
agery, it was not associated with a very spectacular wind field,
as can be seen from Figure 4.3.2. Upon close inspection of the
section from about 0600-1300 UTC, it can be seen that the tail of
the comma cloud was accompanied by a weak trough.

A time-height section of isogons (isopleths of wind direc-
tion), Figure 4.3.3, makes the pattern of wind variations more
apparent. It can be seen that the approach of the comma tail was
accompanied by a backing in the wind field from northwesterlies
to westerlies, followed by a rapid 30-50 degree clockwise shift
(veering) of the wind as the rear (west) edge of the comma tail
passed to the east.

A time-height section of the wind speed, Figure 4.3.4, shows
that the tail of the comma cloud was accompanied by a wind speed
maximum at 0900 UTC in a layer from 7-9 km. The wind field pat-
terns of Figs. 4.3.3 and 4.3.4 suggest that the trough line was
nearly vertical from the surface to the upper troposphere. It
may even have leaned forward with height, since the winds at 9
km shifted from having a northerly component to a southerly com-
ponent about 2 hours before those in mid-troposphere (Figs. 4.3.2
and 4.3.3). Since meteorologists have been trained that troughs
tilt westward with height, the patterns in Figs. 4.3.3 and 4.3.4
are rather unexpected. One suspects that the time of the wind
shifts aloft in this case are likely to have been forecasted too
late in the absence of wind profiler data.

Upper-air analyses indicated that the trough was farther to
the west. Figure 4.3.5 shows that the 300 mb streamline analysis
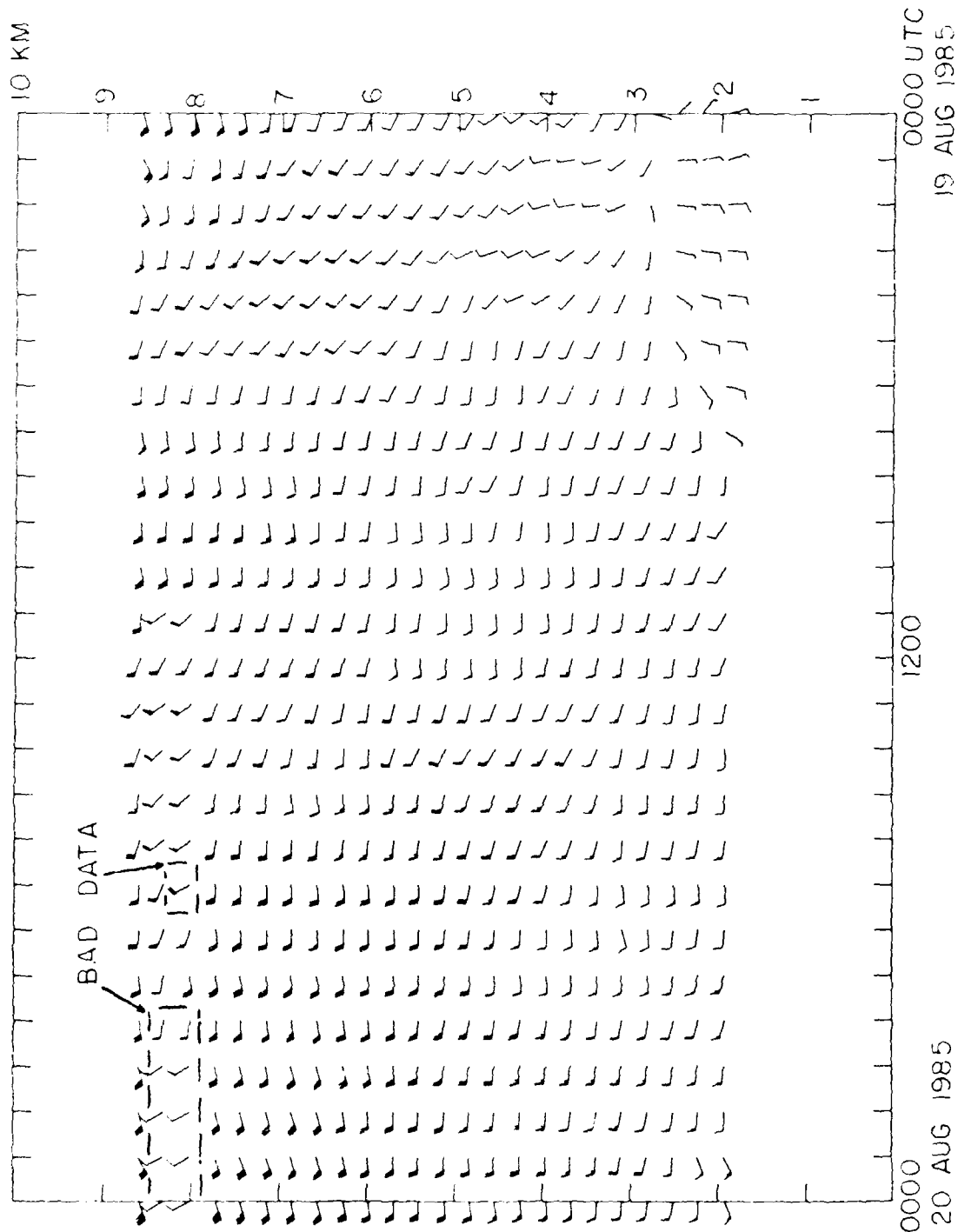
Figure 4.3.2., Time-height section of winds from the McAlevy's Fort, PA wind profiler on 19-20 August 1985. A full barb represents 10 kts (about 5 m/s), and a pennant represents 50 kts (about 25 m/s). Observations likely to be contaminated by noise are not indicated. Vertical velocities are not indicated; a wind vector pointing toward the top of the diagram is blowing from the south.
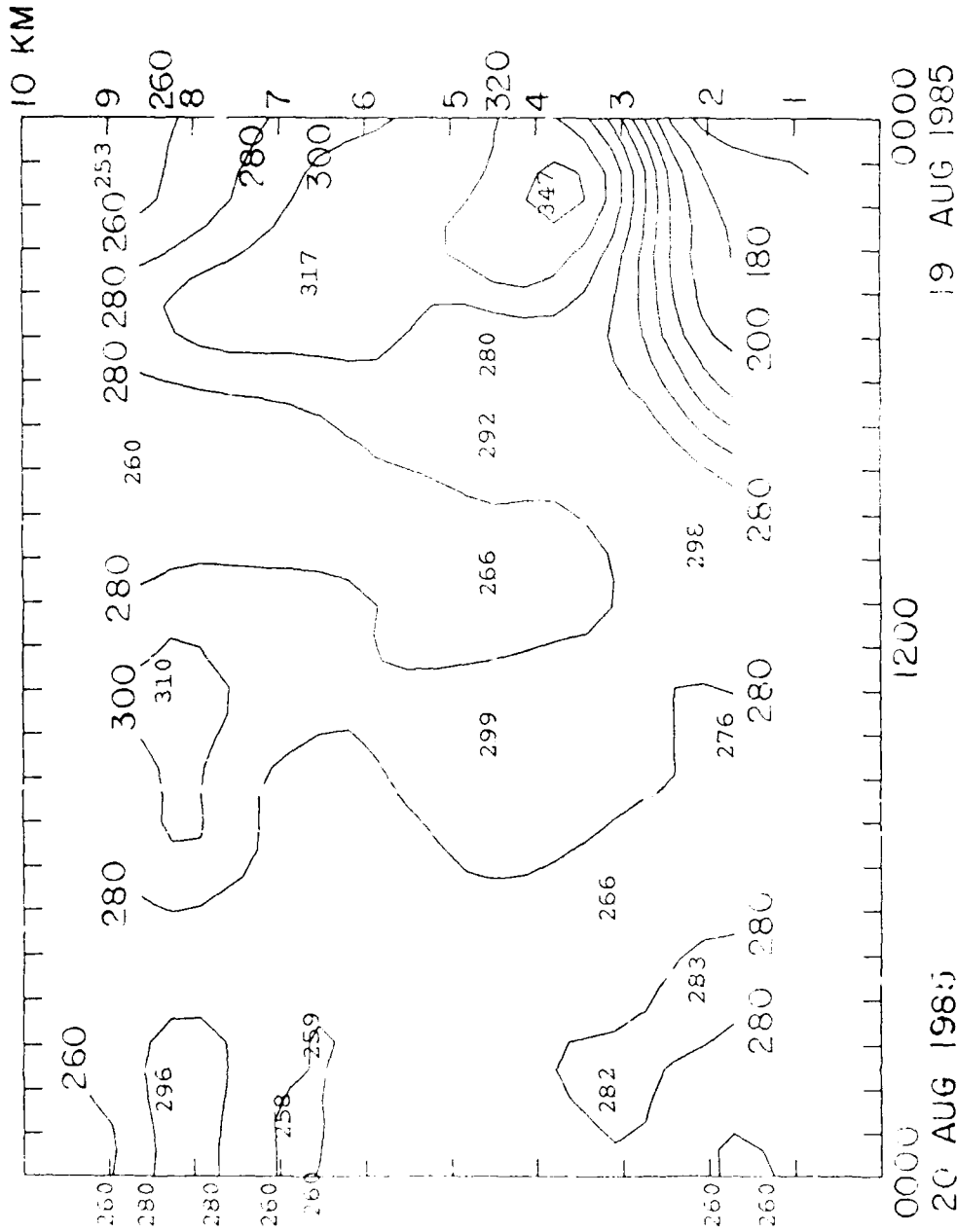
Figure 4.3.3. Analysis of wind direction (isogons at 20° azimuth intervals) corresponding to Fig. 4.3.2.
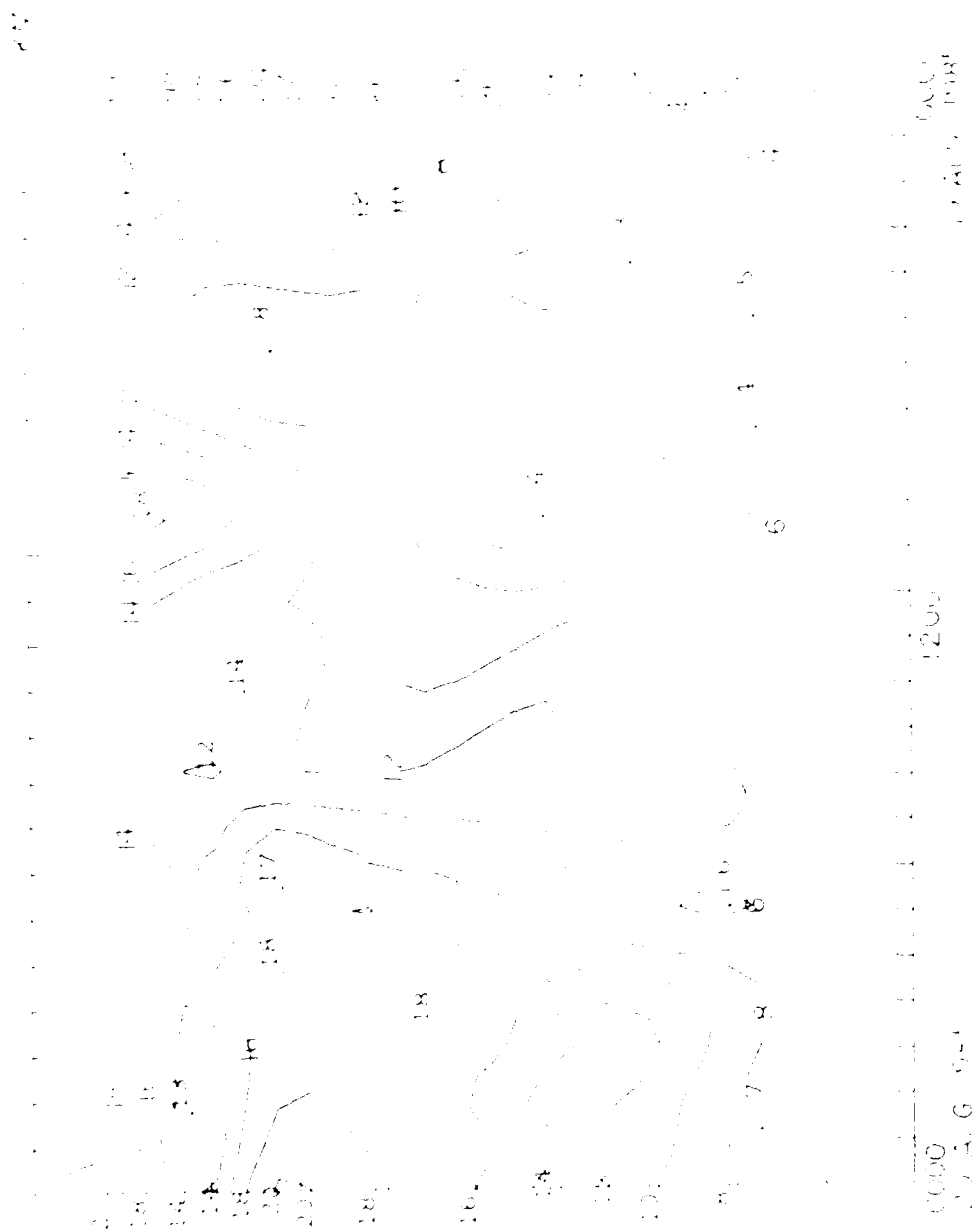
Figure 4.3.4. Analysis of wind speed (2 m/s intervals) corresponding to Fig. 4.3.2.

constructed from rawinsonde data alone yielded a trough axis located about 200 km west of its true location. The analysis using wind profiler data is shown for comparison in Figure 4.3.6. A trough is induced over Central PA, along with a ridge over western PA. This represents a rather short wavelength of only about 600 km; less than can be resolved with rawinsonde data. The satellite image of Fig. 4.3.1 lends credence to this wavelength, as the trough portion of another comma cloud system can be seen near Lake Superior.

With short-wavelength features present and only rawinsonde data available outside of central PA, however, the analysis of Fig. 4.3.6 becomes more suspect the further away one looks from central PA. The confluence zone in southeastern PA is suspect. While a confluence zone is expected when a comma cloud tail is present, this location is not a good match. The tail of the comma cloud is usually in the confluence zone, and in this case the confluence zone should probably extend from eastern NY southwestward to be affiliated with the trough detected by the profiler.

Figure 4.3.7 is an analysis of the pressures of the 330oK isentropic surface and the streamlines of flow within it, relative to the travelling comma cloud system. The relative winds, as usual, exaggerate the confluence, and bring the confluence zone somewhat westward. Inclusion of wind profiler data is likely to have improved the analysis by bringing the confluence zone even more westward. Nevertheless, the orientation of the relative streamlines with the isobars help to explain the exist-
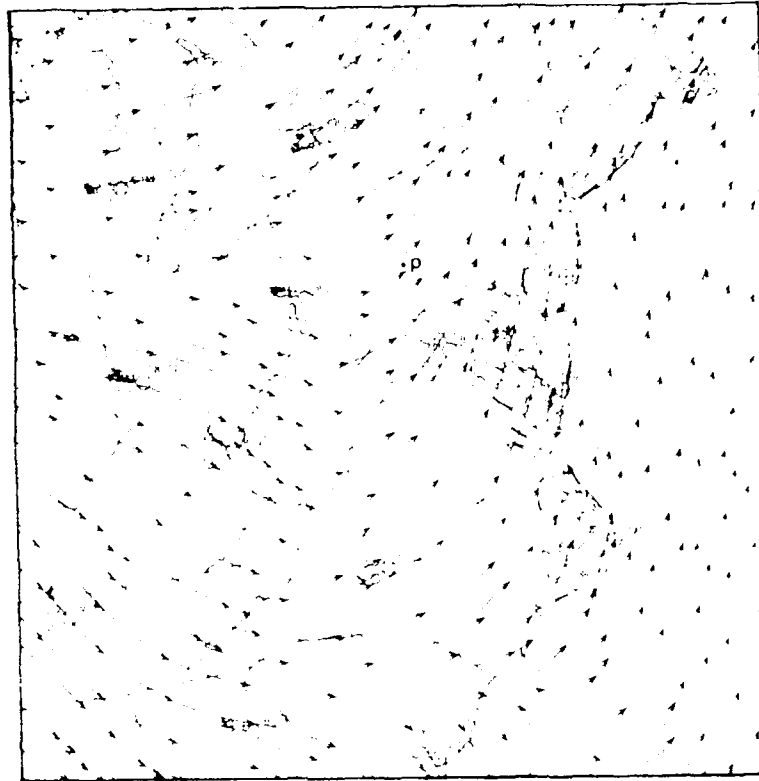
Figure 4.3.5. 300 mb rawinsonde observations and streamlines for 1200 UTC 19 August 1985. Wind profiler location is marked by "p", but data are not included in the streamline analysis.
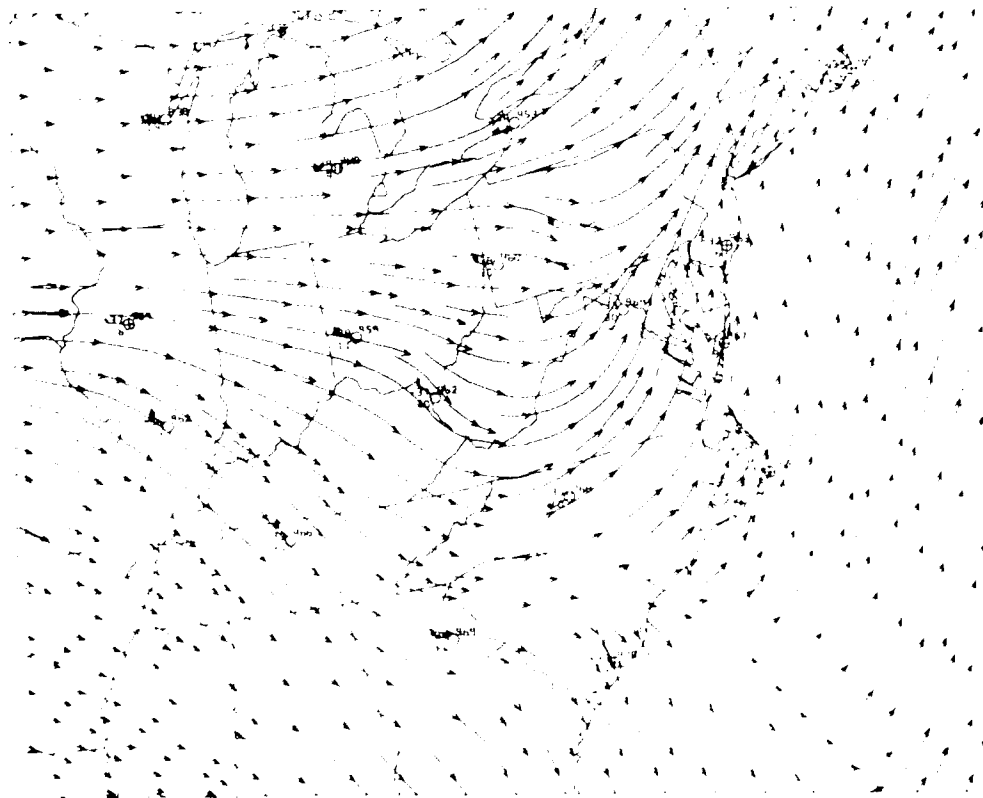
Figure 4.3.6. 300 mb rawinsonde observations, hourly profiler winds, and streamlines for 1200 UTC 19 August 1985. In contrast to Fig. 4.3.5, profiler data are now included in the streamline analysis.

ence of a comma cloud tail in the region. The streamlines ascend from about a pressure of greater than 400 mb to a pressure somewhat less than 350 mb across ext me eastern PA, NJ, and New England. This sloping ascent is typical of the warm conveyor belt of the tail of a comma cloud system.

Figure 4.3.8 is an analysis of the pressures of the 310ok isentropic surface and the streamlines of flow within it. There is again a marked confluence zone, but this time located over north central PA, central NY, and northward. Inclusion of the profiler winds is likely to have extended the confluence zone into central PA.

Equally noticeable in Fig. 4.3.8, however, is a diffluence zone over southeastern PA, which is at about the 700 mb level. This diffluence region at low levels in the region south of the confluent region aloft is quite atypical of comma tail and warm conveyor belt structure. Undoubtedly this helps to explain the rather abrupt end to the tail of the comma cloud over Pennsylvania in Fig. 4.3.1. Additionally, a satellite picture a few hours later, Figure 4.3.9, indicates that the tail was weakening with time as it moved eastward.

The tail of a developing or strong, mature comma cloud more typically extends southward at least to 35oN, and often into the subtropics. In well-defined comma cloud tails, there is a marked confluence zone extending into the top of the planetary or marine boundary layer (PBL or MBL) at low latitudes that feeds a plume of moist PBL (often MBL) air into the warm conveyor belt that comprises the tail of the synoptic-scale comma cloud. The air
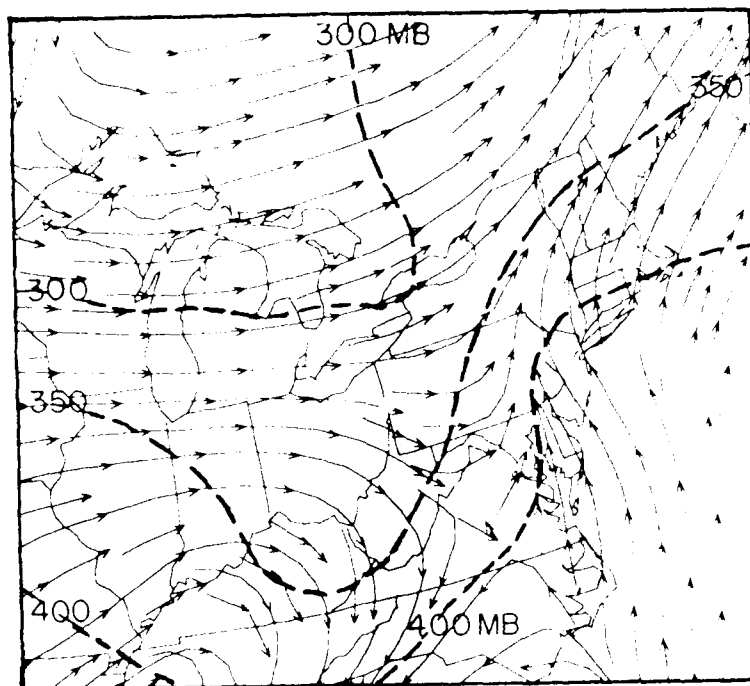
Figure 4.3.7. Analysis of the pressure levels (mb) of the 330°K potential temperature surface (dashed), and streamlines of the relative wind on this surface (with respect to the travelling upper-air disturbance). Based upon conventional rawinsonde data.
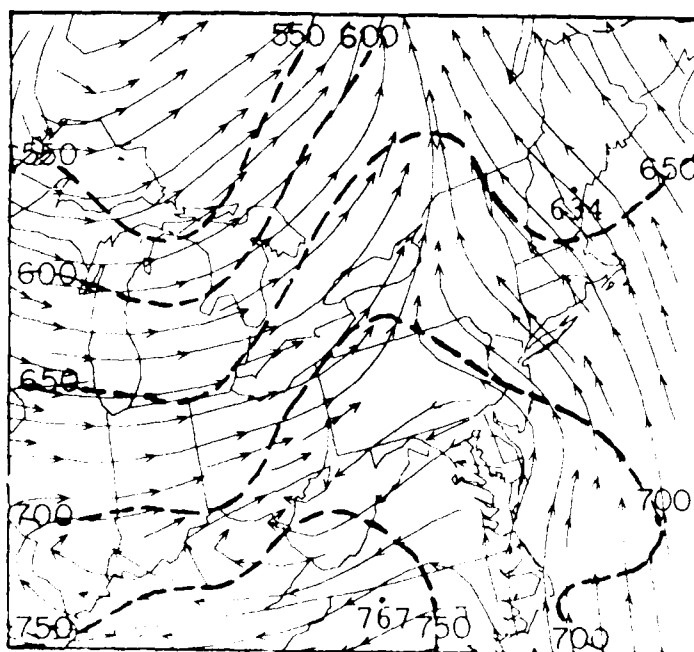
Figure 4.3.8. Analysis of the pressure levels (mb) of the 310°K potential temperature surface (dashed), and streamlines of the relative wind on this surface (with respect to the travelling upper-air disturbance). Based upon conventional rawinsonde data.

2001 19AU85 38A-1 01977 24312 DA3
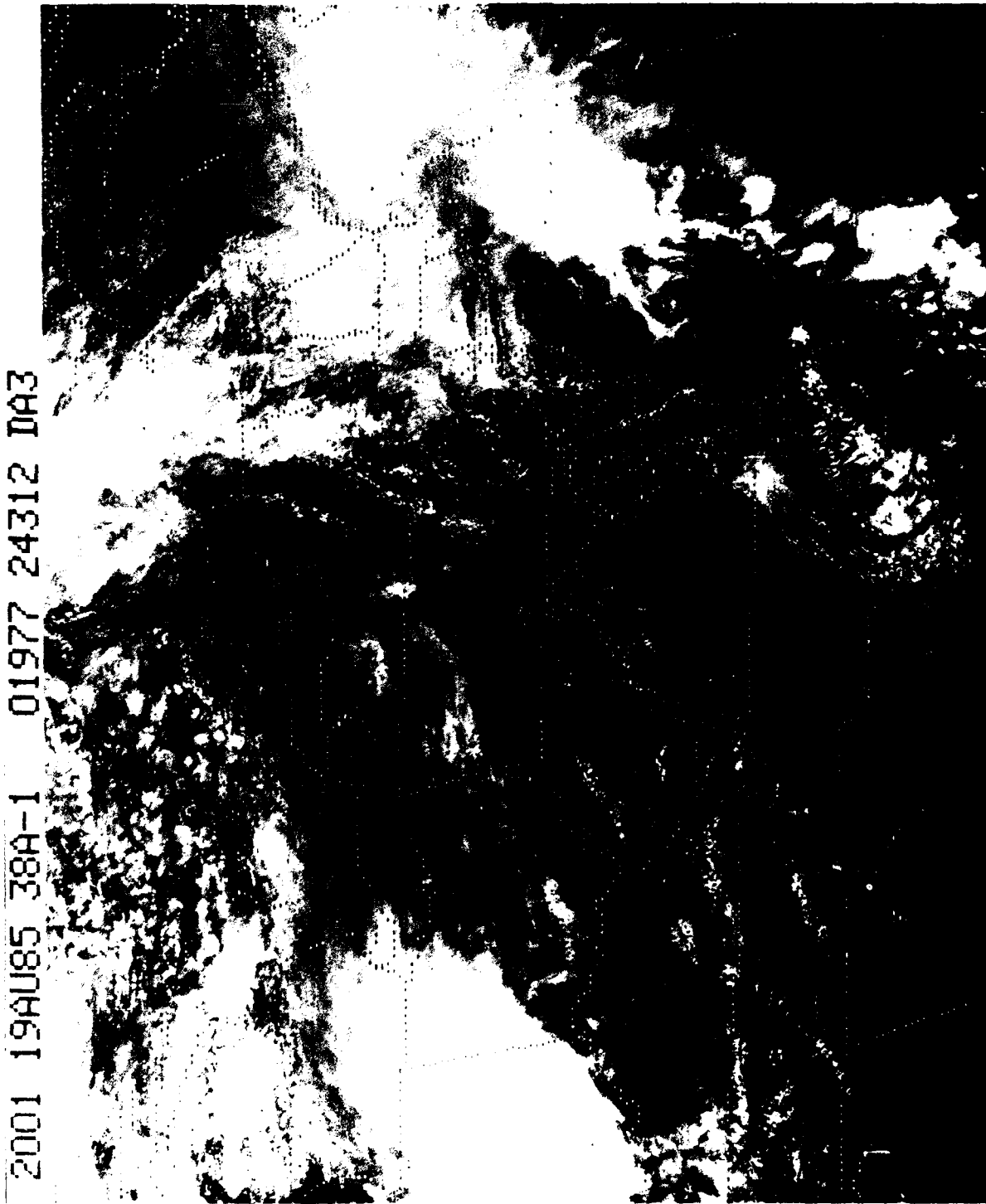
Figure 4.3.9. Visible satellite image at 2001 UTC 19 August 1985.

ascends as it travels northward, reaching the jet stream level farther to the north. In the case of 19 August, the low-level confluence did not begin until 41° N, so that the comma tail and warm conveyor belt tail began there.

Some of the abnormality of this case may be related to events transpiring just off the East Coast. Fig. 4.3.1 shows that there is a disturbance off Delaware, and Fig. 4.3.9 shows a definite circulation center there.

Figure 4.3.10 shows the surface analysis at 1200 UTC. There is, indeed, a cyclone center offshore. Even at this later time, 2-4 hours after the trough line and wind speed maximum passed over McAlevy's Fort, PA, the surface cold (or occluded) front has barely passed the profiler site, if at all. This bears out the forward tilt with height indicated in Fig. 4.3.2. While a full explanation is beyond the scope of this example, it is quite common that when secondary coastal cyclogenesis is occurring the upper-level weather systems leave their original surface front and pressure trough behind, and shift eastward to support the coastal cyclone. However, the coastal cyclogenesis is clearly beyond the range of diagnosis using the Penn State wind profiler.

What is clear from Fig. 4.3.9 is that drier air has invaded Pennsylvania by afternoon. This dry air was already present over Pittsburgh, PA at 1200 UTC, as can be seen from Figure 4.3.11. This shows up in the powers received by the wind profiler, Figure 4.3.12, which peaked at about 1000 UTC at 6km and at about 1200 UTC at 3 km. Powers dropped to a mimimum at about 1800 UTC and rose thereafter, probably in association with some cirrus and
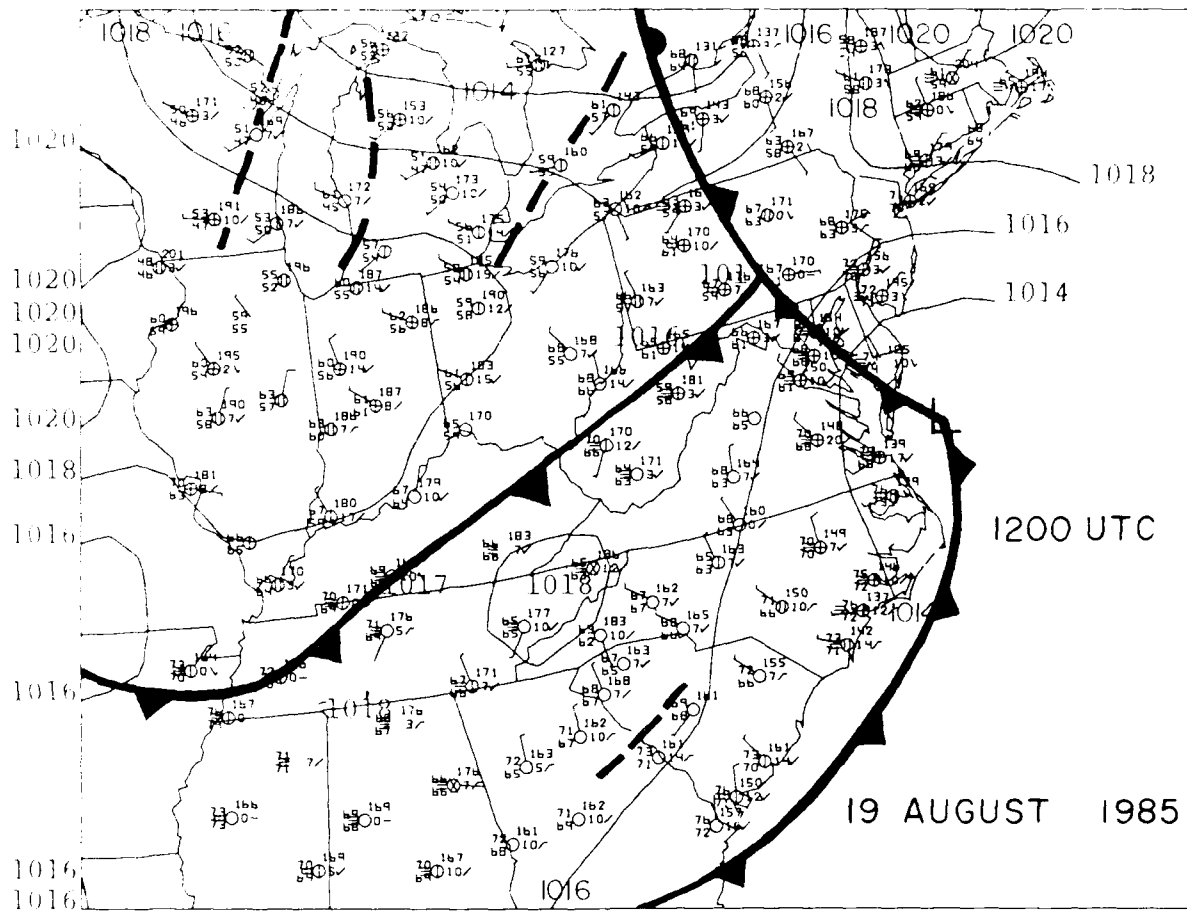
Figure 4.3.10. Surface observations, fronts, trough lines, and sea-level pressure analysis (2 mb intervals, solid lines) for 1200 UTC 19 August 1985.

P	T	TD	RH	HT	WS	WD
100	-63			540	23	250
115	-65			500	29	260
150	-61			480	40	270
219	-47			420	49	250
300	-38	-68	2	390	36	245
390	-22	-52	4	370	44	275
500	-8	-38	6	350	37	265
567	-3	-11	53	340	32	265
601	1	-29	8	320	31	290
636	4	-6	47	300	32	290
700	8	-22	9	260	35	290
754	12	-18	10	250	37	285
773	12	8	76	210	32	275
825	15	9	67	200	34	275
850	14	13	93	160	35	290
974	18	17	93	140	34	285
				120	37	285
				90	21	280
				80	24	275
				70	26	270
				60	26	265
				40	15	275
				30	8	310
				20	8	320
				00	1	300

STATION: 72520
12Z 19-AU-85

Figure 4.3.11. Skew-T log P diagram of temperature (^oC, heavy line) and dew point (^oC, thin line) for Pittsburgh, PA at 1200 UTC 19 August 1985. Conventions as in Fig. 4.2.5 .
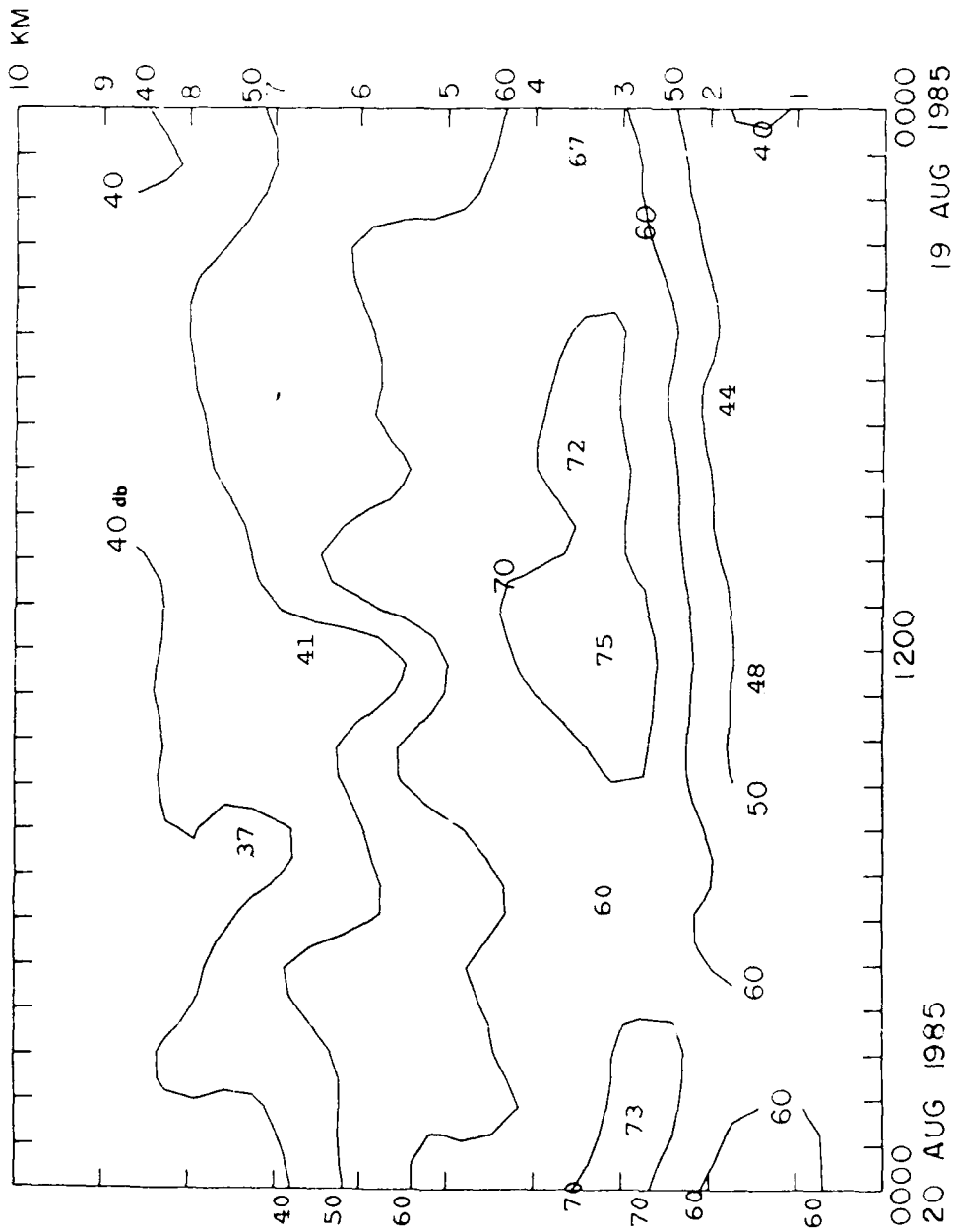
Figure 4.3 12. Time-height section of the wind profiler returned power (db), corresponding to Fig. 4.3.5.

middle clouds seen entering western and north-central PA in Fig. 4.3.9. This is an example of the profiler power-humidity relationship mentioned previously.

4.4 Structure of Unexpected Minor Trough and Cloud Band

During the morning hours of 19 September 1985 an unexpected thin patch of clouds drifted across central PA. These accompanied a rather dramatic pattern of wind shifts shown in Figure 4.4.1. The clouds occurred near the axis and to the rear of a minor short-wave trough at the 3-5 km levels, from about 0500-1300 UTC.

A careful inspection of the wind directions on Fig. 4.4.1 actually shows two wind shifts. The first wind shift is a minor and temporary shift at all levels in the 3-5.5 km layer at about 2000-2100 UTC on 18 September, sloping down to the 2 km level at between 1900 and 2000 UTC, and sloping up to 6km at about 0000 UTC 19 September. No well-defined wind shift can be found above 6 km, although the isogon pattern suggests a shift there at about 0500 UTC.

The second and more substantial shift began a few hours later. The data suggests that the second windshift was associated with a trough whose axis was tilted, passing the 2 km level at 2200 UTC, the 3 km level at 2300 UTC 18 September and the 4 km level at 0000 UTC 19 September. At the 5 km level there appears to be a shift at 0000 UTC and again at 0400 UTC on 19 September, suggesting that the trough (i.e., the second wind shift) may have become nearly horizontal at about that level.

112
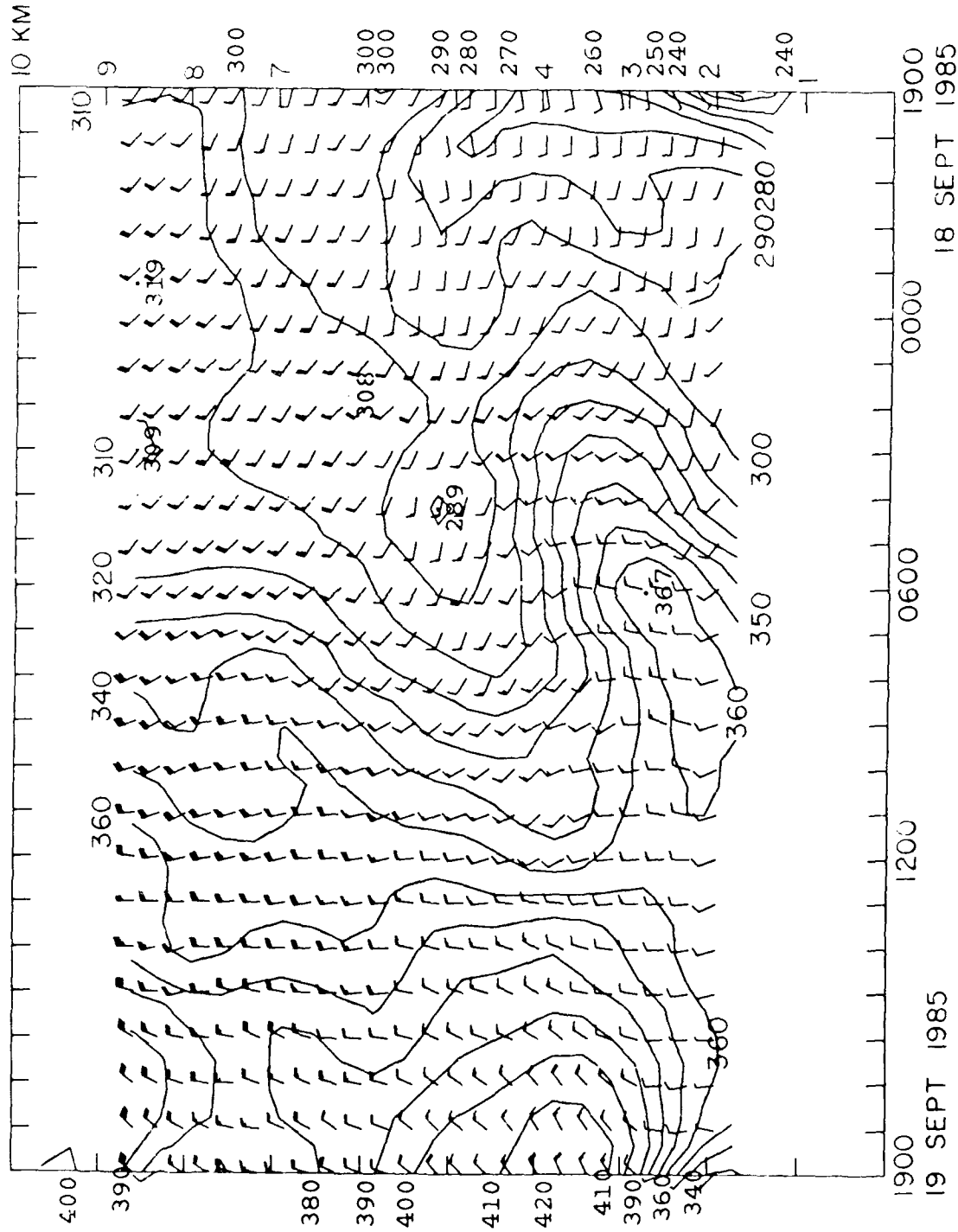
Figure 4.4.1. Time-height section of the profiler winds at McAlevy's Fort, PA on 18-19 September 1985. Solid lines are isogons at 10° azimuth intervals. To avoid excess contours where winds shift from northwest to northeast, wind directions from east of north have been depicted as greater than 360°. Wind barbs are in knots.

The approach and passage of the trough (i.e., second wind-shift) was marked by a shift of the winds from northwesterly to almost westerly before veering back to north. Following the passage of the axis of the trough at about 0400 UTC at 5 km, wind speeds increased at levels above 5 km, as shown in Figure 4.4.2. It is not clear whether these increases were associated with a diffuse upward extension of the first wind shift, an extension of the second wind shift, or a combination of both.

There was no reason to expect multiple windshifts or a distinct trough based upon the 0000 UTC upper-air charts, unless wind profiler data were included. The winds and streamlines at 500 mb, Fig. 4.4.3, do indicate a trough near Flint, MI, but the curvature of the streams is quite large and, accordingly, the trough rather weak. The profiler winds, inserted via time-space conversion, force a trough into northwestern PA on a scale smaller than could be resolved with the rawinsonde network.

Figure 4.4.4 shows the 500 mb data and streamlines 12h later, at 1200 UTC 19 September. A trough can now be more readily detected, from Massachusetts into southeastern PA. It is embedded within northwesterly flow and heading southeastward at this time, having previously apparently travelled eastward across southern MI along the northern flank of an impressive anticyclone centered over southern IL.

In this case, as in previous examples, the time-space converted profiler winds make a perfect fit with the rawinsonde data if and only if it is realized that there was actually some mesoscale trough moving through the region. If one presumed that

114
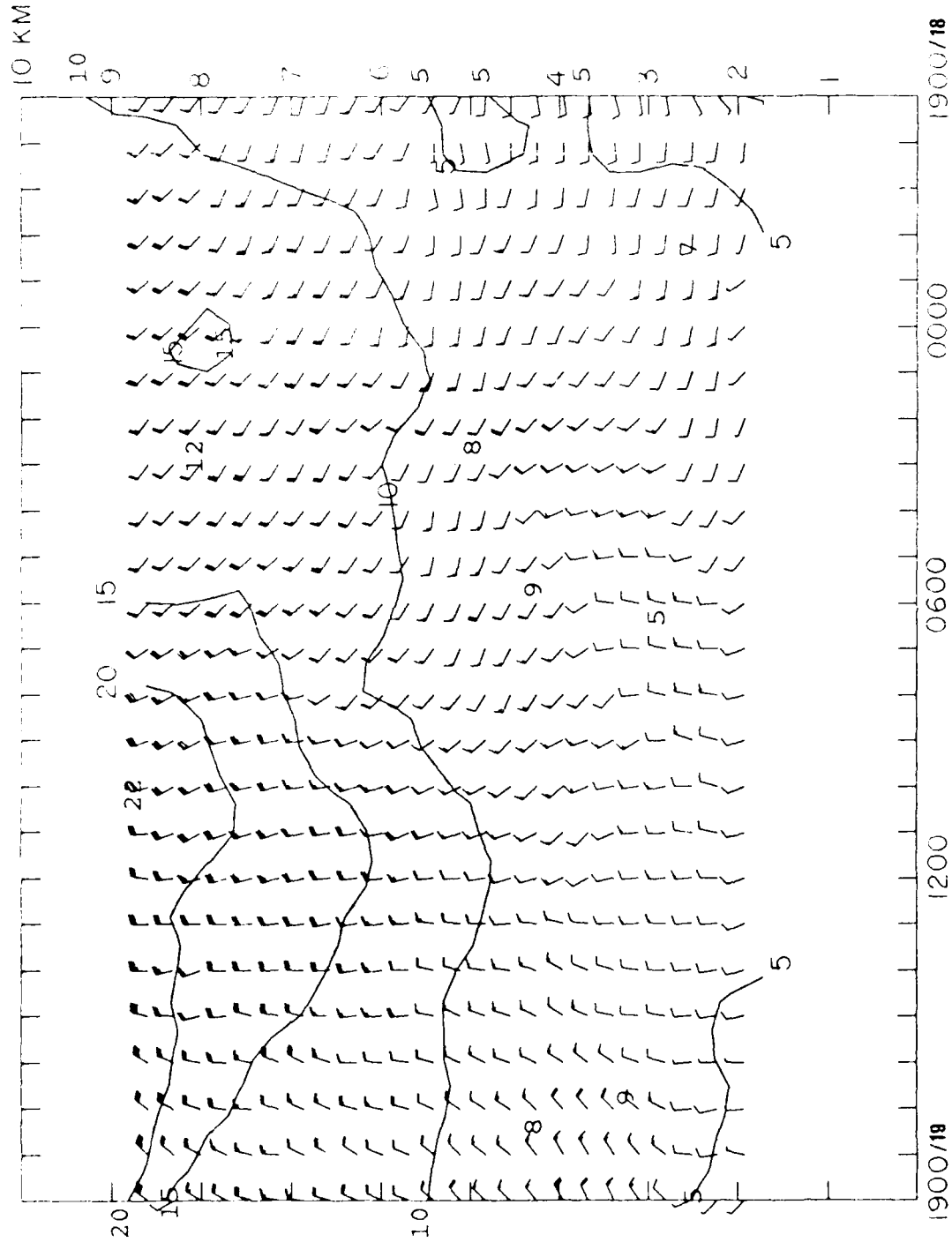
Figure 4.4.2. Time-height section of the profiler winds and isotachs (m/s) at McAlevy's Fort, PA on 18-19 September 1985, corresponding to Fig. 4.4.1.
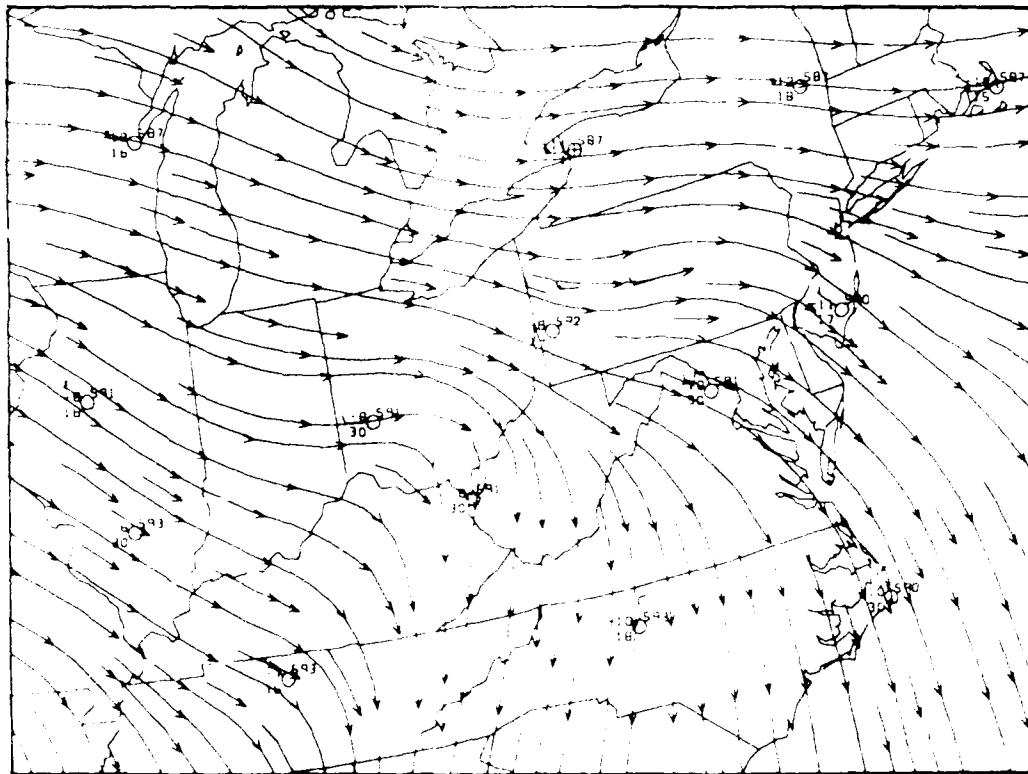
Figure 4.4.3.   500 mb rawinsonde observations, hourly profiler winds, and streamlines at 0000 UTC 19 September 1985.
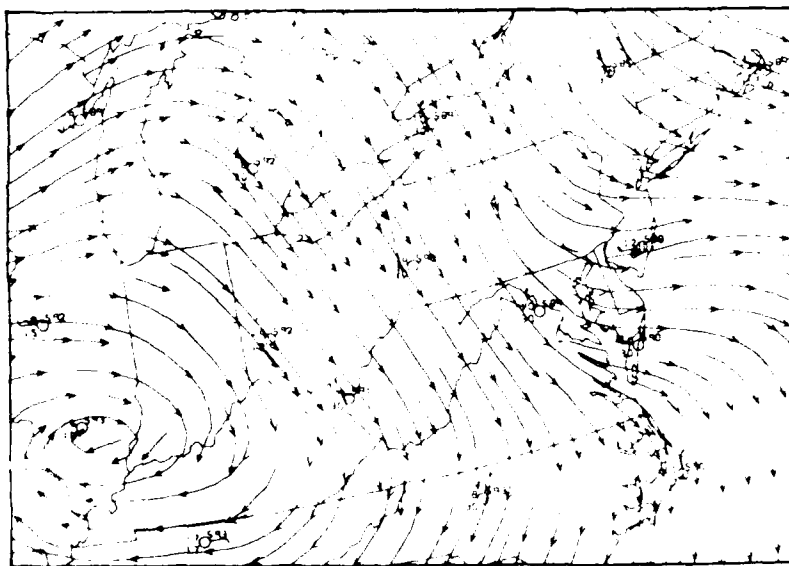
Figure 4.4.4.   500 mb rawinsonde observations, hourly profiler winds, and streamlines at 1200 UTC 19 September 1985.

there were only synoptic-scale waves present, the profiler winds of Figs. 4.4.3 and 4.4.4 would appear to be in error! Had the meteorologist not witnessed the passage of an unexpected patch of clouds, and relied on the surface chart in Figure 4.4.5, he or she might have overlooked the broken or overcast skies at three reporting stations in northern and central PA and western NY, and presumed that all was tranquil aloft so near the center of the surface anticyclone.

Some profiler-derived thermodynamic data are displayed in Figure 4.4.6 and subsequent figures. Fig. 4.4.6 is a plot of profiler-derived temperature advection tendencies from the 0500-0600 UTC 19 September hourly wind profiler data. Subject to the validity of the thermal wind, cold advection is indicated between 3km and 5km, near 7 km, and above 8 km. Warm advection is indicated below 3 km and near 6 km. These diagnoses compare favorably with the 12h temperature changes at Pittsburgh, PA ending at 1200 UTC 19 September, Figure 4.4.7, with the exception of the "spike" of cold advection near 7 km. Temperatures at Pittsburgh decreased from about 750 to 550 mb (2.5 5 km), and increased from about 550 to 230 mb (5-11 km).

A hodograph of the McAlevy's Fort profiler low-resolution winds is shown in Figure 4.4.8. Backing and veering of the wind correspond to cold and warm advections, respectively, by thermal wind assumptions discussed in Section 3.2. Veering between hodograph points 9 and 11, corresponding to 9.8-11.6 km, therefore, represents warm temperature advection. This agrees well with the warming observed at Pittsburgh from 550 to 230 mb. Further

Figure 4.4.5. Surface observations and sea level pressure analysis (2 mb intervals) for 1200 UTC 19 September 1985.
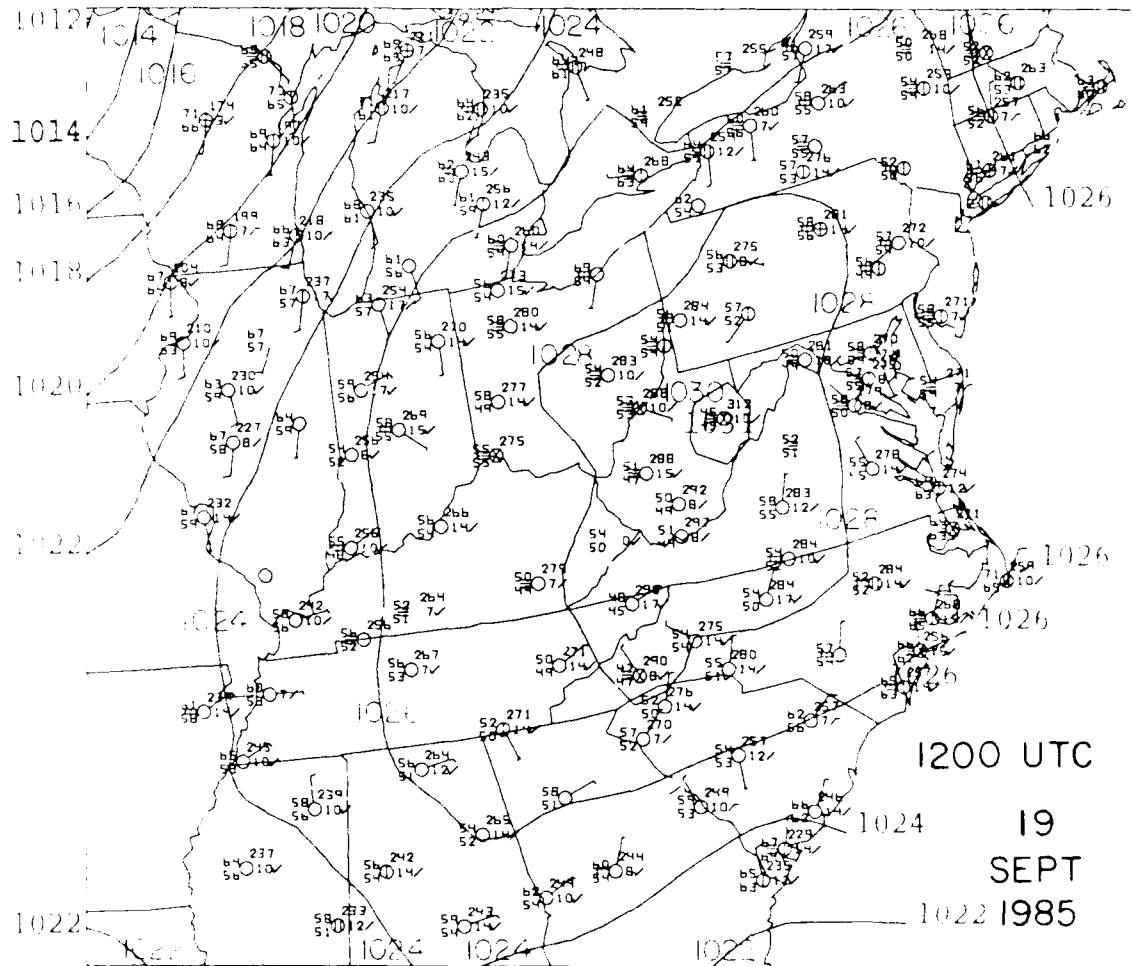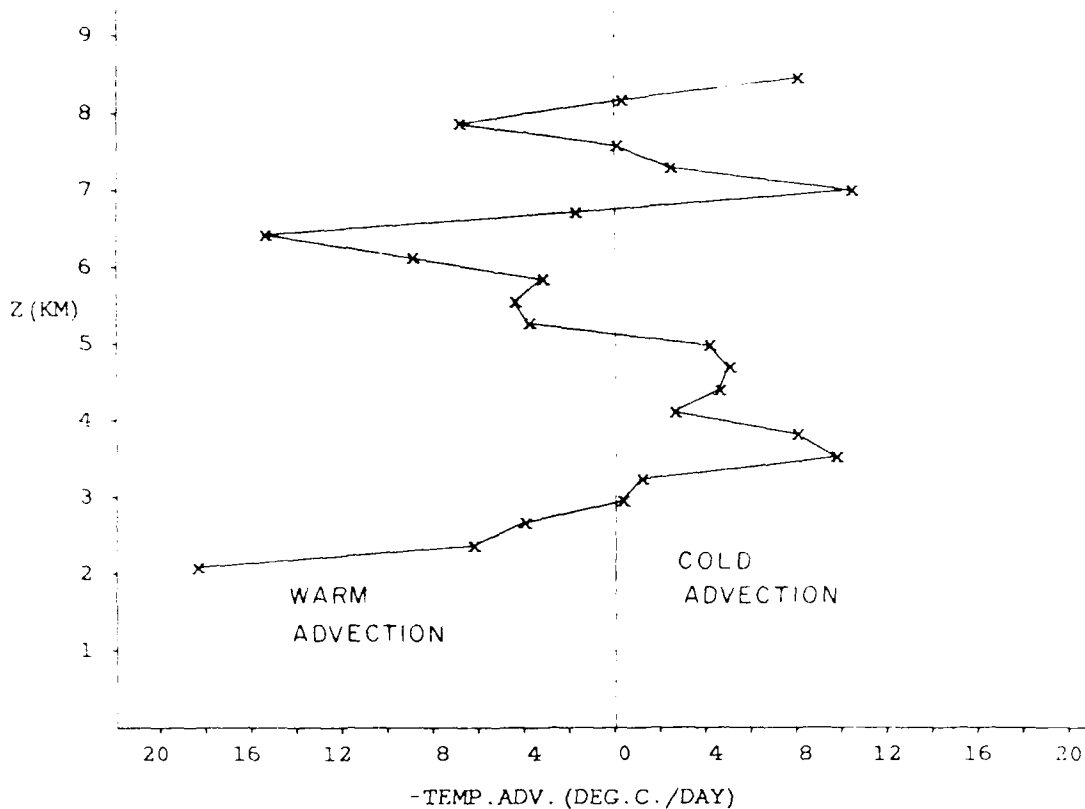
Figure 4.4.6. Vertical profile of wind-profiler-derived temperature advection ($^{\circ}$C per day).

P	T	TD	RH	HT	WS	WD
100	-66					
105	-68					
139	-67					
222	-52					
289	-39	-53	20			
300	-37	-67	2			
367	-25	-55	4			
500	-9	-39	6			
556	-6	-24	22			
729	8	-7	33			
743	8	2	65			
762	8	6	87			
800	10	7	81			
929	19	10	55			
970	21	13	60			
985	15	9	67			
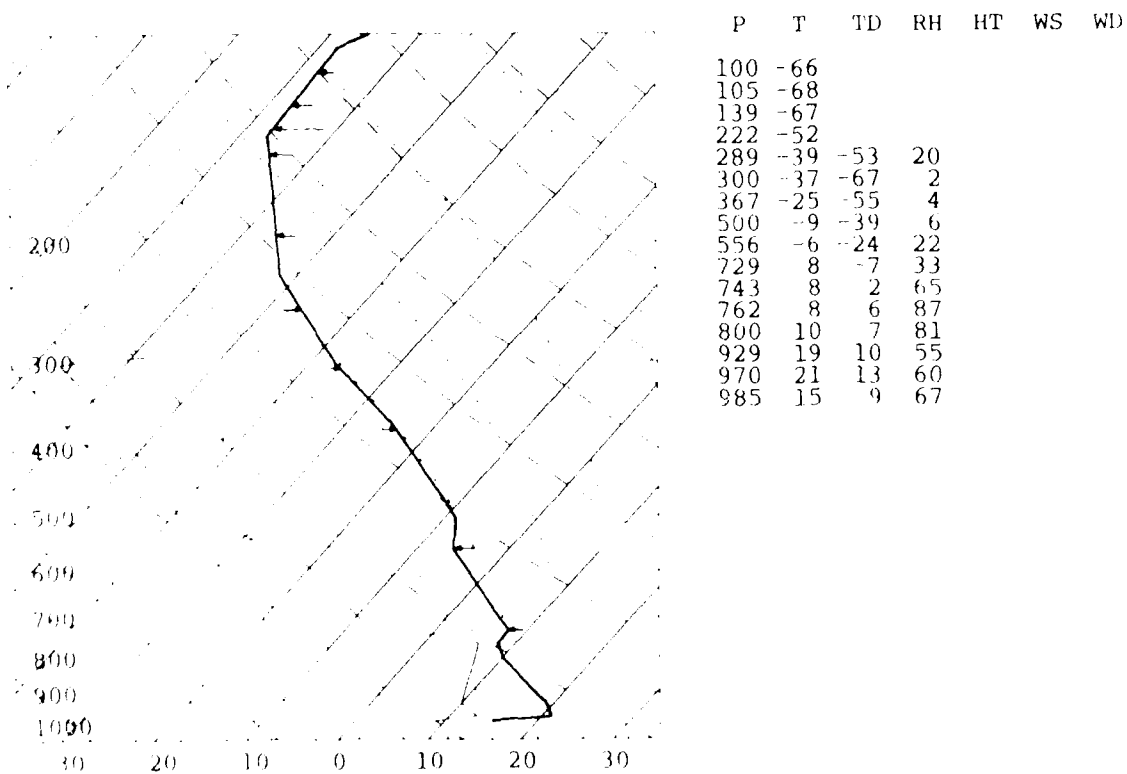
Figure 4.4.7. Skew-T log P diagram of rawinsonde temperatures (heavy line) and dew points (thin line) from Pittsburgh, PA at 1200 UTC on 19 September 1985. Arrows indicate change of temperature at selected altitudes since 0000 UTC 19 September.

HEIGHTS	POINT
2.8	1
4.6	3
6.3	5
8.1	7
9.8	9
11.6	11
13.3	13
15.0	15
16.8	17

5   10   15   20   25   30   35 M/S
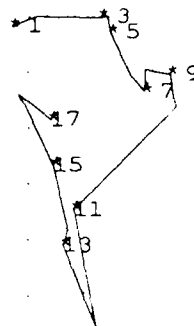
FAR RANGE

SE198506
SCALE=5M/S

Figure 4.4.8.   Hodograph of low-resolution profiler hourly winds from McAlevy's Fort at 0600 UTC on 19 September 1985.   Table at upper right relates numbers along hodograph to altitudes (in km).

Z (KM)

60   50   40   30   20   10   0   10   20   30   40   50   60

(-)   VCOMP SPEED (M/S)   (+)
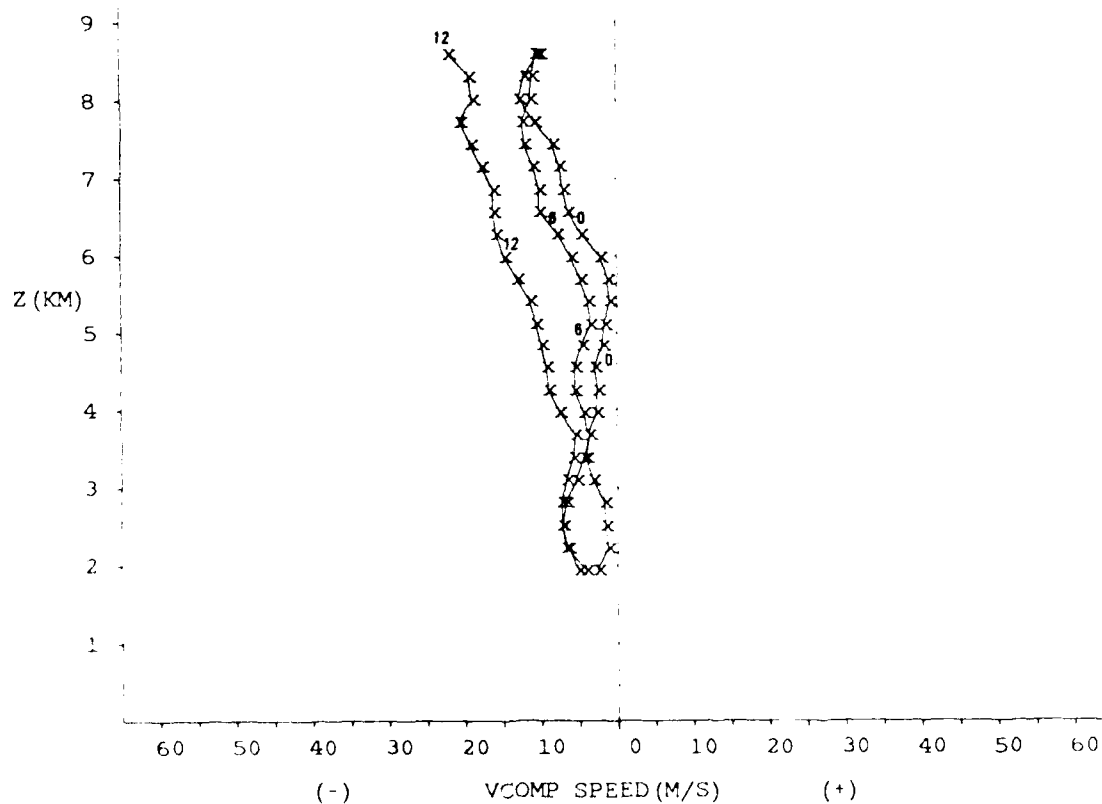
Figure 4.4.9.   Vertical profile of the evolution of the V component (m/s, southerlies positive) of the profiler winds at McAlevy's Fort, PA on 19 September 1985.   Numbers along the profiles   indicate the hour in UTC.

aloft, Pittsburgh cooled, while there were layers of near-zero advection, slight warm advection, and slight cold advection manifested by the hodograph.

Several other profiler displays, Figures 4.4.9 and 4.4.10, indicate that the temporal changes measured by the McAlevy's Fort wind profiler were not very noisy. Sequential profilers of the v component, Fig. 4.4.9, are well correlated, showing inflection points at approximately the same altitudes and changing altitude only slowly. A time series of the u component at 5.12 km shows a curve largely free of fluctuations having a two-hour period, which would have been characteristic of a random noise signal.

4.5 Wind Structure of Jet Stream and Warm Conveyor Belt

The rear edge of a warm conveyor belt cloud pattern passed over the McAlevy's Fort profiler at about 1200 UTC on 20 August 1985. Figure 4.5.1 shows the satellite picture a few hours earlier, when middle and high clouds were over the profiler site. While the cloud pattern was not extremely organized, that is often true during the summer season.

Figure 4.5.2 shows the time-height section of high-resolution profiler winds on 20-21 August 1985. At first glance the most noticeable features are noise in the upper left and right sections of the diagram. Closer inspection, however, shows that winds veered from southwesterly to westerly at all altitudes near the center time of the diagram. Wind speed changes are harder to inspect, by virtue of the small size of the flags.

Figure 4.5.3 shows the isotach field corresponding to Fig.
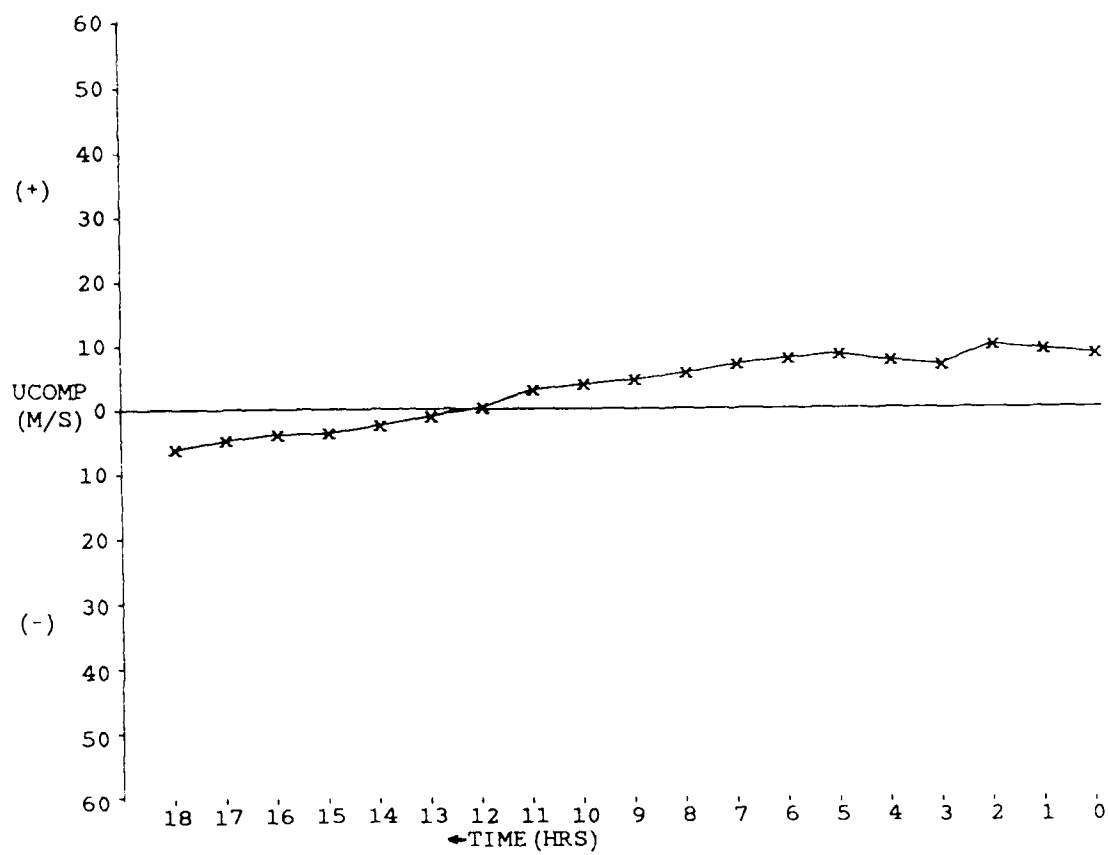
Figure 4.4.10. Time series of the U (m/s, westerlies positive) component of the profiler wind at McAlevy's Fort, PA on 19 September 1985.

0901 30AU85 IUE-IIB 01501 24772 DE1
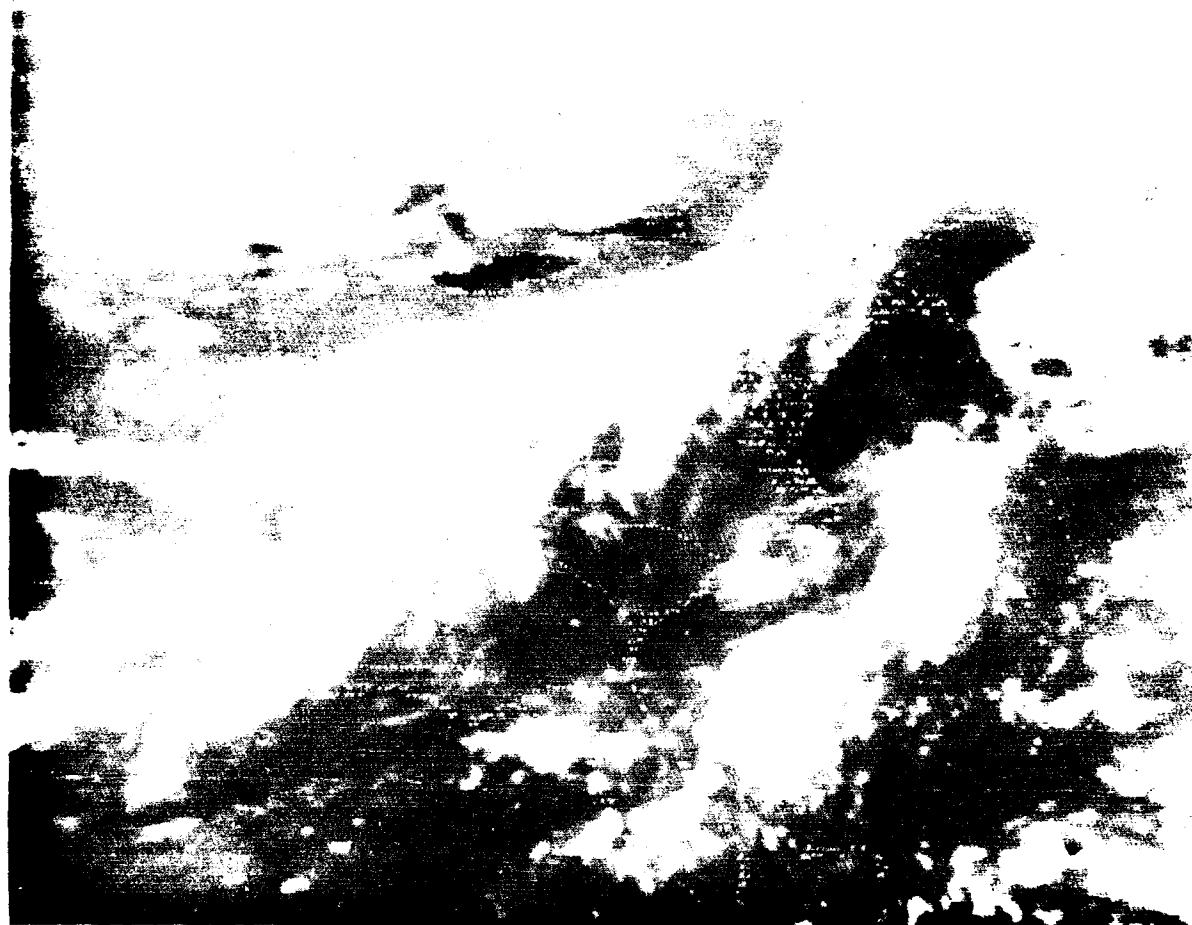
Figure 4.5.1. Enhanced infrared satellite imagery from 0901 UTC 20 August 1985.
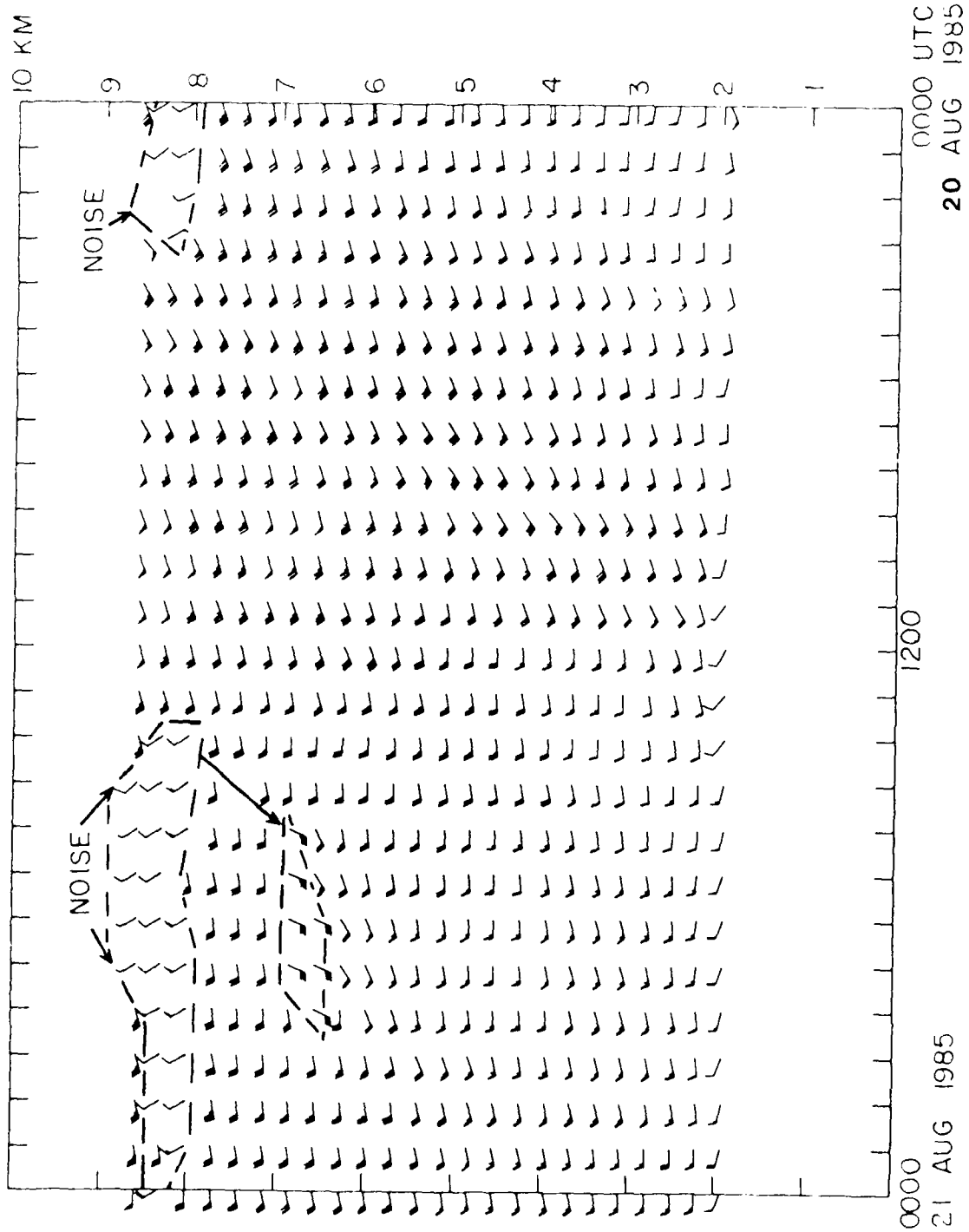
Figure 4.5.2. Time-height section of profiler winds from McAlevy's Fort, PA on 20-21 August 1985. A full barb represents 10 kts (about 5 m/s) and a pennant signifies 50 kts (about 25 m/s). Erroneous winds (noise) are indicated.

124
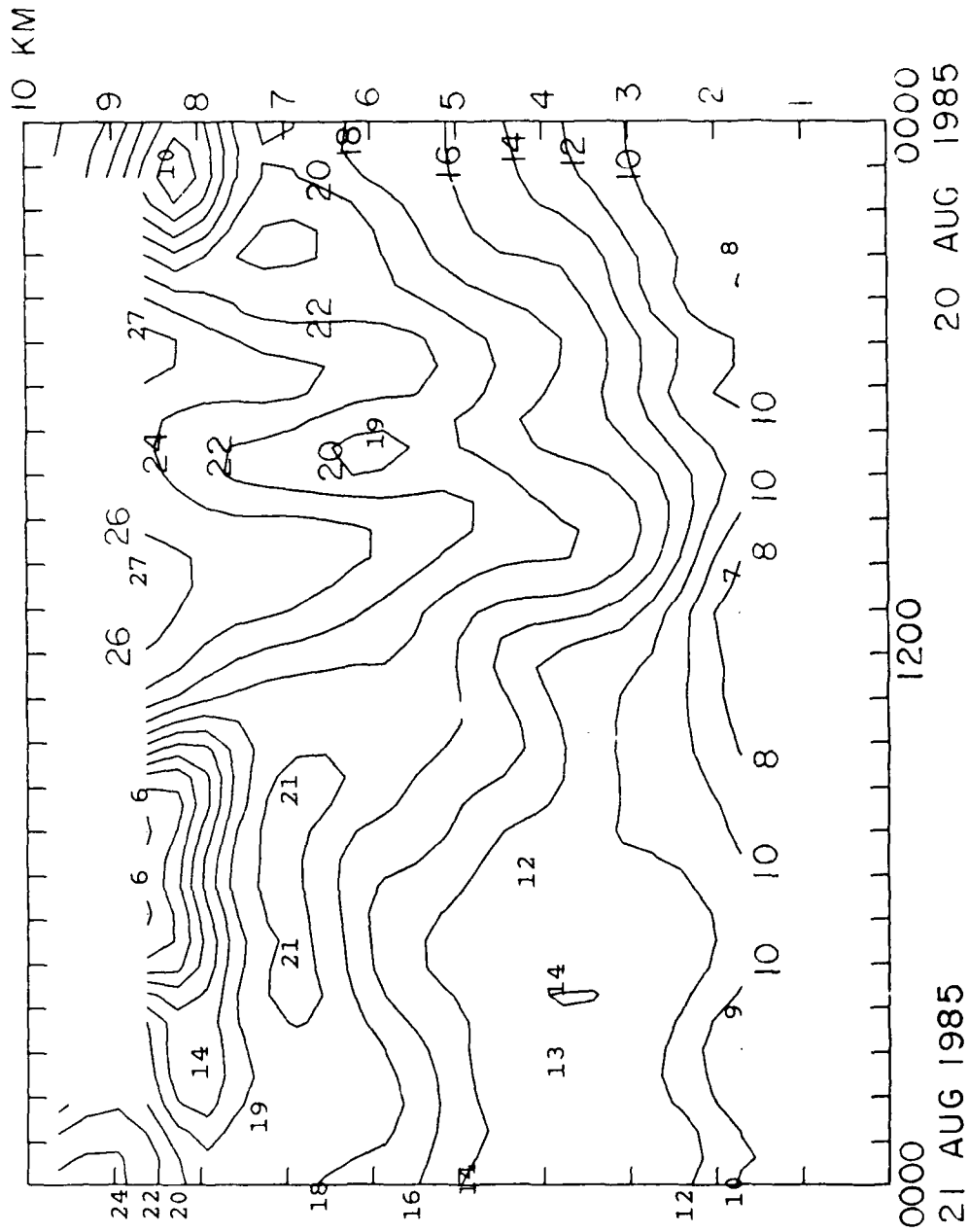

Figure 4.5.3. Time-height section of McAlevy's Fort, PA profiler wind speeds (m/s) on 20-21 August 1985, corresponding to Fig. 4.5.2.

4.5.2. Aside from some "bullseyes" associated with the noise of Fig. 4.5.2, the feature that stands out is a protruding wind maximum at all levels during the period between 0800 and 1100 UTC 20 September. A previous, less-pronounced, "stalactite"-shaped (geologic term for mineral deposit hanging from the ceiling of a cave) wind maximum is also evident at about 0500-0600 UTC.

A comparison between the times of the "stalactites" of Fig. 4.5.3 and the cloud bands of Fig. 4.5.1 is rather interesting. The overall conveyor belt cloud band actually has two high-topped bands. The western one is over the wind profiler at the time of the picture, 0901 UTC, during the passage of the second "stalactite". The eastern of the two high-topped cloud bands is about 100-120 km east of the profiler site at that time, and is likely to have been over McAlevy's Fort at 0500-0600 UTC when the first "stalactite" passed overhead. Again, without careful inspection of independent weather data, one would have been tempted to dismiss the wind speed minimum, at 0700-0800 in Fig. 4.5.3, as bad data. This would yield a smoother pattern of wind variations, more like meteorologists have become accustomed to while using rawinsonde data. If we assume that the wind data are correct, however, then each wind maximum corresponds to a band of high-topped clouds in Fig. 4.5.1. This again points out the potential time and space difficulties in performing wind profiler-rawinsonde intercomparisons. As far as the authors are concerned, however, there is no doubt that the profiler winds are more representative of the true atmospheric structures present, provided that truly noisy wind profiler data have been elimi-

nated.

Returning now to the overall structure of the warm conveyor belt, wind speeds were high within the conveyor belt, in excess of 20 m/s at all levels above 3.5 km, and decreased as the west edge of the cloud pattern passed. Speed decreases were most rapid near 4km, but were obscured above 7km by the presence of noisy winds as drier air moved in aloft. Wind directions also began to veer aloft, Figure 4.5.4, as the west edge of the clouds passed. Again, the extent of the veering is obscured by the presence of noise in the drier air near 7km and above 8km (Fig. 4.5.2).

The sounding at Pittsburgh, PA, Figure 4.5.5, shows the approach of the dry air at levels about 3 km. A cross section, Figure 4.5.6, shows both the dry air west of the conveyor belt and the humid air within the conveyor belt over Washington, DC. As has been discussed previously, the arrival of this dry air is coincident with a decrease in returned power and an increase in noisy (bad) data received by the wind profiler.

This case can be compared to the one in Section 4.3, in which there was an abrupt southern end to the tail of the comma cloud, Figs. 4.3.1 and 4.3.9. In each case the rawinsonde data tended to underestimate the amount of confluence associated with the warm conveyor belt, and caused its location to be too far to the east in middle and upper troposphere, with respect to the satellite imagery. This can be seen in the case of 20 August in Figure 4.5.7, near 500 mb, and from the case of 19 August 1985 in Fig. 4.3.7. It can again be seen that on 20 August the inclusion
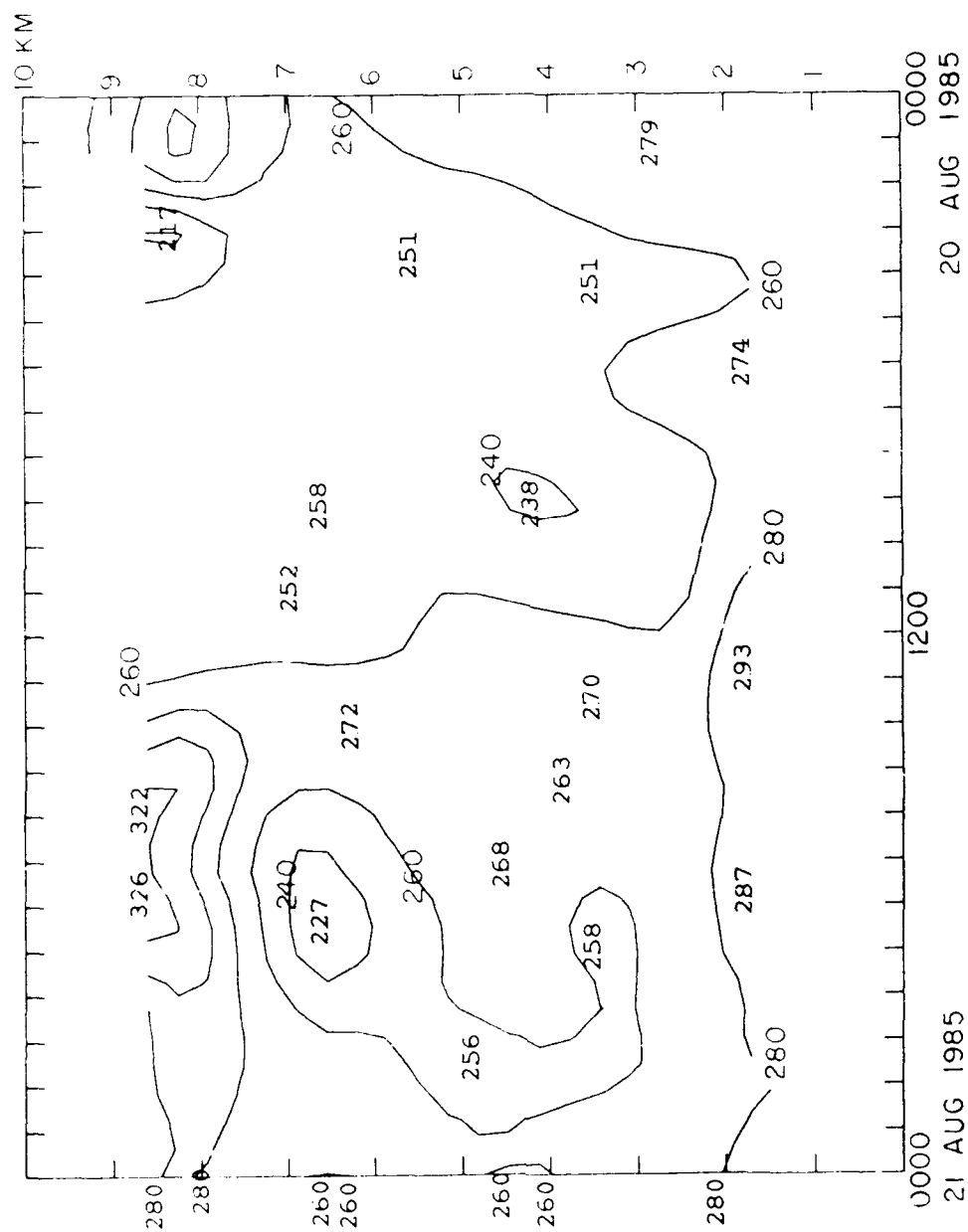
Figure 4.5.4. Time-height section of McAlevy's Fort, PA profiler wind
directions (° azimuth) on 20-21 August 1985, corresponding to Fig. 4.5.2.
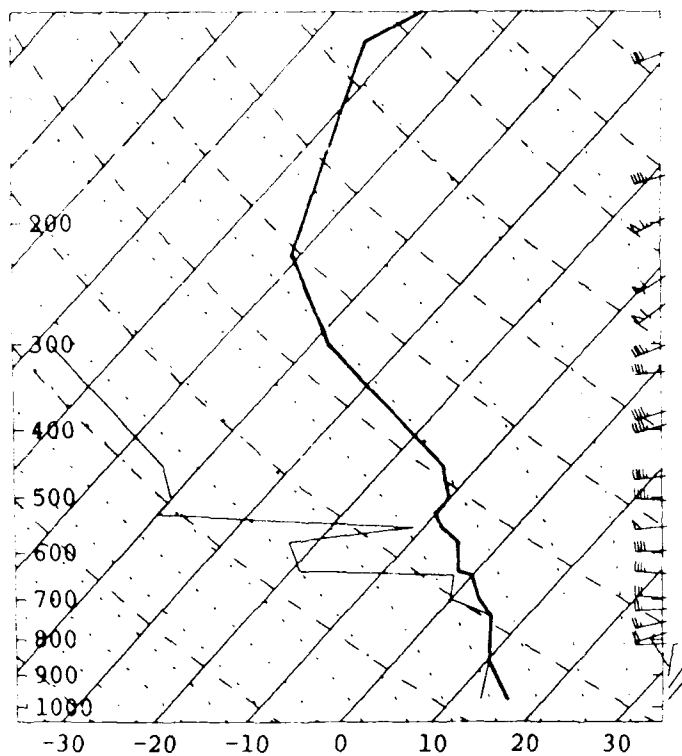
P	T	TD	RH	HT	WS	WD
100	-61			530	29	270
110	-64			500	38	250
222	-51			420	46	255
300	-38	-68	2	390	63	245
450	-14	-44	5	350	60	240
500	-10	-40	6	330	59	235
528	-10	-40	6	300	44	250
552	-8	-11	78	280	44	265
577	-5	-23	22	250	43	255
637	-2	-19	25	240	43	255
646	0	-2	86	200	47	265
700	3	0	80	180	43	275
738	6	6	100	160	48	265
850	10	10	100	140	38	270
977	16	13	82	120	35	275
				100	32	275
				90	27	270
				80	23	260
				70	21	255
				60	17	270
				40	6	330
				30	4	10
				20	3	35
				00	2	40

Figure 4.5.5. Skew-T log P diagram of temperature ($^\circ$C, heavy line) and dew point ($^\circ$C, thin line) from Pittsburgh, PA at 1200 UTC on 20 August 1985.
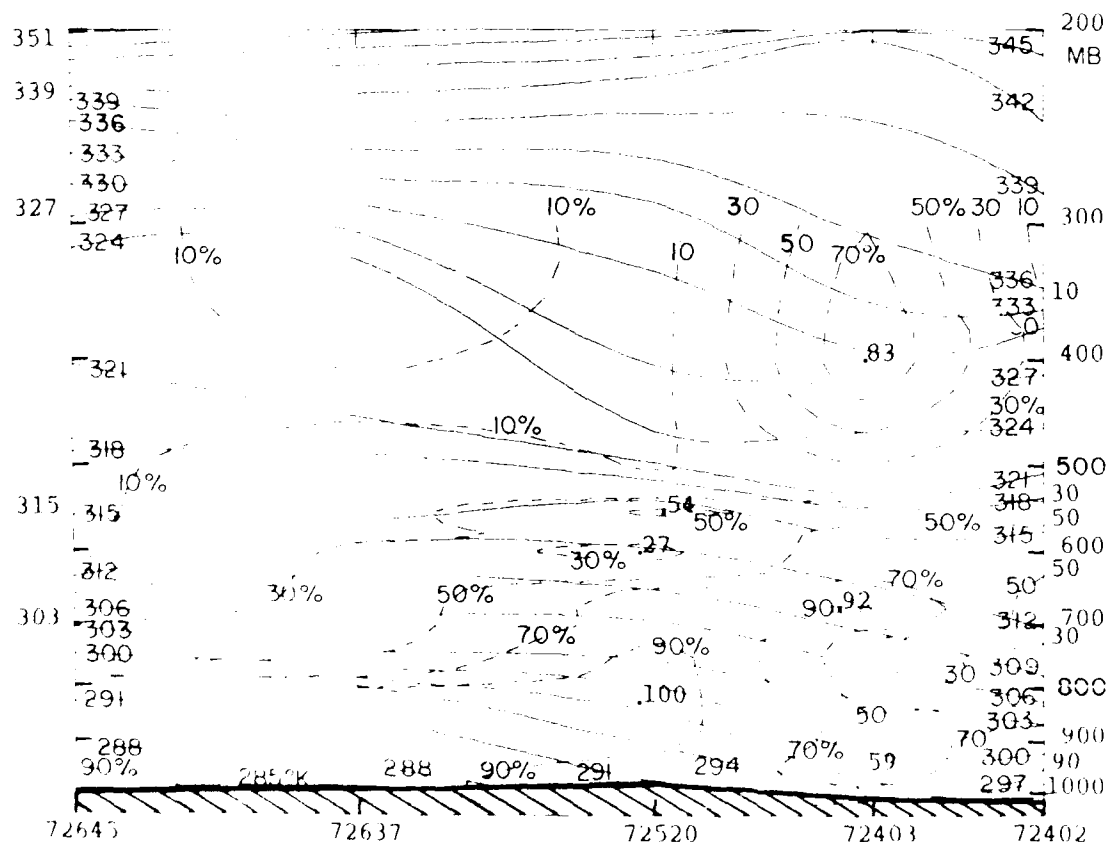
Figure 4.5.6. Northwest-southeast cross section of potential temperature ($^\circ$K, solid) and relative humidity (%, dashed) for 1200 UTC 20 August 1985. Rawinsonde stations used are: 72645, Green Bay, WI; 72637, Flint, MI; 72520, Pittsburgh, PA; 72403, Washington DC Dulles Int'l. Airport, VA; 72402, Wallops Island, VA.

of profiler winds would have improved the analysis, as it forced a short-wavelength trough into west-central PA in the 500 mb streamlines, Figure 4.5.8.

In the 19 August 1985 case of Section 4.3, the confluence zone of the relative winds at low elevations began only in northern or central PA, with diffluence to the south (Fig. 4.3.8). Figure 4.5.9 shows the comparable analysis for the case of 20 August. In this situation the confluence zone near 700 mb extends southwestward into southwestern VA. This allows the conveyor belt on the 20th to tap moist PBL air farther to the south, such that the clouds of the conveyor belt (Fig. 4.5.1) extended into VA, where they were broken. Again, the confluence zone is somewhat too far to the east when only rawinsonde data have been used.

4.6 Wind Structure of Coupled Upper and Lower Jet Streak Circulations

Several wind maxima were observed in the upper troposphere by the McAlevy's Fort, PA wind profiler on 1 September 1985. These can be seen in the low-resolution, far-range time-height sections of Figures 4.6.1 and 4.6.2, at the 12-14 km levels. A few noisy (bad) winds can be seen above the 16 km level. The first wind maximum occurred at about 0600 UTC, followed by a secondary, weaker, one at about 1900 UTC. From wind profiler time series alone at a particular level, it is not possible to determine whether the wind maxima were due to the passage of the core of a quasi-uniform jet stream, or due to the passage of a well-defined jet streak (i.e., wind maximum) within the overall jet
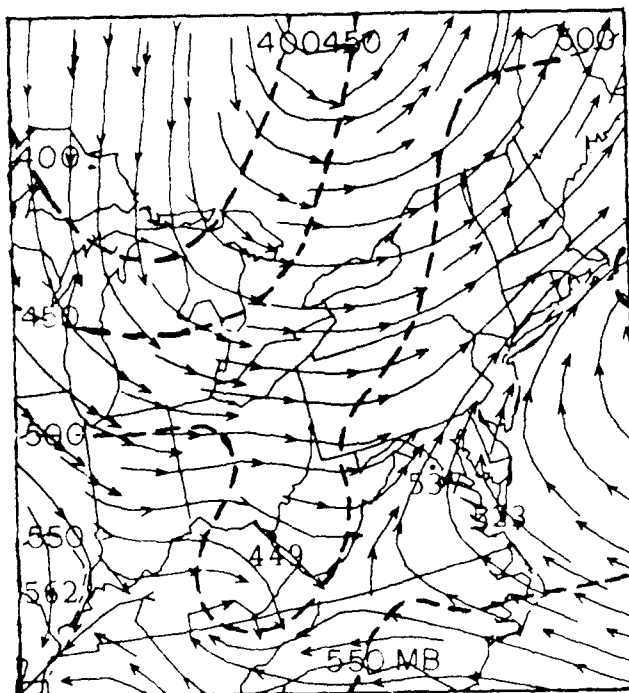
Figure 4.5.7. Analysis of the pressure levels (mb, dashed) of the 320°K isentropic surface and streamlines of the airflow relative to the moving upper-air system, for 1200 UTC 20 August 1985.
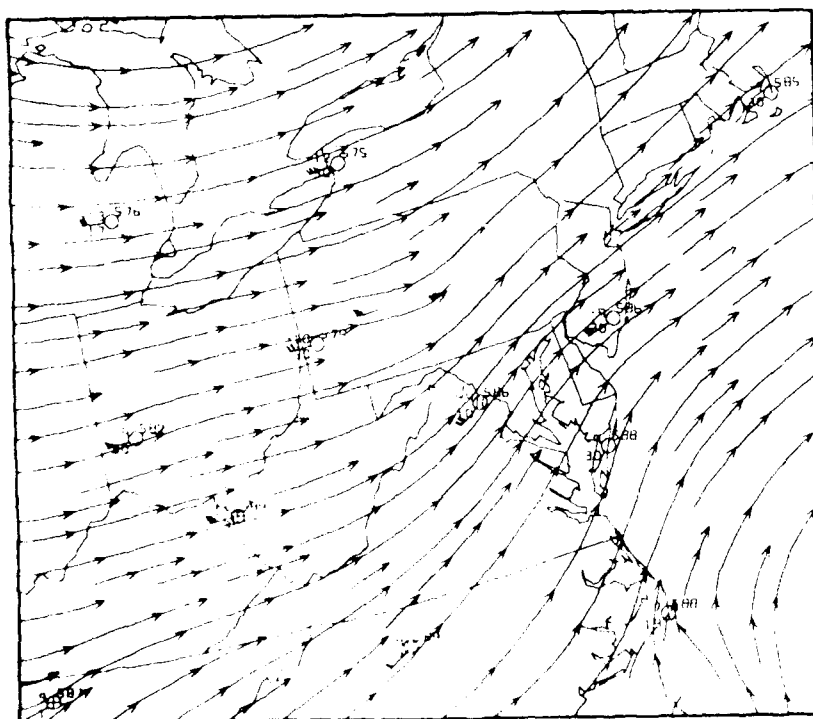
Figure 4.5.8. 500 mb observations and streamlines, incorporating time-space-converted winds from the McAlevy's Fort, PA wind profiler, valid 1200 UTC 20 August 1985.
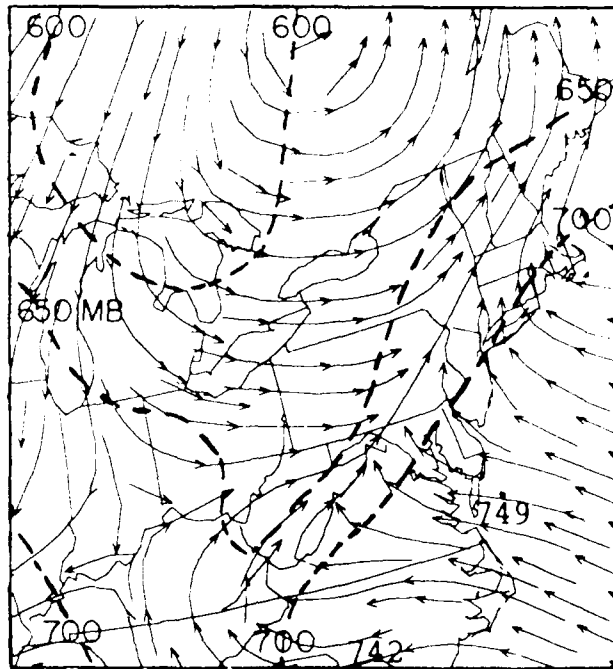
Figure 4.5.9. Analysis of the pressure levels (mb, dashed) of the 310°K isentropic surface and streamlines of the airflow relative to the moving upper-air system.
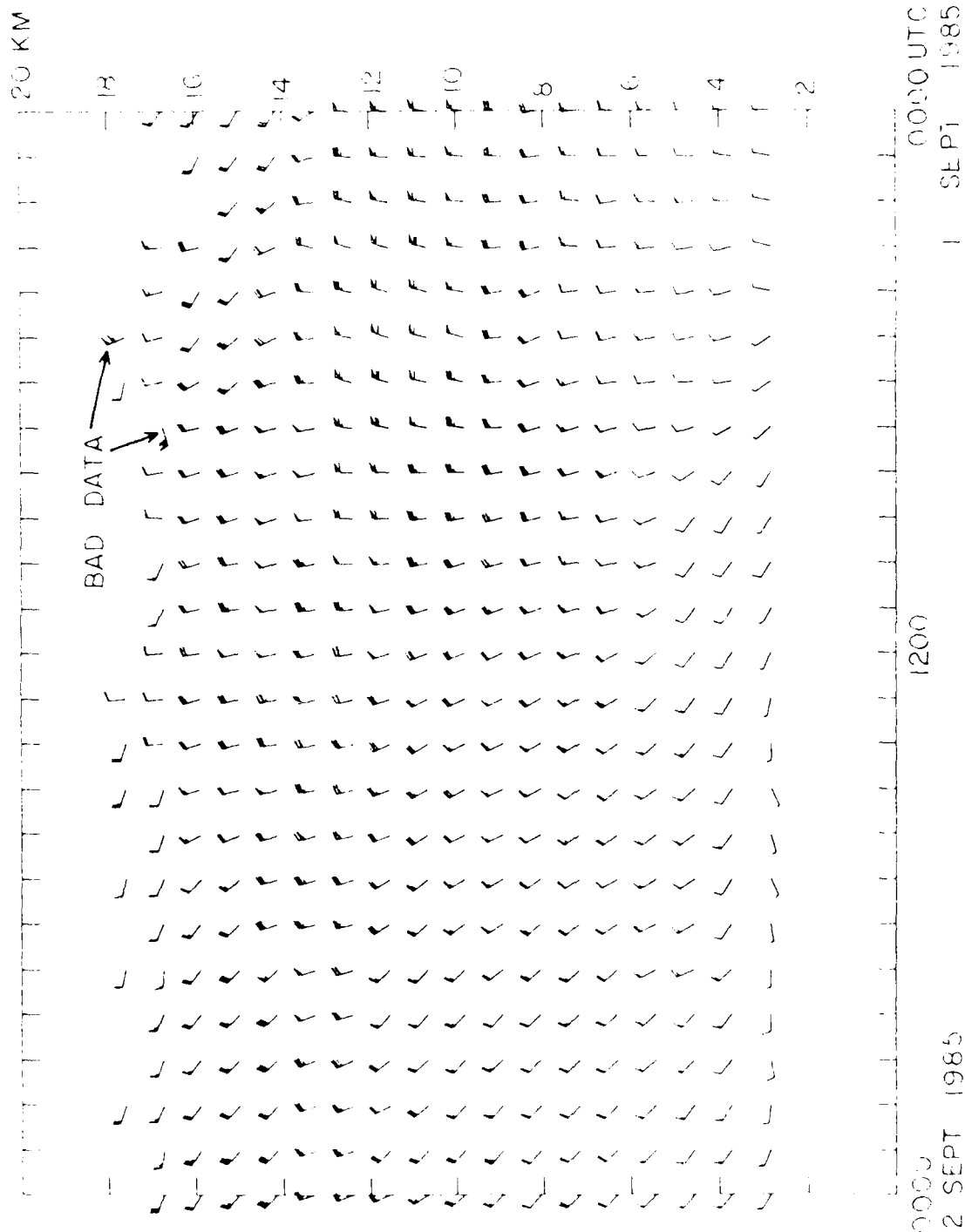
Figure 4.6.1. Time-height section of low-resolution (far-range) winds from the McAlevy's Fort, PA wind profiler on 1-2 September 1985. A barb represents 10 kts (about 5 m/s) and a pennant indicates 50 kts (about 25 m/s).
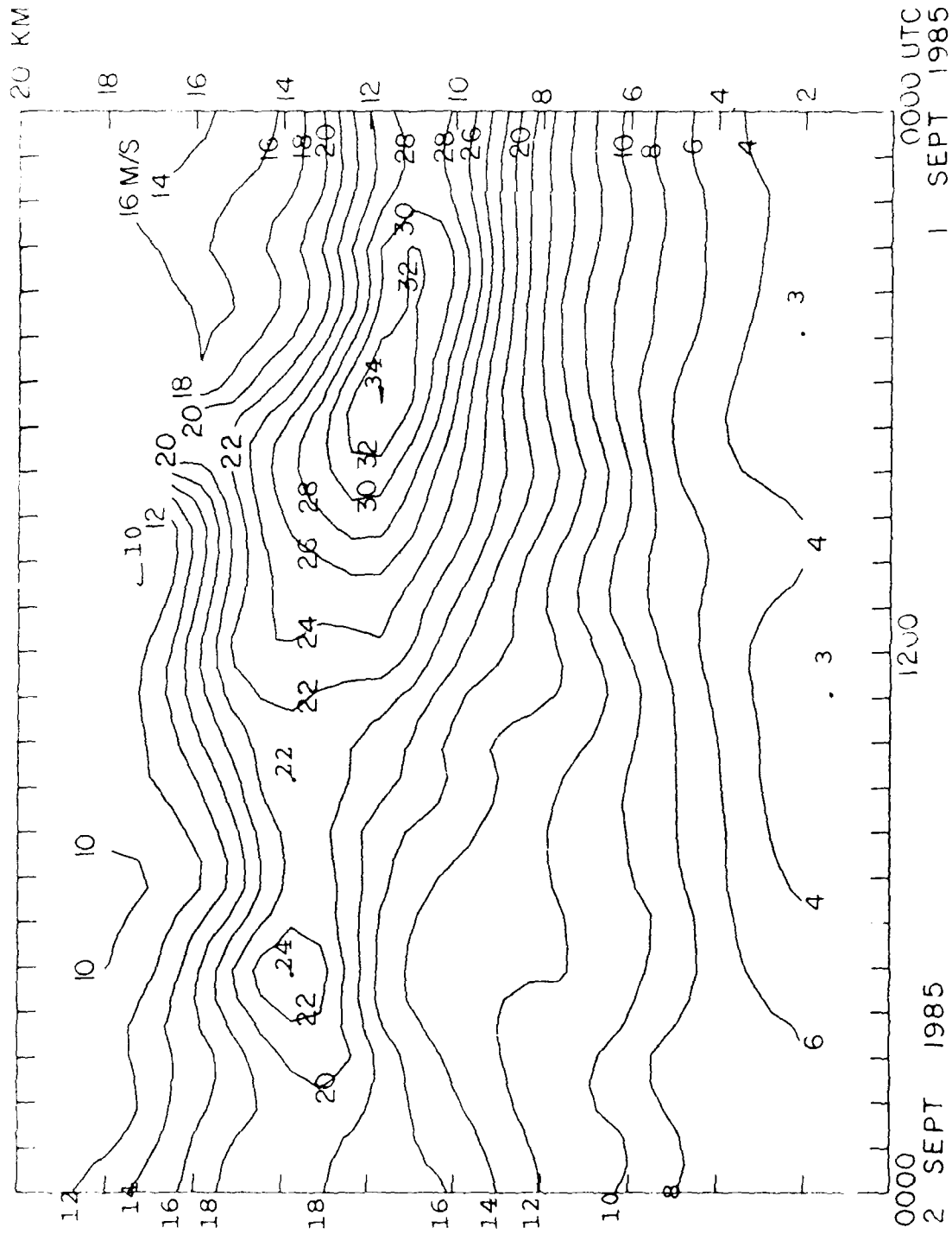
Figure 4.6.2. Time-height section of low-resolution (far-range) wind speeds
(m/s) from the McAlevy's Fort, PA wind profiler on 1-2 September 1985.
Corresponds to Fig. 4.6.1.

stream. This case study shall explore additional procedures which can be used to diagnosis which of these possibilities occurred.

The response of low-level winds to upper-tropospheric jet streaks has been discussed by Uccellini and Johnson (1979). Briefly, at low levels beneath the exit region of an upper-tropospheric jet streak there is an indirect vertical circulation and a transverse flow toward the cold side of the jet. Below the entrance region of an upper-level jet streak there is a direct circulation, and a transverse flow directed toward the warm side of the affiliated baroclinic zone. Since the prevailing flow on 1 September 1985 was from the northwest, as can be seen in Fig. 4.6.1, in this situation a transverse flow in the exit region of a jet streak would be directed from the southwest toward the northeast, and the low-level transverse flow in the entrance region of a jet streak would be directed from the northeast toward the southwest.

Figure 4.6.3 is a time-height section of the high-resolution profiler winds at altitudes from about 2-9 km. Figures 4.6.4 and 4.6.5 are diagrams of wind direction and speed that correspond to Fig. 4.6.3. It can be seen that winds in the layer between about 3 km and 9 km were almost northerly from 0000 to about 0700 UTC, and remained almost northerly until 1000 UTC in the layer between about 5 and 9 km. After these times, winds shifted to a more westerly component (i.e., becoming northwesterly or westerly). We shall use these winds, and the expected jet-streak-related wind directions determined above, to decide whether the upper-
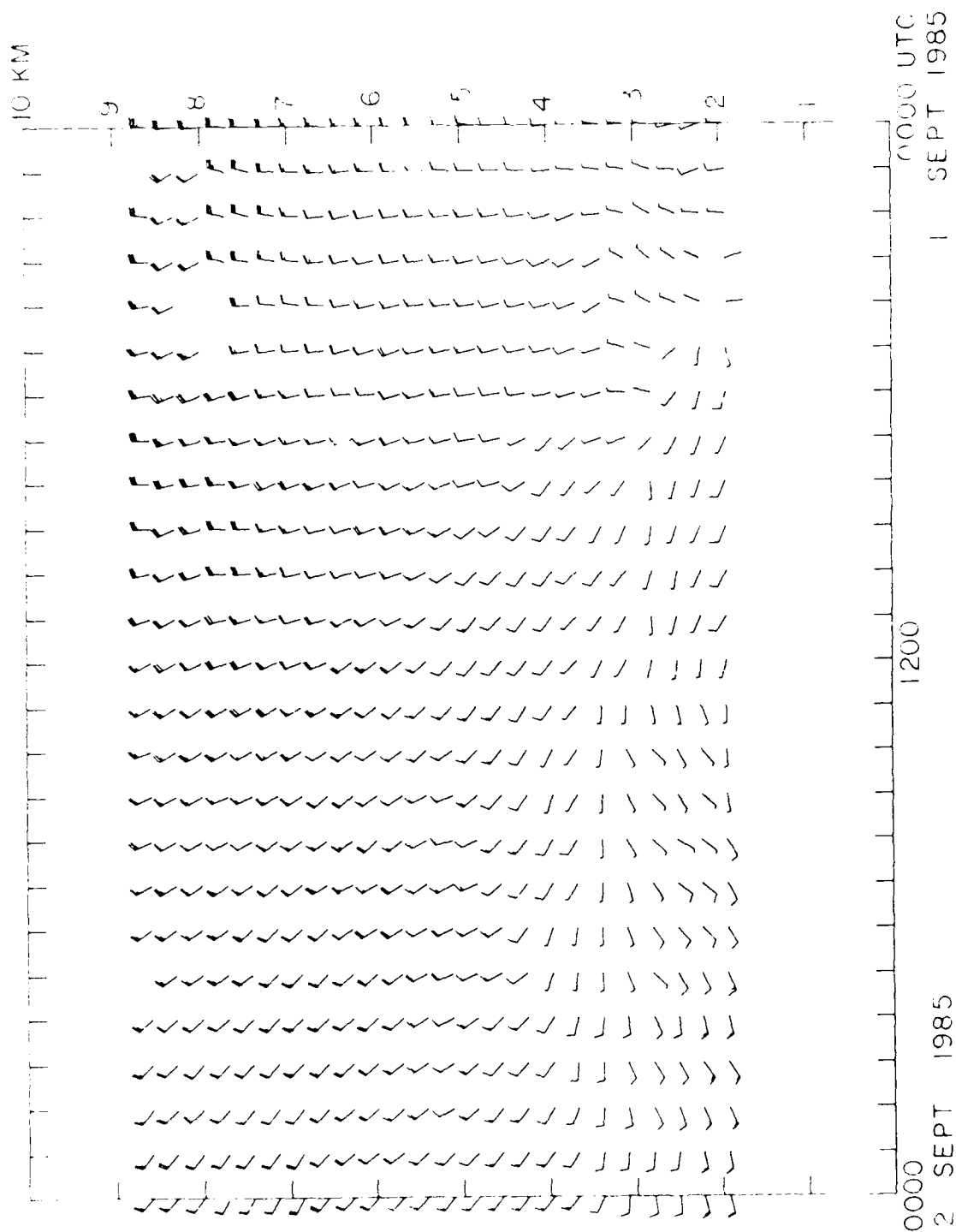
Figure 4.6.3. Time-height section of winds from the McAlevy's Fort, PA wind profiler from 1-2 September 1985. A barb represents 10 kts (about 5 m/s) and a pennant signifies 50 kts (about 25 m/s).

Figure 4.6.4. Time-height section of wind directions (° azimuth) from 1-2
September 1985 from the McAlevy's Fort, PA wind profiler, corresponding to
Fig. 4.6.3.
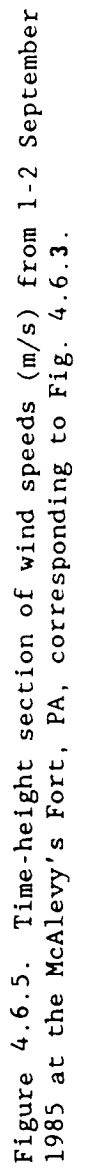
Figure 4.6.5. Time-height section of wind speeds (m/s) from 1-2 September 1985 at the McAlevy's Fort, PA, corresponding to Fig. 4.6.3.

tropospheric wind maxima were from a uniform jet stream passage or from a jet streak.

Prior to 0600 UTC, winds at the lower levels would have been in the exit region if the upper-tropospheric wind maximum at 12 km at 0600 UTC had been affiliated with a jet streak. The observed low-level winds have directions not characteristic of an exit region, since they have a component more from the north than the prevailing winds (say, averaged over the 24h of the time-height section). Exit region winds should have had a southwesterly component at low levels.

If the wind maximum at 14 km at 1900 UTC were due to a jet streak, then low-level winds should have had a southwesterly component while in the exit region sometime prior to that. Indeed, the winds at 2-3 km are southwesterly from about 1400 to 2200 UTC. Winds below 4 km have a southwesterly component (i.e., are more westerly than the prevailing northwesterlies) from about 1500 to 1900 UTC. Hence, the second wind maximum is more likely to have been affiliated with a jet streak than the more impressive wind maximum at 0600 UTC.

The enhanced northerlies in the 2-3 km layer from 0100 to 0400 UTC actually suggest that the wind profiler was in an entrance region at that time. Some of the winds actually became north-northeasterly for a few hours. However, upper-level winds do not support this hypothesis.

Deciding on jet stream versus jet streak presence can be aided through use of quasi-horizontal mappings. Figure 4.6.6 is the 300 mb chart from 1200 UTC, with the 1200 UTC profiler wind
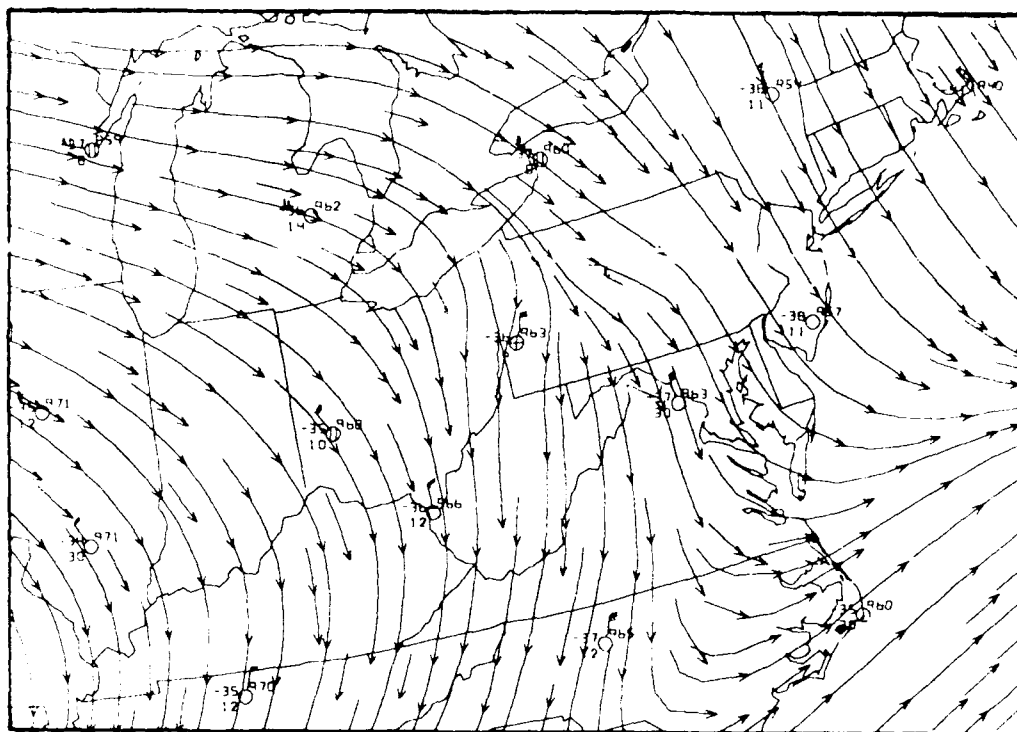
Figure 4.6.6. 300 mb rawinsonde observations, profiler winds, and streamlines for 1200 UTC 1 September 1985.
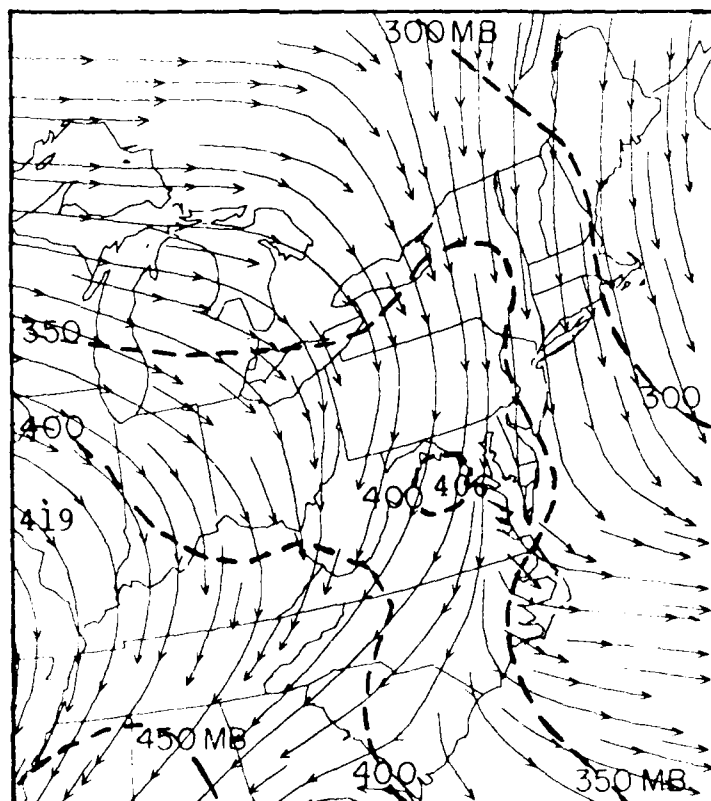
Figure 4.6.7. Analyses of the pressure levels (mb, dashed) of the 330°K isentropic surface and streamlines of the observed wind from 1200 UTC 1 September 1985.

added.   Strong winds can be seen at Albany, NY and Chatham, MA,

and the wind is missing at Atlantic City, NJ (often a sign of

strong winds).   Streamlines at these sites are from just slightly

west of north, and the jet stream or streak flows offshore by the

time it reaches the latitude of McAlevy's Fort.   This jet stream

or streak may have been as far west as Atlantic City, and appears

to be the core of the 0600 wind maximum.

Figure 4.6.7 shows winds on the 3300K isentropic surface.

Since the   character of the pertinent disturbance (i.e., jet

stream or   streak) has   not been determined, a pertinent disturb-

ance phase velocity cannot be determined, and the streamlines

are of the observed winds rather than relative to the moving

disturbance.   These streamlines, nevertheless, show a confluence

over the region north of New York and New England and a difflu-

ence over the Chesepeake Bay and the eastern Carolinas. This

would support a jet streak over northeastern PA or thereabouts at

the 1200 UTC analysis time. Unfortunately, further diagnosis on

the nature of the first McAlevy's Fort, PA wind maximum is not

possible, as there is no data over water or over northeastern PA,

no winds at Atlantic City, NJ, and no report from Wallops Island,

VA.   This is sometimes the case: when counting on coarse-density

operational rawinsonde data to help clarify profiler-detected

signatures, disappointments can arise!

Strong winds are also seen at Green Bay, WI in Fig. 4.6.6.

Streamlines head ESE from there, flow between Flint, MI and Buf-

falo, NY, and turn more southward into central PA.   This airflow

appears to be affiliated with the second wind maximum. The dif-

141

fluence between the Pittsburgh, PA and profiler winds would support a jet streak somewhere near Lake Erie, hidden between the coarse-density rawinsonde observations. Likewise, the confluence between the profiler wind and the Albany, NY wind at 700 mb, Figure 4.6.9, is supportive of a jet streak over Lake Erie at 1200 UTC.

From the available profiler and rawinsonde data and analyses, then, the best analysis is that a jet stream over New York, western New England, and along the NJ Coast—and possibly an entrance region of a jet streak within it—affected the McAlevy's Fort, PA site from 0000 UTC to about 1200 UTC. Thereafter, the exit region of an upper-tropospheric jet streak which was over or near Lake Erie at 1200 UTC began to affect the McAlevy's Fort profiler site. This upper-level jet streak induced a low-level transverse flow in its exit region that caused winds to become southwesterly in the 2-3 km layer, and more westerly at other low levels. The maximum impact at low elevations was felt at about 1600 UTC. While there was little speed increase at the 2.5 km level, there was a marked backing of the flow to a southwesterly direction (Figs. 4.6.3 and 4.6.4), becoming almost normal to the prevailing flow in this region. The upper-level jet streak passed the profiler site sometime between 1900 UTC (when speeds peaked) and 2200 UTC (when low-level flow lost its southwesterly component), after which time the exit region was no longer overhead.
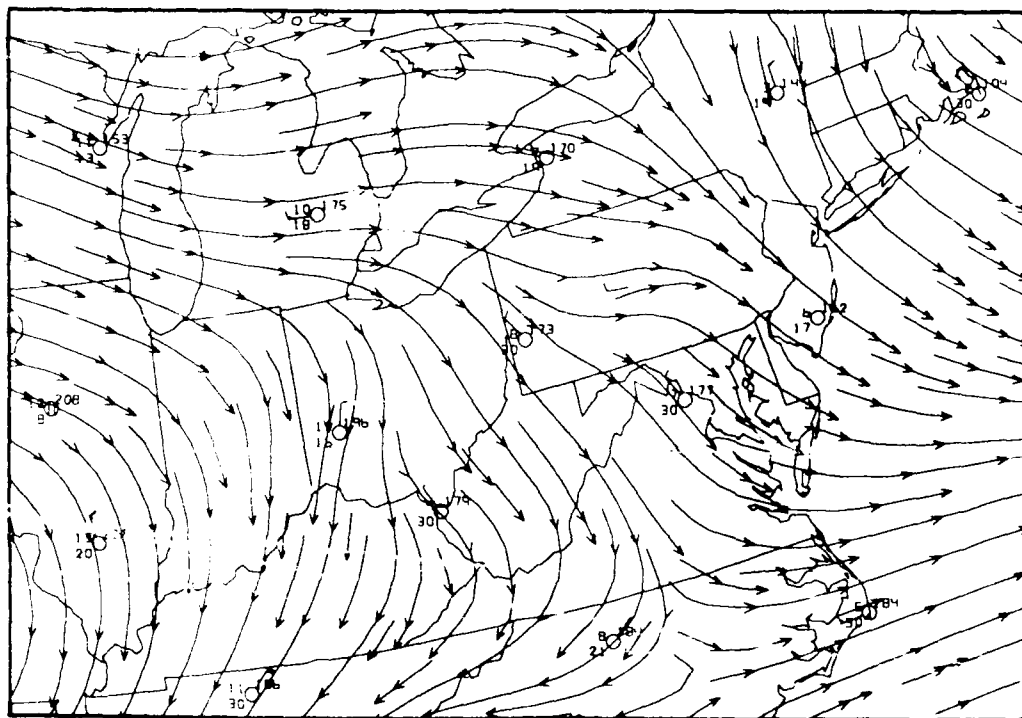
Figure 4.6.8. 700 mb rawinsonde observations, profiler winds, and streamlines from 1200 UTC 1 September 1985.

4.7   Detection and Structure of Unexpectedly Sharp Ridge Axis

Figure 4.7.1 shows a rather rapidly evolving pattern of wind directions at most levels on 20 September 1985, even if the noise in the upper left corner is ignored.   The winds progressively evolved from easterly to southwesterly at elevations below about 5 km MSL.   At about 6 km, using the principles of Section 3.2, it can be deduced that a high-pressure center passed just to the north of the McAlevy's Fort profiler.   This allowed winds to retain an easterly component throughout the period and to shift from ENE to ESE.   Figure 4.7.2, showing isotachs corresponding to Fig. 4.7.1, reveals light winds throughout, characteristic of an anticyclone.

Indeed, the atmosphere at most levels was under the influence of a sprawling anticyclone. Figure 4.7.3 shows the surface chart at 1200 UTC on 20 September 1985.   The anticyclone is somewhat elliptical, with long axis from southern New England, approximately along the Appalachians, and into MS.

Figure 4.7.4 shows the 700 mb chart at 0000 UTC on 20 September, with McAlevy's Fort, PA profiler wind included.   A sharp ridge axis runs southwestward from Lake Ontario to the crest of the Appalachians from WV to GA.

Figure 4.7.5 shows the 700 mb chart at 1200 UTC on 20 September, with the McAlevy's Fort profiler wind and two time-space-converted profiler winds superimposed.   These blend in quite well with the rawinsonde winds, to form an analysis that shows that the ridge axis has moved eastward and is splitting into two anticyclone centers.   One center has moved offshore of New England,
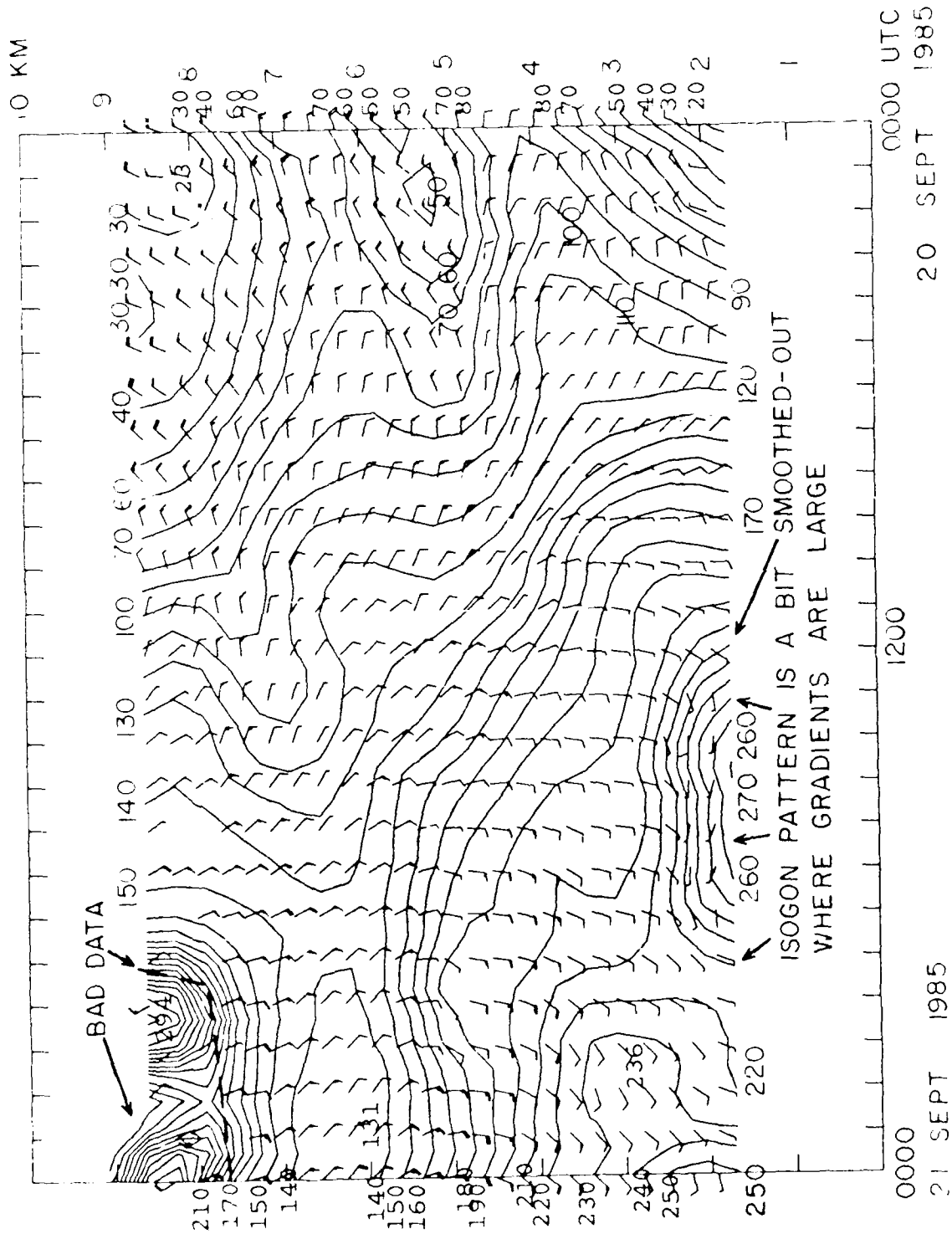
Figure 4.7.1. Time-height section of winds and wind directions (10° azimuth intervals) from the McAlevy's Fort, PA wind profiler on 20-21 September 1985.
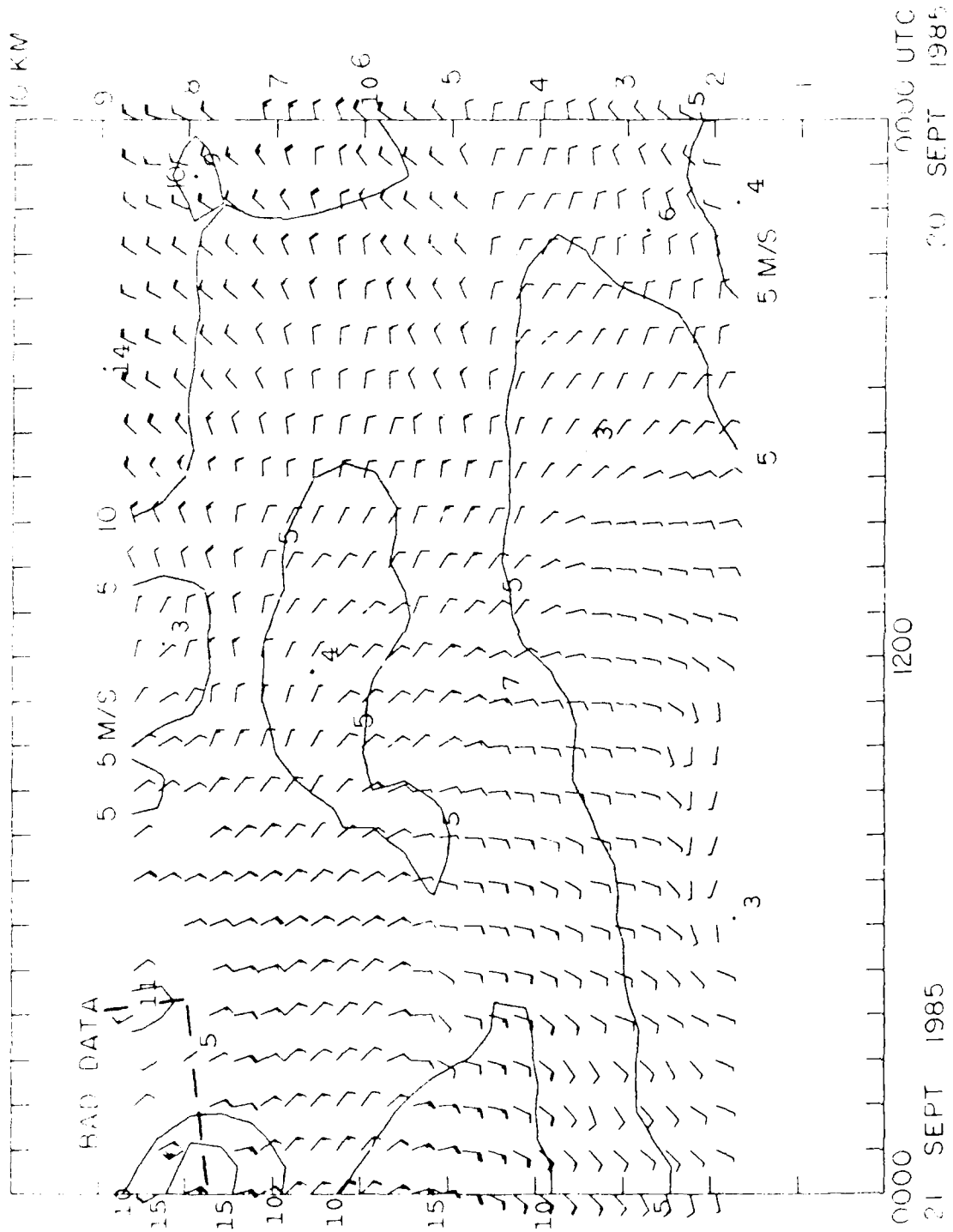
Figure 4.7.2. Time-height section of winds and wind speeds (m/s) from the McAlevy's Fort, PA wind profiler on 20-21 September 1985.
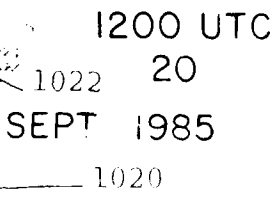
Figure 4.7.3. Surface observations, cold front, and sea-level pressure
analysis (2 mb intervals) for 1200 UTC 20 September 1985.
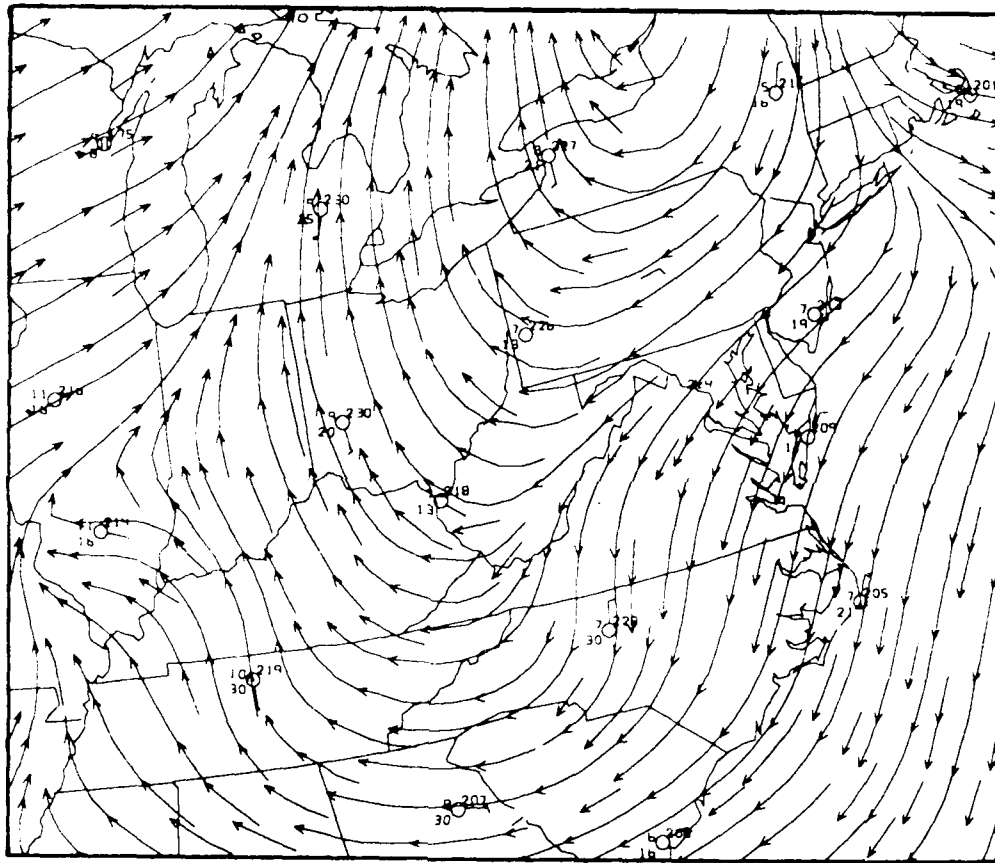
Figure 4.7.4. 700 mb rawinsonde observations, profiler winds, and streamlines for 0000 UTC 20 September 1985.
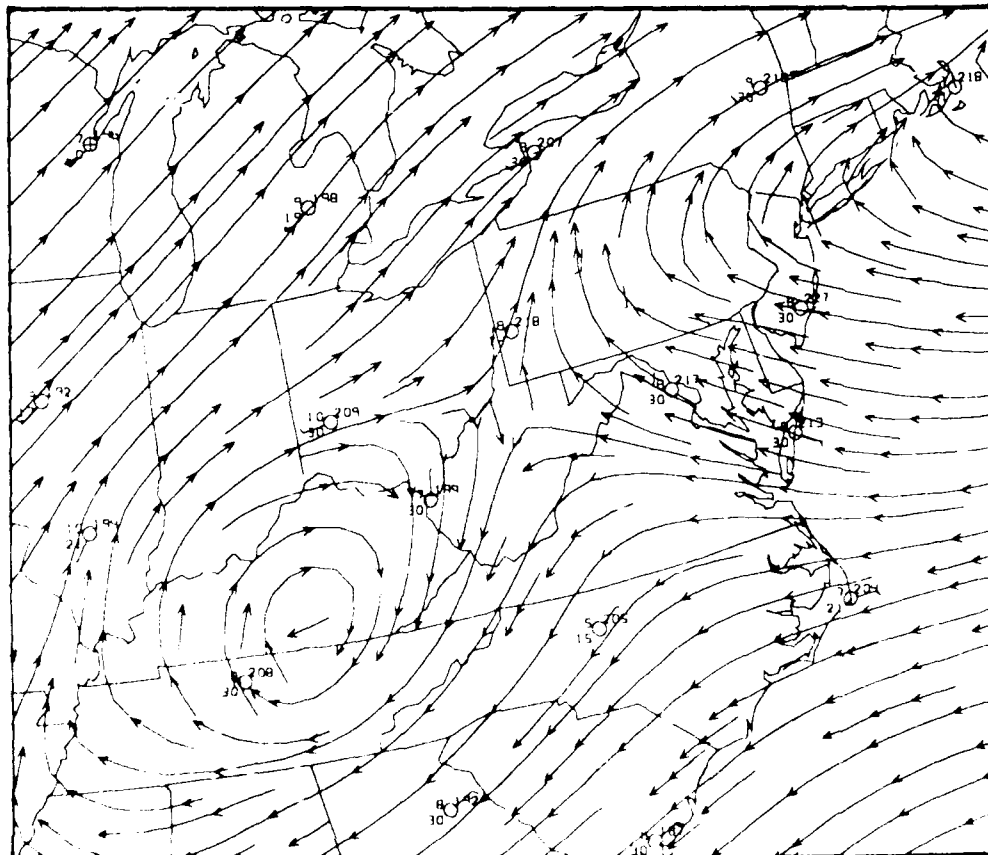
Figure 4.7.5. 700 mb rawinsonde observations, profiler winds, and streamlines for 1200 UTC 20 September 1985.

while the other is heading westward and has formed in southern KY. The veering of the profiler winds with time from north-easterly through south-southwesterly is consistent with an anti-cyclone passing to the north of the site.

Figure 4.7.6 is the 500 mb chart from 0000 UTC 20 September 1985, with the McAlevy's Fort, PA profiler wind included. This analysis shows a closed anticyclone center in eastern OH, and a ridge extending NNE-SSW from it.

Figure 4.7.7 is the 500 mb chart from 1200 UTC, including the McAlevy's Fort, PA profiler wind and two time-space converted winds. They, again, blend well with the rawinsonde winds, and show that the anticyclone center has passed over PA into the New York City area. The profiler wind shift from easterly to south-erly indicates that the anticyclone center passed north of the site, which is consistent with an extrapolation between Figs. 4.7.6 and 4.7.7, although the anticyclone center should not have been very far north of the profiler site.

It was of interest to determine what impact the profiler winds and time-space converted winds would have on the computed vorticity within the ridge axis. Figure 4.7.8 shows the absolute vorticity computed using only rawinsonde winds at 500 mb. Values of 0 to 2×10^{-5} s-1 are obtained along the ridge axis. Figure 4.7.9 shows the absolute vorticity analysis using rawinsonde data and the 1200 UTC wind from the McAlevy's Fort, PA wind profiler. The absolute vorticity values are not changed appreciably, rang-ing from -1 to 1×10^{-5} s-1. Figure 4.7.10 shows the absolute vorticity analysis when two time-space-converted profiler winds
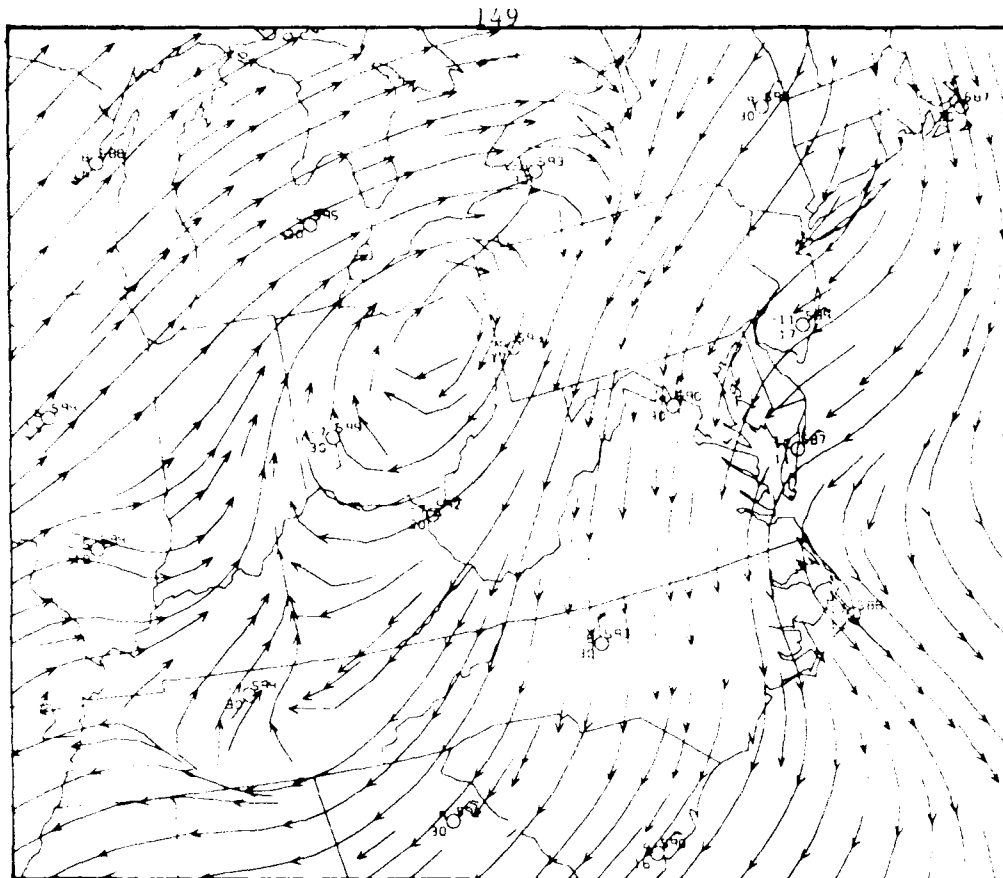
Figure 4.7.6. 500 mb rawinsonde observations, profiler winds, and streamlines for 0000 UTC 20 September 1985.
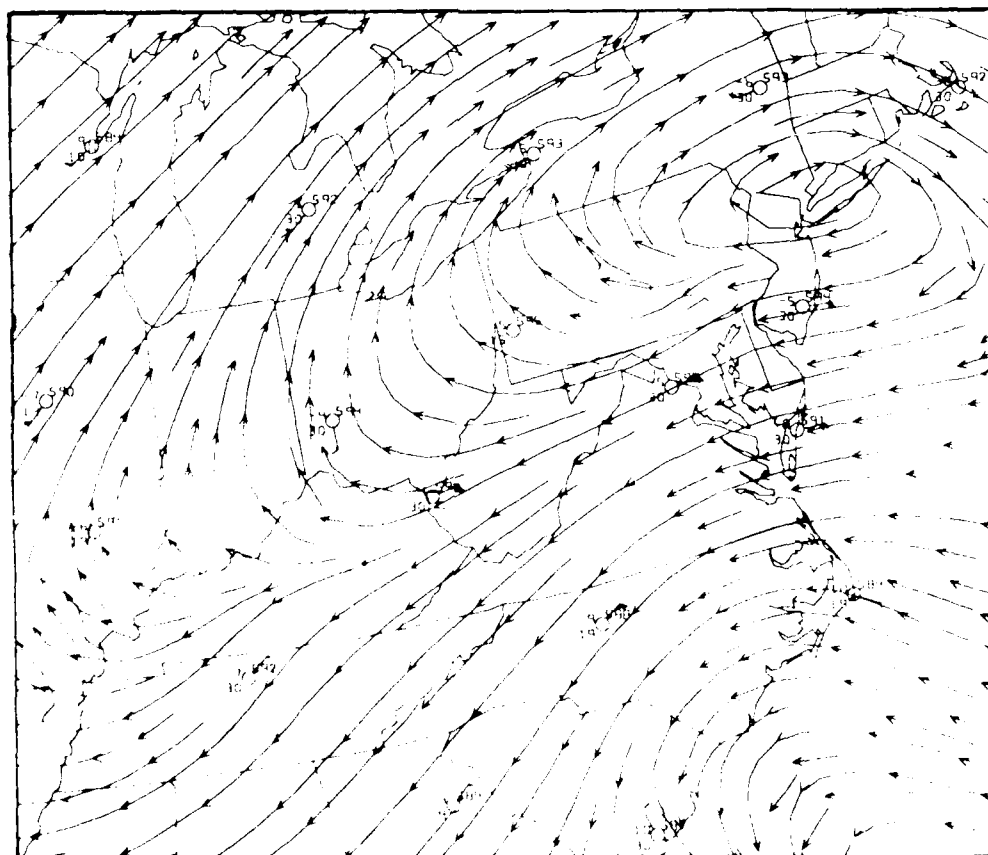
Figure 4.7.7. 500 mb rawinsonde observations, profiler winds, and streamlines for 1200 UTC 20 September 1985.
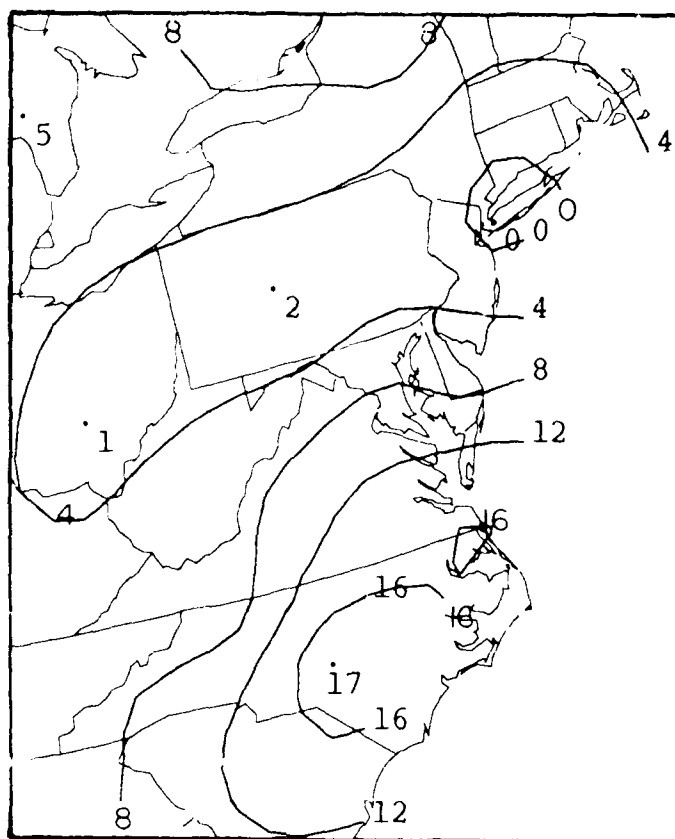
Figure 4.7.8.   500 mb absolute vorticity (units of 10^{-5} s^{-1}), using only rawinsonde data, from 1200 UTC 20 September 1985.
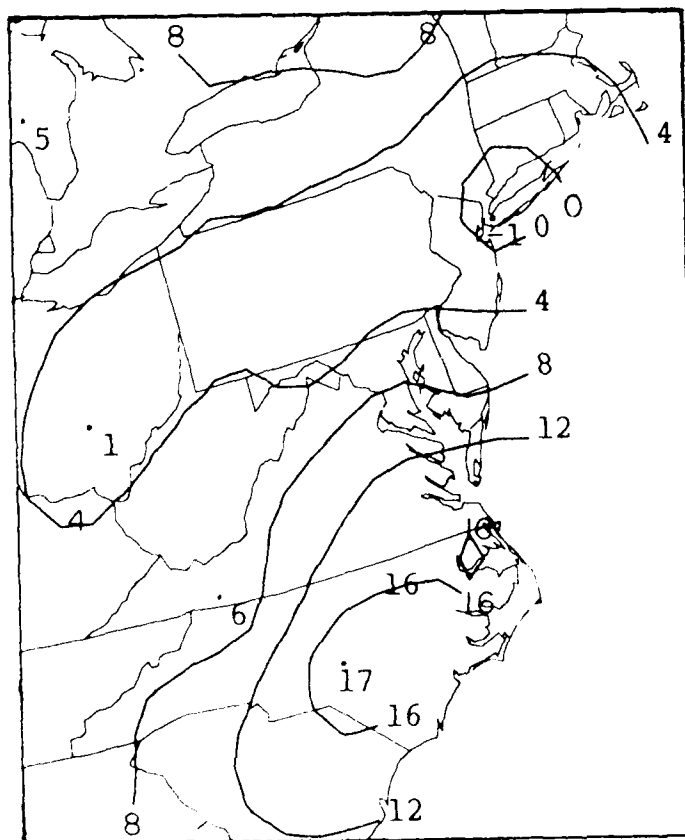
Figure 4.7.9.   500 mb absolute vorticity (units of 10^{-5} s^{-1}), using rawinsonde winds and the McAlevy's Fort, PA hourly wind from 1200 UTC 20 September 1985.

are also used, from 6h before and after 1200 UTC. The absolute vorticity pattern is now changed appreciably in western PA, where a small vorticity maximum of $7 \times 10-5$ s-1 appears.

It is tempting to dismiss the analysis using time-space-converted winds as being inferior, since it injects "cyclonic" vorticity (actually, it's still anticyclonic, but just an anti-cyclonic vorticity minimum) into the region of a ridge. However, there are reasons to be more cautious. First, the 700 mb analysis of Fig. 4.7.5, which looked fine, actually shows a trough near the OH-PA border. Second, it is the 1800 UTC time-space converted wind that would have caused the appearance of the $7 \times 10-5$ s-1 maximum. An inspection of the 1931 UTC satellite imagery, Figure 4.7.11, shows a field of cumulus and congestus clouds over western PA (and western NY where there is no enhanced analysis). Might these clouds be affiliated with slightly cooler air aloft accompanying such a minor trough? No quick decisions are possible in this case, of course. However, future work is planned to explore the utility of the time-space conversion of profiler winds (by Ming-Tzer Lee, and by Forbes [see Forbes and Bankert, 1987]).

4.8 Ambiguity--Diurnal Oscillations or Travelling Mesoscale Ridges?

This case, from 7-8 September 1985, has some things in common with the case of 20 September 1985, discussed in Section 4.7. Pronounced wind variations have been observed during a quiescent period dominated by ridge axis. In the case of 7-8 September 1985, however, the ridge axis remained several hundred kilometers
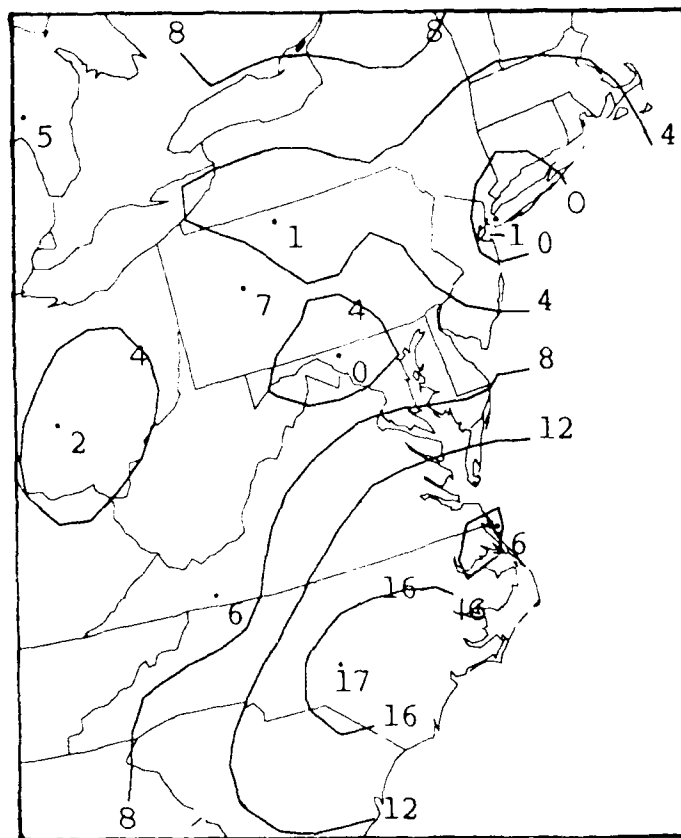
Figure 4.7.10. 500 mb absolute vorticity (units of 10^{-5} s^{-1}), using rawinsonde winds, the McAlevy's Fort, PA hourly winds from 1200 UTC and 1800 UTC (time-space-converted) 20 September 1985 to produce the analysis pertaining to 1200 UTC.

Figure 4.7.11. Visible satellite image from 1931 UTC 20 September 1985.

southwest or west of the McAlevy's Fort profiler although moving toward the northeast. Unlike the case of 20 September 1985, this ridge axis did not pass the wind profiler during the case under examination. Without cloud patterns to supply some independent mesoscale data, interpretation of the variations has been difficult.

A good example of an ambiguous wind variation is the north/ west/north pattern at about 3 km on Figure 4.8.1, with apparent period of about 18-19 hours. This is approximately the period of an inertial oscillation at the latitude of the profiler (about 41.5 N). It is, of course, well known that there is an oscillation of the wind induced by the diurnal mixing cycle (Blackadar, 1957), wherein winds that are subgeostrophic at the top of the boundary layer in late afternoon undergo an inertial oscillation during the nighttime and become supergeostrophic at some time before sunrise. In the case of Fig. 4.8.1, the geostrophic winds were from the northwest, such that the wind oscillation shown appears to have the proper phase.

Alternatively, the wind fluctuations may also have been due to some substructure within the ridge, with short-wavelength ridges or lobes travelling around its periphery. As these approached, winds would become more northerly, and then become more westerly as the mesoscale disturbance passed to the south of the profiler. Upper-air observations were inadequate to definitively resolve these features, if they did exist. Some insight, however, can be gained.

Figure 4.8.2 is the surface analysis for 1200 UTC 7 Septem-
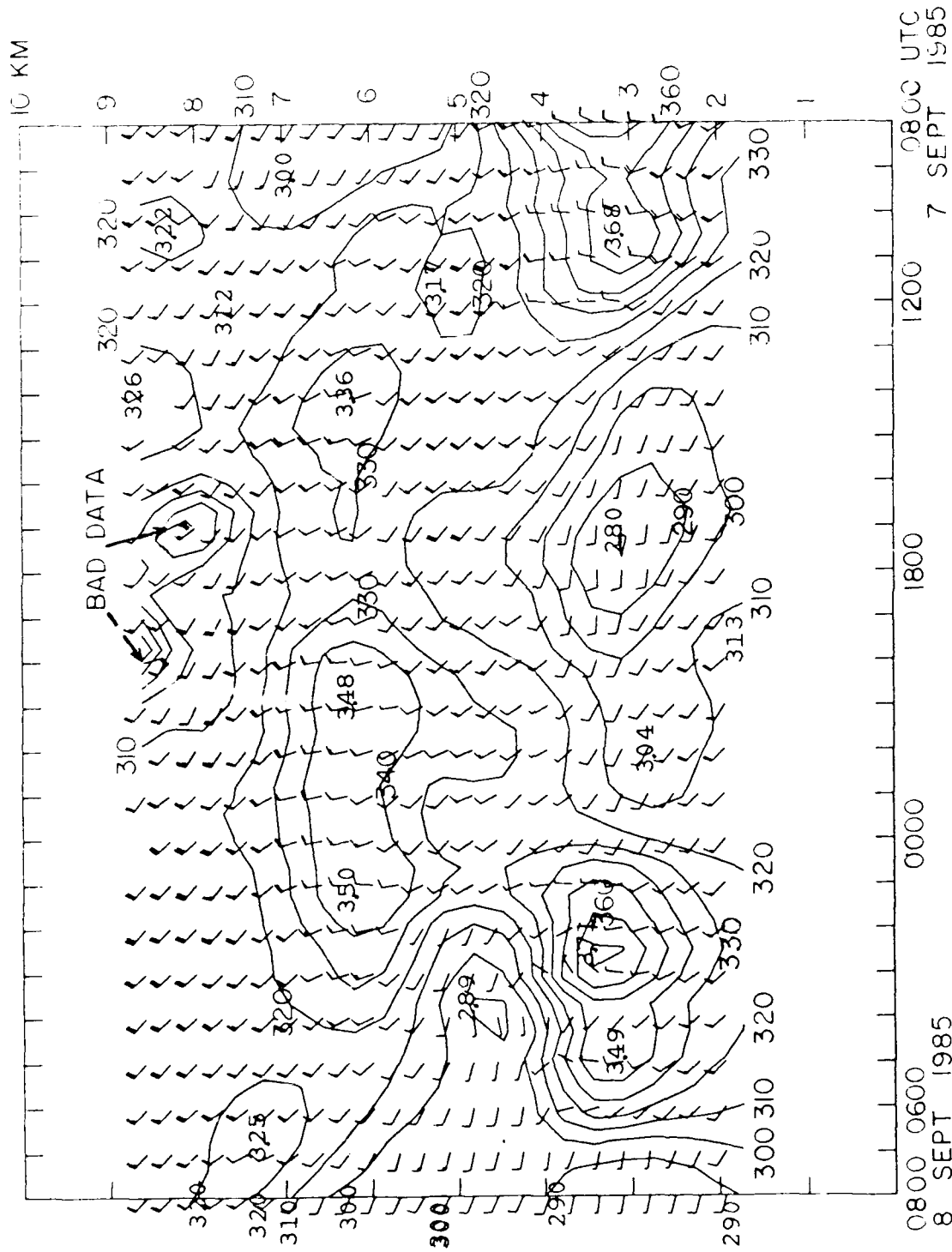
Figure 4.8.1. Time-height section of winds and wind directions (10° azimuth intervals) from the McAlevy's Fort, PA wind profiler on 7-8 September 1985.

ber 1985. A ridge of high pressure lies over the Appalachians from PA southward, broken across NY and NJ by a frontal zone. Northerlies across southern New England are driving this front southward toward the region east of the Appalachians as a back-door cold front. Figure 4.8.3 is a SW-NE cross section, and shows that the depth of the cold air extends to about 700 mb over Portland, ME.

Figure 4.8.4 shows the 700 mb streamline analysis using rawinsonde and time-space-converted profiler winds for 1200 UTC 7 September. The profiler winds force a trough into central PA, which actually matches well with the winds at Atlantic City, NJ and Albany, NY. From this figure it can be seen that the trough was moving from the NW around the flank of a large-scale cyclone over northeastern New England. A confluence zone over central PA is quite visible. Pittsburgh, PA and areas to the south and west were "protected" from the trough by virtue of being on the anti-cyclonic side of the confluence zone. Figure 4.8.5, for 500 mb, gives a similar picture, but the trough and confluence zone are not as pronounced.

Figure 4.8.6 is the surface analysis for 0000 UTC 8 September 1985. By this time the back-door cold front has pushed southward into the central Carolinas, and has begun to dissipate along the slopes of the Appalachians there. The eastern boundary of this back-door cold surge remains visible as a front just in-land of the coasts. This front was moving within the northerly flow along the New England side of the confluence zone of Fig. 4.8.4.
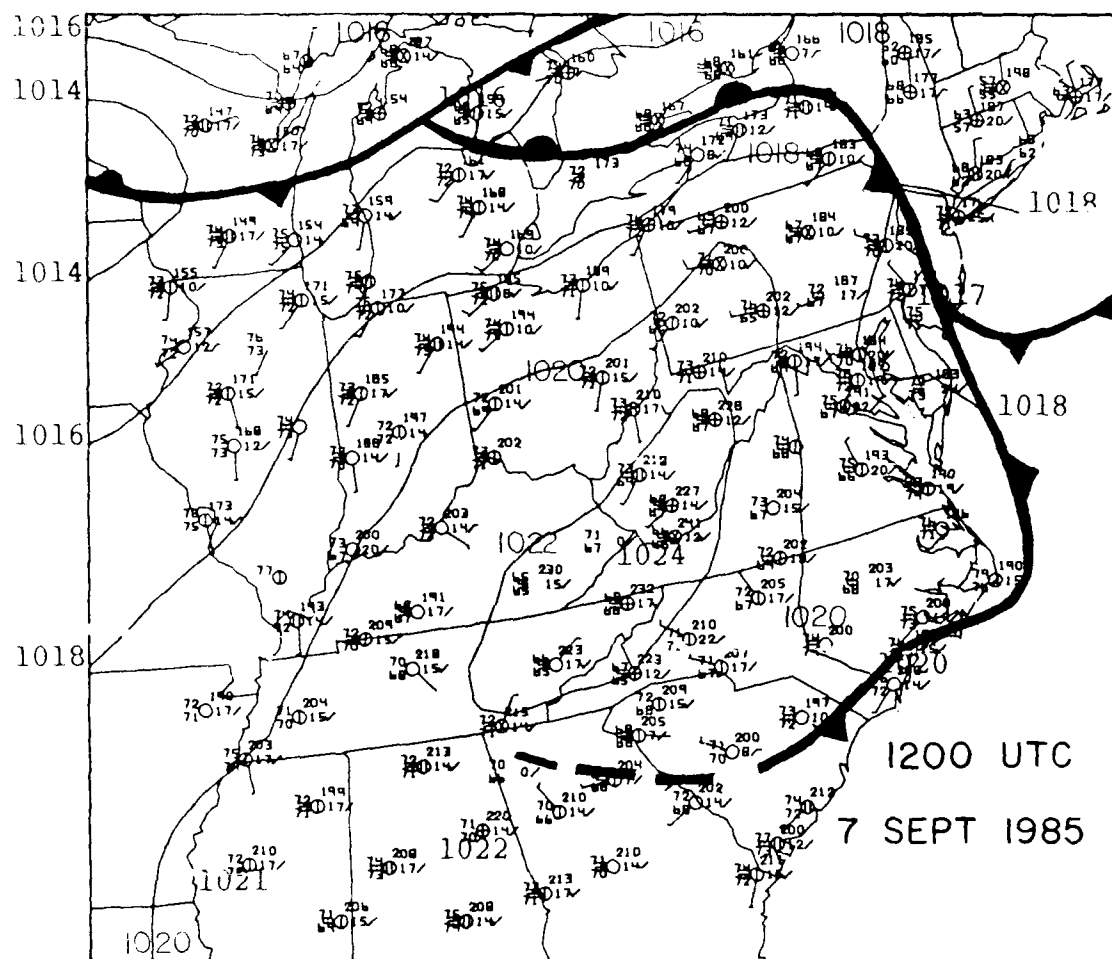
Figure 4.8.2. Surface observations, fronts, and sea-level pressure analysis (2 mb intervals) for 1200 UTC 7 September 1985.
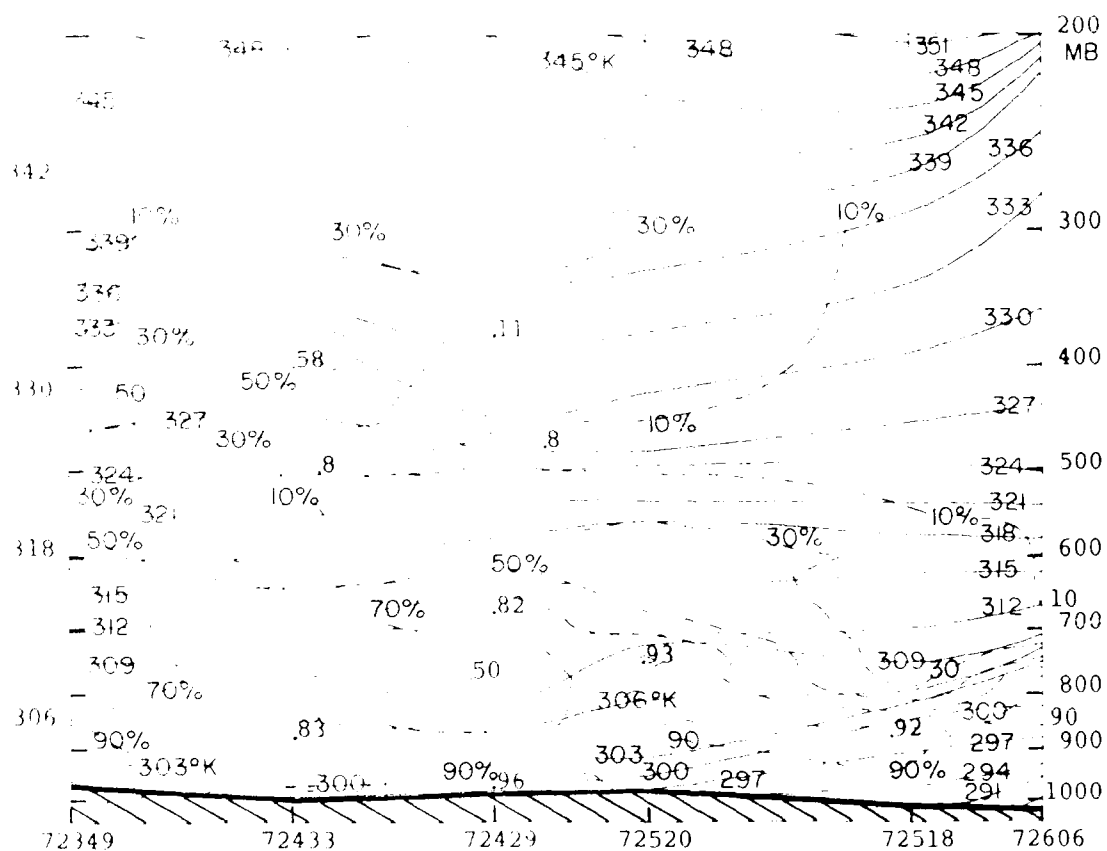
Figure 4.8.3. West-southwest - east-northeast cross section of potential temperatures (^{O}K, solid) and relative humidity (%, dashed) for 1200 UTC 7 September 1985. Rawinsonde stations used are: 72349, Monett, MO; 72433, Salem, IL; 72429, Dayton, OH; 72520, Pittsburgh, PA; 72518, Albany, NY; 72606, Portland, ME.
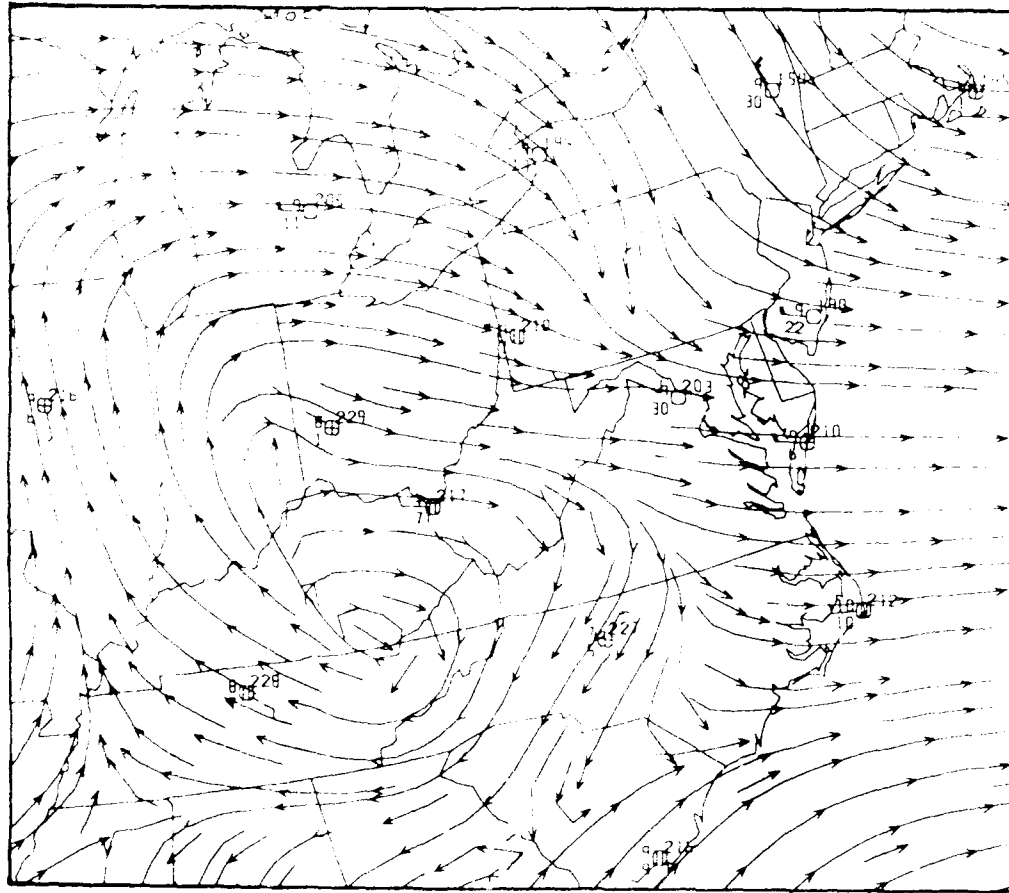
Figure 4.8.4. 700 mb rawinsonde observations, profiler winds, and streamlines from 1200 UTC 7 September 1985.
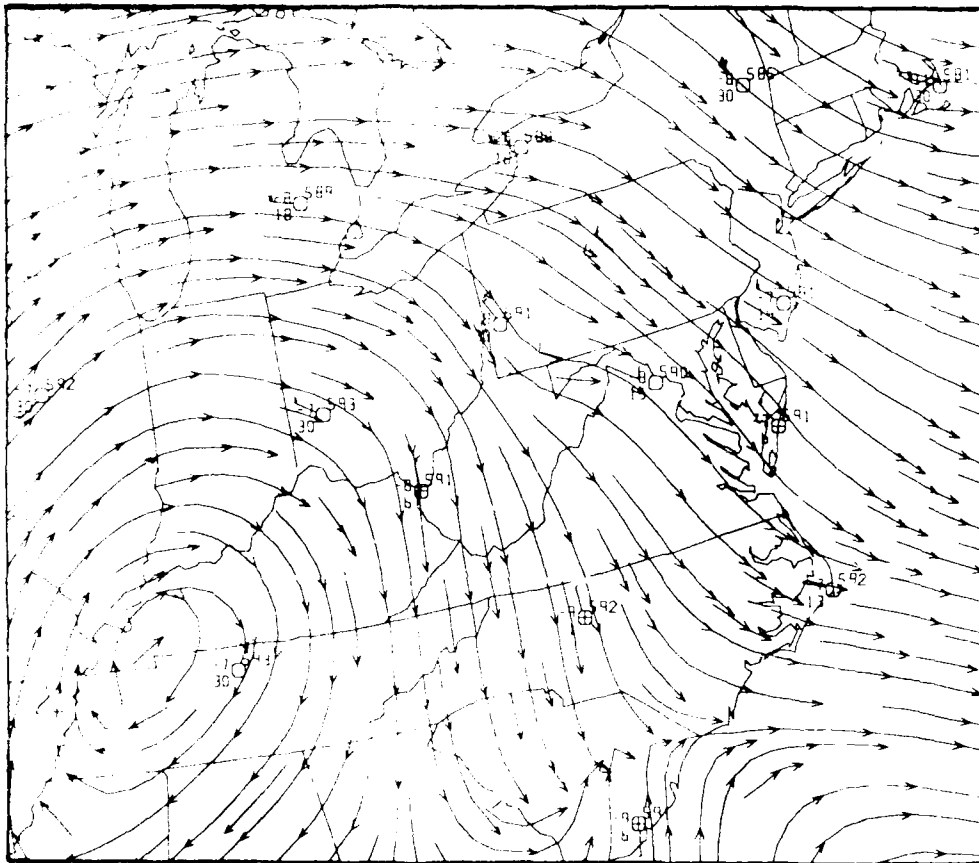
Figure 4.8.5. 500 mb rawinsonde observations, profiler winds, and streamlines from 1200 UTC 7 September 1985.
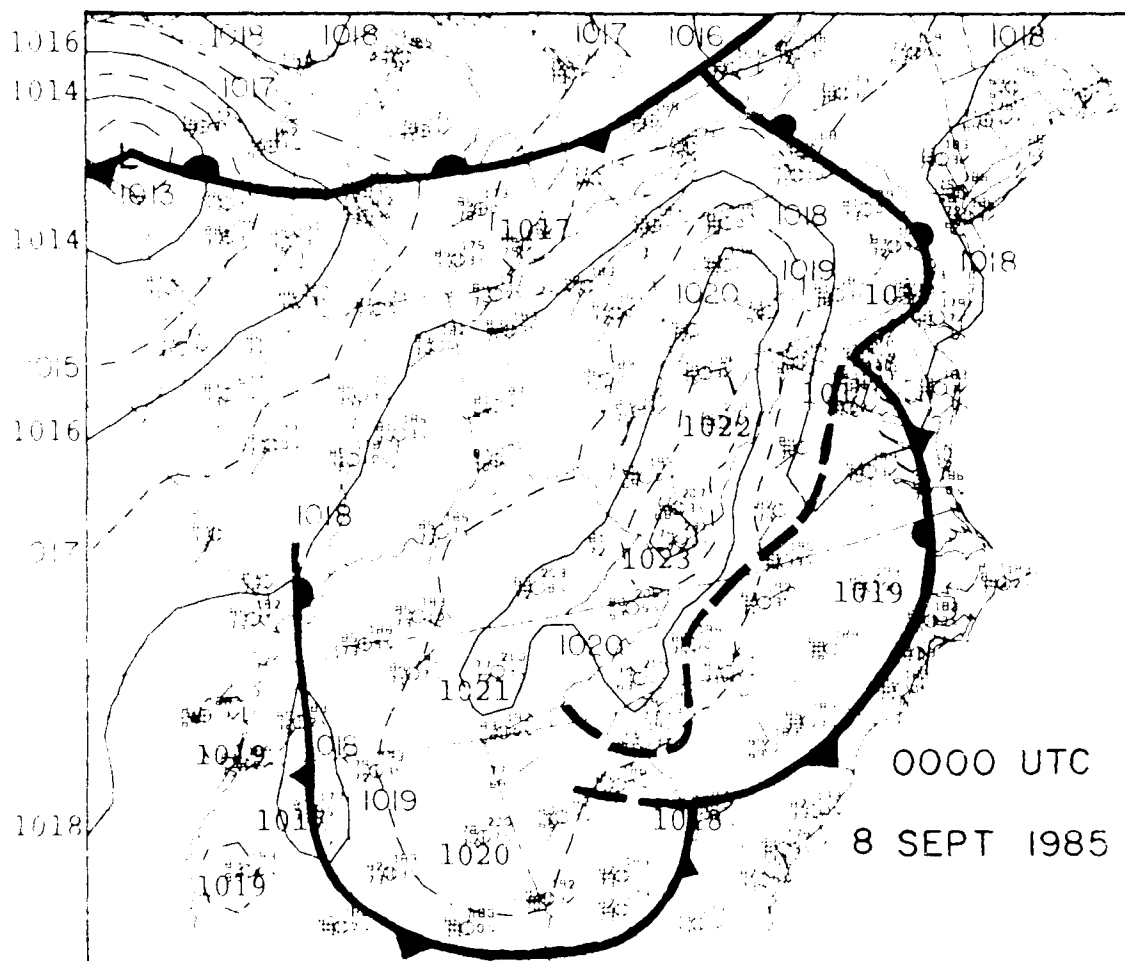
Figure 4.8.6. Surface observations, fronts, trough line, and sea-level pressure analysis (even mb, solid; odd mb, dashed) for 0000 UTC 8 September 1985.

Figure 4.8.7 is the 700 mb streamline analysis for 0000 UTC
8 September, incorporating time-space-converted profiler winds.
A mesoscale ridge has now be forced over central PA by the pro-
filer winds, but it blends in well with the winds at Atlantic
City, NJ, Albany, NY, and Buffalo, NY. Winds everywhere along
the NJ, VA, and NC coast have become northerly, during the back-
door cold front passage. The large-scale anticyclone center has
moved into western OH. The confluence zone which was over
central PA has disappeared.

To summarize, while some role of the diurnal inertial oscil-
lation cannot be ruled out, it is clear that at least one meso-
scale trough and one mesoscale ridge travelled southward or
southeastward through central and eastern PA. Non-translating
and local influences such as diurnal inertial oscillations,
mountain-induced gravity waves, and local mountain-valley circu-
lations, have yet to be examined at some later date.
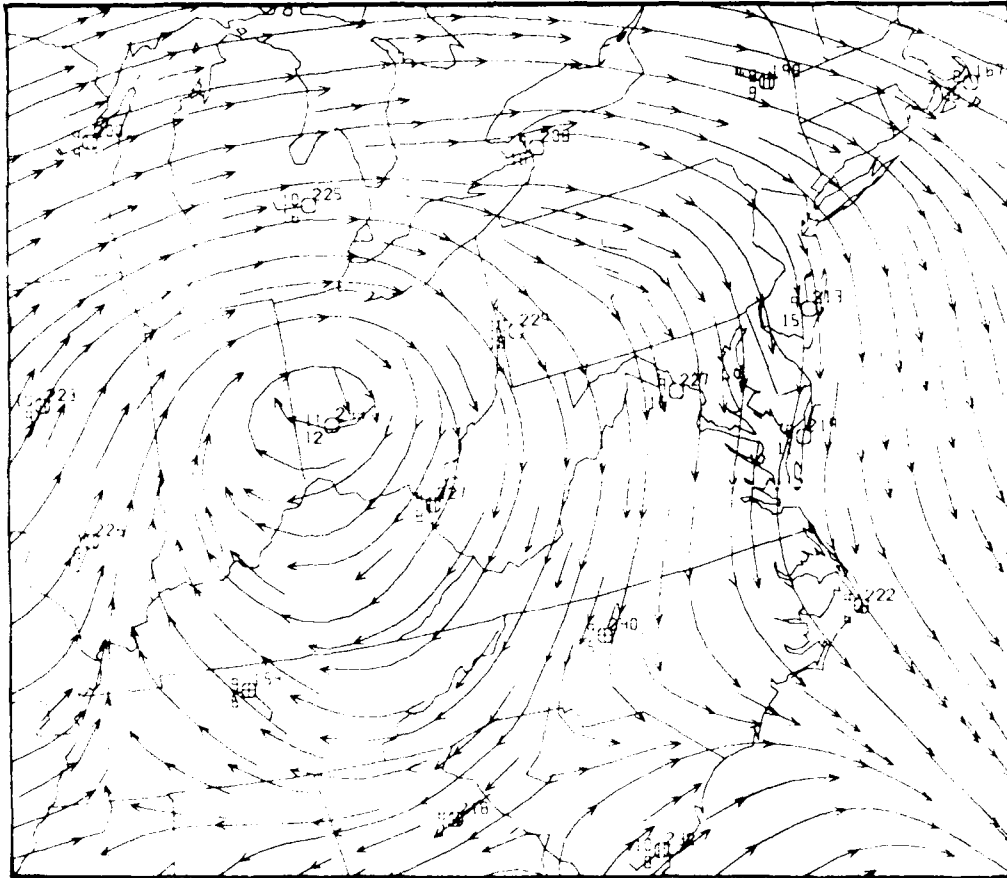
Figure 4.8.7. 700 mb rawinsonde observations, profiler winds, and streamlines from 0000 UTC 8 September 1985.

5. SINGLE-STATION CASE STUDY: EXAMINATION OF THERMODYNAMIC QUANTITIES

5.1 Undulating Frontal Surface and Frontal Waves

Figures 5.1.1 and 5.1.2 show the hourly Fleming, CO profiler wind velocities on 25-26 November 1984. Easily identified as the overall pattern in the section is the prevalence of low-level northwesterly flow and upper-level southerly flow during the period from about 0600 UTC/25 to 1800/26. Separating these flow regimes is a layer of considerable vertical shear, at an altitude that varies rather regularly over a range of about 3 km, between about 4 km and 7km. In view of the connection of this shear zone to the region of low-level wind shifts at about 0600/25, this shear zone is interpreted as a frontal zone which is meandering vertically as time progresses. This sequence of wind profiler data is among the most striking seen to date.

Assuming that the meandering wind shear zone is a frontal surface, then Figs. 5.1.1 and 5.1.2 indicate that the cold air was deep at Fleming, CO at 0700-0800/25 November, again at 0300-0500/26 November, and progressively deeper after 1200/26 November. The figures also indicate that the cold layer was shallow at 1400/25 November and 0900-1000/26 November. Some other wind-shift features also exist further aloft.

Analyses from synoptic-scale data are consistent with the meandering frontal zone hypothesis. However, the situation is not exactly as would have been imagined. An easily imagined scenario would have had a quasi-stationary surface front over the Plains east of CO, with a sequence of small frontal waves riding
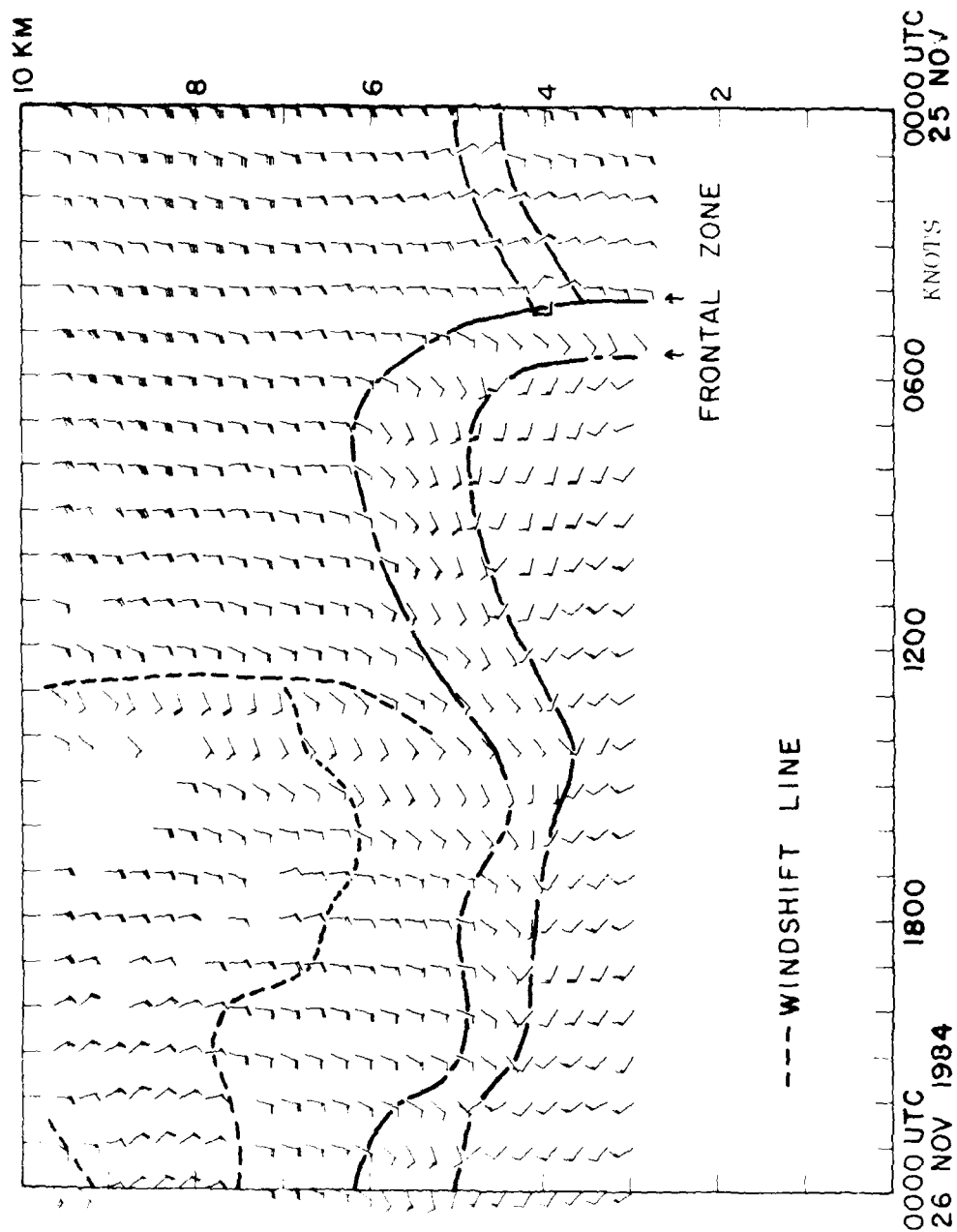
Figure 5.1.1. Time-height section of Fleming, CO profiler winds on 25-26 November 1984. Solid lines denote frontal zones, as inferred from contiguous patterns of wind shifts. Dashed lines represent other wind shift lines.
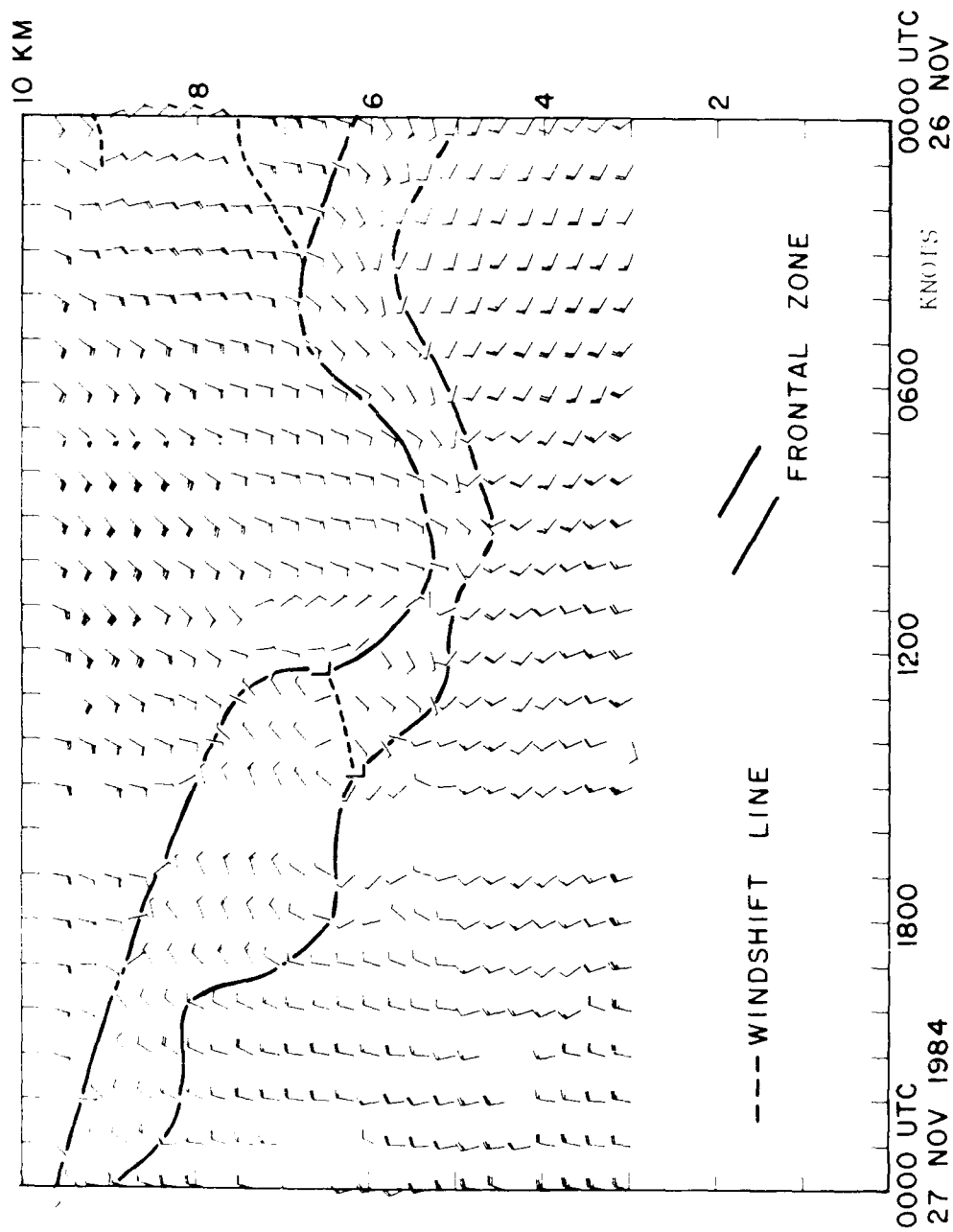
Figure 5.1.2. Time-height section of Fleming, CO profiler winds on 26-27 November 1984. Solid lines denote frontal zone, as inferred from contiguous patterns of wind shifts. Dashed lines represent other wind shift lines.

northward along it, causing the front to oscillate westward as the trough of the wave approached and causing the front to oscillate eastward as the wave trough moved away. This was not the case, as will be shown in the detailed case study which follows. Since the meandering frontal zone was located primarily near the 5 km level, and the cold layer always included the 3 km level after 0500 UTC on 25 November, a sequence of 500 mb and 700 mb analyses will be presented to illustrate the evolution of the case.

The case had some aspects similar to that of Section 4.2, of 16 December 1984, in that the case began with the lifting out northeastward of a closed low pressure system from the Southwest. Figure 5.1.3 shows the 700 mb temperature analysis for 1200 UTC on 24 November 1984. Cold air from the southwestern cutoff low (labelled cold pocket C1) is approaching the Fleming, CO profiler site (the dot in the northeastern corner of the State) from the southwest. Another major cold pocket (C3) is approaching from the northwest, and there is a hint of a weak cold pocket (C2) pushing eastward across Wyoming.

Figure 5.1.4 shows the satellite imagery at about the time of Fig. 5.1.3, revealing conveyor belts of clouds along the two major cold fronts and a patch of clouds over NM, the TX panhandle, and southeastern CO in advance of the center of the cutoff low.

Figure 5.1.5 shows a surface analysis for 0000 UTC 25 November. At this time there is a surface low over eastern CO, a sprawling anticyclone over the Gulf Coast States, and a warm
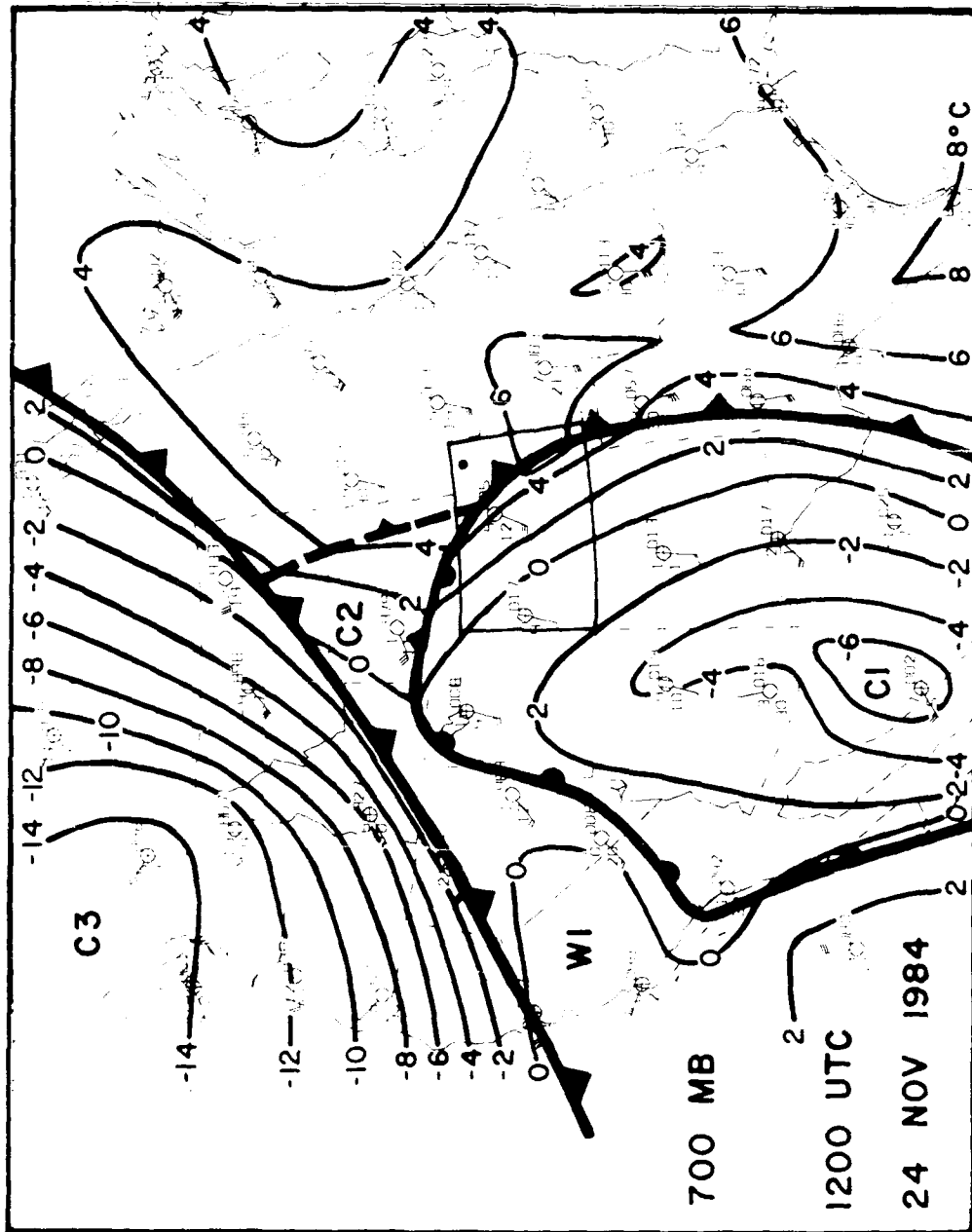
Figure 5.1.3. 700 mb rawinsonde observations, fronts, and isotherms (2°C intervals) for 1200 UTC 24 November 1984. Dot in northeastern CO locates Fleming, CO wind profiler site. Warm and cold pockets or tongues are labelled W and C, respectively, and assigned numbers for monitoring their movement and evolution over time.
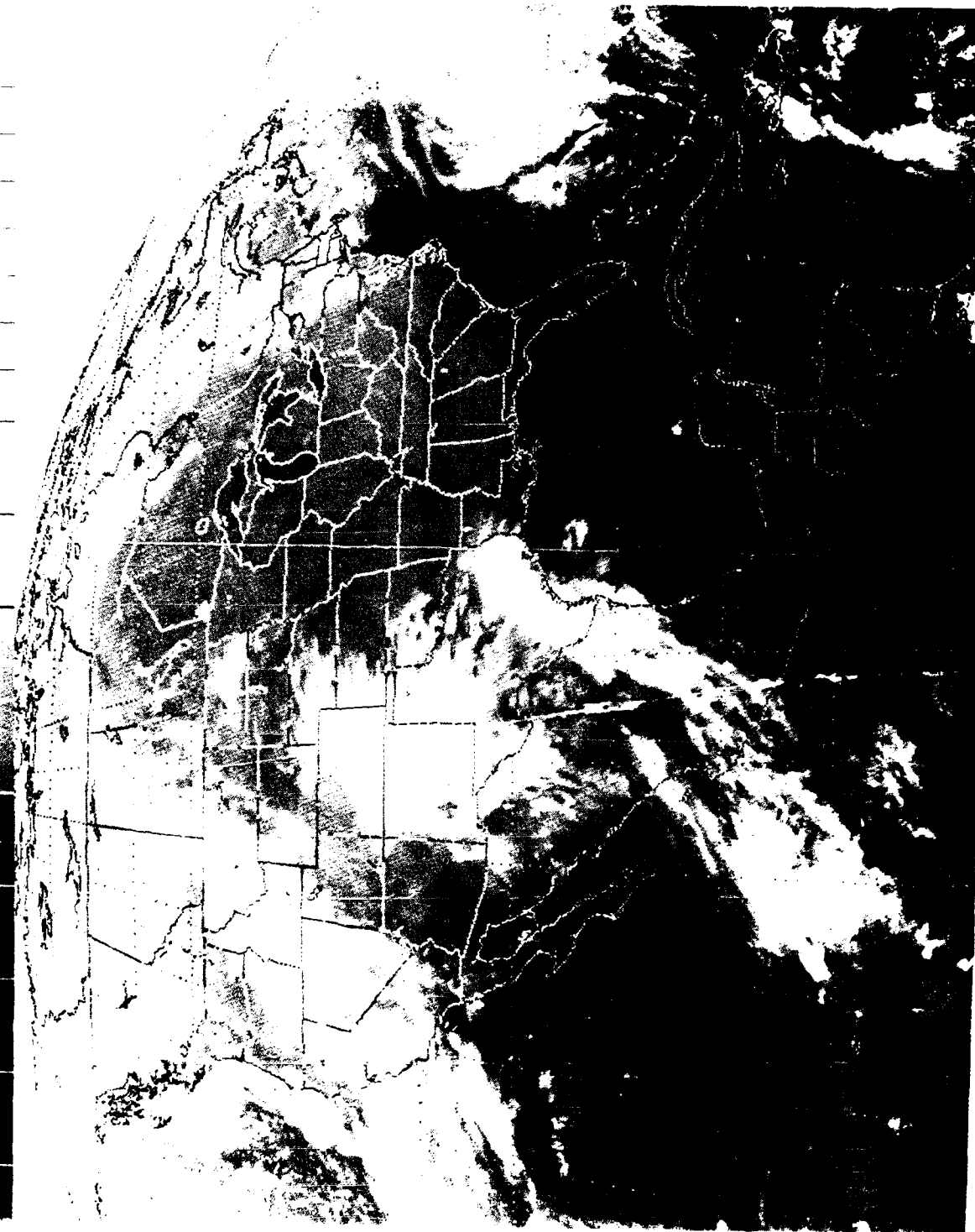
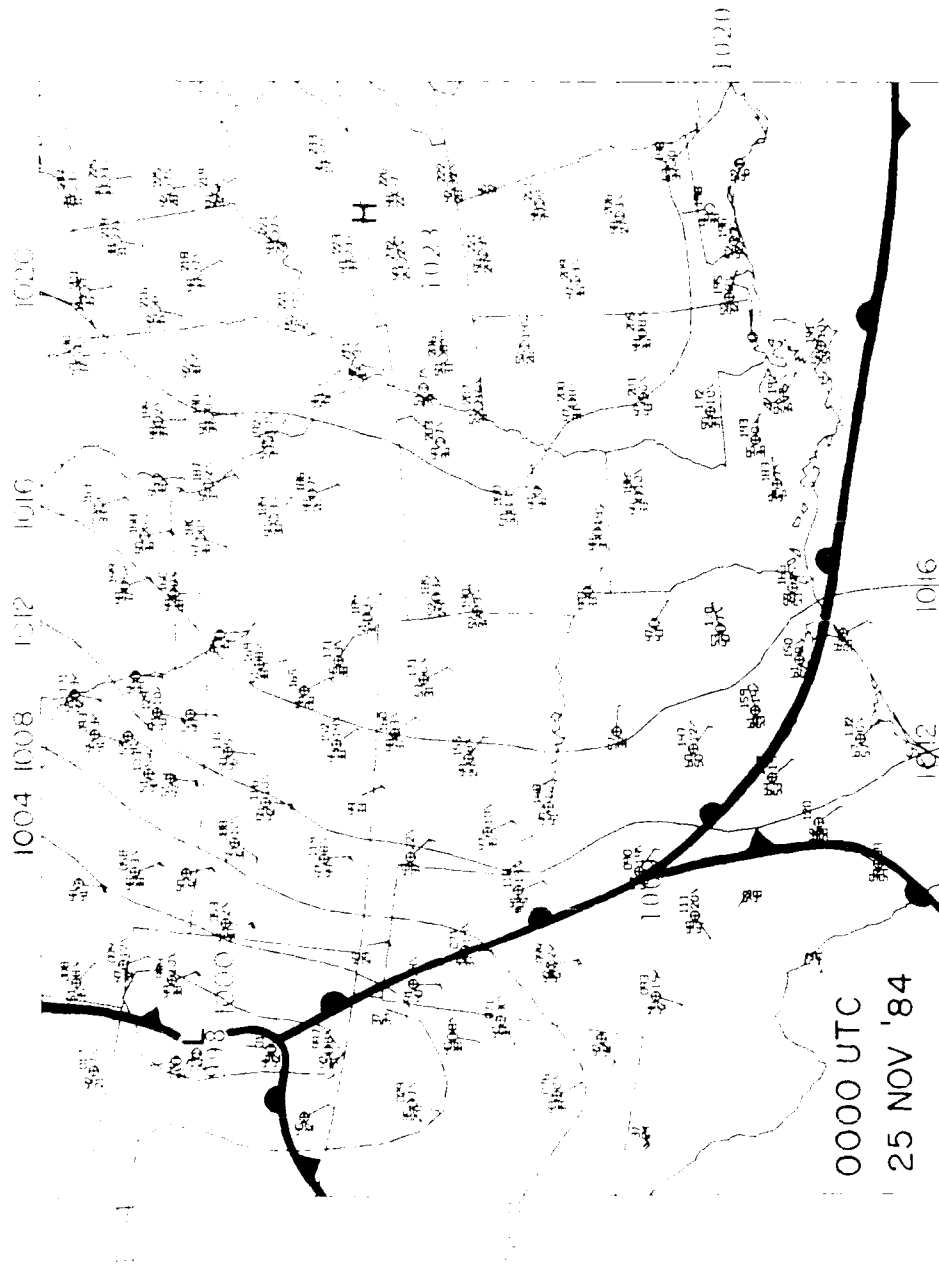Figure 5.1.4. Unenhanced infrared satellite image from 1230 UTC 24 November 1984.

Figure 5.1.5. Surface observations, fronts, and sea-level pressure analysis (4mb intervals) for 0000 UTC 25 November 1984.

front across TX. The trough of low pressure across the TX pan-
handle into CO is partly a lee trough and partly dynamically
forced (by the approaching upper-level cutoff low) at this time.
Figure 5.1.6 shows a more detailed surface chart at this time,
revealing a more complicated pattern of fronts and orographically
influenced surface lows. The main item of interest for the case
study is that the Fleming, CO wind profiler site at this time is
in SSE flow of relatively warm air, in advance of the cold air
push from any of the cold pockets C1, C2, or C3.

Figure 5.1.7 shows the 700 mb isotherm analysis at 0000 UTC
25 November 1984. The southwestern cold pocket has pushed far-
ther to the northeast across OK and KS, but is lagging behind
along the slopes of the Rockies in CO and has not reached the
Fleming profiler site yet. Likewise, the fronts with cold pock-
ets C2 and C3 have not reached Fleming at the 700 mb level. How-
ever, the front associated with C2 has passed the Denver, CO
rawinsonde site.

Figure 5.1.8 shows the 500 mb isotherm analysis at 0000 UTC
25 November. There is no 500 mb reflection of the 700 mb cold
pocket C2, but the major southwestern and Pacific cold pockets
(C1 and C3, respectively, at 700 mb) are readily apparent. Sev-
eral trough or windshift lines are also detectable.

Figure 5.1.9 shows the Denver, CO rawinsonde data from 0000
UTC 25 November 1984. A marked backing of the winds accompanies
the moist layer near 600 mb (587 mb), which is interpreted as the
altitude at which the front from cold dome C3 (Fig. 5.1.7) inter-
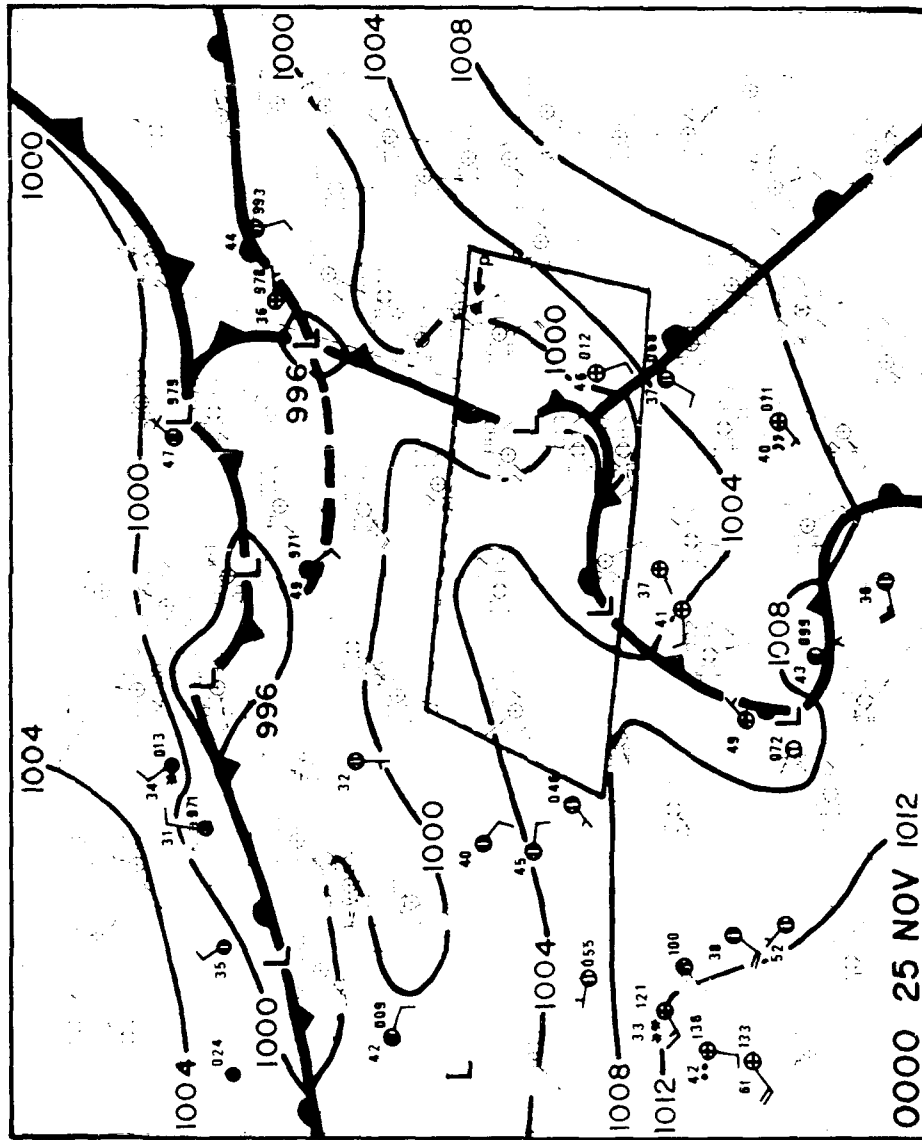sects the sounding. This front is easily seen in the cross sec-

Figure 5.1.6. Detailed map of surface observations, fronts, sea-level pressure analysis (4mb intervals) for 0000 UTC 25 November 1984.
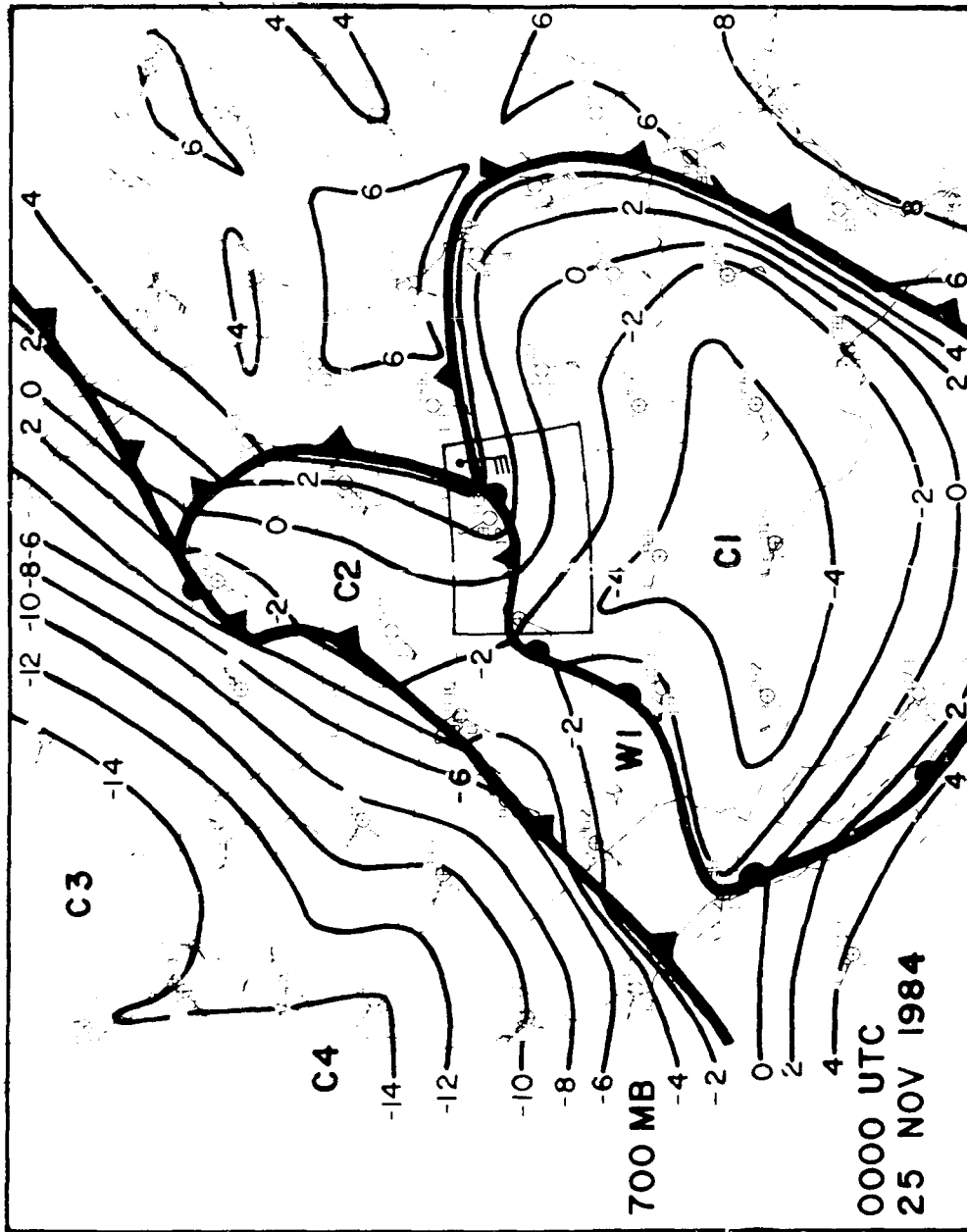
Figure 5.1.7. 700 mb rawinsonde observations, profiler wind, fronts, and isotherms (2°C intervals) for 0000 UTC 25 November 1984. Warm and cold pockets are labelled by W or C and assigned number.
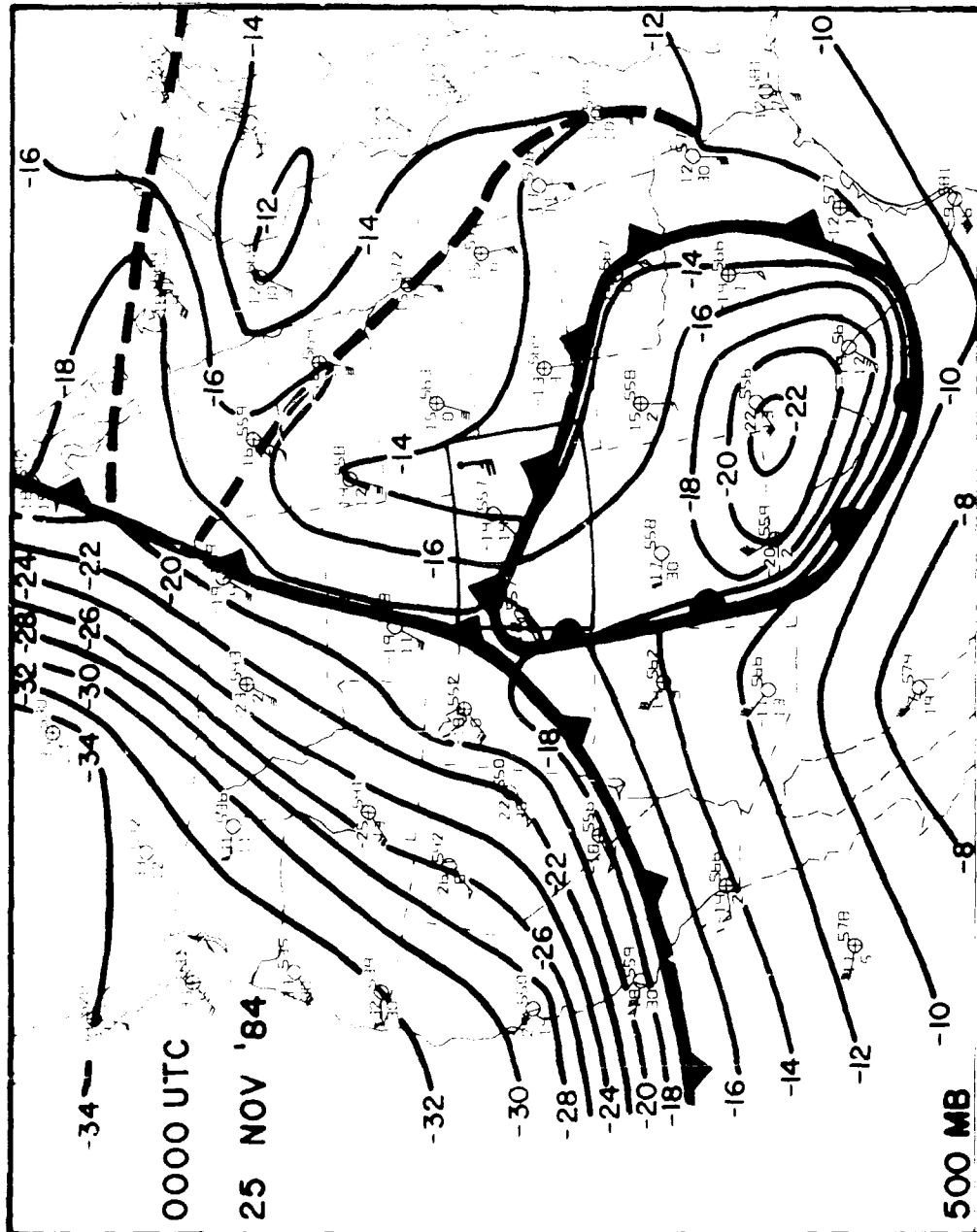
Figure 5.1.8. 500 mb rawinsonde observations, profiler wind, fronts, and isotherms (2°C intervals) for 0000 UTC 25 November 1984.
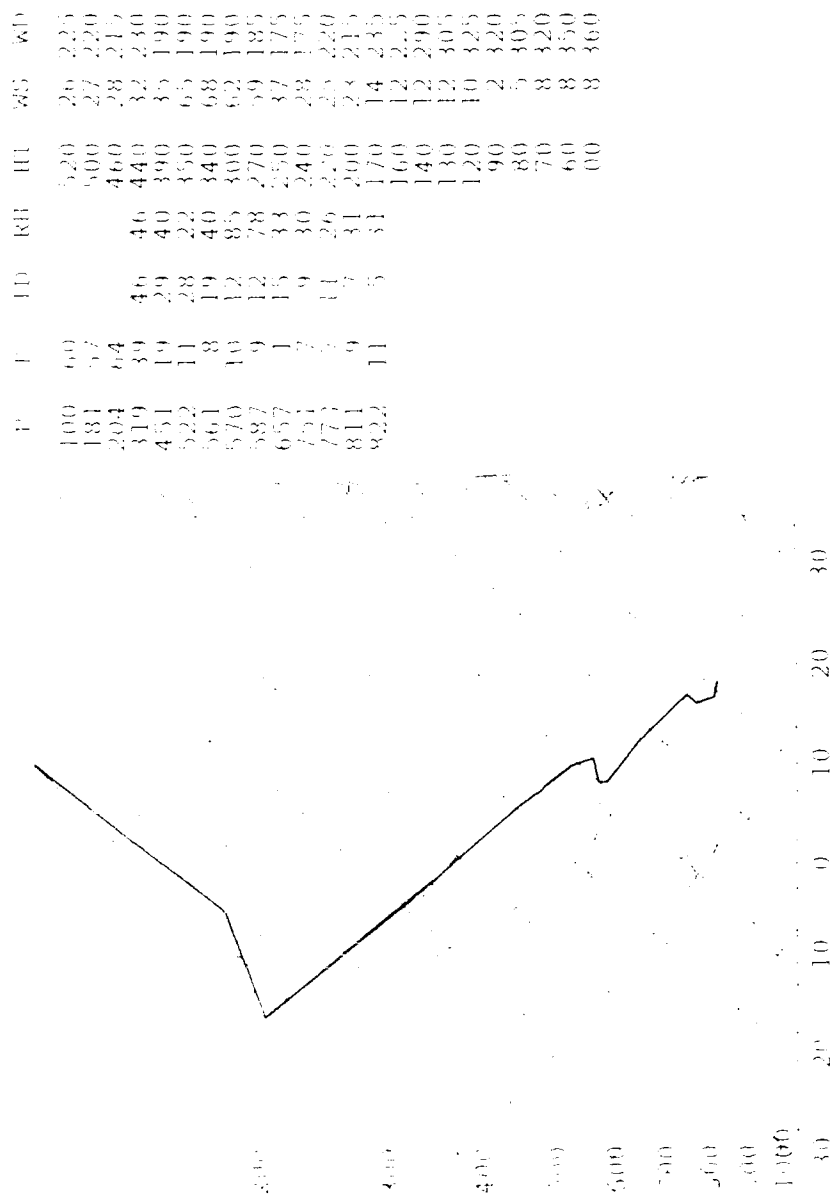
Figure 5.1.9. Skew-T log P diagram of temperatures (^{o}C, heavy) and dew points (^{o}C, thin) at Denver, CO on 0000 UTC 25 November 1984.

tion of Figure 5.1.10, as is the front associated with C3.   Actu-
ally, the front associated with C1 is also easily seen, humping
up from the surface just east of Denver, although its location
becomes vague thereafter.

By 1200 UTC on 25 November 1984, the surface analysis of
Figure 5.1.11 is still rather complicated.   Most cold fronts are
still hung up in the mountains, but a front characterized pri-
marily as a warm front has passed north of the Fleming profiler
site.   The surface is still largely influenced by orographic
effects, however.

At 700 mb, in contrast, Figure 5.1.12, the cold front assoc-
iated with C1 has passed the Fleming profiler site and is heading
for the Great Lakes.   Hereafter, the 700 mb level is remains
within cold, northwesterly flow (according to the wind profiler
time-height section).   Actually, the coldest air of C1 has passed
well beyond Fleming, CO, and the relative warm tongue along the
front of C2 is near the wind profiler site.   Also near the pro-
filer, to the SW, is the northeastern portion of cold air mass
C1', which is a portion of original cold dome C1 that has been
left behind in NM.   Thus, the 700 mb analysis agrees well with
the analysis of the undulating frontal zone of Fig. 5.1.1.   Once
the cold front of C1 passed (0500 UTC), the frontal zone rose
until about 0800 UTC, and began descending thereafter as the
coldest air passed NE beyond the profiler site.

Figure 5.1.13 shows the 12h change of the 700 mb temper-
atures ending at 1200 UTC 25 November 1984.   These confirm that
the coldest temperatures have passed beyond Fleming.   Denver, CO
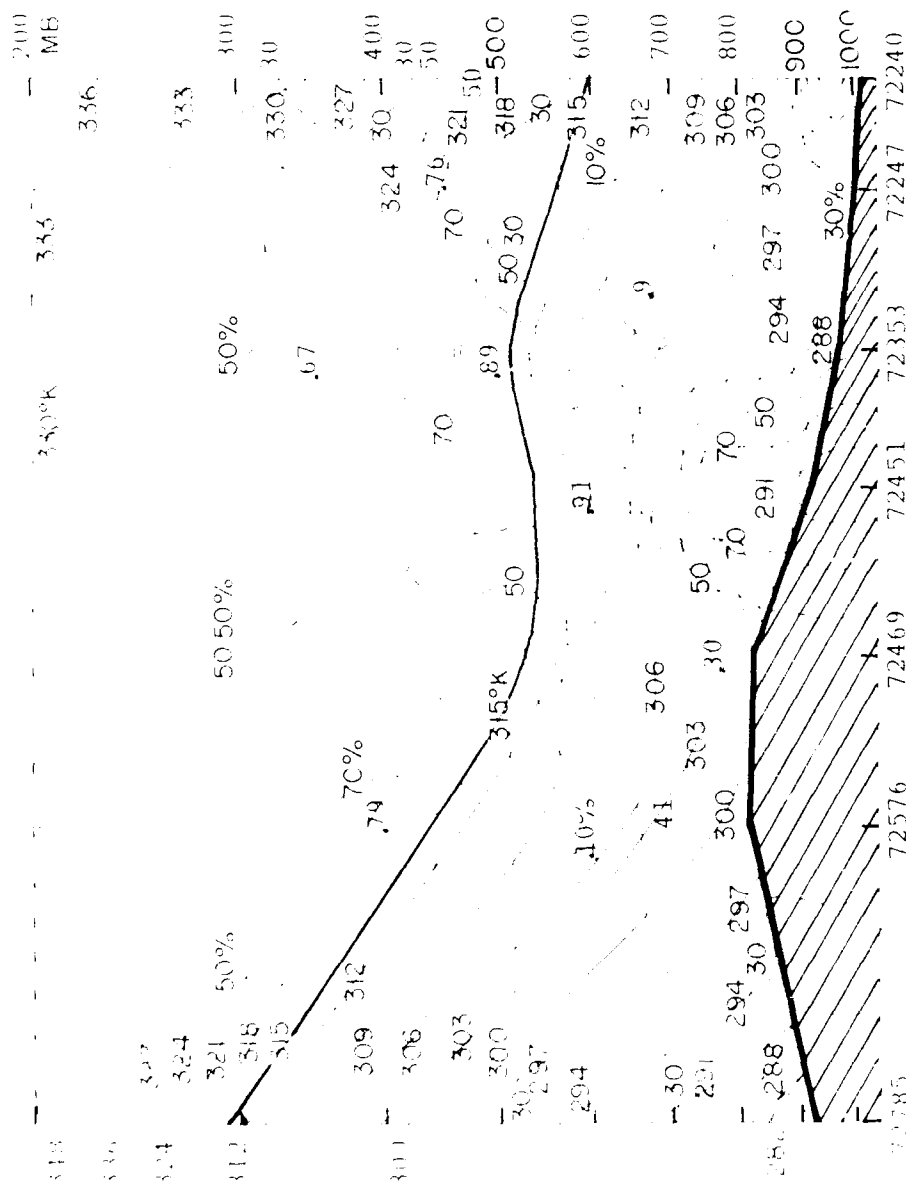
Figure 5.1.10. Northwest-southeast cross section of potential temperatures (°K, solid) and relative humidities (%, dashed) for 0000 UTC 25 November 1984. Rawinsonde stations used are: 72785, Great Falls, MT; 72576, Lander, WY; 72469, Denver, CO; 72451, Dodge City, KS; 72353, Oklahoma City, OK; 72247, Longview, TX; 72240, Lake Charles, LA.
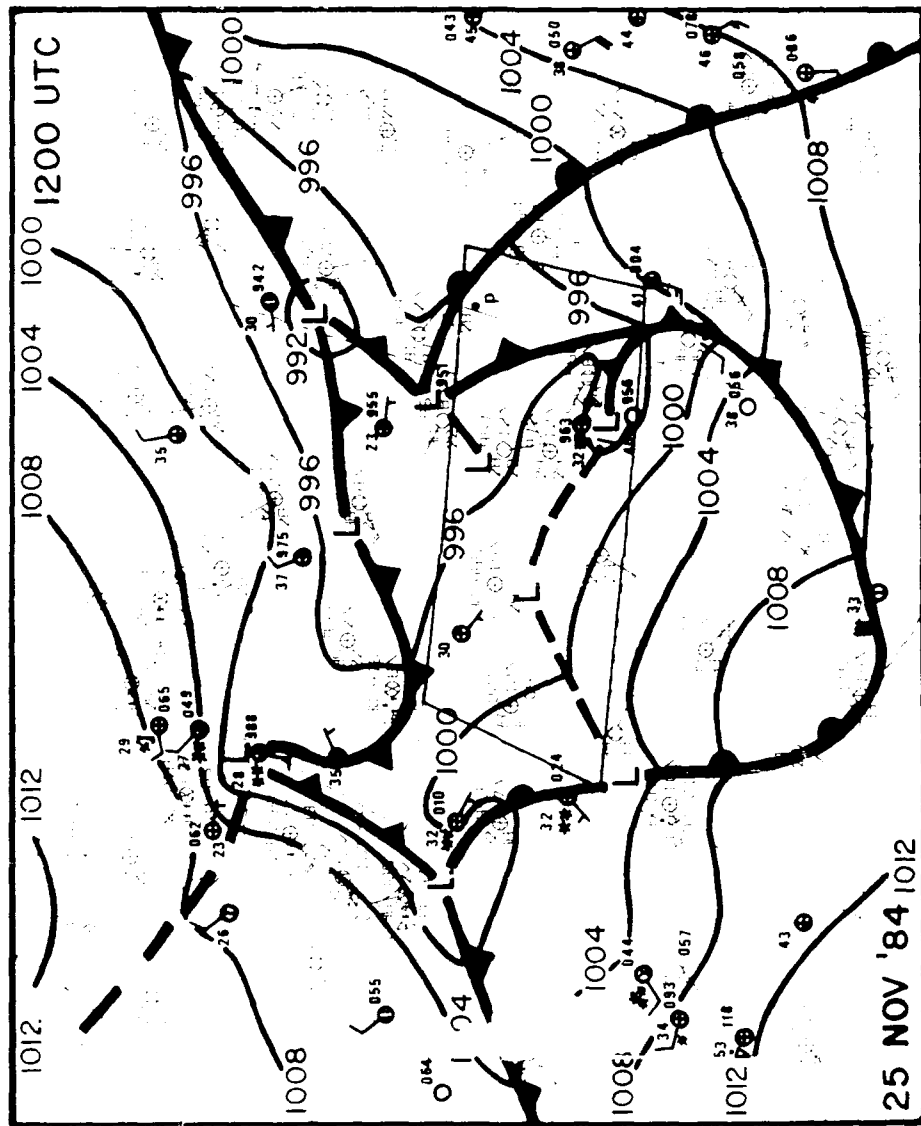
177

Figure 5.1.11. Surface observations, fronts, and sea-level pressure analysis
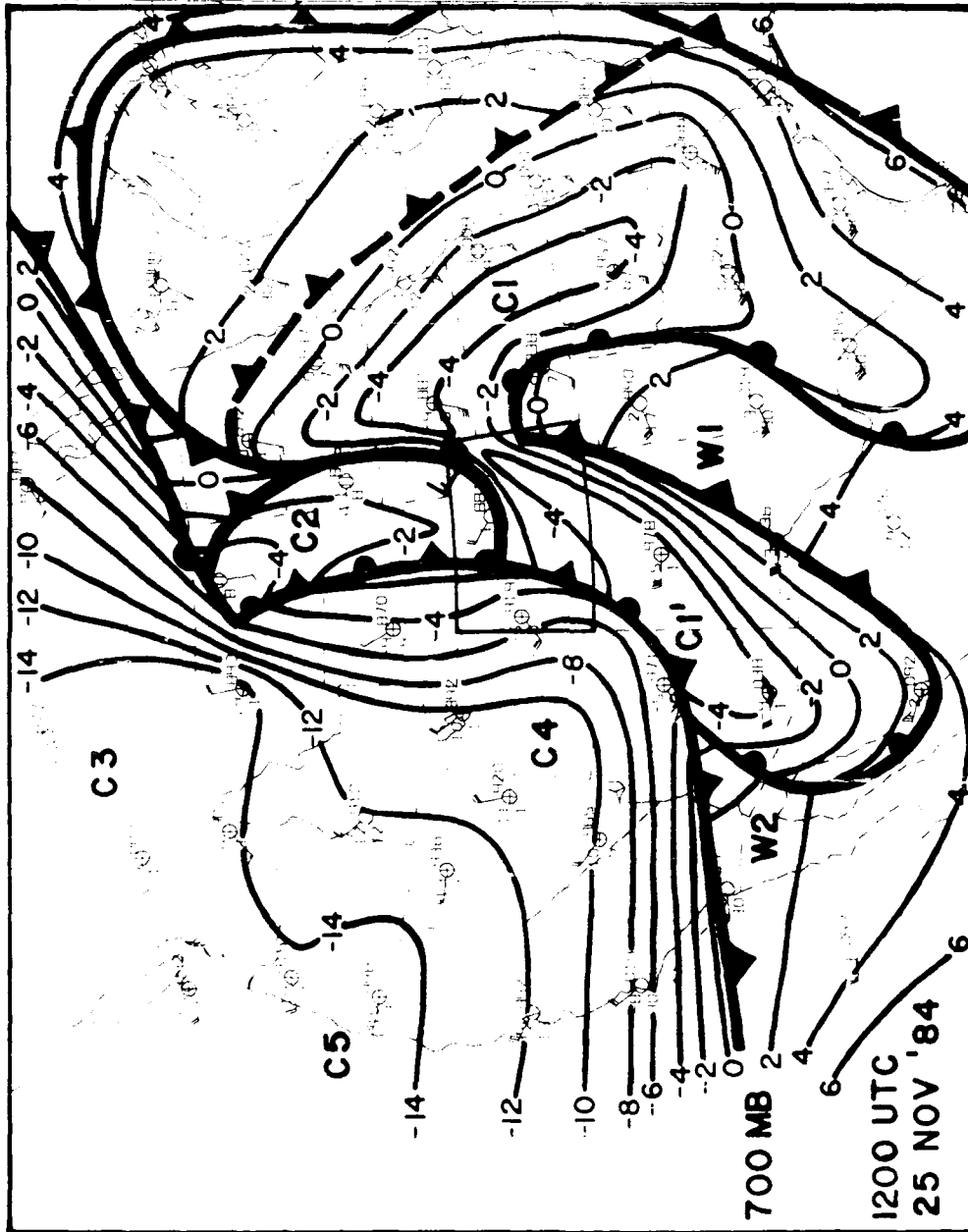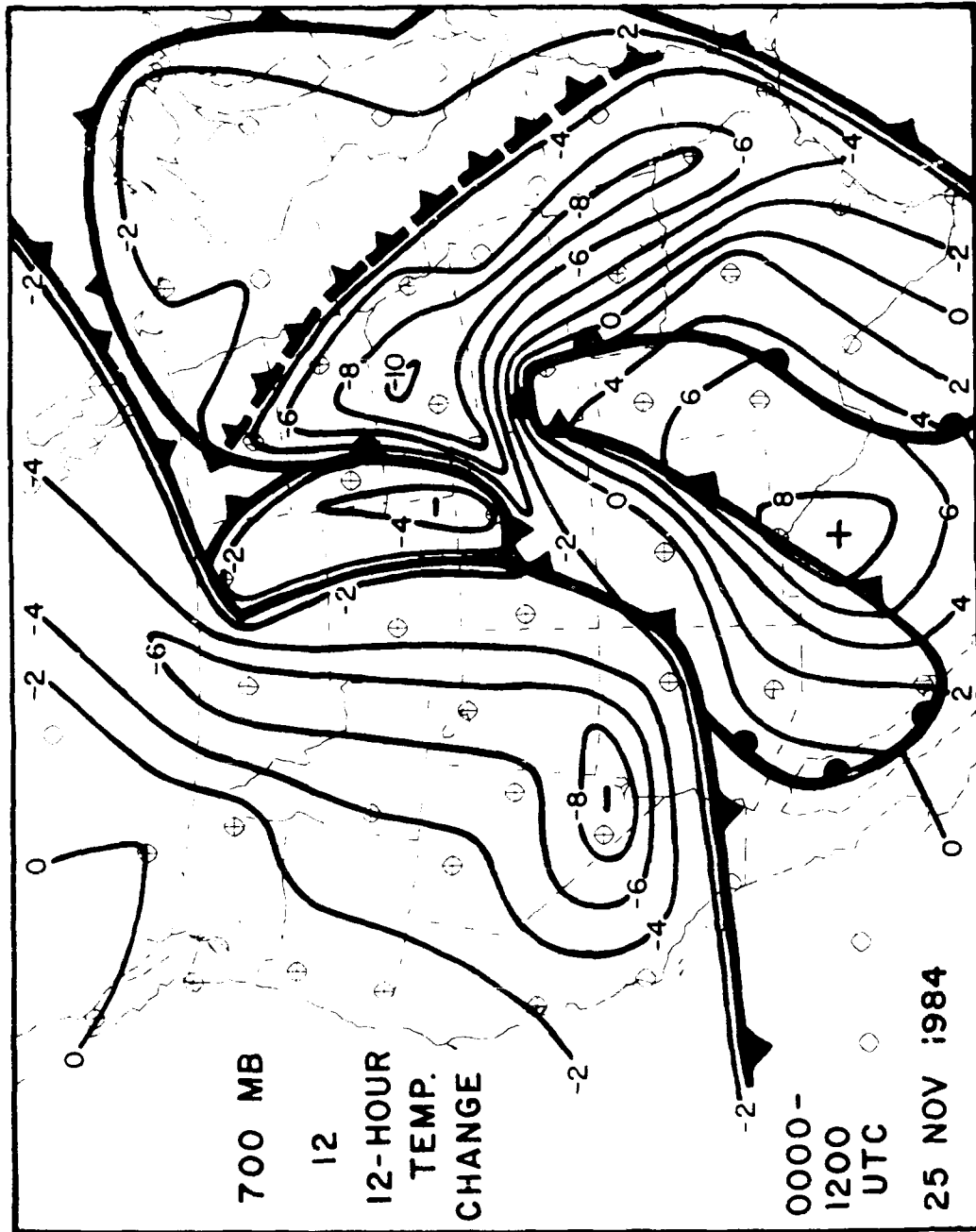(4 mb intervals) for 1200 UTC 25 November 1984.

178

Figure 5.1.12. 700 mb rawinsonde observations, profiler wind, fronts, and isotherms (2°C intervals) for 1200 UTC 25 November 1984. Warm and cold pockets are labelled by W or C and assigned number.

700 MB

12

12-HOUR
TEMP.
CHANGE

0000-
1200
UTC

25 NOV 1984

Figure 5.1.13. Change of 700 mb temperature (°C) during the past 12h, and front locations, for 1200 UTC 25 November 1984.

and Rapid City, SD are near a minimum of temperature decrease, as they are near the relative warm tongue along the front of C2.

Figure 5.1.14 shows the 500 mb temperatures at 1200 UTC 25 November. The NNE-moving cold front from the Southwest has passed Fleming, CO, and the Pacific front has caught up to it just west of the profiler site. That occluded-type front between air masses C1 and C3 is approaching Fleming, CO from the west.

Figures 5.1.15 and 5.1.16 show the Denver sounding and a cross section for 1200 UTC 25 November. An intercomparison with Figs. 5.1.9 and 5.1.10, the 0000 UTC counterparts, shows that there has been a cooling at Denver at all altitudes in the troposphere. At pressures below about 230 mb, in the stratosphere, a warming has occurred, and the tropopause has descended. The cross section shows that a deeper portion of C1 has pushed over Oklahoma City, OK (72353), and that the western portion of C1 has pushed westward to Denver, where it intercects the Pacific front.

Figure 5.1.17 shows the surface analysis for 0000 UTC 26 November. By this time the dynamics are beginning to push eastward, and frontal waves can be seen over western KS/NE and over SD. Other low pressure centers linger over the Rockies, where the Pacific front passage is apparently being delayed by the terrain.

Figure 5.1.18 shows the 700 mb isotherms for 0000 UTC 26 November. The Pacific front has clearly passed through the entirety of CO at this level. The 700 mb analysis again agrees with the behavior of the frontal zone of Fig. 5.1.1. The frontal zone began to ascend after 1400 UTC and is still rising, in
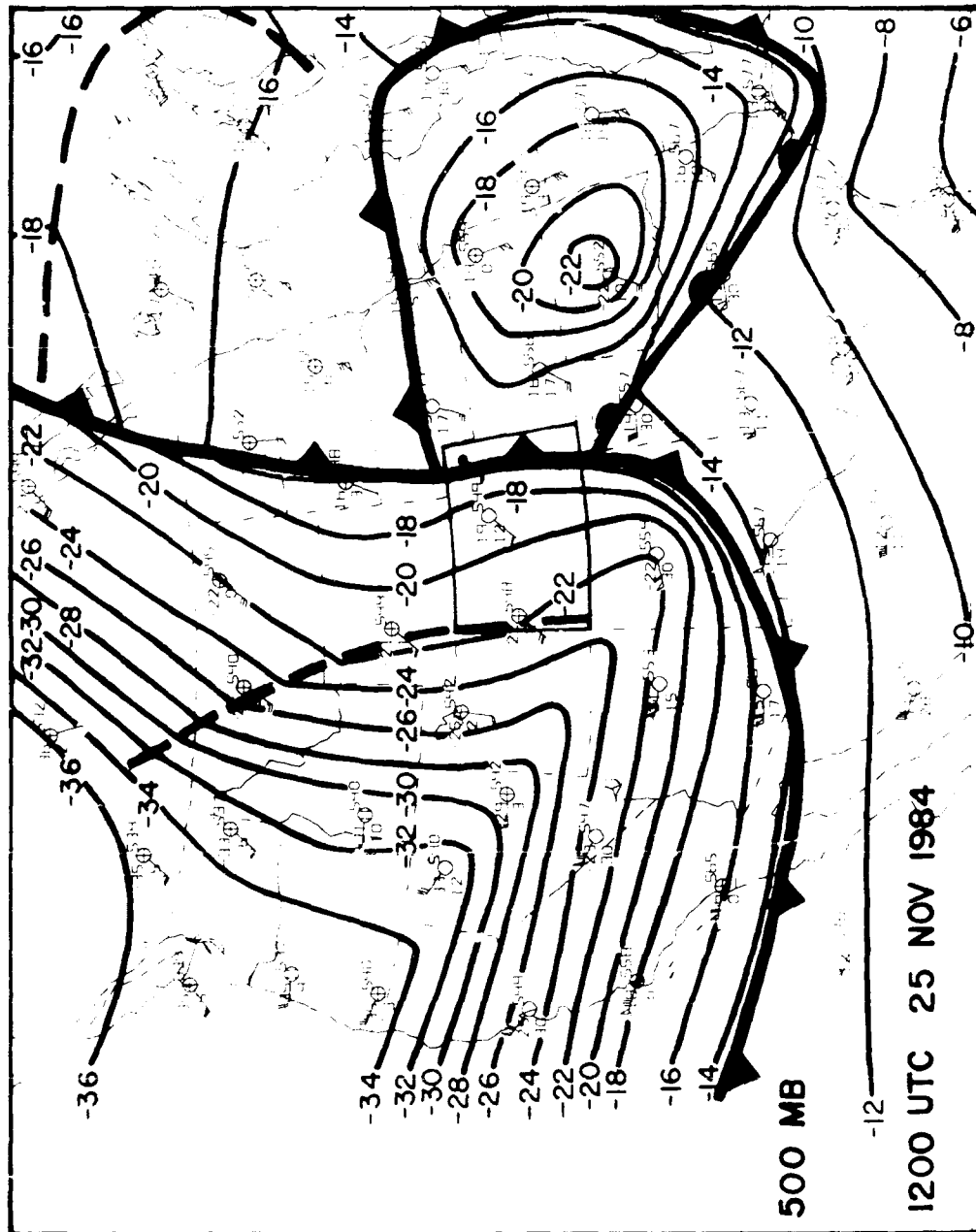
Figure 5.1.14. 500 mb rawinsonde observations, profiler wind, fronts, and isotherms (2°C intervals) for 1200 UTC 25 November 1984.
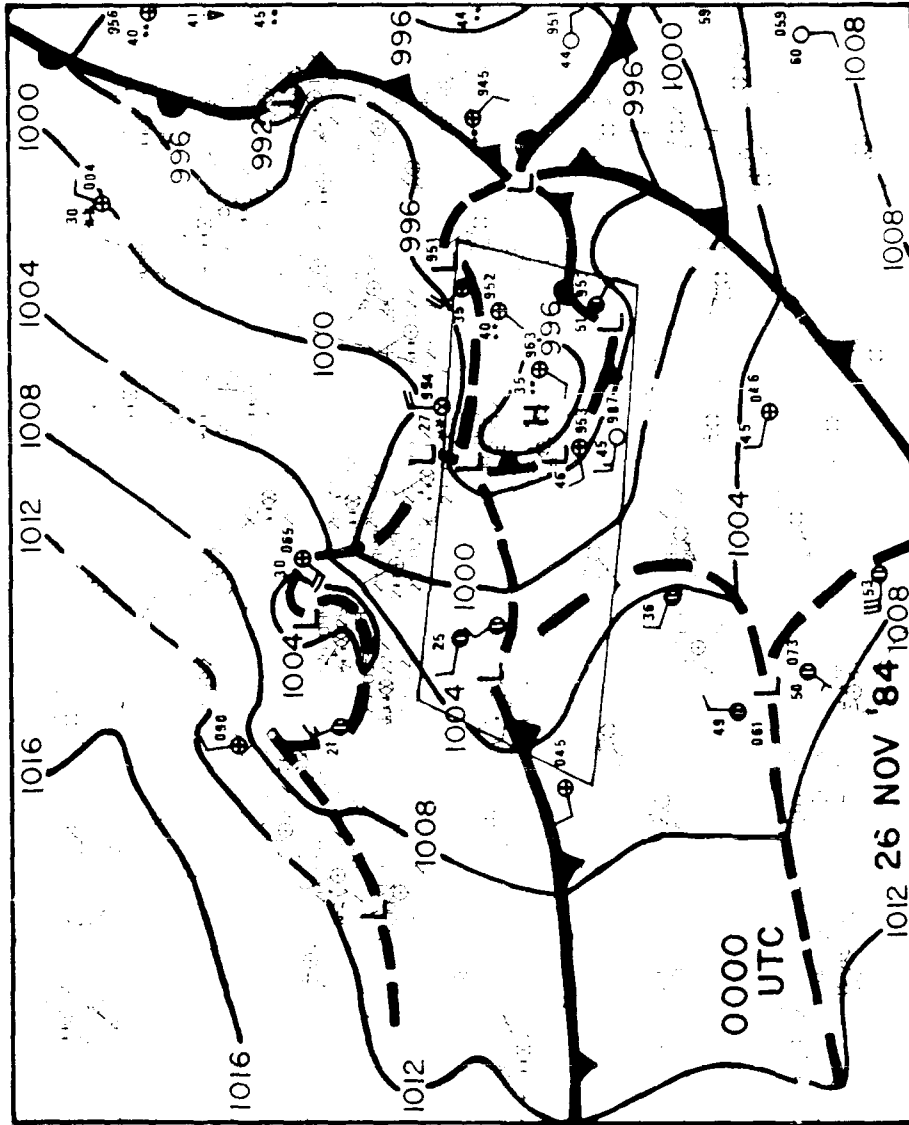
P	T	Td	RH	HT	WS	WD
100	-58			480	34	220
115	-58			460	36	235
150	-52			440	47	225
167	-54			430	33	215
200	-50			400	35	235
238	-57			370	42	210
330	-39	-41	26	350	27	190
374	-31	-42	32	340	24	185
395	-29	-32	74	300	28	225
431	-24	-31	51	270	21	215
456	-22	-27	63	250	27	225
500	-19	-31	33	240	31	230
524	-15	-31	23	200	21	250
637	6	-17	40	180	18	225
775	6		38	160	12	250
794	4	-6	47	140	13	260
804	3	-3	93	130	10	250
814	2	-1	80	120	9	235
819	-2	-5	79	110	14	275
				100	20	305
				90	18	305
				80	11	260
				70	4	220
				60	1	175
				00	0	0

Figure 5.1.15. Skew-T log P diagram of temperatures (°C, heavy) and dew points (°C, thin) at Denver, CO on 1200 UTC 25 November 1984.

Figure 5.1.16. Northwest-southeast cross section of potential temperatures (°K, solid) and relative humidities (%, dashed) for 1200 UTC 25 November 1984. Stations as in Fig. 5.1.10.

Figure 5.1.17. Surface observations, fronts, and sea-level pressure analysis (4mb intervals) for 0000 UTC 26 November 1984.
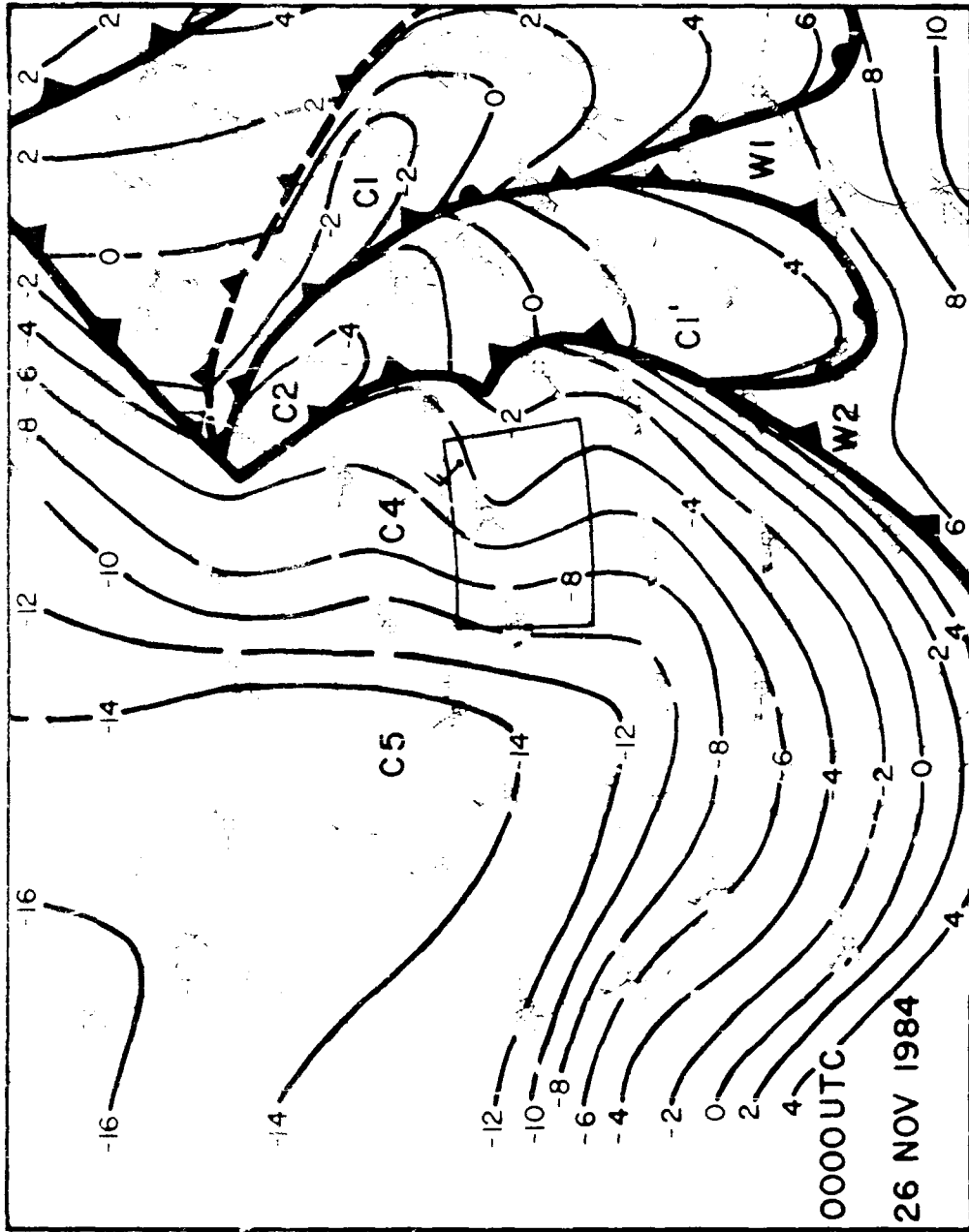
Figure 5.1.18. 700 mb rawinsonde observations, profiler wind, fronts, and isotherms (2°C intervals) for 0000 UTC 26 November 1984. Warm and cold pockets are labelled by W or C and assigned number.

response to the reinforcement of ... . Since all features of interest have now passed at 700 mb, the 700 mb level will no longer be examined.

At 500 mb, Figure 5.1.19, the Pacific front has entered central CO. The Denver winds have become easterly, presumably under the influence of the frontal trough or closed low pressure center.

Figures 5.1.20 and 5.1.21 show the 0000 UTC 26 November Denver sounding and cross section. In comparison to Figs. 5.1.15 and 5.1.16 from 12h earlier, Denver can be seen to have again cooled at all levels in the troposphere, except for a shallow layer near the surface. The tropopause has descended to about 300 mb, above which warming has continued. The cold pocket C1 has now almost entirely passed northeast beyond the plane of the cross section.

Figure 5.1.22 shows the surface analysis at 1200 UTC 26 November. A well-defined cyclone formed along the Plains and has tracked into northeastern ND. The approaching Pacific front has triggered a modest cyclone center in north-central CO, and the front is bearing down on the profiler site.

Figure 5.1.23 shows infrared satellite imagery from 1100 UTC 26 November. A conveyor belt of cloud extends from western TX into southeastern KS aloft in advance of the Pacific cold front. A patch of clouds over CO and Wyoming accompanies the Pacific trough.

Figure 5.1.24 shows the 500 mb analysis at 1200 UTC 26 November. The Pacific cold pocket, which may have split into
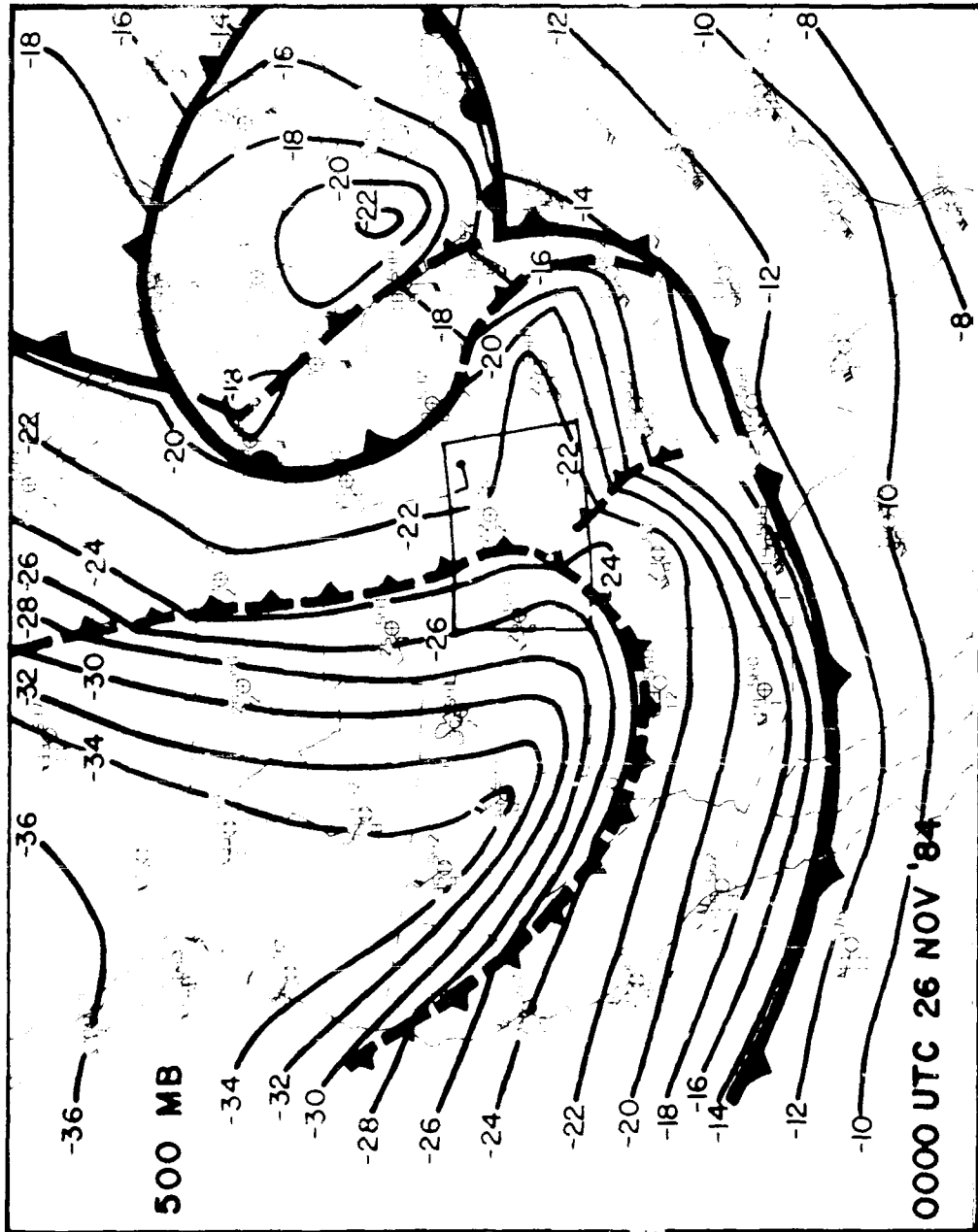
Figure 5.1.19. 500 mb rawinsonde observations, profiler wind, ..s, and
isotherms (2°C intervals) for 0000 UTC 26 November 1984.
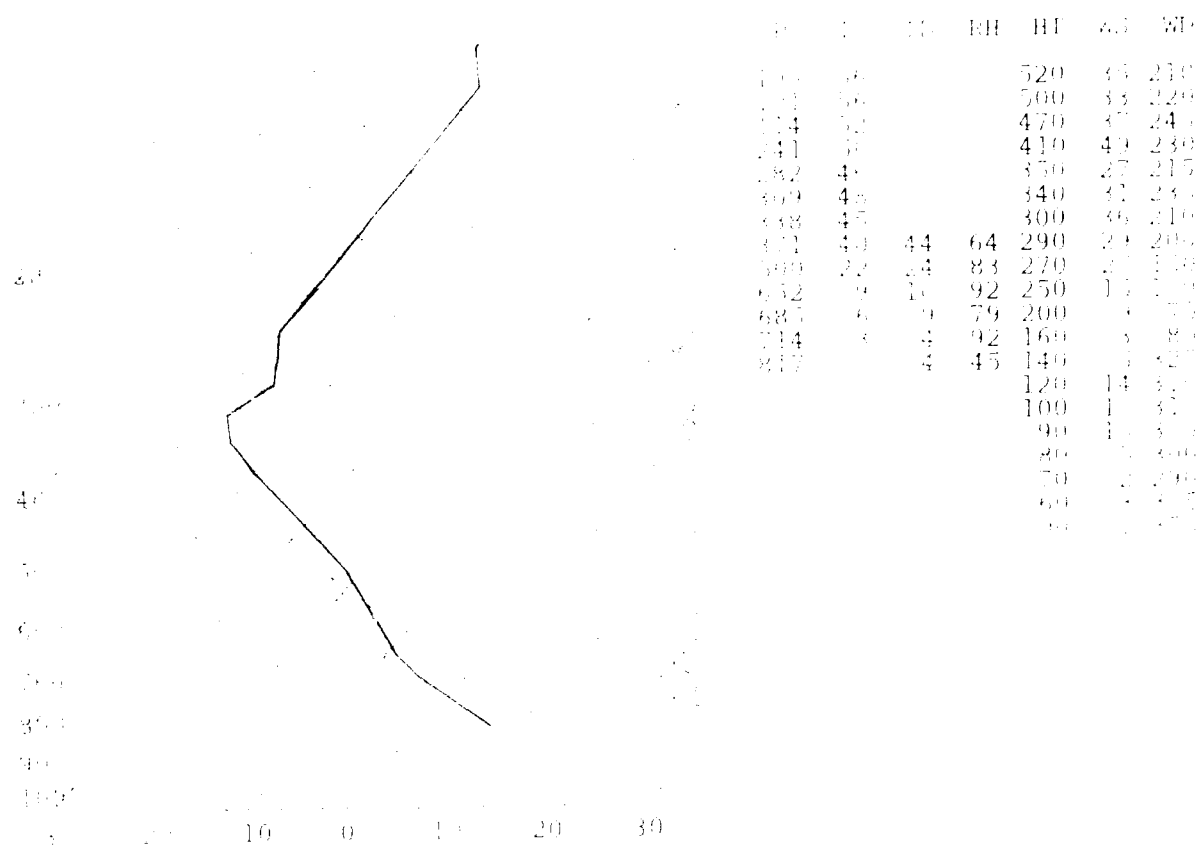
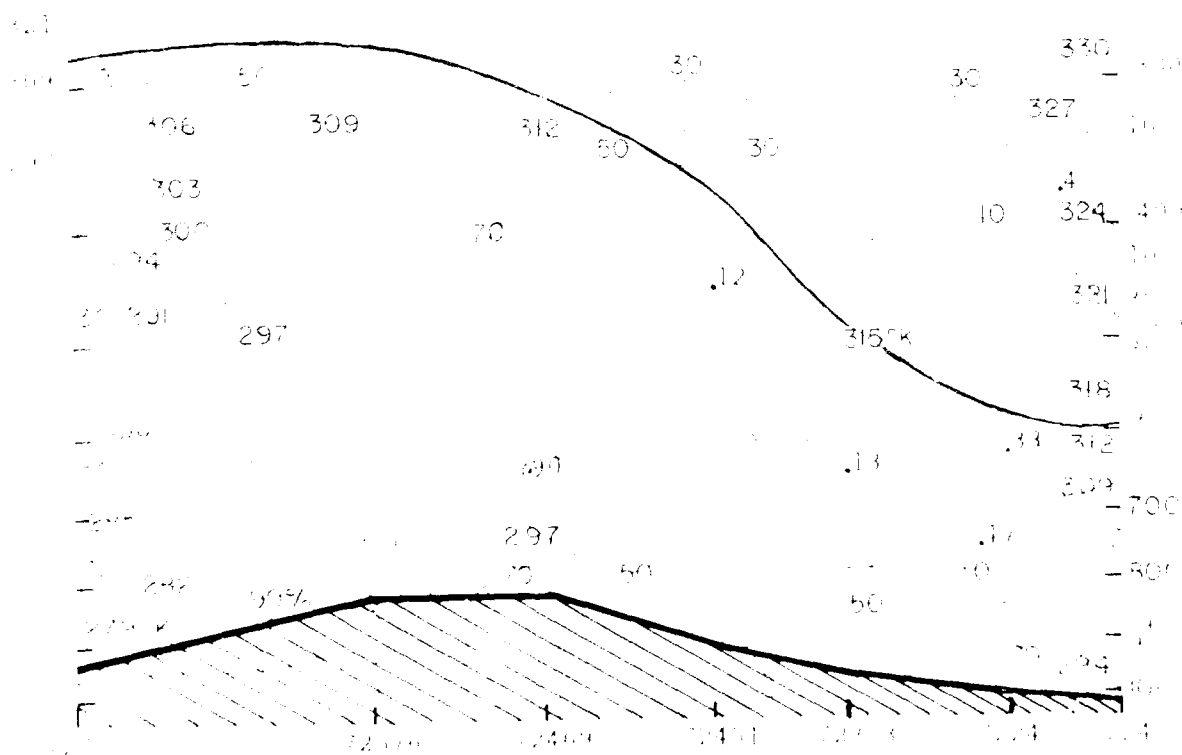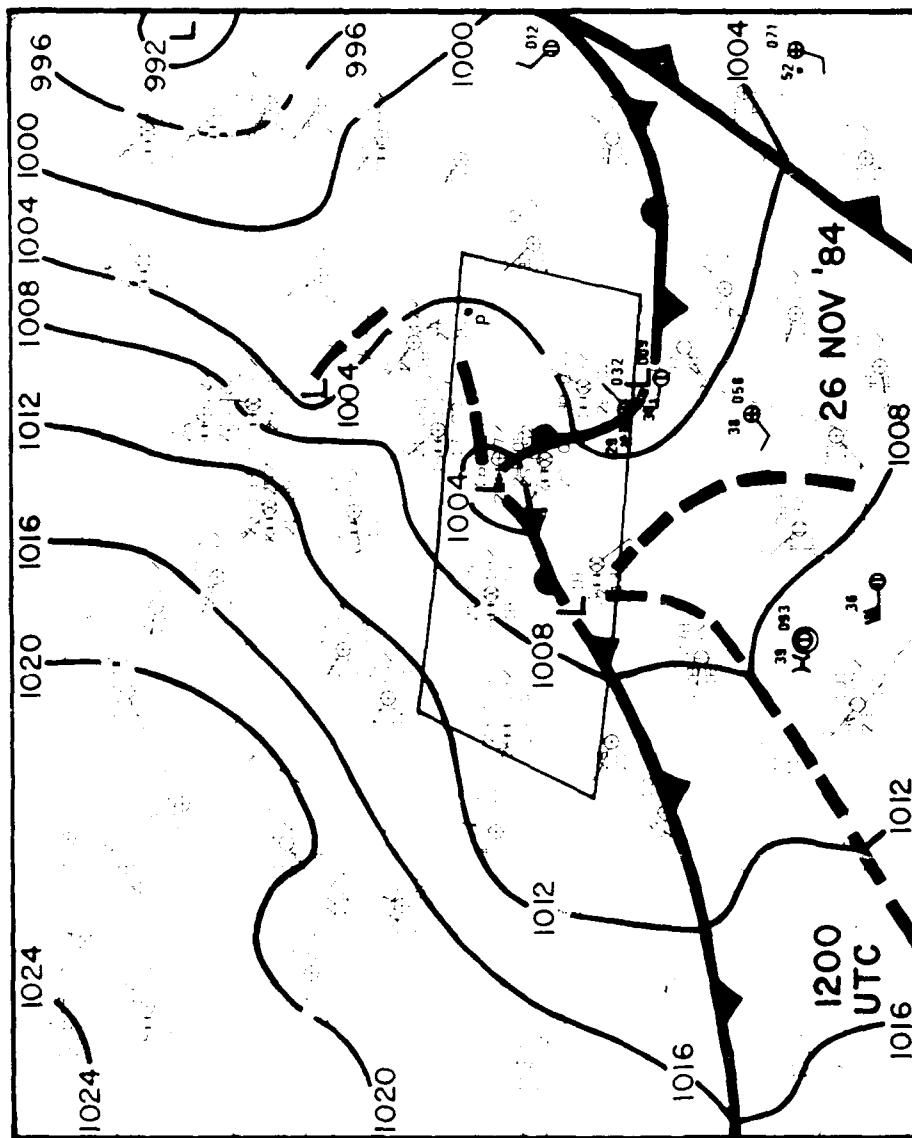Figure 5.1.20. Skew-T log P diagram of temperatures (°C, heavy) and dew points (°C, thin) at Denver, CO on 0000 UTC 26 November 1984.

Figure 5.1.21. Northwest-southeast cross section of potential temperature (°K, solid) and relative humidities (%, dashed) for 0000 UTC 26 November 1984. Stations as in Fig. 5.1.10.

Figure 5.1.22. Surface observations, fronts, and sea-level pressure analysis
(4mb intervals) for 1200 UTC 26 November 1984.
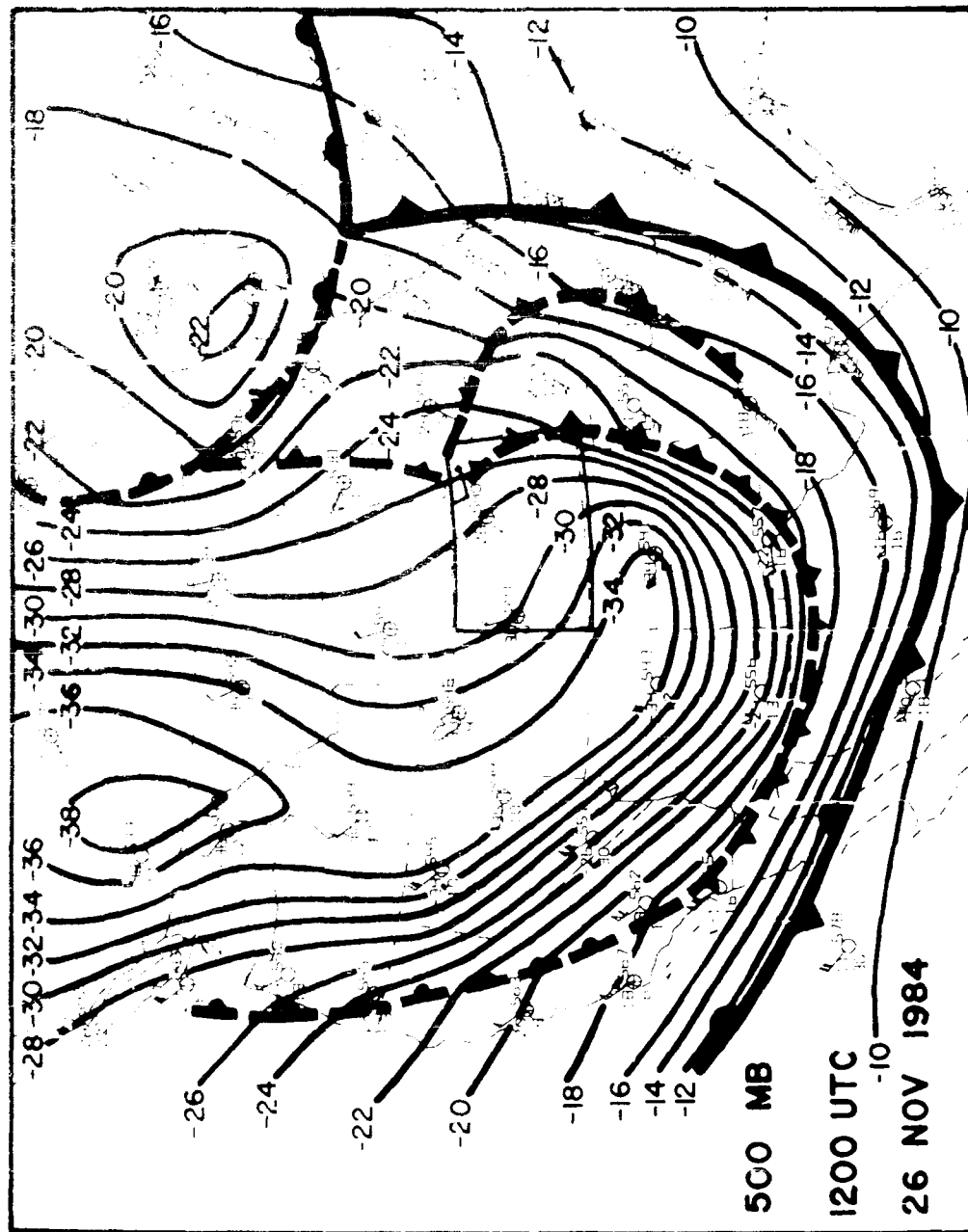
Figure 5.1.24. 500 mb rawinsonde observations, profiler wind, fronts, and isotherms (2°C intervals) for 1200 UTC 26 November 1984.

several cold pockets, is advancing toward the profiler, and is nearby. The temperatures at all tropospheric levels over Denver continue to cool, Figure 5.1.25, but the tropopause has apparently levelled off, as has the stratospheric warming.

The cross section, Figure 5.1.26. shows that all of the baroclinic zones have passed east of Denver. With deep cold air at all levels, and no more disturbances approaching aloft, it is not surprising that the frontal surface has stopped undulating in Fig. 5.1.2, and is in a period of steady ascent.

The profiler data, Fig. 5.1.2, suggested the passage of an upper-level low pressure center shortly after 1200 UTC 26 November 1984. The 500 mb analysis of Fig. 5.1.24 suggests that a trough axis is near Denver at 1200 UTC. Some of the Denver winds near 400 mb, Fig. 5.1.25, are still easterly at 1200 UTC, so the wind profiler diagnosis at Fleming, CO is probably accurate. In some other evidence, there remains a surface pressure trough across central CO at 1800 UTC (Figure 5.1.27), perhaps mirroring a low pressure center aloft. Satellite imagery, Figures 5.1.28 and 5.1.29, suggests a weakly formed comma cloud center over eastern CO at this time.

Figures 5.1.30 through 5.1.34 are time-height sections of profiler-derived thermodynamic parameters derived from the raw Fleming, CO winds and vertical wind shears. They should be compared to the front locations in Figs. 5.1.1 and 5.1.2.

Figures 5.1.30 and 5.1.31 depict the magnitude and orientation of the profiler-derived horizontal temperature gradients on 25 and 26 November 1984, respectively. These are based upon the

P	T	TD	RH	HT	WS	WD
126	50			470	30	225
156	51			440	36	215
215	47			410	27	230
313	50			360	30	205
373	45			350	35	215
408	40	-41	89	340	42	215
500	28	-30	82	320	25	225
737	8	-8	100	300	43	205
758	8	-8	100	270	14	200
824	3	-4	92	260	10	180
				250	21	85
				240	23	70
				200	4	155
				160	8	315
				150	11	325
				140	15	330
				120	15	325
				100	21	310
				90	6	320
				80	7	340
				70	7	360
				60	2	60
				00	4	180
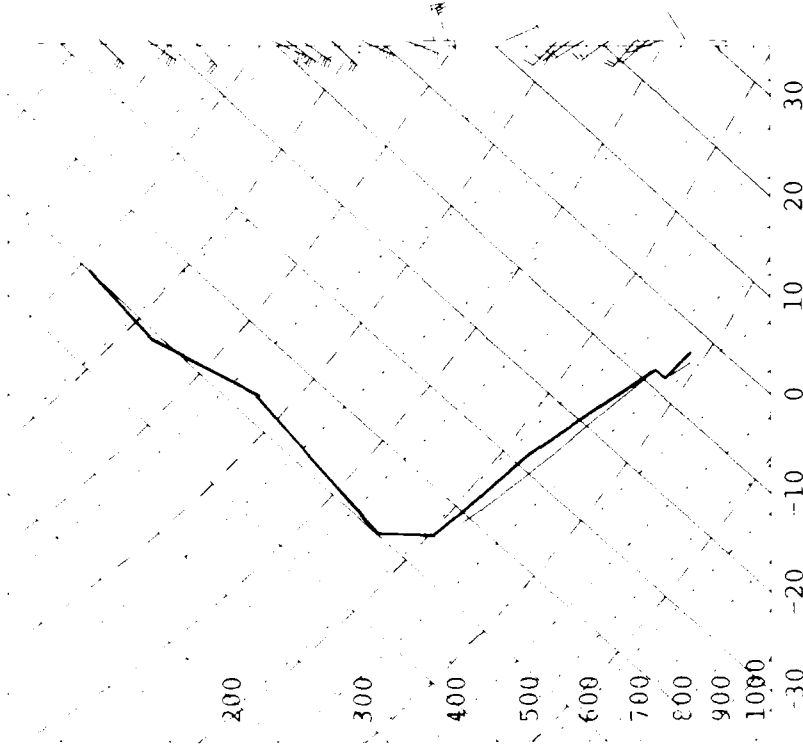
Figure 5.1.25. Skew-T log P diagram of temperatures ($^{\circ}$C, heavy) and dew points ($^{\circ}$C, thin) at Denver, CO on 1200 UTC 26 November 1984.

193
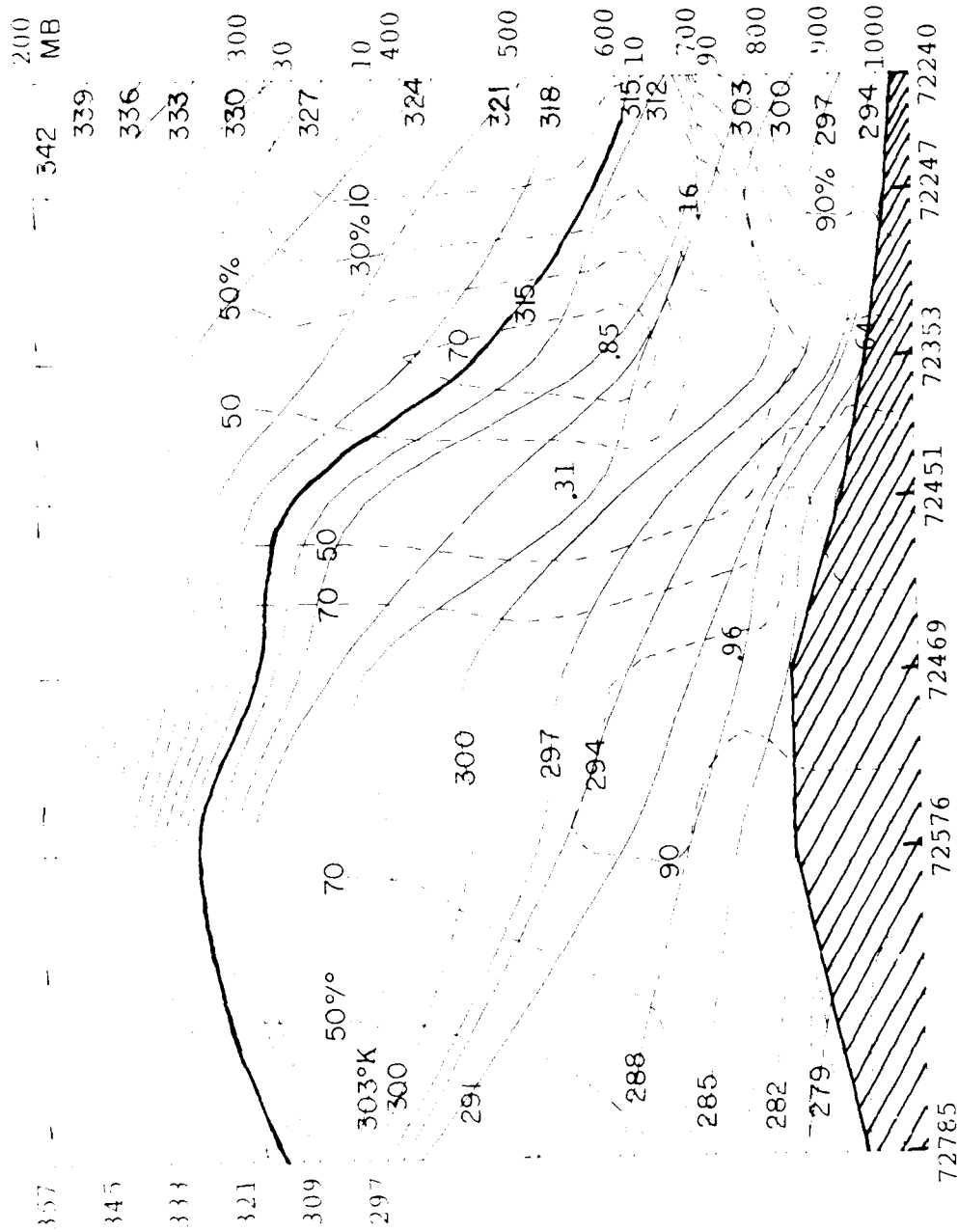
Figure 5.1.26. Northwest-southeast cross section of potential temperatures (°K, solid) and relative humidities (%, dashed) for 1200 UTC 26 November 1984. Stations as in Fig. 5.1.10.

194
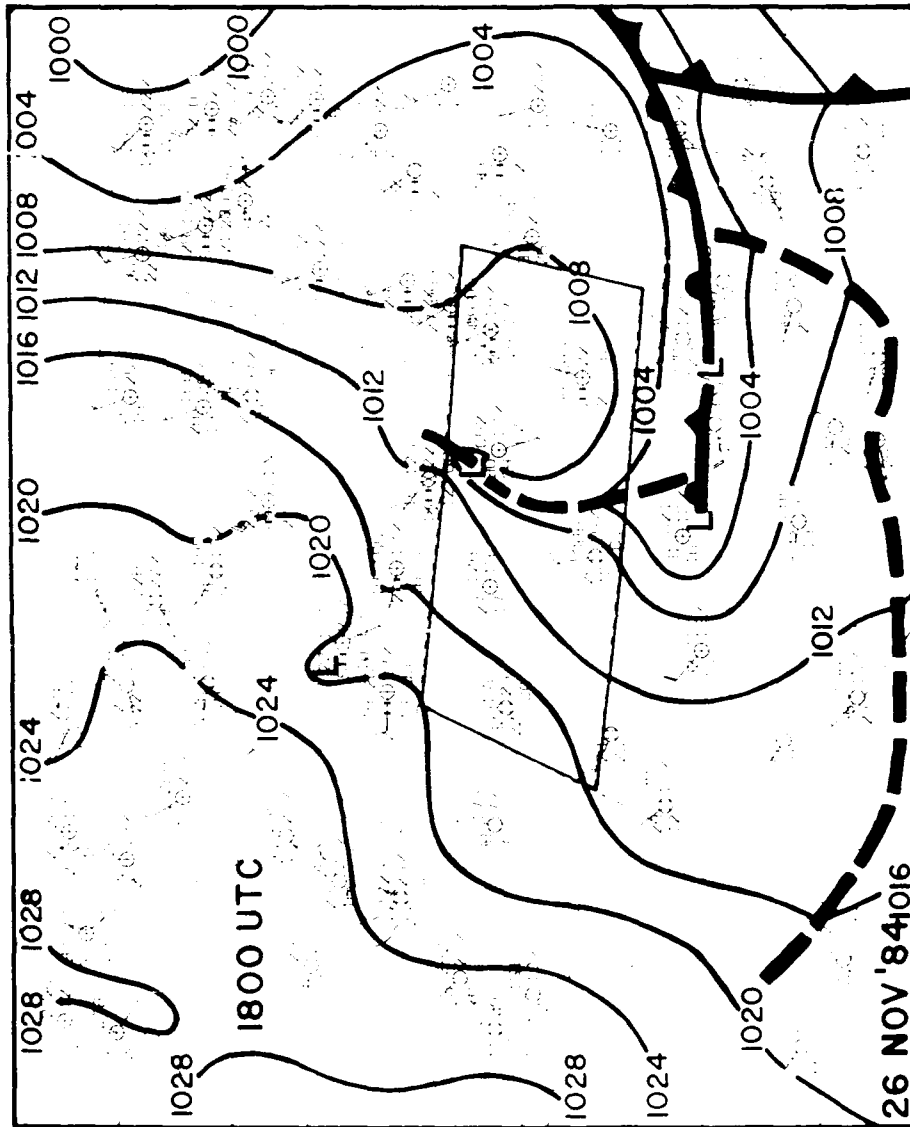
Figure 5.1.27. Surface observations, fronts, and sea-level pressure analysis (4mb intervals) for 1800 UTC 26 November 1984.

Figure 5 1.78. .... 17 .... 1984.
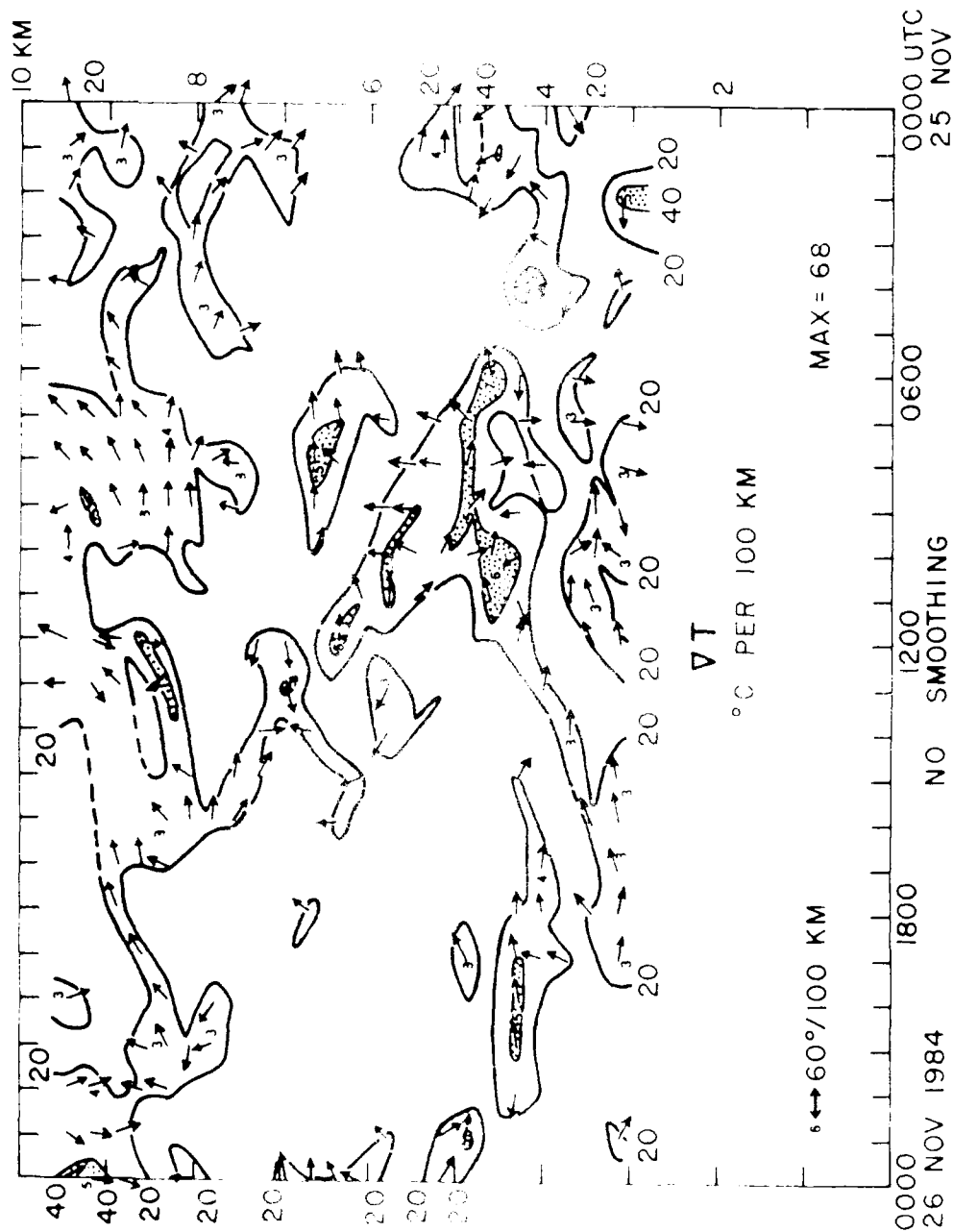
Figure 5.1.30. Time-height section of wind profiler-derived horizontal temperature gradients (°C per 100 km) on 25-26 November 1984. Vectors indicate orientation of large gradient values; a vector toward the top of the page indicates warmer air toward the north. Stippling indicates values greater than 40°C per 100 km.
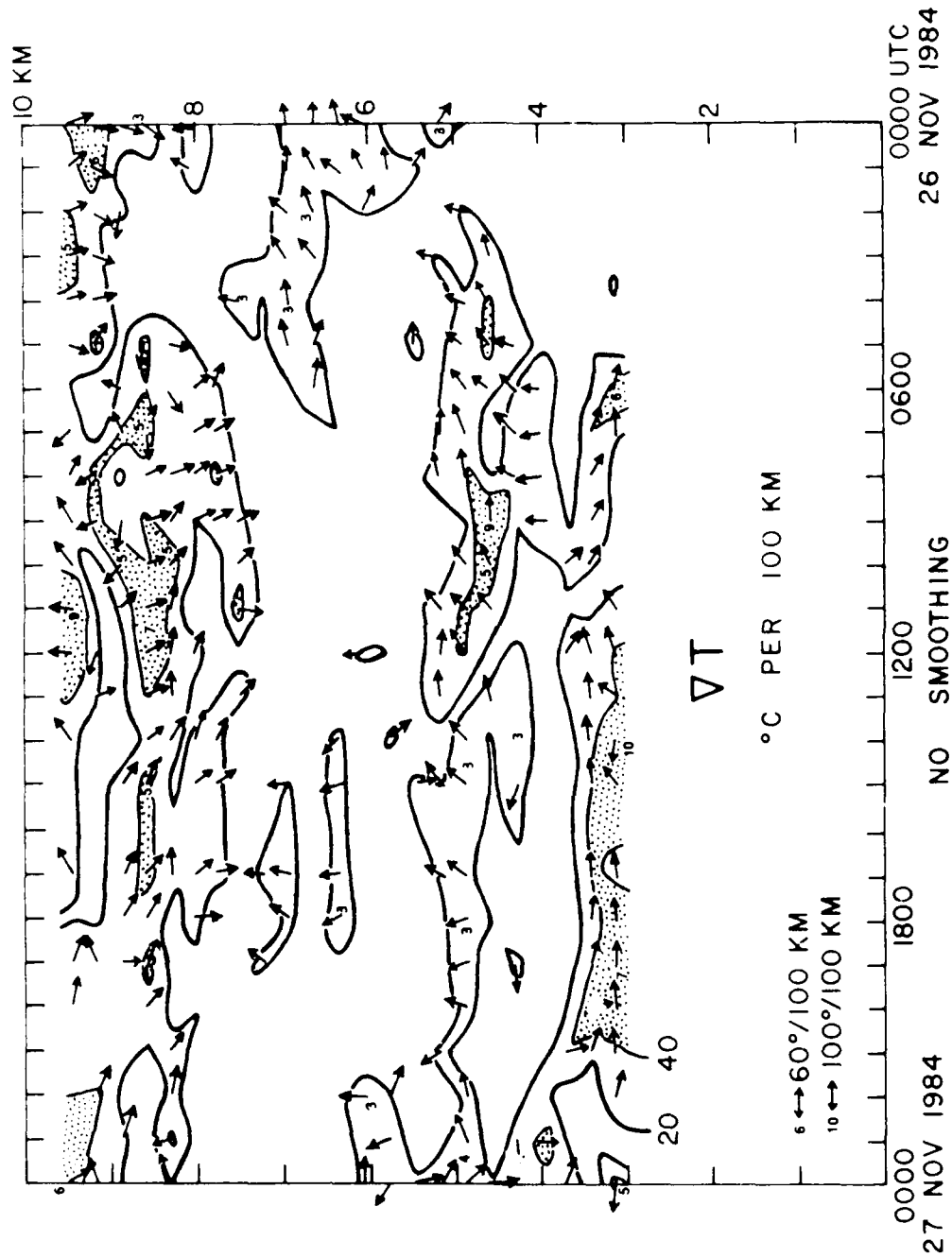
Figure 5.1.31. Time-height section of wind profiler-derived horizontal temperature gradients (°C per 100 km) on 26-27 November 1984. Vectors indicate orientation of large gradient values; a vector toward the top of the page indicates warmer air toward the north. Stippling indicates values greater than 40°C per 100 km.

principles of Section 3.2. It can be seen that the meandering frontal zone usually contains large temperature gradients, with warmer air located to the east. There are sometimes large gradients indicated in the lowest few elevation gates, which may be unduly influenced by friction-induced turning of the wind with height. There are also some large gradients persistent above 8 km, which may be the result of increased noise in the winds at these levels because of reduced powers from the drier air.

The sloping zone of temperature gradient going upward from about 5 km at 1000 UTC 25 November to 7 km at 1400 UTC 25 November is interesting. It extends from the crest of the first deep cold frontal meander of Fig. 5.1.1 to the wind shift line further aloft on that Figure. It may have been some upper front, detached from the surface-based cold domes, as suggested by the cross section in Fig. 5.1.16.

Figures 5.1.32 and 5.1.33 are time-height sections of profiler derived temperature advections on 25 and 26 November 1984, respectively. These are based upon the principles of Section 3.2. While interesting, these do not match the meandering frontal zone nearly as well as was anticipated. One period of cold advection matched the first ascent of the frontal zone at about 0600-1200 UTC 25 November. Some weak cold advection matched a modest ascent near 0000 UTC 26 November. Thereafter, the largest advections were beneath the frontal zone within the cold layer, or above 8 km where noise effects were probably at work.

Figure 5.1.34 shows the time-height section of wind profiler derived lapse rate gradients on 25 November 1984, based
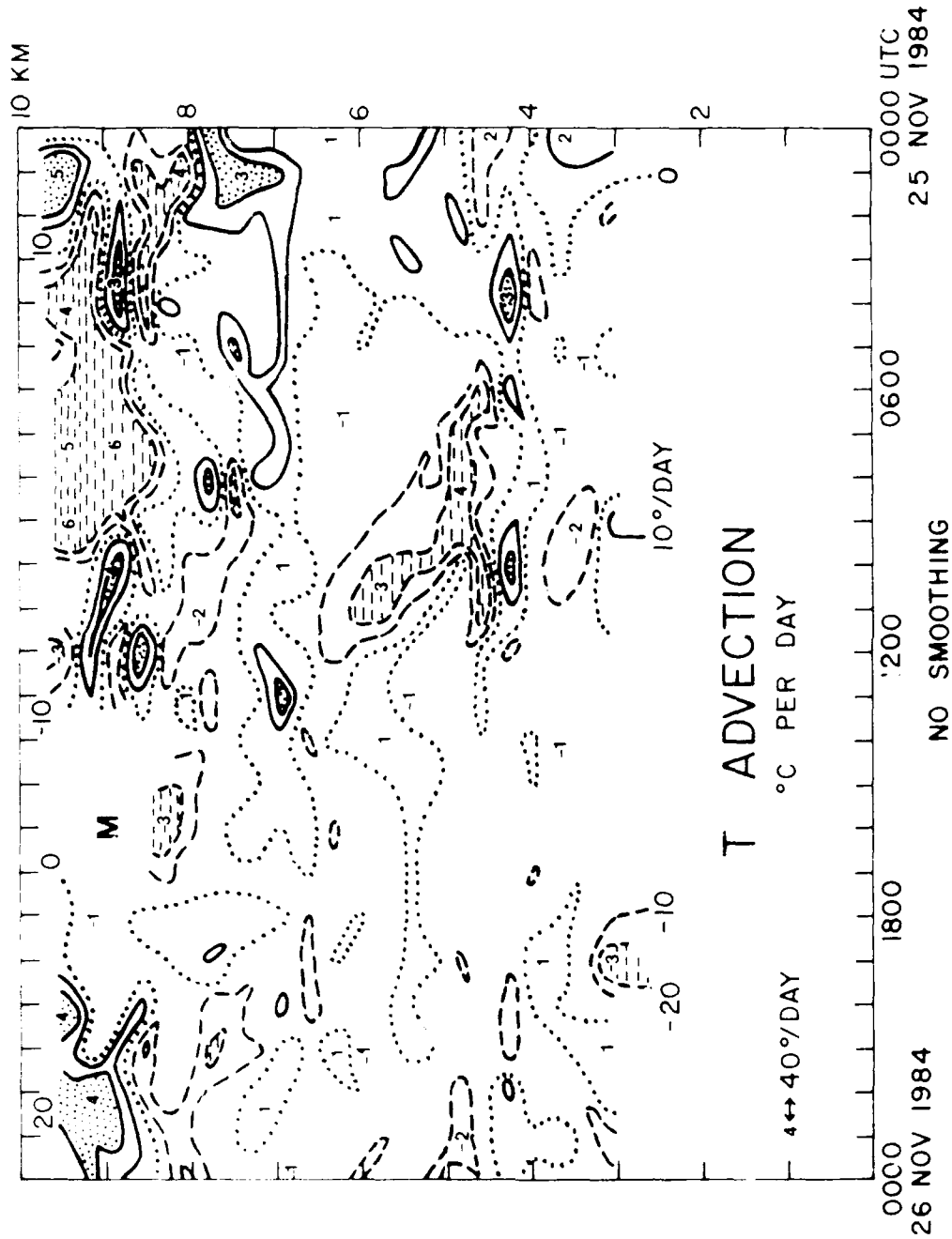
Figure 5.1.32. Time-height section of wind profiler-derived horizontal temperature advection (°C per day) on 25-26 November 1984. Dotted regions indicate warm advection at instantaneous rates of more than 20°C per day; dashed regions indicate cold advection at instantaneous rates of more than 20°C per day.
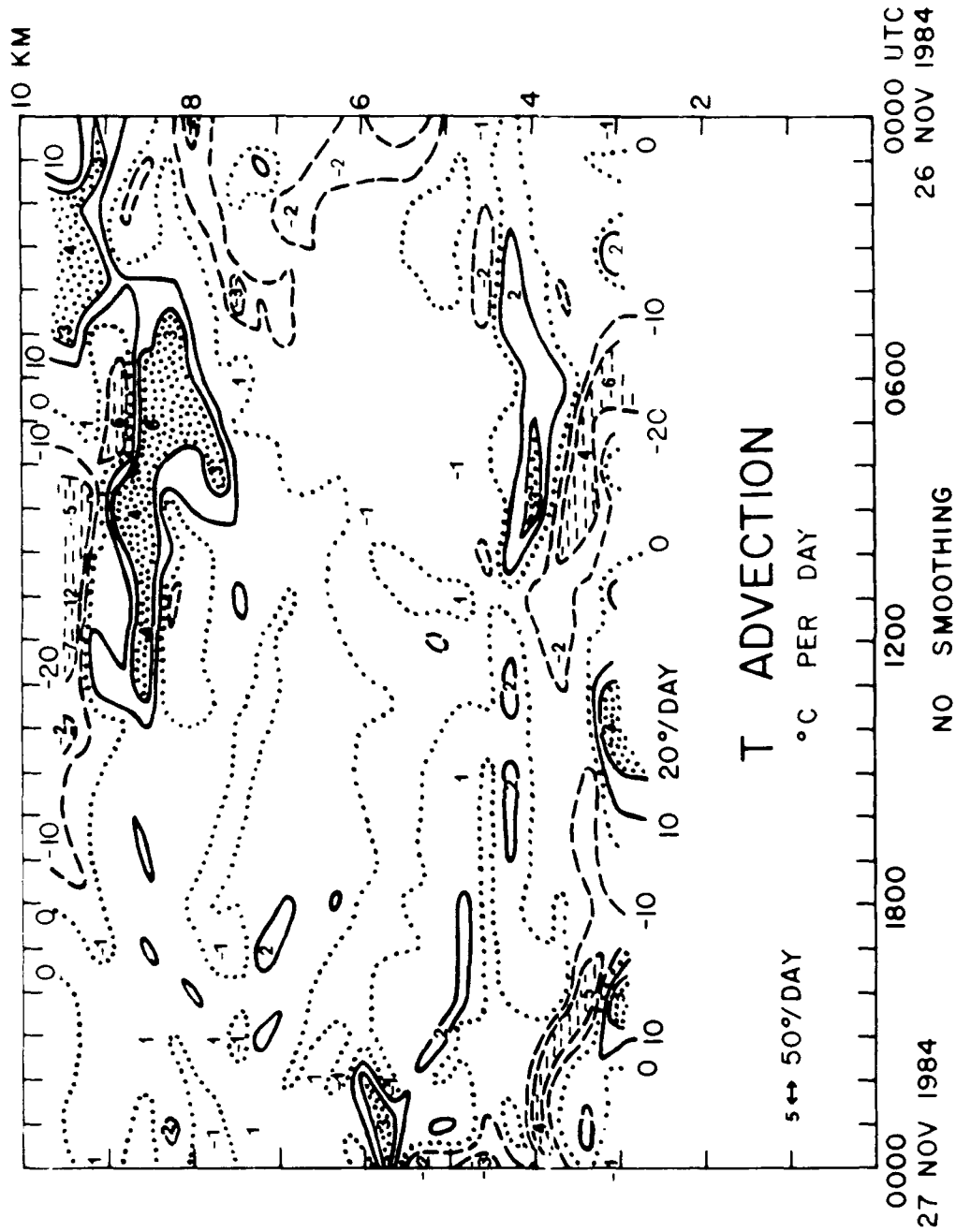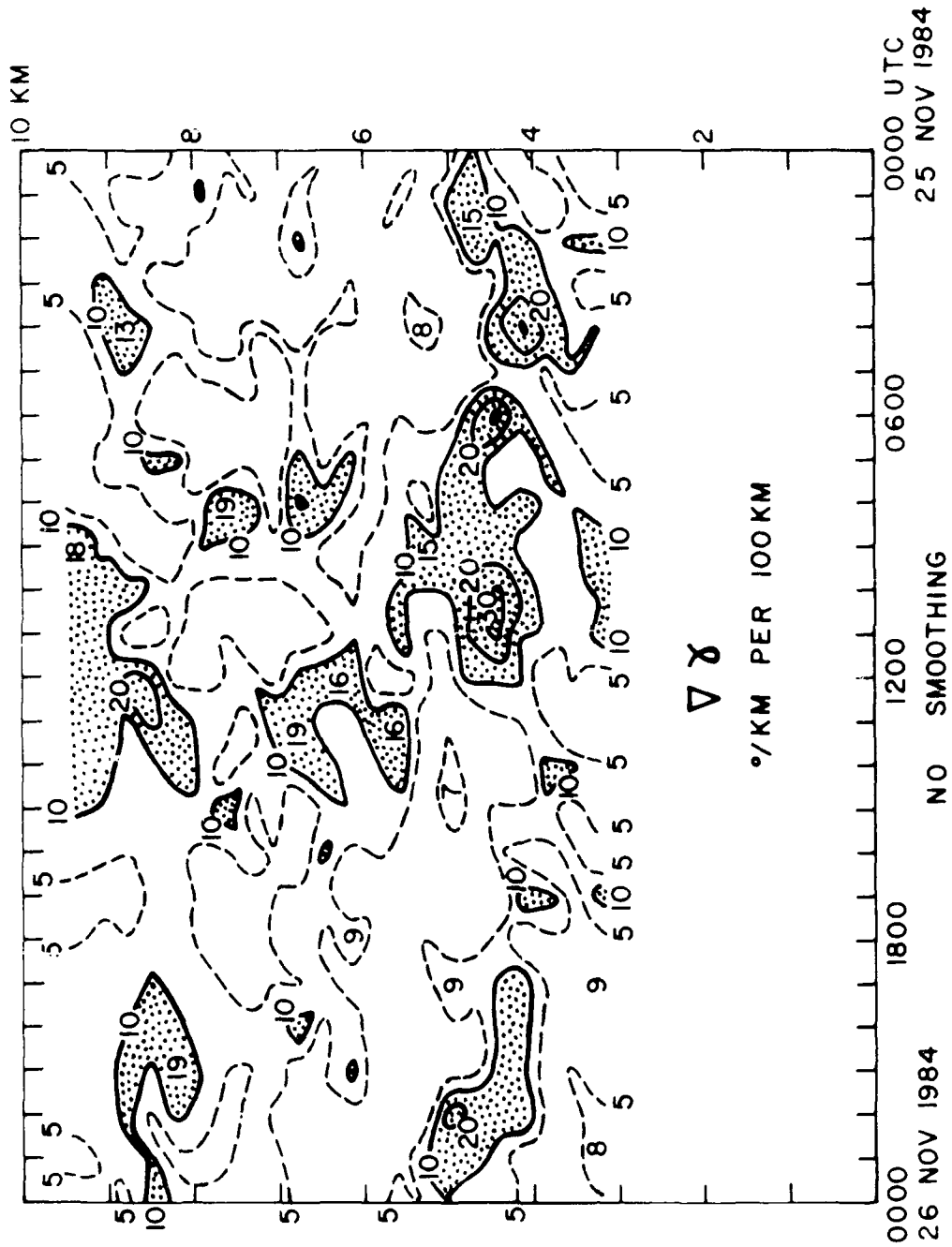
Figure 5.1.33. Time-height section of wind profiler-derived horizontal temperature advection (°C per day) on 26-27 November 1984. Dotted regions indicate warm advection at instantaneous rates of more than 20°C per day; dashed regions indicate cold advection at instantaneous rates of more than 20°C per day.

Figure 5.1.34. Time-height section of wind profiler-derived horizontal gradient of lapse rate (°C per km per 100 km) on 25-26 November 1984. Stippled regions indicate values greater than 10°C per km per 100 km.

upon the principles of Section 3.2.   Quite surprisingly, this parameter may have best followed the meandering frontal zone. The correlation between the shaded areas of Fig. 5.1.34 and the indicated frontal zone of Fig. 5.1.1 is impressive. It had been anticipated that this parameter would be least meaningful, since it involves the difference of two profiler-derived temperature gradients, each of which could contain noise-induced and ageo-strophic-induced errors.

Overall, this case gave several surprises. First, the ori-gin of the meandering frontal zone was more complicated than would have been anticipated.   Rather than oscillating as waves passed along the front, the front moved upward when a cold surge reinforced the existing frontal zone, receded when the cold pock-et moved away from the site, and saw repeated cold surges rein-force the cold dome before the front had the opportunity to de-scend to the 700 mb level.

A second surprise was that the profiler-derived temperature advections were probably less impressive in this case of a strong mesoscale signal in the winds than they had been in the more subtle cases of Chapter 4. The ascending stages of the undulat-ing front (i.e., when the surface-based cold layer was deepen-ing) were generally associated with cold advection reasonably well. The descending stages of the undulating front, however, were not accompanied by much systematic warm advection. It may be that the frontal descent during these periods was dominated by downward vertical motion rather than by horizontal advection.

A third surprise was that the wind profiler-derived lapse

rate gradient appeared to be a useful parameter; probably more so than temperature advection. The overall impression is that the vertical depth of the frontal zone may have been too shallow to be handled well by the wind profiler techniques, in that the frontal zone contained so few profiler wind observations.

5.2 Effect of Vertical and Temporal Smoothing of Winds

Inasmuch as the temperature gradients and temperature advections computed from the raw profiler vertical wind shears appear to be quite realistic, and certainly not excessive when noisy areas are eliminated, there is no obvious need to apply vertical or temporal smoothing schemes to eliminate "noise" in the hourly data (unless, of course, the intent is to eliminate the effect of mesoscale variations). However, there is a tendency to perform such smoothing, because it tends to make the values more comparable to those obtained using the coarse rawinsonde data. In this section the effects of temporal and vertical smoothing of the winds on profiler-derived temperature gradient and temperature advection are examined.

Figures 5.2.1 to 5.2.5 illustrate the impact of vertical and temporal smoothing on the temperature gradient field. By comparison with Fig. 5.1.30, it can be seen that the magnitude of the temperature gradient is decreased slowly as greater time periods are used in the smoothing scheme, and that vertical smoothing has a more rapid impact. Details of the thin frontal zone are degraded somewhat more rapidly, whereas the more extensive features farther aloft are less slowly damped.
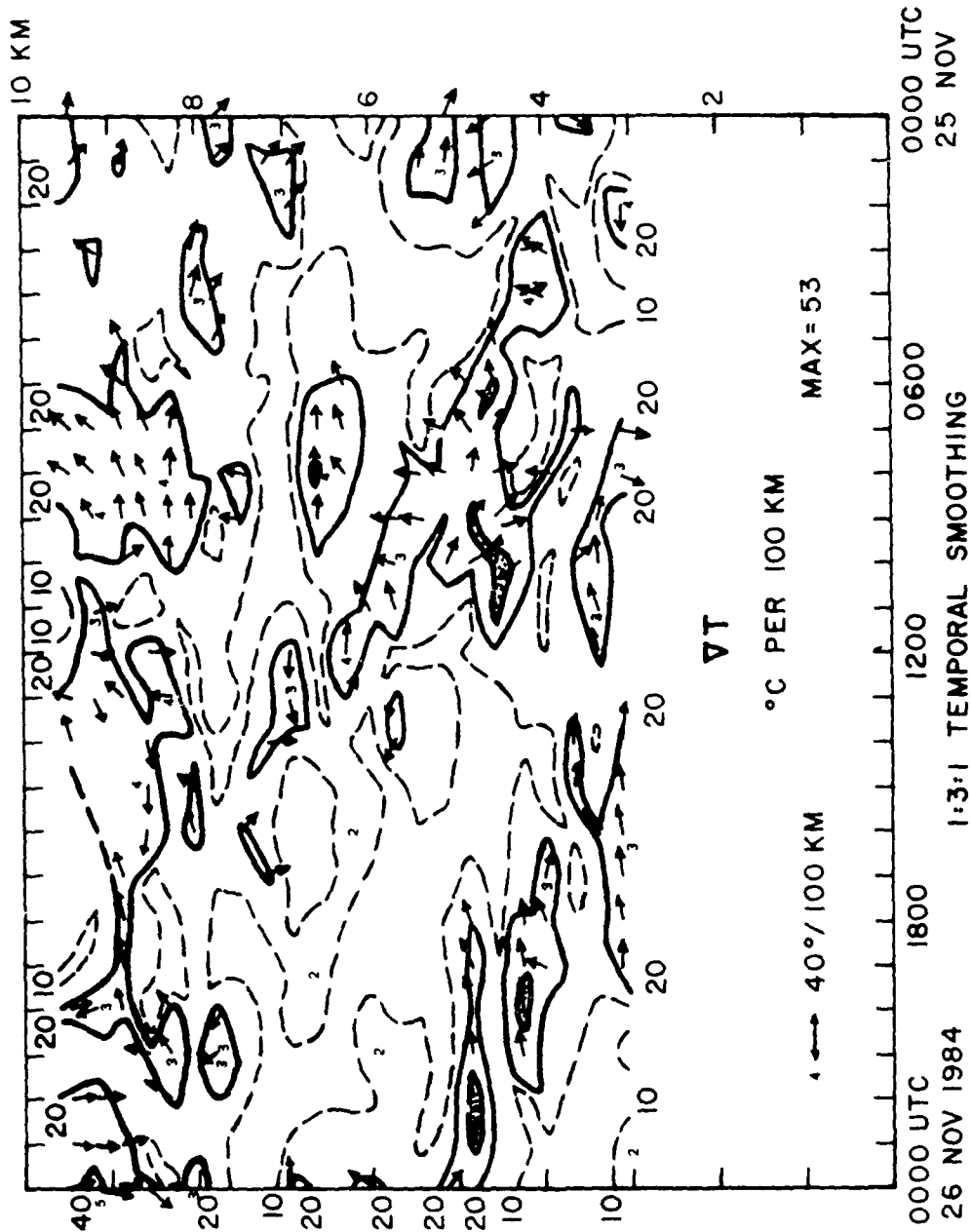
Figure 5.2.1. Time-height section of wind profiler-derived horizontal temperature gradients (°C per 100 km) on 25-26 November 1984, with 1:3:1 temporal smoothing applied. Vectors indicate orientation of large gradient values; a vector toward the top of the page indicates warmer air toward the north. Stippling indicates values greater than 40°C per 100 km. Contrasts with Fig. 5.1.30.
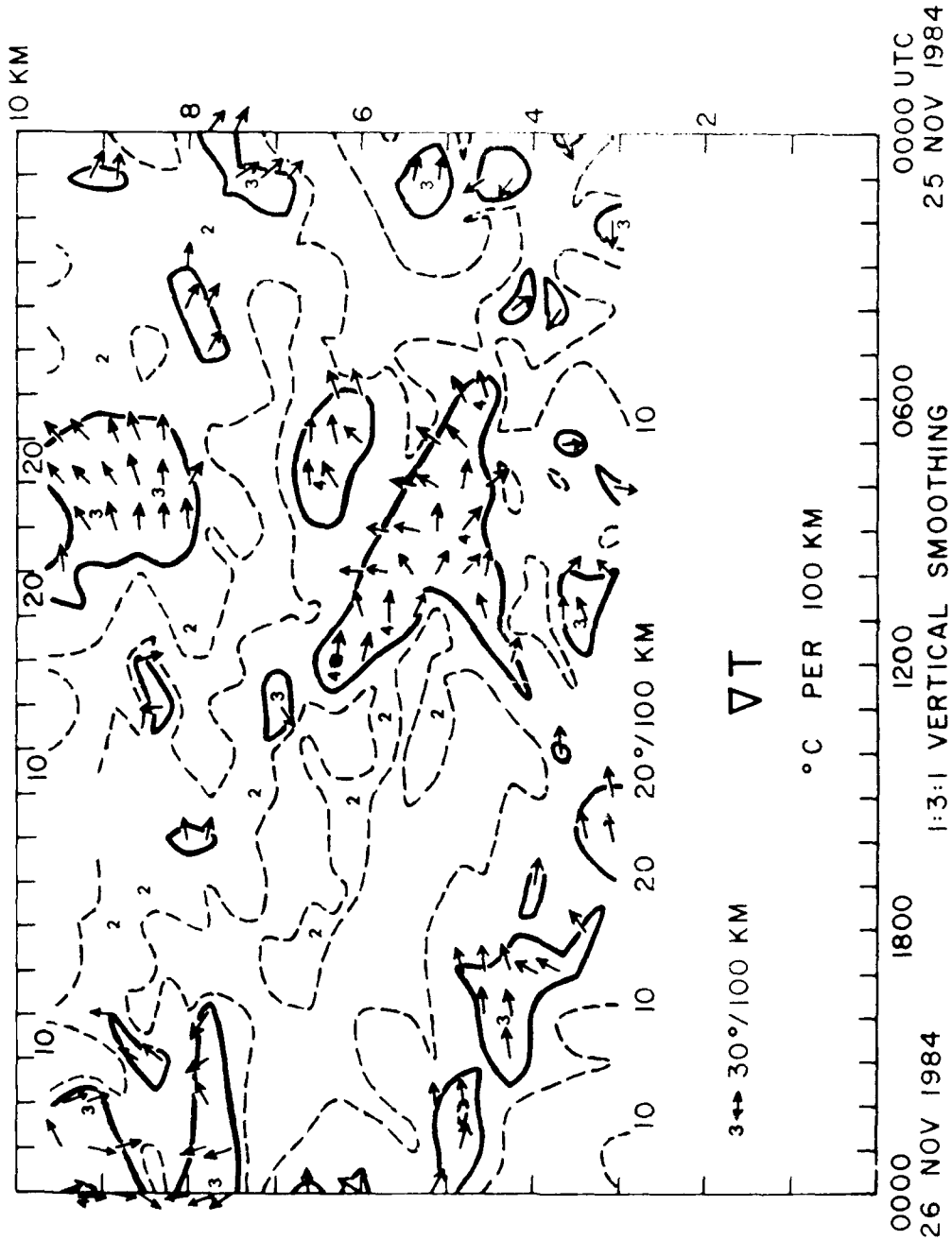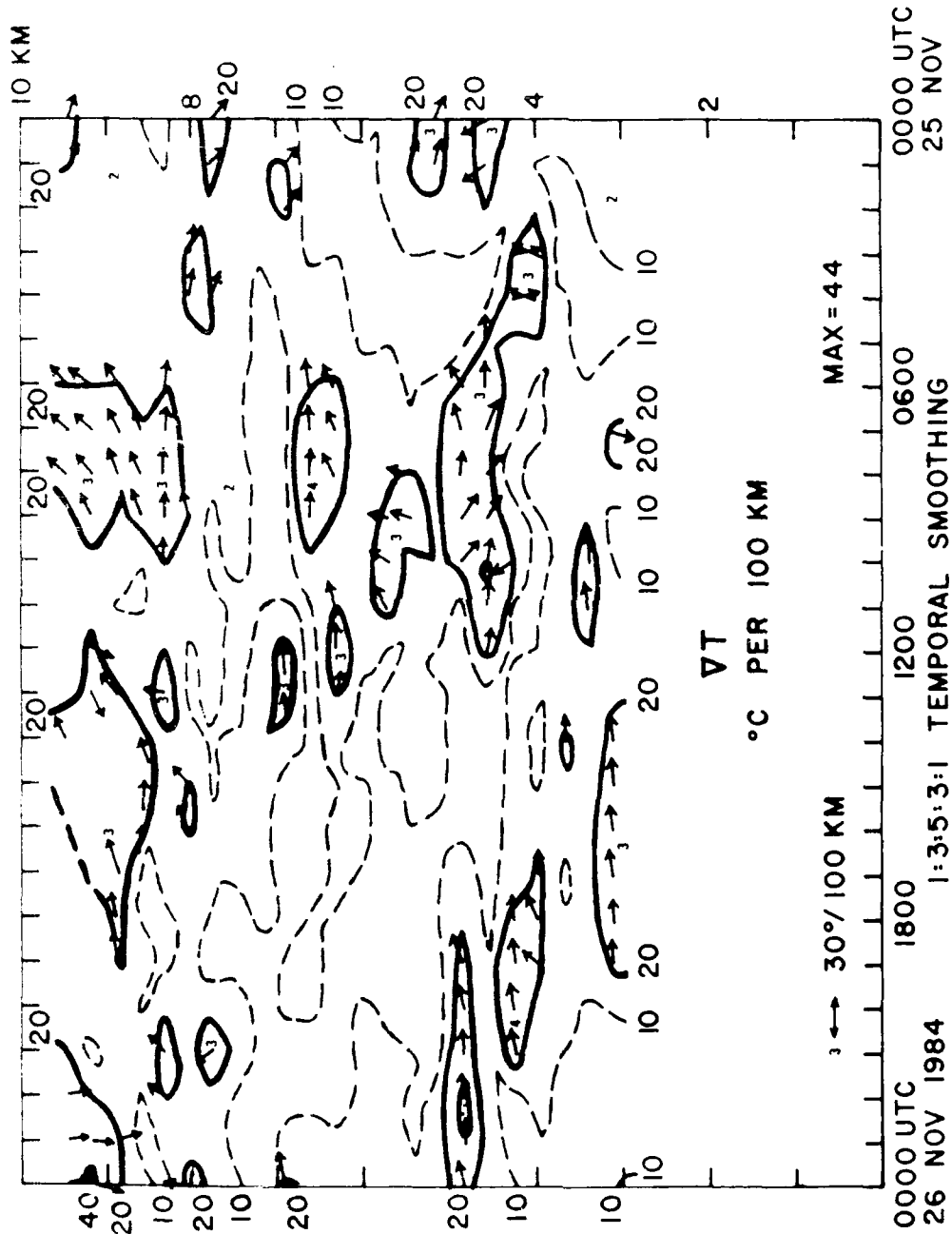
Figure 5.2.2. Time-height section of wind profiler-derived horizontal temperature gradients (°C per 100 km) on 25-26 November 1984, with 1:3:1 vertical smoothing applied. Vectors indicate orientation of large gradient values; a vector toward the top of the page indicates warmer air toward the north. Stippling indicates values greater than 40°C per 100 km. Contrasts with Fig. 5.1.30.
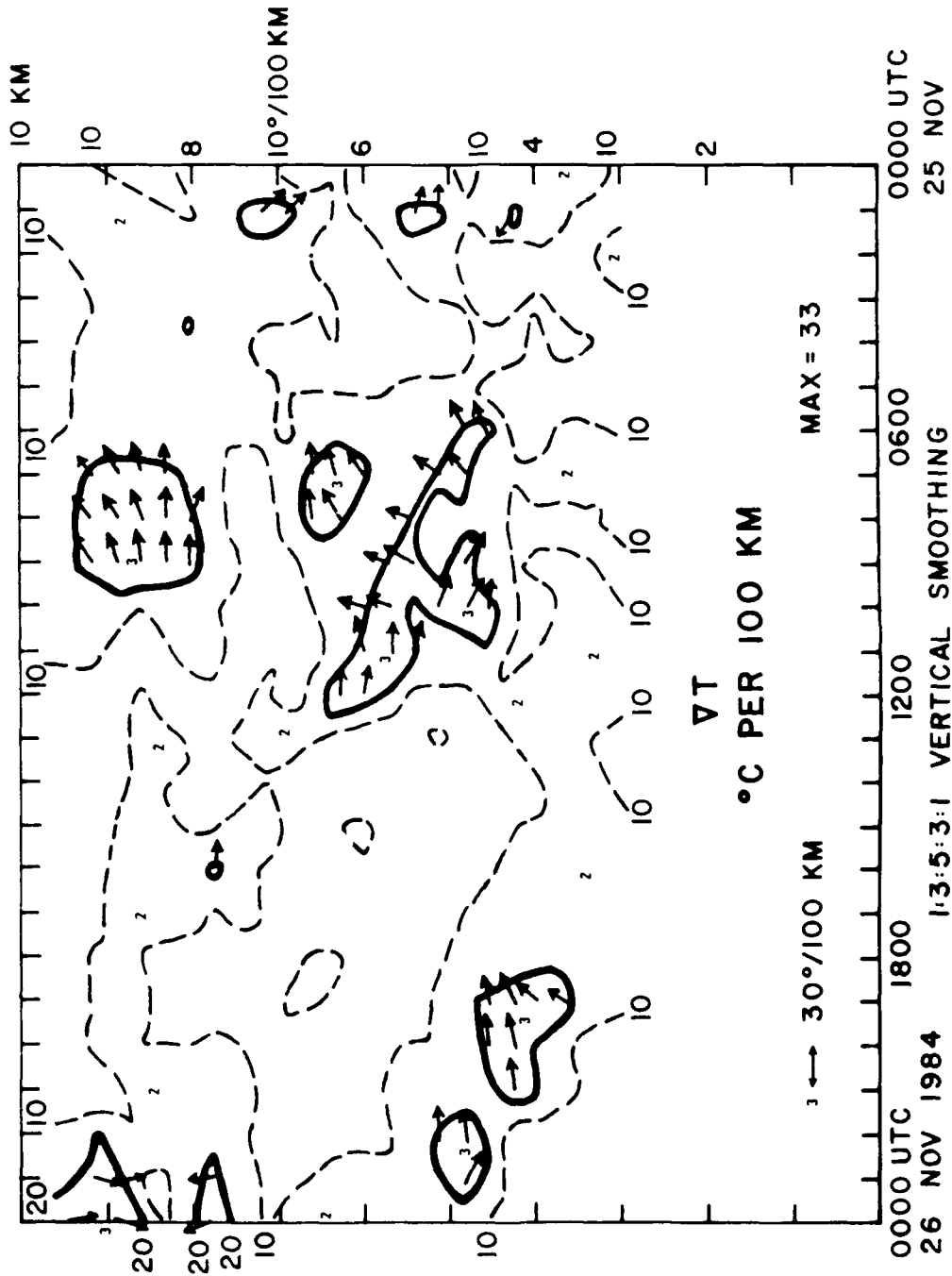
Figure 5.2.3. Time-height section of wind profiler-derived horizontal temperature gradients (°C per 100 km) on 25-26 November 1984, with 1:3:5:3:1 temporal smoothing applied. Vectors indicate orientation of large gradient values; a vector toward the top of the page indicates warmer air toward the north. Stippling indicates values greater than 40°C per 100 km. Contrasts with Fig. 5.1.30.
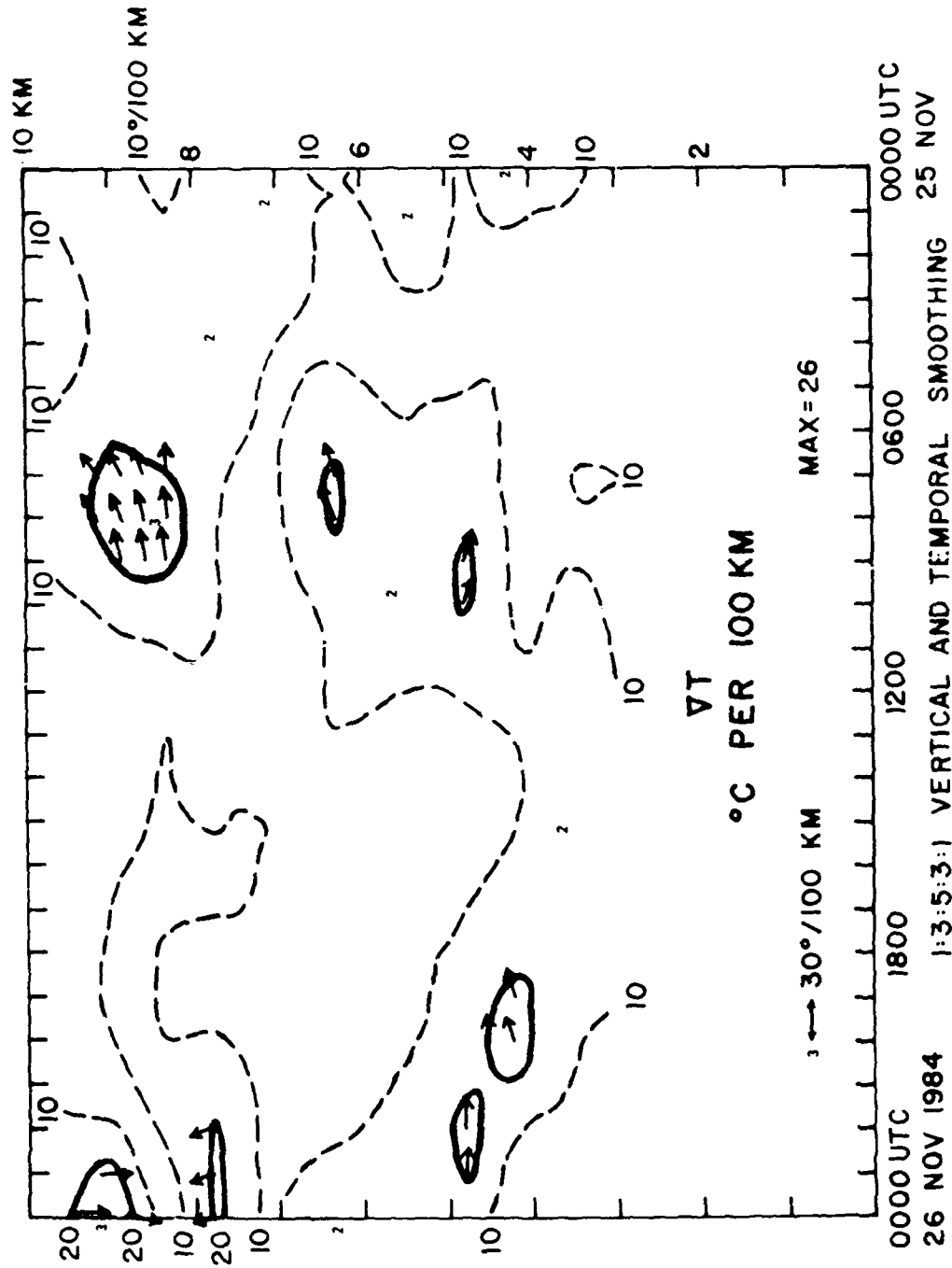
Figure 5.2.4. Time-height section of wind profiler-derived horizontal temperature gradients (°C per 100 km) on 25-26 November 1984, with 1:3:5:3:1 vertical smoothing applied. Vectors indicate orientation of large gradient values; a vector toward the top of the page indicates warmer air toward the north. Stippling indicates values greater than 40°C per 100 km. Contrasts with Fig. 5.1.30.

Figure 5.2.5. Time-height section of wind profiler-derived horizontal temperature gradients (^oC per 100 km) on 25-26 November 1984, with 1:3:5:3:1 temporal and vertical smoothing applied. Vectors indicate orientation of large gradient values; a vector toward the top of the page indicates warmer air toward the north. Stippling indicates values greater than 40°C per 100 km. Contrasts with Fig. 5.1.30.

Figures 5.2.6 and 5.2.7 illustrate the effect of vertical smoothing on profiler-derived temperature advection. Fig. 5.1.32 should be inspected for comparison. Smoothing again damps the values, with somewhat greater impact on the shallow frontal features.

Table 5.2.1 summarizes the effect of the smoothing schemes by displaying the value of the maximum gradients and maximum advections remaining after each smoothing procedure. In general, vertical smoothing damps the values of the parameters more rapidly than a comparable temporal smoothing.

5.3   Other Displays of Derived Thermodynamic Quantities

This section will end the chapters on use of wind profiler data with a procedural note. All of the wind-profiler-derived thermodynamic parameter values of Sections 5.1 and 5.2 were computed from the original wind profiler data, level by level and time by time. A problem can occur if profiler winds are first interpolated to a grid mesh and then manipulated. This problem can be seen through examination of Figures 5.3.1 and 5.3.2.

Figure 5.3.1 illustrates the effect of a mismatch of the number of grid points in the vertical dimension of a time-height diagram and the location of the wind data points. While wind data are inserted almost directly to some grid points, such as numbers 13 and 29, other grid points receive essentially the mean of two adjacent data points. An example of the latter is grid point 21. Thus, there is an implicit smoothing in the wind data that is variable with height, unless the meteorologist is careful
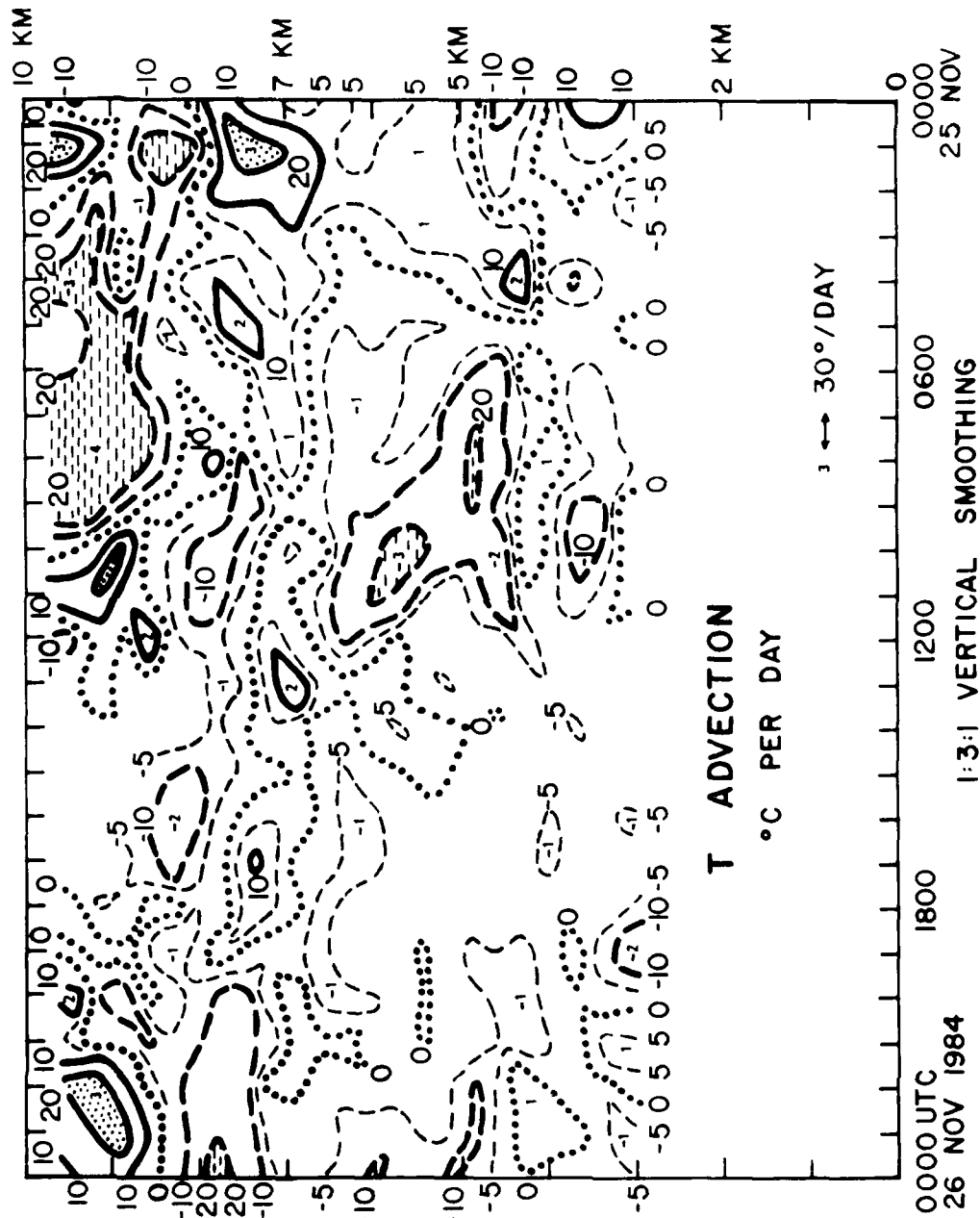
Figure 5.2.6. Time-height section of wind profiler-derived horizontal temperature advection (°C per day) on 25-26 November 1984, with 1:3:1 vertical smoothing applied. Dotted regions indicate warm advection at instantaneous rates of more than 20°C per day; dashed regions indicate cold advection at instantaneous rates of more than 20°C per day. Contrasts with Fig. 5.1.32.
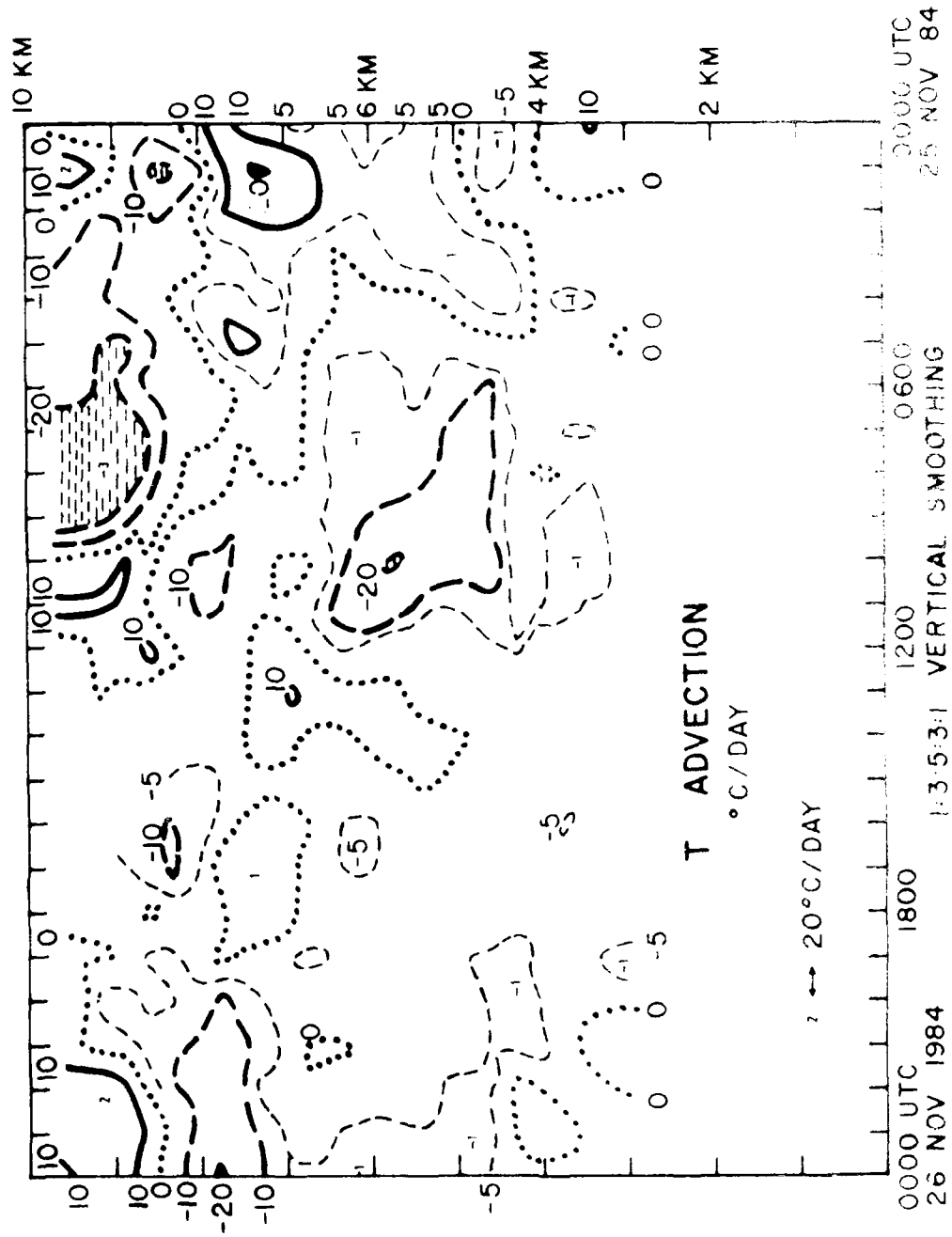
Figure 5.2.7. Time-height section of wind profiler-derived horizontal temperature advection (°C per day) on 25-26 November 1984, with 1:3:5:3:1 vertical smoothing applied. Dotted regions indicate warm advection at instantaneous rates of more than 20°C per day; dashed regions indicate cold advection at instantaneous rates of more than 20°C per day. Contrasts with Fig. 5.1.32.

TABLE 5.2.1

EFFECT OF TEMPORAL AND VERTICAL SMOOTHING OF PROFILER WINDS

ON WIND PROFILER DERIVED

TEMPERATURE GRADIENTS AND TEMPERATURE ADVECTIONS

0000 UTC 25 November - 0000 UTC 26 November 1984

Wind Smoothing	Maximum T Gradient (oC per 100 km)	Maximum T Advection (oC per day)
None (Raw winds)	68	63
1:3:1 Temporal	53	48
1:3:5:3:1 Temporal	44	42
1:3:1 Vertical	45	44
1:3:5:3:1 Vertical	33	33
1:3:5:3:1 Vertical and Temporal	26	27

enough to avoid this type of situation when designing his or her analysis schemes. It is easy to imagine that the vertically sharp frontal windshift zone of Figs. 5.1.1 and 5.1.2 could have been totally smeared out by use of an improper grid point scheme like that of Fig. 5.3.1.

Figure 5.3.2 shows the effect of a mismatch of temporal data points and x-coordinate grid points of a time-height section diagram. Like in Fig. 5.3.1, some of the data points are ingested almost fully at grid points, while other grid points are almost exact means of two adjacent times. Again, let the meteorologist/ analyst beware!
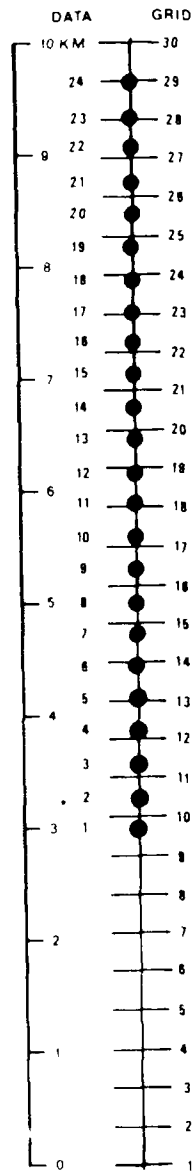
Figure 5.3.1. Potential mismatch between altitude of profiler observations (dots) and a 30-mesh grid of points covering the layer (horizontal ticks).
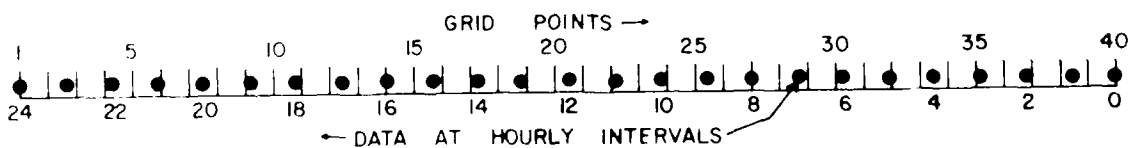

Figure 5.3.2. Potential mismatch between time of profiler observations (dots) and a 40-mesh grid of points covering the tie period (vertical ticks).

6. MULTIPLE-PROFILER NETWORK CALCULATIONS

The principles of making multiple-profiler network calcula-
tions of various kinematic and dynamic quantities have been pre-
sented in Chapter 3. Case studies applying these techniques be-
gan late during this Contract period, and continued during the
subsequent Contract. Case studies by Cathy Carlson (1987) ap-
plied the techniques to a triangle of Colorado wind profilers.
Studies using both Colorado and Pennslyvania wind profilers have
been performed by Larry Knowlton (1987). The interested reader
is referred to these M.S. Theses for additional details, and to a
brief summary in the Final Report of the subsequent Contract
(Forbes et. al, 1989b).

7. CONCLUDING REMARKS

This manuscript described the first stage of a sequence of two AFGL Contracts over the period between 1985 and 1989, in which the authors investigated the use of wind profiler data to diagnose and predict mesoscale weather systems. The research performed during this Contract period was used mainly to develop the techniques needed to use and display the profiler data and derived quantities. At the end of the period, some case studies were performed as preliminary tests of the utility of the techniques and displays.

Some of the case studies blended wind profiler data into analyses using primarily rawinsonde data. Some of these blends involved insertion of time-space-converted profiler winds, in addition to winds at the profiler site at the time of the analysis. That the observed and time-space-converted profiler winds blended well into the background supplied by rawinsonde data seemed to both lend confidence regarding the accuracy of the wind profiler data and assist greatly in the interpretation of the cause of the signatures portrayed in the profiler time-height sections.

Analyses using wind profiler data enabled the detection and resolution of weather phenomena that would have gone unnoticed if only rawinsonde data and derived analyses were used. In some real-time uses of wind profiler data not reported, wind profiler time-height sections were used as proof that upper-air troughs had already passed State College, PA, when the upper-air analyses and numerical model prognoses indicated that the trough had yet

to pass. This type of evidence is a "smoking gun" to a forecaster in such a situation, signifying that he or she can indicate that the threat of precipitation has passed.

Examinations of wind profiler-derived thermodynamic variables were performed on several cases. While the inferred temperature advection inferred was generally of the correct sign, the magnitudes could not be assessed as either correct or incorrect due to a lack of adequate independent information. In the case of the undulating frontal zone, probably the strongest mesoscale feature examined, the temperature advections were not overly large. Of course, there may be a reason for this, since ageostrophic motions may have been rather large. Qualitative use of the wind profiler-derived thermodynamic data appears to be justified.

A simple scheme was introduced by which wind profiler-derived temperature gradient information could be used to fine-tune the location of frontal zones on quasi-horizontal mappings based primarily on rawinsonde data. While additional testing is needed, that approach also appears to be justified.

Perturbation winds, computed as departures from a temporal mean, appeared to be very useful quantities. Their coherence in height and time lent confidence regarding the accuracy of the profiler winds, and it often highlighted the existence of an organized mesoscale feature that might have been masked by the presence of a large mean wind.

Future studies using wind profiler data under AFGL Contract will concentrate on (1) the computation of multiple profiler

quantities such as vorticity, divergence, and mesoscale vertical velocity; (2) multi-profiler examination of frontal circulations; (3) high-temporal-resolution studies of rainbands; (4) the use of the time-space conversion technique with wind profiler and rawin-sonde data to study the mesoscale structure of satellite-detected weather systems.

ACKNOWLEDGEMENTS

REFERENCES

Balsley, B.B., 1981: The MST technique -- a brief review. J. Atmos. Terr. Phys., 43, 495-509.

Balsley, B.B. and K.S. Gage, 1982: On the use of radars for operational wind profiling. Bull. Amer. Meteor. Soc., 63, 1009-1018.

Blackadar, A.K., 1957: Boundary layer wind maxima and their significance for the growth of nocturnal inversions. Bull. Amer. Meteor. Soc., 38, 283-290.

Carlson, C.A., 1987a: Kinematic quantities derived from a triangle of VHF Doppler wind profilers. M.S. Thesis, The Pennsylvania State University, University Park, PA, 136pp.

Carlson, C.A., 1987b: Kinematic quantities derived from a triangle of VHF Doppler wind profilers. AFGL-TR-87-0265, Air Force Geophysics Lab, Hanscom AFB, MA, 136pp. ADA207542

Carlson, H.C. and N. Sundararaman, 1982: Real-time jet stream tracking: National benefit from an ST radar network for measuring atmospheric motions. Bull. Amer. Meteor. Soc., 63, 1019-1026.

Dodge, J., J. Arnold, G. Wilson, J. Evans, T. Fujita, 1986: The Cooperative Huntsville Meteorological Experiment (COHMEX). Bull. Amer. Meteor. Soc., 67, 417-419.

Forbes, G.S., 1986: Examples of mesoscale structures and short-term wind variations detected by VHF Doppler radar. Workshop on Technical Aspects of MST Radar, Aguadilla, Puerto Rico, 1985. Middle Atmosphere Handbook, 20, 17-29. [SCOSTEP Secretariat, Univ. of Illinois, 1406 Green St., Urbana, IL 61801]

Forbes, G.S. and R. Bankert, 1987: Satellite imagery and conceptual models in mesoscale forecasting. Proc., Symposium on Mesoscale Analysis and Forecasting, Vancouver, Canada, ESA SP-282, 251-261.

Forbes, G.S., D.W. Thomson, and J.J. Cahir, 1985: Hourly wind profiles in a region of frequent air traffic--the Penn State profiler network. Preprints, 2nd Int'l. Conf. Aviation Weather System., Amer. Meteor. Soc., Montreal, 172-176.

Forbes, G., et. al, 1989b: Final Report on Contract F19628-86-C-0092. [To be published during the fall of 1989.]

Gage, K.S. and B.B. Balsley, 1978: Doppler radar probing of the clear atmosphere. Bull. Amer. Meteor. Soc., 59, 1074-1093.

Hoehne, W.E., 1980: Precision of National Weather Service upper air measurements. NOAA Tech. Rept. NWS T&ED-16, 23pp.

Hogg, D.C., et. al, 1983: An automatic profiler of the temperature, wind and humidity in the troposphere. J. Climate Appl. Meteor., 22, 807-831.

Kessler, E., M. Eilts, and K. Thomas, 1985: A look at profiler performance. Workshop on Technical Aspects of MST Radar, Aguadilla, Puerto Rico, 1985. Middle Atmosphere Handbook, 20. [SCOSTEP Secretariat, Univ. of Illinois, 1406 Green St., Urbana, IL 61801]

Knowlton, L., 1987: Kinematic diagnoses of frontal structure and circulations derived from two and three-station VHF Doppler wind profiler networks. M.S. Thesis, The Pennsylvania State University, University Park, PA, 84pp.

Larsen, M.F. and J. Rottger, 1982: VHF and UHF Doppler radars as tools for synoptic research. Bull. Amer. Meteor. Soc., 63, 996-1008.

Lawrence, T.R., B.F. Weber, M.J. Post, R.M. Hardesty, R.A. Richter, N.L. Abshire, and F.F. Hall, Jr., 1986: A comparison of Doppler lidar, rawinsonde, and 915 MHz UHF wind profiler measurements of tropospheric winds. NOAA Tech. Mem. ERL WPL-130, Boulder, CO.

Neiman, P., 1987: Wind profiler-derived temperature gradients and advections. M.S. Thesis, The Pennsylvania State University, University Park, PA, 214 pp.

Steinberg, R., 1984: MERIT -- a new approach to upper air forecasting for aviation. Preprints, 10th Conf. Wea. Forecasting and Analysis, Clearwater Beach, FL, Amer. Meteor. Soc., 249-254.

Strauch, R.G., 1986: Methods for verifying the accuracy of wind profilers. Workshop on Technical Aspects of MST Radar, Aguadilla, Puerto Rico, 1985. Middle Atmosphere Handbook, 20, 273-278. [SCOSTEP Secretariat, Univ. of Illinois, 1406 Green St., Urbana, IL 61801]

Thomson, D.W., 1988: New perspectives on atmospheric structure and dynamics. Earth and Mineral Sciences, 57(1), 1-6.

Uccellini, L.W. and D.R. Johnson, 1979: The coupling of upper and lower tropospheric jet streaks and implications for the development of severe convective storms. Mon. Wea. Rev., 107, 682-703.

Vincent, R.A., 1986: Session summary and recommendations. Workshop on Technical Aspects of MST Radar, Aguadilla, Puerto Rico, 1985. Middle Atmosphere Handbook, 20, 254-255. [SCOSTEP Secretariat, Univ. of Illinois, 1406 Green St., Urbana, IL 61801]

Williams, S.R. and R.M. Peters, 1986: The Penn State Doppler network progress report. Workshop on Technical Aspects of MST Radar, Aguadilla, Puerto Rico, 1985. Middle Atmosphere Handbook, 20, 339-341. [SCOSTEP Secretariat, Univ. of Illinois, 1406 Green St., Urbana, IL 61801]

Williams, S.R. and D.W. Thomson, 1986: An evaluation of errors observed in the measurement of low wind velocities. Workshop on Technical Aspects of MST Radar, Aguadilla, Puerto Rico, 1985. Middle Atmospheric Handbook, 20, 256-262. [SCOSTEP Secretariat, Univ. of Illinois, 1406 Green St., Urbana, IL 61801]

APPENDIX 1

PROJECT PERSONNEL

The following personnel were supported, in part, by AFGL Contract F19628-85-K-0011:

John J. Cahir
Catherine A. Carlson
Gregory S. Forbes
Paul Neiman
Arthur A. Person
Dennis W. Thomson
Scott Williams

APPENDIX 2

REPORTS AND PUBLICATIONS PREPARED

Forbes, G.S., D.W. Thomson, and J.J. Cahir, 1985: Hourly wind profiles in a region of frequent air traffic--the Penn State profiler network. Preprints, 2nd Int'l. Conf. Aviation Weather System., Amer. Meteor. Soc., Montreal, 172-176.

Forbes, G.S., 1986: Examples of mesoscale structures and short-term wind variations detected by VHF Doppler radar. Workshop on Technical Aspects of MST Radar, Aguadilla, Puerto Rico, 1985. Middle Atmosphere Handbook, 20, 17-29. [SCOSTEP Secretariat, Univ. of Illinois, 1406 Green St., Urbana, IL 61801]

Williams, S.R. and R.M. Peters, 1986: The Penn State Doppler network progress report. Workshop on Technical Aspects of MST Radar, Aguadilla, Puerto Rico, 1985. Middle Atmosphere Handbook, 20, 339-341. [SCOSTEP Secretariat, Univ. of Illinois, 1406 Green St., Urbana, IL 61801]

Williams, S.R. and D.W. Thomson, 1986: An evaluation of errors observed in the measurement of low wind velocities. Workshop on Technical Aspects of MST Radar, Aguadilla, Puerto Rico, 1985. Middle Atmosphere Handbook, 20, 256-262. [SCOSTEP Secretariat, Univ. of Illinois, 1406 Green St., Urbana, IL 61801]

PUBLICATIONS BEGUN UNDER CONTRACT SUPPORT

Carlson, C.A., 1987a: Kinematic quantities derived from a triangle of VHF Doppler wind profilers. M.S. Thesis, The Pennsylvania State University, University Park, PA, 136pp.

Neiman, P., 1987: Wind profiler-derived temperature gradients and advections. M.S. Thesis, The Pennsylvania State University, University Park, PA, 214 pp.